UNIVERSITY OF TECHNOLOGY, SYDNEY

REMOVAL AND RECOVERY OF PHOSPHORUS FROM MUNICIPAL WASTEWATER BY ADSORPTION COUPLED WITH CRYSTALLIZATION

By

THI AN HANG NGUYEN

A Dissertation

Submitted in fulfillment for the degree of

DOCTOR OF PHILOSOPHY

In

Environmental Engineering

University of Technology, Sydney

New South Wales, Australia

June 2015

CERTIFICATE OF ORIGINAL AUTHORSHIP

I certify that the work in this thesis has not previously been submitted for a degree nor has it been submitted as part of requirements for a degree except as fully acknowledged within the text.

I also certify that the thesis has been written by me. Any help that I have received in my research work and the preparation of the thesis itself has been acknowledged. In addition, I certify that all information sources and literature used are indicated in the thesis.

SIGNATURE OF STUDENT:

Thi An Hang Nguyen

DATE: 30 June 2015

ACKNOWLEDGEMENTS

First and foremost, I would like to express the sincere gratitude to my principal supervisor, Prof. Dr. Huu Hao Ngo, for providing me with an interesting topic and helping me to overcome all challenges during my candidature. I am indebted to him for his valuable guidance and emotional supports. I also would like to thank my supervisory committee, Dr. Wenshan Guo and Dr. Tien Vinh Nguyen for their mentor supports and useful comments on this dissertation.

I gratefully acknowledge the Australian Government for awarding me the Australia Awards Scholarship. The financial support from Centre for Technology in Water and Wastewater, UTS is highly appreciated.

This project would not have been possible without substantial help of Dr. Andrzej from Sydney Olympic Park Authority, Mr. Tyrelk from Sydney Olympic Park Wastewater Treatment Plant, and Mrs. Nga from Nhu Quynh tofu and soy milk workshop. Thank you very much for providing me with municipal wastewater and okara for use in my experiments.

I would like to extend my gratitude to M.E. Johir, UTS Environmental Engineering Laboratories Manager for his patience guidance on the use of the laboratory equipment. I am grateful to Dr. Nga for her sincere help. I appreciate Lijuan for collecting samples at night and friendship. I am thankful to Son for his assistance with SEM and XRD analysis. I also would like to thank Van for preparing some illustrations. Many thanks go to Anwar, Danious, Chung, and Tanjina for their useful discussions. I am very grateful to Tram for her sincere help with binding this thesis. Thanks a lot to other fellow post-graduate colleagues at School of Civil and Environmental Engineering for making UTS a dynamic and pleasant study place.

My heartfelt thanks go to M.Sc. Quang, my husband for his help with on-site wastewater sampling, the true love and sacrifice. My warmest thanks go to Giang and Minh, my dearest daughter and son for giving me a great motivation to complete my Ph.D. study. My love and special thanks go to my parents for encouraging me to fulfill my dreams. I owe Hung, Le, De, and Sao a big "THANH YOU" for their love and emotional supports.

Thank you all for making my Ph.D. study at UTS and my stay in Australia a wonderful and enjoyable experience!

DEDICATION

To my dearest husband, daughter and son

for their love and inspiration

TABLE OF CONTENTS

LIST OF TABLES

LIST OF FIGURES

NOMENCLATURES

Symbol	Description	Unit
A	Bed cross-sectional area	cm^2
Å	Angstrom	
AER	Adsorbent exhaustion rate	g/L
Al^{3+}	Aluminum (III) ion	
As	Arsenic	
BOD_5	Biochemical oxygen demand after 5 days	mg/L
BV	Bed volume	cm^3
C_b	Phosphorus concentration at breakthrough time	mg/L
C_o	Initial concentration of phosphorus	mg/L
C_t	Concentration of phosphorus at time t	mg/L
Ca^{2+}	Calcium ion	
$CaCO_3$	Calcium carbonate	
CaO	Calcium oxide	
$Ca(OH)_2$	Calcium hydroxide	
$Ca_3(PO_4)_2$	Tricalcium phosphate	
Cd	Cadmium	
Cl^-	Chloride ion	
ClO_4^-	Perchlorate ion	
CO_2	Carbon dioxide	
CO_3^{2-}	Carbonate ion	
COD	Chemical oxygen demand	mg/L
Cu^{2+}	Copper ion	
D	Column inner diameter	cm

DMF	N,N-dimethylformamide	
E	Activation energy	kJ/mol
EBCT	Empty bed contact time	min
EDA	Ethylene diamine triethylamine	
EDTA	Ethylene diamine tetra acetic acid	
F^-	Fluoride ion	
Fe^{2+}	Iron (II) ion	
Fe^{3+}	Iron (III) ion	
g/L	Gram per liter	
HCl	Hydrochloric acid	
Hg	Mercury	
HNO_3	Nitric acid	
H_3PO_4	Phosphoric acid	
$H_2PO_4^-$	Di hydrogen phosphate ion	
HPO_4^{2-}	Hydrogen phosphate ion	
H_2SO_4	Sulfuric acid	
IS	Ionic strength	M
k_{AB}	Adams-Bohart kinetic constant	L/mg.min
K_F	Freundlich constant	$(mg/g)(L/mg)^{1/n}$
K_L	Langmuir constant related to the energy of adsorption	L/mg
k_{Th}	Thomas rate constant	mL/min.mg
k_{YN}	Yoon-Nelson rate velocity constant	1/min
KCl	Potassium chloride	
m	Mass of dry adsorbent	g
m^2/g	Square meter per gram	
m^3	Cubic meter	
m^3/d	Cubic meter per day	
kg/d	Kilogram per day	
km^3	Cubic kilometer	
m_f	Mass of empty flask	
m_{f+w}	Mass of filled volumetric flask + water	
m_{s+f}	Mass of ZLO + volumetric flask	
m_{s+f+w}	Mass of ZLO + volumetric flask + water	
Mg^{2+}	Magnesium ion	
$MgCl_2$	Magnesium chloride	
$MgCl_2.6H_2O$	Magnesium chloride hexahydrate	

$MgNH_4PO_4.6H_2O$	Magnesium ammonium phosphate hexahydrate	
MgO	Magnesium oxide	
$Mg(OH)_2$	Magnesium hydroxide	
$MgSO_4.7H_2O$	Magnesium sulfate heptahydrate	
mg/L	Milligram per liter	
mg P/L	Milligram phosphorus per liter	
mg PO_4/g	Milligram phosphate per gram	
min	Minute	
mL/min	Milliliter per minute	
MoO_4^{-2}	Molybdate ion	
MPa	Mega Pascal	
MSBG	Modified sugarcane baggase	
µm	Micrometer	
µM	Micro molar	
mM	Mill molar	
Mn	Manganese	
mV	mill volt	
n	Freundlich constant	
N	Nitrogen	
NaOH	Sodium hydroxide	
Na_2HPO_4	Disodium hydrogen phosphate	
$NaH_2PO_4.2H_2O$	Sodium dihydrogen orthophosphate dihydrate	
$Na_{3.25}(OH)_{0.25}PO_4.12H_2O$	Trisodium phosphate dodecahydrate	
NH_4^+	Ammonium ion	
NH_4Cl	Ammonium chloride	
Ni^{2+}	Nickel ion	
NO_2^-	Nitrite ion	
NO_3^-	Nitrate ion	
N_o	Saturation phosphorus concentration	mg/L
NTUs	Nephelometric turbidity units	
P	Phosphorus	
Pb^{2+}	Lead ion	
P_s	Particle size	mm
PO_4^{3-}	Phosphate ion	
Q	Volumetric flow rate	mL/min
q_b	Amount of phosphorus adsorbed per unit of dry	mg/g

	weight of adsorbent at breakthrough time	
q_e	Equilibrium adsorption capacity of the adsorbent	mg/g
q_m	Maximum adsorption capacity of the adsorbent	mg/g
q_s	Amount of phosphorus adsorbed per unit of dry weight of adsorbent at saturation time	mg/g
q_{total}	Total mass of phosphorus adsorbed	mg
R_b	Removal percentage of phosphorus at breakthrough time	%
R_s	Removal percentage of phosphorus at saturation time	%
rpm	Revolutions per minute	
SBG	Sugarcane baggase	
SO_4^{2-}	Sulfate ion	
SeO_3^{2-}	Selenite ion	
t	Service time of the column	min
t_b	Service time at breakthrough point	min
t_s	Service time at saturation point	min
TOC	Total organic carbon	mg/L
TSS	Total suspended solids	mg/L
V_b	Volume of water treated at breakthrough time	L
V_e	Volume of water treated at exhaustion time	L
V_s	Superficial velocity	cm/min
VO_3^-	Vanadate ion	
Z	Bed height	cm
Z_o	Critical bed depth	cm
Zn^{2+}	Zinc ion	
Zr^{4+}	Zirconium ion	
$ZrOCl_2.8H_2O$	Zirconyl chloride octahydrate	
ΔG	Change in Gibbs free energy	J/mol
ΔH	Change in enthalpy	J/mol
ΔS	Change in entropy	J/mol/K
$	United States dollar	
€	Euro	

ABBREVIATIONS

Symbol	Description
ATP	Adenosine tri phosphate
AWBs	Agricultural wastes/by-products
BDST	Bed depth service time
BET	Brunauer emmett teller
BSR	Batch stirred reactor
DNA	Deoxyribonucleic acid
FTIR	Fourier transform infrared spectroscopy
HAP	Hydroxyapatite
ILO	Iron loaded okara
ISSA	Incinerated sewage sludge ash
IZLO	Iron/zirconium loaded okara
MAP	Magnesium ammonium phosphate hexahydrate ($MgNH_4PO_4.6H_2O$)
MBR	Membrane bioreactor
MTZ	Mass transfer zone
NOM	Natural organic matter
PAOs	Polyphosphate accumulating organisms
PBR	Packed bed reactor
PHB	Poly hydroxyl butyrate
ppm	Part per million
RNA	Ribonucleic acid
RO	Reverse osmosis
SEM-EDS	Scanning electron microscopy with X-ray microanalysis
TEM	Transmission electron microscope
USEPA	United States environmental protection agency

WWTP	Waste water treatment plant
XRD	Powder X-ray diffraction
ZLO	Zirconium loaded okara

GREEK SYMBOLS

Symbol	Description	Unit
τ	The time required for 50% phosphorus breakthrough	min
ρ_b	Bulk density of the adsorbent	g/cm^3
ρ_p	Particle density of the adsorbent	g/cm^3
ρ_w	Density of water	g/cm^3
η	Porosity of the adsorbent	%

PhD DISSERTATION ABSTRACT

Author: THI AN HANG NGUYEN

Date: 26 June 2015

Thesis title: Removal and recovery of phosphorus from municipal wastewater by adsorption coupled with crystallization

Statistical data: 235 pages, 38 tables, 69 figures, and 185 references

School: Civil and Environmental Engineering

Supervisors: Prof. Dr. Huu Hao Ngo (Principal supervisor)

Dr. Wenshan Guo (Alternative supervisor)

Dr. Tien Vinh Nguyen (Co-supervisor)

Keywords: Phosphorus, Removal, Recovery, Adsorption, Crystallization, Struvite (MAP - Magnesium ammonium phosphate hexahydrate - $MgNH_4PO_4.6H_2O$), Municipal wastewater, Metal loading, Zirconium loaded okara (ZLO), Soybean by-product (okara), Agricultural by-product recycling

Abstract:

Phosphorus is both critical and detrimental so it is desirable to develop a process that can not only remove but also recovery phosphorus. As the global phosphate reserve will be exhausted in 50-100 years, there is a need to explore alternatives to phosphate ores. Municipal wastewater is a significant source of phosphorus for recovery due to extremely high volumes and low levels of hazardous substances. This study investigates the feasibility of removing and recovering phosphorus from municipal wastewater by adsorption coupled with crystallization. Adsorbents were prepared from soybean by-product (okara) using metal loading method. The results indicated that zirconium loaded okara (ZLO) was the best among three developed adsorbents. The maximum adsorption capacity of ZLO was 58.93 mg PO_4/g adsorbent. The rapid adsorption was observed with 95% of the removal efficiency in 30 min. Isotherm data was best fitted by Freundlich model while kinetic data was satisfactorily described by Pseudo-second order model. Thermodynamic results revealed that the adsorption was feasible, spontaneous, and endothermic. The solution pH did not affect PO_4^{3-} uptake in a wide range of 2-11. CO_3^{2-} had a profound effect on PO_4^{3-}retention, whereas SO_4^{2-}, NO_3^- and

Cl^- were trivial inhibitors. Successful desorption and regeneration were achieved with 0.2 M NaOH and 0.1 M HCl, respectively. The ligand exchange was an important pathway for PO_4^{3-} capture by ZLO. The column results showed that the highest dynamic adsorption capacity of ZLO was 50.35 mg PO_4/g adsorbent. Thomas and Bed depth service time (BDST) models were most suitable for the description of the column adsorption behavior. ZLO column could be recycled at least three cycles with a reduction of 18.64% and 8.7% of adsorption capacity and adsorbent weight, respectively. A semi-pilot scale column packed with 100 g ZLO was capable of treating 132.5 L of municipal wastewater to meet the recommended discharge standard (1 mg P/L). The Zr^{4+} detachment from ZLO during its operation was negligible. The struvite (MAP - Magnesium ammonium phosphate hexahydrate - $MgNH_4PO_4.6H_2O$) recovery from desorption solution was most favored at pH 9, Mg: N: P molar ratio of 2:2:1, room temperature, using a combination of $MgCl_2.6H_2O$ and NH_4Cl. The harvested MAP was characterized by 93% MAP and 89% by mass P-bioavailability. Overall, the removal and recovery of phosphorus from municipal wastewater can be achieved by means of adsorption and crystallization. However, further study is necessary to make the process more economically viable.

Graphical Abstract

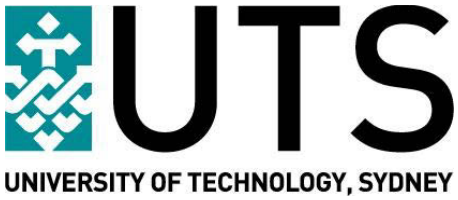

CHAPTER 1

INTRODUCTION

1.1 PROBLEM STATEMENT

1.1.1 Phosphate reserve depletion

Phosphorus is one of the sixteen elements that are essential for the plant growth (Nguyen et al., 2012). It is also a key component of deoxyribonucleic acid (DNA), ribonucleic acid (RNA), adenosine triphosphate (ATP), phospholipids, teeth and bones in animal bodies (Biswas, 2008; Karachalios, 2012). Additionally, phosphorus is a major material for many principal industries, such as fertilizers, detergents, paints, corrosion inhibitors, beverages, and pharmaceuticals (Choi et al., 2012). Though phosphorus plays an important role in daily life, it is a non-renewable resource and cannot be artificially synthesized (Karabegovic et al., 2013). Due to the over-exploitation for different purposes, the global phosphate reserve is at the risk of being exhausted in 50-100 years (Cooper et al., 2011; Eljamal et al., 2013; Ogata et al., 2012). Thus, the search for alternative sources of phosphorus has become a matter of urgency (Anirudhan et al., 2006; Zhang et al., 2012).

1.1.2 Phosphorus related environmental concerns

In another perspective, the phosphorus level above 0.02 mg/L can be responsible for eutrophication (Ismail, 2012; Mallampati and Valiyaveettil, 2013). This phenomenon is characterized by excessive growth of algae. Due to the extensive consumption of oxygen for the dead algae decay, the aquatic medium may become lack of dissolved oxygen, and thus threatening the life of aquatic creatures (Jyothi et al., 2012). As a result, the loss of water quality, biodiversity, economic and recreational value may occur (Okochi, 2013). To protect the surface water from eutrophication, the United States Environmental Protection Agency (USEPA) has recommended that the total phosphorus level in streams that enter lakes should not exceed 0.05 mg/L (Benyoucef and Amrani, 2011a). Therefore, the appropriate treatment technology is required to meet the stringent regulations (Kalmykova and Fedje, 2013).

1.1.3 Phosphorus removal and recovery technologies

Phosphorus is shown to be both an essential and harmful element (Gibbons, 2009). Thus, there is a need to develop a technology that can both remove and recovery this finite resource (Jia, 2014). To date, numerous technologies have been developed for phosphorus elimination, namely chemical precipitation, biological processes, electrodialysis, reverse osmosis, ion exchange, and adsorption (Biswas et al., 2008; Boujelben et al., 2008). However, only adsorption can facilitate the phosphorus

recovery (Loganathan et al., 2014). The significant advantages of adsorption include high efficiency for the treatment of diluted wastewater, good selectivity in presence of foreign anions, great potential of the phosphate pre-concentration, and production of a reusable phosphorus (Lanning, 2008; Li et al., 2009; Zhang et al., 2011). Although phosphorus can be recovered by various methods, the phosphorus recovery as magnesium ammonium phosphate (MAP) is preferred. This is because this process allows a simultaneous elimination of both nitrogen and phosphorus from wastewater (Ackerman, 2012; Muster et al., 2013). Moreover, the use of MAP as a slow release fertilizer mitigates the nutrient leaching and thus protecting the surface water from eutrophication (Garcia-Belinchón et al., 2013). Besides, the controlled MAP crystallization is believed to protect engineered systems from MAP scaling (Jia, 2014; Perera et al., 2007). So far, the full-scale applications of MAP crystallization from wastewater include Ostara Pearl® in Canada, Phosnix in Japan, and AirPrex in Germany (Karabegovic et al., 2013).

In the past, sludge used to be a typical raw material for MAP recovery. However, high cost resulted from chemical consumption for phosphorus leaching, is a main factor limiting its wide application (Bottini and Rizzo, 2012; Nieminen, 2010). Moreover, due to the risks of heavy metals and/or pathogen from the sludge, the use of sludge for MAP recovery is increasingly restricted (Karabegovic et al., 2013). As a result, there is a growing trend in using wastewater for MAP recovery.

1.1.4 Potential and challenges to MAP recovery from municipal wastewater

It is well-recognized that municipal wastewater with low levels of phosphorus but vast volumes can provide high mass loads of phosphorus for MAP recovery. Hence, there is a growing trend to consider the municipal wastewater as a source of phosphorus rather than an environmental concern (Huchzermeier, 2011). It has been calculated that around 250,000 tons of phosphorus can be recycled from wastewater in Western Europe annually, equivalent to the requirement of the phosphate industry (Biswas et al., 2007). According to Shu et al. (2006), every 100 m^3 of municipal wastewater can form 1 kg of MAP. Annually, around 330 km^3 of municipal wastewater are generated worldwide (Mateo-Sagasta et al., 2015). The industrial price of MAP is 1885 USD/ton (Seymour, 2009). It means that more than 6 billion USD can be saved each year if the phosphorus in municipal wastewater is recycled as MAP. Unless an adequate attention is paid to this process, the profit estimated above will be zero and simultaneously money has to be paid for phosphorus pollution treatment. Moreover, low concentrations of heavy metals

in municipal wastewater likely result in a high purity of the recovered MAP. This can be considered as a dominant advantage of municipal wastewater over other raw materials (e.g. sludge, ash) for MAP recovery (Lanning, 2008).

Till date, the MAP recovery from municipal wastewater has not become an established process (Nieminen, 2010). This is possibly due to the low concentration of phosphorus in municipal wastewater. The typical level of phosphorus in municipal wastewater was in the range of 4-16 mg/L (Nieminen, 2010). However, to make phosphorus recovery as MAP an economically feasible process, it was recommended to use the solution with the phosphorus concentration above 50 mg/L (Cornel and Schaum, 2009). Therefore, it is important to develop a viable process that can pre-concentrate phosphorus in municipal wastewater to a sufficiently high level prior to MAP recovery (Tyagi and Lo, 2013).

Meanwhile, it is well-documented that adsorption is an excellent method for the pre-concentration of pollutants. Özkütük et al. (2008) reported that the concentration of phosphate was increased 147.9 times by metal chelating polymer. Similarly, Ohura et al. (2011) found that 55-fold pre-concentration of phosphate was achieved with Zr^{4+} loaded orange waste. Likewise, Li et al. (2012) observed that the phosphorus in desorption solution was enriched 530 times compared to the feed solution by XDA-7 resin. Hence, it is believed that the combination of adsorption and crystallization can enable the phosphorus recovery from municipal wastewater (Ebie et al., 2008).

1.1.5 Research gaps

MAP has been successfully recovered from many kinds of P-rich wastewater, such as swine wastewater (Perera et al., 2007; Song et al., 2007), cola beverage (Foletto et al., 2013), eutrophic water (Li et al., 2012), sludge liquor (Karabegovic et al., 2013; Okano et al., 2013), membrane concentrate (Bradford-Hartke, 2012). However, the MAP recovery from desorption solution has rarely been tested (Nur, 2014). Furthermore, though some studies have been available on the MAP reclamation by means of adsorption/ion exchange and crystallization, little work has been done on the beneficial use of agricultural wastes/by-products (AWBs) for this purpose.

1.2 RESEARCH HYPOTHESES

The primary hypothesis for this research is the removal and recovery of phosphorus from municipal wastewater can be achieved using adsorption onto zirconium-loaded okara (ZLO) followed by crystallization as MAP.

The secondary hypotheses were:

- ZLO will be an efficient, affordable and sustainable medium for the adsorption of phosphorus from municipal wastewater.
- ZLO can pre-concentrate phosphorus in desorption solution to a sufficiently high level for an economical recovery of MAP.
- With the recycling of Zr^{4+} loading solution and ZLO be conducted, the MAP recovery from municipal wastewater by means of adsorption and crystallization will be economically feasible.

1.3 RESEARCH OBJECTIVES AND SCOPE

1.3.1 Research objectives

The overall objective of this study is to develop a viable process for removing and recovering phosphorus from municipal wastewater by means of adsorption onto ZLO and crystallization as MAP. The specific objectives of this study are as follows:

- To investigate characteristics of raw municipal wastewater to determine the potential and challenges to the phosphorus removal and recovery;
- To develop different phosphorus adsorbents from soybean by-product (okara) by metal loading method, and select the best adsorbent for next experiments;
- To investigate the phosphorus removal using the selected adsorbent (ZLO) in batch and column experiments, with synthetic and municipal wastewater;
- To appraise the phosphorus pre-concentration ability of ZLO for MAP recovery;
- To design, operate and evaluate a lab-scale batch reactor of MAP recovery from desorption solution; and
- To conduct economic assessment of ZLO development and MAP recovery.

1.3.2 Research main tasks and scope

This study involves the development of three kinds of metal load okara, which include iron-loaded okara (ILO), iron/zirconium-loaded okara (IZLO), and zirconium-loaded okara (ZLO). Of these, the best adsorbent (ZLO) was selected and applied for the next experiments. Two categories of ZLO were used at different stages of this study.

ZLO, prepared from the homemade okara, was utilized for batch experiments and characterization tests. Considering the actual application, ZLO, developed from the industrial okara, was subsequently employed for column experiments. The isotherm and kinetic studies of ZLO were performed in the batch mode with synthetic wastewater. Isotherm data were described by Langmuir, Freundlich, and Temkin models while kinetic data were fitted with Pseudo first order, Pseudo second order, and Intra particle diffusion models. The effects of different operating variables as well as the breakthrough curve modeling were investigated in mini-columns with the synthetic wastewater. The modeling of the column data was done using Thomas, Bohart-Adams, Yoon-Nelson, and Bed depth service time (BDST) models. The column adsorption, desorption and regeneration tests of ZLO were conducted with both synthetic and municipal wastewaters for comparison purpose. The phosphorus recovery as MAP was carried out with the column desorption solution. The raw municipal wastewater was collected from Sydney Olympic Park Wastewater Treatment Plant while the synthetic wastewater was prepared from disodium hydrogen phosphate (Na_2HPO_4).

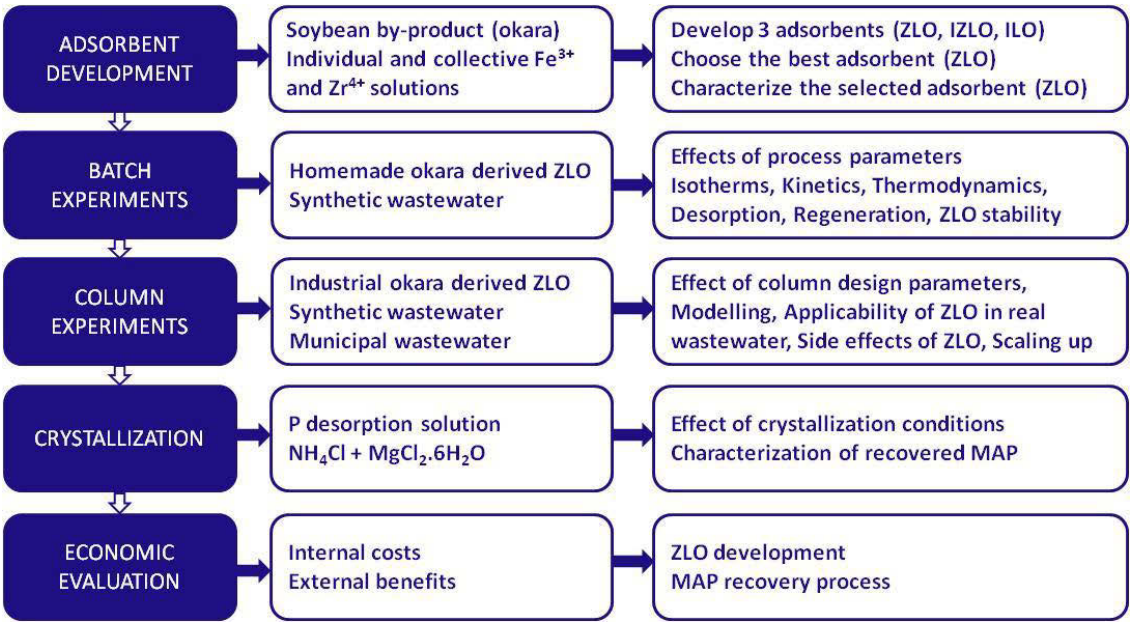

Figure 1.1 The main tasks and scope of this study

1.4 RESEARCH SIGNIFICANCE

The recycling of soybean by-product (okara) as a phosphorus adsorbent results in double environmental benefits. It does not only give a chance to reduce okara as an agricultural waste in a green way but also provide an efficient, beneficial and sustainable technology for MAP recovery from municipal wastewater. The proposed

process can be applied wherever municipal wastewater and soybean by-product are readily available enough for a practical application.

1.5 THESIS OUTLINE

This thesis has been completed by 8 Chapters. The main contents of each chapter are presented below.

Chapter 1 introduces a context for this study and defines the research problem. The research objectives, main tasks and scope, and significance are highlighted. Chapter 1 comes to an end with the layout of the thesis.

Chapter 2 provides a research background for this study. A majority part of this chapter is devoted to evaluating the current technologies for phosphorus removal and recovery. The focus is placed on MAP crystallization, with respect to influential factors, cases studies, and economic evaluation. The applicability of AWBs based adsorbents for phosphorus removal and recovery is discussed. The effects of process parameters are investigated in conjunction with mechanisms and applications. The use of soybean by-product (okara) for the development of phosphorus adsorbents is justified. The characteristics of the municipal wastewater are also presented in this chapter. Chapter 2 concludes with key findings from literature review and determines the proper research direction.

Chapter 3 presents the materials and methods used in this study. All experiments in this study are described in detail. Contents of experiments, such as chemical preparation, experimental setup, analytical methods as well as instruments used are introduced. To better understand the approach of this study, a general experimental procedure is illustrated.

Chapter 4 focuses on the development of phosphorus adsorbents from okara by a metal loading method. A comparative study on different kinds of metal loaded okara was carried out to determine the best adsorbent. Characterization of the selected adsorbent was then implemented to verify effects of metal loading and to elucidate adsorption mechanisms.

Chapter 5 refers to the performance of ZLO in batch experiments. The influential factors of the adsorption process were investigated. The maximum adsorption capacity of ZLO for phosphate was determined and compared with those of other adsorbents in the literature. The common isotherm and kinetic models are applied to analyze the

experimental data. The thermodynamic study was also carried out. The final part of this chapter is dedicated to appraising desorption and regeneration abilities of ZLO.

Chapter 6 investigates the performance of ZLO in column experiments, from the laboratory to semi-pilot scale. The maximum dynamic adsorption capacity of ZLO was estimated in association with column design parameters. The breakthrough curve modeling was performed with well-known empirical models. The efficacy of ZLO in the real and synthetic wastewater was compared. The scale-up of the column adsorption system brings an end to this chapter.

Chapter 7 deals with the phosphorus recovery from desorption solution as MAP. The effects of solution pH, the Mg: N: P molar ratio, the chemical combination, and reaction temperature were discussed. The characteristics of the harvested precipitates were identified using Scanning electron microscope (SEM), Fourier transform infrared spectroscopy (FTIR), Powder X-ray diffraction (XRD), and elemental analysis methods. The economic evaluation was implemented to determine the cost of ZLO preparation and MAP recovery. On the basis of the results encountered, the feasibility of the hybrid adsorption - crystallization system was appraised.

Chapter 8 summarizes major findings of this work. Additionally, the unique contributions of this study to the field of phosphorus removal and recovery are highlighted. Chapter 8 ends with recommendations for future research.

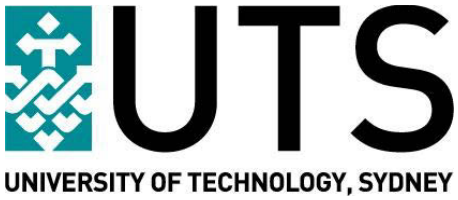

CHAPTER 2

LITERATURE REVIEW

2.1 INTRODUCTION

This Chapter begins with an investigation into the nature of municipal wastewater that paves the way to the selection of the appropriate treatment technology. By introducing merits and demerits of a wide variety of technologies currently available for phosphorus removal, the advantages of adsorption over other methods are highlighted. Chapter 2 continues with discussion on the phosphorus recovery with respect to drivers, technologies and barriers. Much attention has been paid to the crystallization of phosphorus as magnesium ammonium phosphate (MAP, struvite), the most favored recovered product. As the main part of this literature review, the next section evaluates the potential of using agricultural by-products based adsorbents for phosphorus removal and recovery. This section provides deep insights into modification methods, influential factors, mechanisms and application for phosphorus removal and recovery. Additionally, Chapter 2 also justifies the selection of the soybean by-product (okara) for the development of phosphorus adsorbents in this study. Chapter 2 ends with major findings and research gaps, which guide the present research.

A major part of Chapter 2 was published in the two following papers:

1) **Nguyen, T.A.H.,** Ngo, H.H., Guo, W.S., Nguyen, T.V., 2012. Phosphorus removal from aqueous solutions by agricultural by-products: A critical review. *J. Water Sustain.* 2, 193-207.
2) **Nguyen, T.A.H.,** Ngo, H.H., Guo, W.S., Zhang, J., Liang, S., Lee, D.J., Nguyen, P.D., Bui, X.T., 2014. Modification of agricultural waste/by-products for enhanced phosphate removal and recovery: Potential and obstacles. *Bioresour. Technol.* 169C, 750-762.

2.2 MUNICIPAL WASTEWATER CHARACTERISTICS AND PHOSPHORUS RELEVANT REGULATIONS

2.2.1 Municipal wastewater characteristics

Understanding the municipal wastewater characteristics is essential for designing and operating the treatment facilities. Thus, this section deals with the characterization of municipal wastewater and factors influencing its composition.

Table 2.1 Physical and chemical characteristics of raw municipal wastewater with minor contributions of industrial wastewater (adapted from Henze and Comeau, 2008)

Parameter	Unit	High	Medium	Low
Alkalinity	mg/L as $CaCO_3$	7	4	1
Conductivity	mS/m	120	100	70
pH	-	8.0	7.5	7.0
Viscosity	kg/m.s	0.001	0.0001	0.001
Biochemical oxygen demand (BOD)	mg/L	560	350	230
Chemical oxygen demand (COD) total	mg/L	1200	750	500
Chemical oxygen demand (COD) soluble	mg/L	480	300	200
Chemical oxygen demand (COD) suspended	mg/L	720	450	300
Total suspended solids (TSS)	mg/L	600	400	250
Volatile fatty acids (VFA) (as acetate)	mg/L	80	30	10
Volatile suspended solids (VSS)	mg/L	480	320	200
Total nitrogen (TN)	mg/L	100	60	30
Ammonia nitrogen ($N\text{-}NH_4$)	mg/L	75	45	20
Nitrate + nitrate nitrogen ($N\text{-}NO_2$/ $N\text{-}NO_3$)	mg/L	0.5	0.2	0.1
Organic nitrogen	mg/L	25	15	10
Total Kjeldahl nitrogen	mg/L	100	60	30
Total phosphorus (TP)	mg/L	25	15	6
Ortho phosphorus (Ortho P)	mg/L	15	10	4
Organic P	mg/L	10	5	2
Chloride (Cl^-)	mg/L	600	400	200
Cyanide (CN^-)	mg/L	0.05	0.03	0.02

Table 2.2 Typical content of metals in municipal wastewater with minor contributions of industrial wastewater (adapted from Henze and Comeau, 2008)

Metal (µg/L)	High	Medium	Low
Aluminum (Al)	1000	600	350
Cadmium (Cd)	4	2	1
Chromium (Cr)	40	25	10
Copper (Cu)	100	70	30
Lead (Pb)	80	60	25
Mercury (Hg)	3	2	1
Nickel (Ni)	40	25	10
Silver (Ag)	10	7	3
Zinc (Zn)	300	200	100

Table 2.3 Biological characteristics of municipal wastewaters, number of microorganisms per 100 ml (adapted from Henze and Comeau, 2008)

Micro organisms	High	Low
E. coli	$5*10^8$	10^6
Coliforms	10^{13}	10^{11}
Cl. perfringens	$5*10^4$	10^3
Fecal Streptococcae	10^8	10^6
Salmonella	300	50
Campylobacter	10^5	$5*10^3$
Listeria	10^4	$5*10^2$
Staphylococcus aureus	10^5	5.10^3
Coli phages	$5*10^5$	10^4
Giardia	10^3	10^2
Roundworms	20	5
Enterovirus	10^4	10^3
Rotavirus	100	20

According to urban wastewater treatment Directive 91/271/EEC municipal or urban wastewater can be defined as domestic wastewater or a mixture of domestic wastewater with industrial wastewater and/or run-off rain water (Frost, 2009).

Municipal wastewater consists of 99.9% water and a small percentage of organic and inorganic solids. The organic substances in municipal wastewater include carbohydrates, lignin, fats, soaps, synthetic detergents, proteins. The municipal wastewater may contain a wide range of inorganic substances, including heavy metals, such as copper, zinc, lead, cadmium, mercury. Besides, pathogenic viruses, bacteria, protozoa and helminthes may be present in raw municipal wastewater. The typical composition of municipal wastewater is illustrated in Tables 2.1, 2.2, and 2.3.

As the above tables show, the composition of municipal wastewater varies considerably. This could be mainly attributed to the difference in water consumption from one location to another (Henze and Comeau, 2008). Low water consumption often leads to concentrated municipal wastewater, characterized by high concentrations of major components and vice versa. For example, Jordan is a country in an arid area, where the water consumption is usually very low (90 L/d per person). Consequently, the levels of most pollutants in municipal wastewater of Amman city, Jordan were even higher than those proposed for high contaminated municipal wastewater as listed in Table 2.1. Specifically, the composition of the municipal wastewater of Amman city was characterized as follows: total solid 1200 mg/L, total nitrogen 150 mg/L, total phosphorus 25 mg/L, alkalinity 850 mg/L as $CaCO_3$, BOD_5 770 mg/L, COD 1830 mg/L, TOC 220 mg/L (Matouq, 2008). The implementation of more stringent regulations might also be responsible for the enhanced quality of municipal wastewater. In a review on the effect of phosphorus control measures on water quality in the United States, Litke (1999) reported that the concentration of phosphorus in the WWTPs effluent was proportional to the consumption of phosphate for detergent. The concentration of total phosphorus in raw effluent increased from 3 to 11 mg/L from the 40s to 70s, when the phosphorus consumption for detergent reached a maximum. With the prohibition of phosphate- based detergents, the raw effluent contained about 5 mg/L of total phosphorus in the early 1990s. The authors concluded that the phosphate detergent bans resulted in 50% reduction in the phosphorus concentration in the WWTPs effluent. In addition, the different levels of treatment could be another important reason for the varying composition of municipal wastewater. This is evidenced by typical effluent quality following various levels of treatment in Table 2.4.

Table 2.4 Typical effluent quality following various levels of treatment (adapted from Australian guidelines for sewerage systems - effluent management, 1997)

Treatment	BOD, mg/L	TSS, mg/L	Total N, mg/L	Total P, mg/L	E. Coli, Org./100 mL	Grease, mg/L
Raw	150-500	150-450	35-60	6-16	10^7-10^8	50-100
A	140-350	150-350	-	-	-	-
B	120-250	80-200	30-55	6-14	10^6-10^7	30-70
C	20-30	25-40	20-50	6-12	10^5-10^6	<10
D	5-20	5-20	10-20	<2	-	<5
E	-	-	-	-	$<10^3$	-
F	2-5	2-5	<10	<1	$<10^2$	<5

Notation:

Treatment process categories: A. Pre-treatment, B. Primary treatment, C. Secondary treatment, D. Nutrient removal, E. Disinfection, F. Advanced treatment

From the public health point of view, pathogenic organisms can be considered as the greatest concern. However, in view of phosphorus recovery, among various pollutants in municipal wastewater, phosphorus and heavy metals are of the most significance. It is observed that the concentration of total phosphorus in municipal wastewater is changeable, such as 4.2 mg/L (Gibbons, 2009), 4-15 mg/L (Mezenner and Bensmaili, 2009; Nieminen, 2010), 8-10 mg/L (Xu et al., 2011a), 10 mg/L (Karachalios, 2012; Kumar et al., 2010; Namasivayam and Sangeetha, 2004), 10-30 mg/L (Zach-Maor et al., 2011). Understanding the existence of phosphorus species in aqueous solution enables the selection of appropriate treatment technologies (Neethling, 2011). In natural water bodies, phosphorus may exist in different forms (Fig.2.1). However, only orthophosphate can accelerate the growth of algae, inducing eutrophication (Bhojappa, 2009). Depending on pH values of aquatic medium, orthophosphate may exist in various species. In strongly alkaline conditions, PO_4^{3-} is the major form, while in weakly alkaline conditions, HPO_4^{2-} is dominant. In weakly acidic conditions, $H_2PO_4^-$ prevails, whereas H_3PO_4 is most common in strong acidic conditions (Karachalios, 2012). The ratio of various forms of phosphorus might be different from case-by- case. However, the researchers agreed that the proportion of orthophosphate in the total phosphorus was approximately 50% (Karachalios, 2012; Kumar et al., 2010; Namasivayam and Sangeetha, 2004; Parsons and Smith, 2008; Xu et al., 2011a).

Notably, Gibbons (2009) stated that the percentage of orthophosphate in the secondary wastewater effluent from Mill Cove pollution control plant, Bedford, Nova Scotia, Canada was 94%. This result verified the effect of the processing level on the phosphorus component of municipal wastewater.

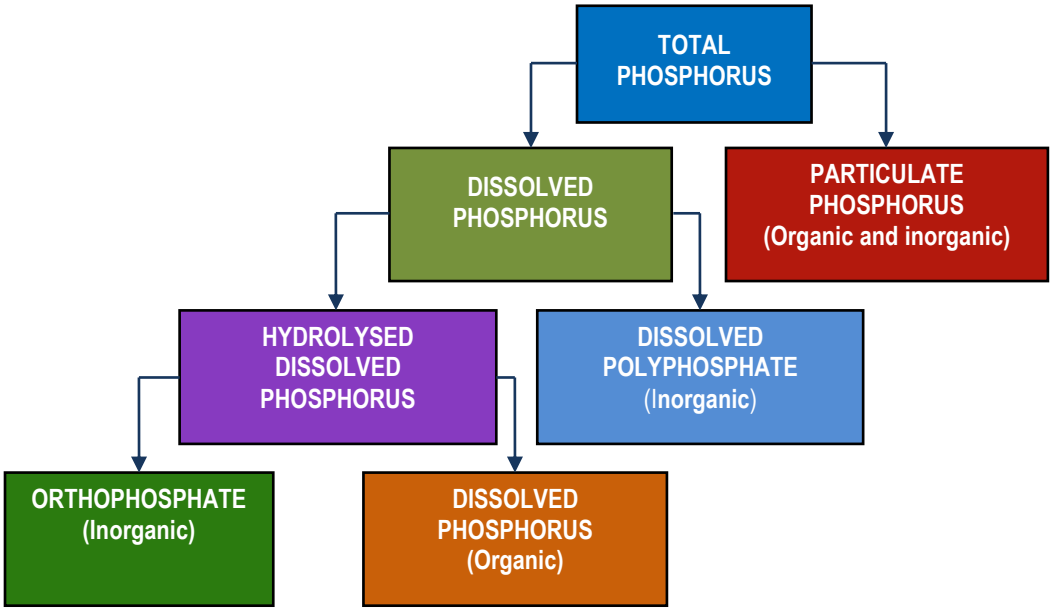

Figure 2.1 Different forms of phosphate in municipal wastewater (modified from Bhojappa, 2009)

The typical content of metals in municipal wastewater is shown in Table 2.2. These results are in good agreement with those recently reported by Chu et al. (2010); Kihampa (2013); and Reyahi-khoram and Sobhanardakani (2014). It is apparent that, the concentration of metals in municipal wastewater was not significant enough to interfere with the quality of phosphorus recovered. It can be considered as an advantage of municipal wastewater over other WWTP's products, for example sludge or ash when being used for phosphorus recovery.

In conclusion, the composition of municipal wastewater may change considerably with the location and the time, depending on the influents and processing levels at Waste Water Treatment Plants (Gibbons, 2009). Typically, municipal wastewater represents low concentrations of phosphorus and metals. While low content of phosphorus may hinder the recovery of phosphorus, low levels of metals in municipal wastewater are beneficial for enhancing the purity of recovered phosphorus. The chemical parameters of stored wastewater can change over time, due to the activity of microbes living in the medium (Ackerman, 2012). The instability of municipal wastewaters makes it difficult to repeat experiments (Huchzermeier, 2011).

2.2.2 Phosphorus relevant regulations

An excessive amount of phosphorus may result in negative impacts on ecosystems. Hence, several standards and guidelines come into existence for controlling phosphorus pollution in natural water bodies and wastewater effluents (Gibbons, 2009).

Table 2.5 Effluent discharge standards of different countries

Country	Total phosphorus unless otherwise indicated (mg/L)	Year, source
Australia, Tasmania	0.5 (50% of samples must be less than the specified limit) 1 (90%) 3 (100%)	2001, Emission Limit Guidelines for Sewage Treatment Plants that Discharge Pollutants in Fresh and Marine Waters June 2001.
Canada	1	1976, Guidelines for Effluent Quality and Wastewater Treatment at Federal Establishments
China	0.5 (Level A) 1 (Level B)	2006, China National Standards
European Union	1 (> 100,000 PE) 2 (10,000 -100,00 PE)	1991, European Union Urban Waste Water Directive (Council Directive 91/271/EEC)
India	5 (dissolved P)	1986, General Standards for Discharge of Environmental Pollutants
Japan	16	1993, Japan National Effluent Standards
Uganda	5 (Soluble P) 10 (Total P)	1999, The National Environment Regulations (Standards for Discharge of Effluent into Water or on Land)
USA, Colorado	0.7 (New plants) 1 (Existing plants)	Colorado Regulation No31 and No85
USA, Montana	1 (TN 10mg/L, Q>1 mgd) 2 (TN 15 mg/L, Q<1 mgd)	Montana Senate Bill 95 and Senate Bill
USA, Wisconsin	1	Wisconsin Dual Legislation
Vietnam	4 (Category A) 6 (Category B) 8 (Category C)	2005, Standard TCVN 5945 - 2005 (Industrial Wastewater Discharge Standards)

References: Clark and Vanrolleghem, 2010; Eldho, 2014; http://epa.tas.gov.au/epa/document?docid=40; http://www.env.go.jp/en/water/wq/nes.html; http://faolex.fao.org/docs/pdf/uga40868.pdf; http://www.gree-vn.com/pdf/TCVN5945-2005.pdf

In many countries, the level of phosphorus in surface water has been regulated lower than or equal to 0.05 mg/L to prevent excessive algae growth (Benyoucef and Amrani, 2011a; Ismail, 2012; Krishnan and Haridas, 2008). According to Awual and Jyo (2011), a maximum permissible level of phosphorus lower than 0.01 mg/L is required to protect surface water from eutrophication. For the same purpose, the USEPA has recommended the total phosphorus level in streams that enter lakes and in the flowing streams should not exceed 0.05 mg/L and 0.1 mg/L, respectively (Benyoucef and Amrani, 2011a).

To control the phosphorus pollution at sources, the effluent discharge standards have been developed and applied in several countries (Table 2.5). As is shown by the table, the effluent discharge standards vary significantly from one country to another. This can be explained by the variation in the level of treatment technologies and the background phosphorus concentration in the water bodies in different countries. Nevertheless, the most stringent regulation has recommended the level of total phosphorus in the effluent should range between 0.5 and 1 mg/L before discharging into the aquatic environment (Xu et al., 2011a). To meet these limits, the search for proper treatment technologies is necessary.

2.3 PHOSPHORUS REMOVAL TECHNOLOGIES

Removal of phosphorus can be achieved with various technologies, such as membrane filtration, reverse osmosis (Greenlee et al., 2009), precipitation, coagulation, crystallization (Ackerman, 2012; Jia, 2014), adsorption (Gibbon, 2009; Okochi, 2013), ion exchange (Awual and Jyo, 2011; Gupta, 2011; Nur et al., 2014a), magnetic separation, biological treatment, and constructed wetland (Martín et al., 2013). Though chemical precipitation and biological treatment are most common, each method represents its own merits and demerits (Table 2.6). In this study, phosphorus removal technologies have been grouped into conventional and non-conventional technologies as follows.

2.3.1 Conventional technologies

A. Physical methods

Physical removal technologies include microfiltration, reverse osmosis, and electrodialysis. These are membrane related processes. Microfiltration involves a size exclusion mechanism. Therefore, its removal efficiency does not rely on process

parameters, such as influent concentration and pressure. In contrast, the primary mechanism of reverse osmosis is diffusion, and thus the elimination efficiency is controlled by the influent concentration, pressure, and water flux rate. In the electrodialysis method, the movement of ions is supported by an electric field applied across a semi-permeable membrane. Ions tend to migrate through the membrane and become more concentrated in one compartment, while decontaminated water remains in the other. While microfiltration suffers from low separation efficiency (≤10%), reverse osmosis and electrodialysis are often prone to extremely high costs (Karachalios, 2012).

B. Chemical methods

Chemical precipitation was first applied in the 1950s, in response to increasing concern over eutrophication. Chemical methods remove phosphorus by addition of salts of multi-valence metal ions to form precipitates of insoluble metal phosphates, which are subsequently separated by sedimentation (Biswas, 2008; Gibbons, 2009).The most common chemicals employed for this purpose are iron and aluminum chloride or sulfate, or calcium hydroxide. These chemicals combine with phosphate as shown by the following reactions (Nieminen, 2010).

$$Al^{3+} + PO_4^{3-} \rightarrow AlPO_4^{\downarrow} \quad (2.1)$$

$$Fe^{3+} + PO_4^{3-} \rightarrow FePO_4^{\downarrow} \quad (2.2)$$

$$5\ Ca^{2+} + 3\ PO_4^{3-} + OH^- \rightarrow Ca_5(PO_4)_3(OH)\downarrow \quad (2.3)$$

Chemical removal has the advantage of being simple, efficient and flexible (Biswas, 2008). It is reported that up to 90% of the total phosphorus can be removed by this method. Though chemical addition can be done at different stages in the wastewater treatment process, the secondary treatment is usually the stage recommended (Nieminen, 2010). Nevertheless, chemical removal method is still subjected to several drawbacks, such as sludge formation, high chemical expense, effluent neutralization requirement, inadequate efficiency for phosphorus dilute solution (Biswas, 2008; Kumar et al., 2010; Mallampati and Valiyaveetttil, 2013; Zhang et al., 2011). The sludge handling will increase the treatment cost and require much space (Lanning, 2008; Sengupta and Pandit, 2011). Neutralization of effluent not only increases the chemical expenditure but also is harmful to the biological treatment process (Biswas, 2008). In addition, the end-products of chemical methods are non-reusable, due to high impurities and low bioavailability (Biswas, 2008; Gupta, 2011; Kalmykova and Fedje, 2013; Midorikawa et al., 2008; Nieminen, 2010). Besides, it is hard to identify the optimal dosing conditions (Biswas, 2008).

C. Biological methods

Biological phosphorus removal was developed in the late 1950s, and it has become a firmly established technology (Biswas, 2008). Biological methods to remove phosphorus from aqueous solutions are characterized by the storage of phosphorus in the cells of polyphosphate accumulating organisms (PAOs), followed by the separation of accumulated phosphorus in the form of biomass. In anaerobic conditions, PAOs use their intracellular polyphosphate as an energy source to assimilate fermentation products, for example acetate, to form polyhydroxy butyrates (PHB) and release orthophosphate. When exposed to aerobic conditions, PAOs use PHB as an energy source for oxidizing organic matter to provide carbon for new cell growth and synthesizing polyphosphate from previously released orthophosphate to store in their cells. The principle of the cell operation for biological removal method is illustrated in Fig.2.2, while concentrations of participating substances in the process are depicted in Fig.2.3. Biological methods hold a number of benefits over their chemical counterparts, such as the formation of biological sludge with better value when used in agriculture and phosphorus recovery and the absence of chemicals (Biwas, 2008). Nevertheless, biological methods have various shortcomings, namely low removal efficiency (≤30%), complex configuration and operating regimes (Biswas, 2008), high energy consumption and high foot print (Gupta, 2011; Karachalios, 2012; Ning et al., 2008; Peleka and Deliyanni, 2009). Especially, biological removal methods require the addition of readily biodegradable organic carbon, which make these processes costly (Gupta, 2011; Nieminen, 2010). The functional micro-organisms (PAOs) are sensitive to the variation of temperature and feed concentrations (Li et al., 2013; Onyango et al., 2007). Furthermore, these processes cannot remove trace levels of phosphorus (Sengupta and Pandit, 2011).

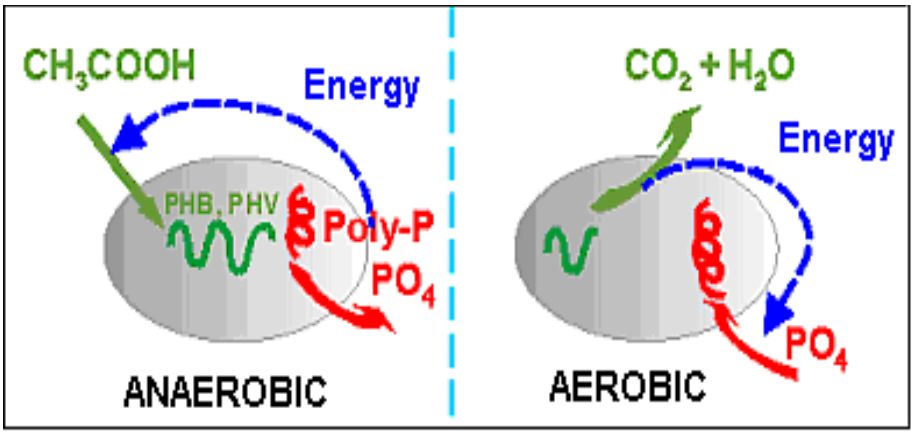

Figure 2.2 The principle of biological phosphorus removal process (adapted from Nieminen, 2010)

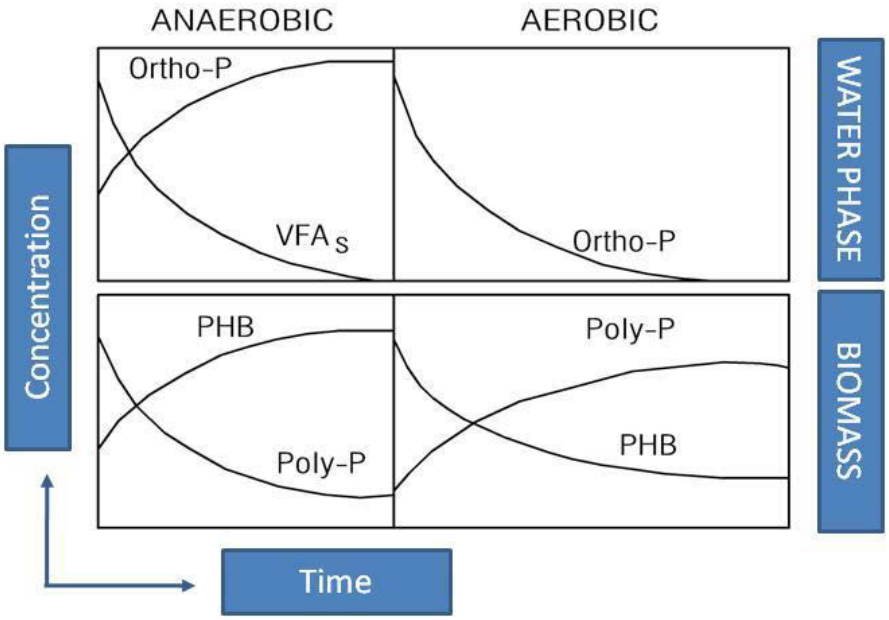

Figure 2.3 The concentrations of involving substances in the biological P removal process (adapted from Nieminen, 2010)

2.3.2 Non-conventional technologies

A. Magnetic separation

Magnetic separation was initially investigated in the 1970s. It is considered as an attractive method because this method can produce an effluent with the phosphorus level of 0.1-0.5 mg/L at the same costs as other methods. Magnetic separation can be used as a reliable add-on technology for chemical removal. Lime is employed to precipitate calcium phosphate, which is attached to the magnet. In the next step, calcium phosphate is separated from the magnet in a separator unit using shear forces and a

drum operator. The significant advantages of this process are high elimination efficacy, compact process, and low energy consumption (Biswas, 2008).

B. Crystallization

The crystallization technology has been developed since the 1970s, as a result of more stringent regulations and a desire to yield a more marketable end-product (Biswas, 2008). This method is based on the crystal nucleation and growth chemistry. It includes MAP (magnesium ammonium phosphate) and HAP (hydroxyapatite) processes. However, the high cost and improper public perception make crystallization an unattractive option for phosphorus pollution treatment. Even so, there are some full-scale WWTPs applying MAP crystallization technology in Canada, United States, Germany, Japan and Australia (Nieminen, 2010).

C. Ion exchange

Ion exchange is defined as the reversible interchange of ions between a solid phase (the ion exchange resin) and a liquid phase (Martin et al., 2009). Ion exchange materials are insoluble acids or bases, which contain loosely held ions in the form of insoluble salts. It allows ion exchange materials to exchange either positively charged ions (cation exchangers) or negatively charged ions (anion exchangers) (Karachalios, 2012).The natural ion exchange materials include proteins, cellulose, living cells while the most common synthetic resins are those consisting of polystyrene with sulfonate groups (cation exchangers) or amine groups (anion exchangers). Ion exchange method is advantageous because of its simple operation, adaptability to changes in feed flow rates, temperatures and compositions (Awual and Jyo, 2011; Li et al., 2012). However, low selectivity with the presence of co-ions and high operation cost caused by frequent use of generation chemicals are major hindrances for its widespread application (Biswas et al., 2007; Gupta, 2011; Karachalios, 2012)

D. Adsorption

Adsorption method removes phosphorus from water by attracting phosphate ions in a liquid to the surface of a solid adsorbent and holding them by intermolecular forces (Biswas, 2008). This method offers various advantages, such as low cost, high efficiency, simple operation, no sludge formation, no influence on wastewater pH (Gupta, 2011; Zhang et al., 2011; Zhang et al., 2014; Zach-Maor et al., 2011). Among numerous technologies available for phosphorus removal, only adsorption holds the potential for phosphorus recovery (Loganathan et al., 2014; Sengupta and Pandit, 2011;

Zhang et al., 2014). It can be explained that adsorption can pre-concentrate phosphorus in the solution to a high level, and therefore enabling phosphorus recovery (Li et al., 2012; Ohura et al., 2011). In addition, it is well-documented that, adsorption is efficient in removing phosphorus from a dilute solution (Krishnan and Haridas, 2008; Zhang et al., 2011). Consequently, it is believed that adsorption can promote phosphorus recovery from wastewaters characterized by low levels of phosphorus, such as municipal wastewater (Ebie et al., 2008; Tan and Lagerkvist, 2011). Nevertheless, the bottleneck for the use of adsorption in water treatment is the development of low-cost and efficient adsorbent (Li et al., 2013). It is supported by Biswas (2008) who stated that the feasibility of the phosphorus adsorption process mostly depends on the preparation of adsorbents.

In the past, activated carbon was used for phosphorus removal. However, the problems relative to the high cost, no renewability and disposal after use hinder its wide application in developing countries (Karthikeyan et al., 2004). Hence, there is a new trend in using low-cost and abundantly biomaterials, such as agricultural by-products, for this purpose (Biswas, 2008). It is desirable to develop adsorbents that have by low-cost, abundant availability, high efficiency, high selectivity, potential renewability, and high adaptability to various operating conditions (Ning et al., 2008).

Table 2.6 Summary of advantages and disadvantages of various phosphorus removal technologies*

Method	Treatment result	Advantage	Disadvantage
Membrane technology	EPC 0.04 (MBR), 0.008 (RO), < 0.005 (electro dialysis)		– High costs in case of RO and electrodialysis – Low removal efficiency (<10%) in case of microfiltration
Magnetic separation	EPC 0.1-0.5	– High P removal – Compact process – Low energy consumption	– Chemicals required – Technology is complex
Chemical precipitation	EPC 0.005-0.04	– Flexible – Easy to install – High P removal – Less space requirement	– High chemical demand – Chemical sludge generation – Effluent neutralization requirement – Difficult to identify optimal dosing conditions – Low bioavailability of end-products – Rule out P recovery possibilities – Unsuitable for wastewater with low P levels
Crystallization	EPC0.3-1.0	– Recycle end-products – Demonstrated technology	– High cost – Chemicals and operation skills required – Complex process
Ion exchange		– Simple operation – High P removal – Adaptability to various solution compositions and flow rates – Can operate in wide range of temperature – MAP produced can be used in agriculture	– High operation cost – Low selectivity – Materials originated from nonrenewable resources

Adsorption	EPC 0.005-0.01 RE > 80	– Simple operation – Cost-effectiveness – Few chemicals involved – No sludge formation – No influence on wastewater pH – Suitable for poor P wastewater – Can pre-concentrate P to high levels – Enable P recovery – Multiple regeneration of adsorbents	– High cost – Disposal problems after use – The feasibility of P adsorption process relies on the development of adsorbent – Technology is unproven
Biological P removal	EPC 0.1-0.3 RE ≤ 30	– Avoiding chemical use – Avoiding the chemical sludge formation – Produce biological sludge with better value when used in agriculture – Potential P recovery – Established technology	– Low removal efficiency – Inability to remove trace P concentration – Can hardly meet discharge standards – Biological sludge handling – Sensitive to changes in P load and temperature
Enhanced biological P removal	0.02 ≤ EPC < 0.1, depending on duration RE up to 97	– Can remove P to very low levels – Modest cost – Minimal sludge formation	– External carbon source requirement – Complex configuration and operating regimes – More energy and space requirement

Notation: EPC- Effluent phosphorus concentration (mg P/L); RE - Removal efficiency (%).

* Adapted from Biswas (2008); Karachalios (2012); Lanning (2008); Li et al. (2012); Loganathan et al. (2014); Nieminen (2010); Ohura et al. (2011); Strom (2006).

2.4 PHOSPHORUS RECOVERY

2.4.1 Drivers for phosphorus recovery

Phosphorus recovery is a process that can (i) convert phosphorus into either plant available form for reuse as fertilizer or a raw material for the phosphorus industry, and (ii) separate valuable phosphorus from harmful substances (Cornel and Schaum, 2009; Petzet et al., 2012). According to Green et al. (2004), phosphorus recovery is defined as a process that allows phosphorus to precipitate or crystallize from wastewater, sewage sludge, and ash into a pure product for recycling purposes. Unfortunately, some authors misused 'phosphorus recovery' for phosphorus desorption in the literature, for example Bottini and Rizzo (2012), Ohura et al. (2011), Gupta (2011). In this study, the term 'phosphorus recovery' was used according to the above definitions.

Recovery of phosphorus has become a matter of interest in recent years. There are many reasons for this. Firstly, it is predicted that rock phosphate reserves cannot last for more than 150 years (Jia, 2014; Loganathan et al., 2014; Tyagi and Lo, 2013). The increasing scarcity of high-quality phosphorus ores leads to the rise in the cost of fertilizer production, and this negatively affects the global economy (Nieminen, 2010). Therefore, there is a need to search for alternative phosphorus sources. Another reason is that the direct use of sludge in agricultural soils is increasingly restricted. It has contributed to the desire to develop a proper technology for recovering phosphorus from sludge (Nieminen, 2010). Moreover, recovery of phosphorus is believed to create revenue by converting waste into commercial products. It is reported that the phosphorus recovery from sewage sludge can produce a profit of about $ 2.1 per capita and year (Tyagi and Lo, 2013). Last but not least, the spontaneous formation of MAP is undesirable since it may cause pipe blockage (Jia, 2014; Kuzma, 2011; Perera et al., 2007). Hence, the controlled crystallization of MAP is expected to protect engineered systems from MAP scale. For all the reasons mentioned, the phosphorus in municipal wastewater should be recycled. Thus, the development of an appropriate technology for phosphorus recovery is necessary.

2.4.2 Phosphorus recovery technologies

In WWTPs, the recovery of phosphorus can be performed at several locations (Fig.2.4). Different products of WWTPs may be used as feed materials for phosphorus recovery, including (1) liquor, (2) sludge, and (3) mono-incinerated sludge ash. The liquors used for phosphorus recovery include effluent from secondary sedimentation

(1a), concentrated side stream from anaerobic treatment (1b), and sludge liquor from digested sludge dewatering (1c). In these cases, phosphorus occurs in the soluble form as orthophosphate. As the phosphorus level in (1a) is typically below 5 mg/L, the (1b) and (1c) are usually preferred. These streams normally have phosphorus content of 20-100 mg/L. The phosphorus can also be recovered with sludge from a digester before (2a) and after (2b) dewatering. These materials contain phosphorus in chemically or biologically bound forms. In the case of using sewage sludge ash, the phosphorus is in the most concentrated form.

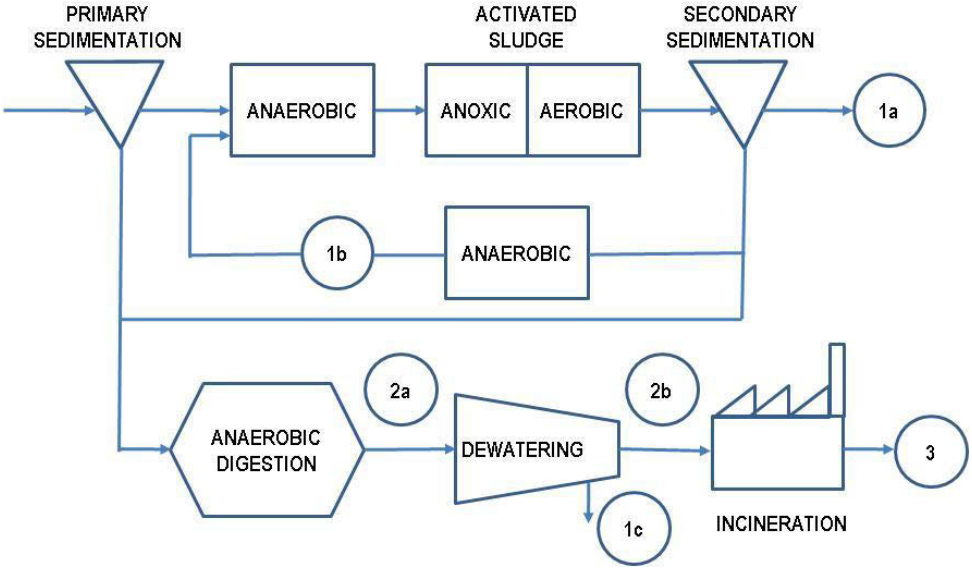

Figure 2.4 Possible places for P recovery in WWTP (adapted from Nieminen, 2010)

Depending on various products of WWTP utilized for phosphorus recovery, the technologies can be classified as precipitation/crystallization, wet-chemical extraction, and thermal treatment (Sartorius et al., 2012). The crystallization and precipitation transfer phosphorus from liquor into the solid phase using pH adjustment and chemical dosage (Fig.2.5). The precipitation differs from crystallization in the reaction speed. Precipitation takes less time than crystallization. Precipitation results in the amorphous product while crystallization yields the crystalloid product. The phosphorus levels in liquors need to be ≥ 50 mg/L to ensure economically viable phosphorus recovery. The pH value can be adjusted with NaOH or CO_2 stripping (Nieminen, 2010). The wet chemical method recovers the phosphorus bound in sludge and ash by chemical leaching combined with precipitation (Fig.2.6). As phosphorus in sludge/ash is in the chemically or biologically bound forms, phosphorus needs to be extracted by acid or base leaching before separation by means of precipitation, ion exchange or nanofiltration. Thermo-chemical method recovers the phosphorus from ash by addition

of chloride chemicals, for example KCl, $MgCl_2$ and thermal treatment (>1000 °C), enabling the evaporation of heavy metal chlorides (Fig.2.7). Due to extensive energy consumption and incineration plant requirement, the thermo-chemical technology is appropriate for countries where sludge is commonly disposed of by incineration.

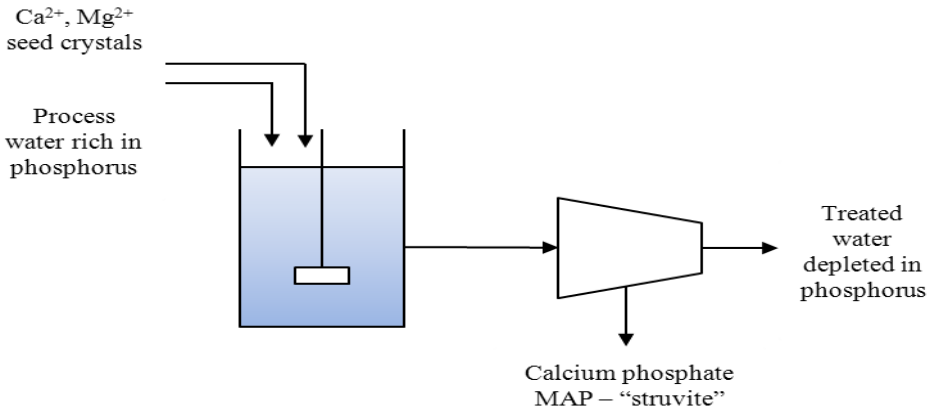

Figure 2.5 The precipitation/crystallization technology (adapted from Cornel and Schaum, 2009)

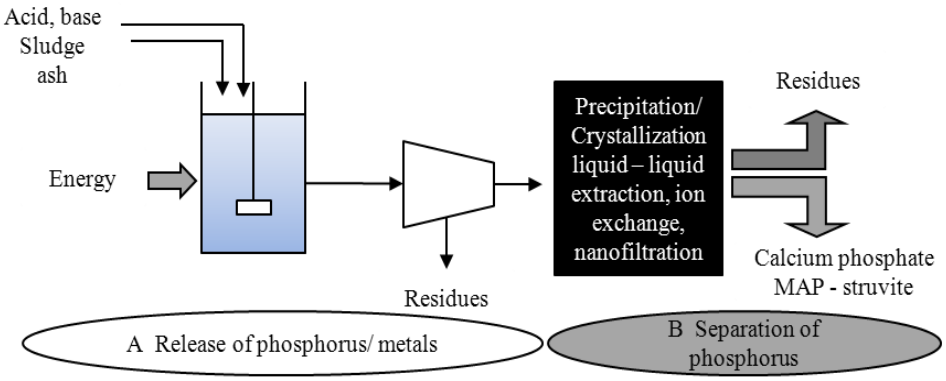

Figure 2.6 The wet-chemical technology (adapted from Cornel and Schaum, 2009)

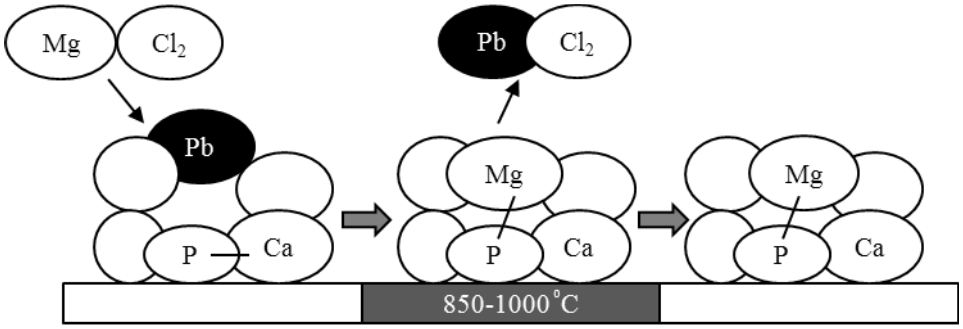

Figure 2.7 The thermo-chemical technology (adapted from Adam, 2011)

Recovery of phosphorus from sludge or ash may result in a higher efficiency than from liquors (Cornel and Schaum, 2009). Nevertheless, this process often suffers from

higher costs, due to chemical and energy consumption for phosphorus leaching and thermal treatment. Thus, from an economic point of view, precipitation/ crystallization technology is usually preferred to wet chemical or thermo-chemical technologies (Nieminen, 2010). So far, the precipitation/crystallization technology has been successfully applied in full scale in several countries such as Canada, Japan, Germany and the United States. In contrast, the wet chemical method has found only limited application in industry. The thermo-chemical process has been restricted to pilot scale applications.

Table 2.7 P recovery potential with different products of WWTPs (adapted from Nieminen, 2010)

	Volume	Phosphorus concentration	Bond	Recovery potential
Effluent	200 l/cap/d	< 5 mg/L	Dissolved	max. 55%
Sludge liquor	1-10 l/cap/d	20-100 mg/L	Dissolved	max. 50%
Dewatered sludge	0.15 l/cap/d	~ 10 g/kg TS	Biological/ chemical	~ 90%
Sewage sludge ash	0.03 kg/cap/d	64 g/kg	Chemical	~ 90%

The summary in Table 2.8 is relevant to the phosphorus recovery from different products of WWTPs. It is evident from Table 2.8 that phosphorus can be recovered via either direct crystallization or crystallization preceded by adsorption/ion exchange. The direct crystallization is often applied to sludge liquors, ash extraction liquors, and wastewaters with high levels of phosphorus (Ackerman, 2012; Foletto et al., 2013; Garcia-Belinchón et al., 2013; Karabegovic et al., 2013; Perera et al., 2007; Xu et al., 2012). The minimal phosphorus concentration for direct MAP crystallization was 50 mg/L while the maximal concentration reached up to 650 mg/L. On the contrary, the crystallization preceded by adsorption/ion-exchange is suitable for phosphorus recovery from wastewaters with moderate content of phosphorus (≤ 5 mg/L). Adsorption/ion-exchange can be used as an add-on technology. Since these methods can pre-concentrate phosphorus in wastewater to a high level, they pave the way to phosphorus recovery (Ebie et al., 2008; Li et al., 2012).

Calcium phosphate and magnesium ammonium phosphate (MAP) are typical products of phosphorus recovery. Calcium phosphate can be recycled in the phosphate industries while MAP can be used as slow-release fertilizer in agriculture (Tyagi and Lo, 2013). MAP seems to be preferred to some calcium phosphate compounds, due to

higher solubility and simultaneous holding of both nitrogen (NH_4^+) and phosphate (PO_4^{3-}) (Ackerman, 2012; Muster et al., 2013). As MAP contains two primary nutrients (P and N) as well as a secondary nutrient (Mg), it would be beneficial to recover phosphorus as MAP to be used in the fertilizer industry (Nieminen, 2010). For this reason, the section 2.4.3 below will focus on the MAP crystallization process.

Table 2.8 P recovery from different products of WWTPs

No	Process	Type of wastewater	P removal efficiency	Recovered products	Reference
1	Large scale	Membrane concentrate: 24-62 mg P/L		MAP	Bradford-Hartke, 2012
2	Field test, Adsorption + Crystallization	Household domestic wastewater	95.6%	$Na_{3.25}(OH)_{0.25}PO_4.12H_2O$: 95%	Ebie et al., 2008
3	Lab scale, direct crystallization	Cola beverage: 415 mg PO_4/L	97%	MAP	Foletto et al., 2013
4	Pilot scale, Ostara's Pearl technology	Anaerobic digester concentrate: 31-150 mg P/L	60-81%	MAP	Garcia-Belinchón et al., 2013
5	Lab scale, direct precipitation	Sewage sludge ash		$CaHPO_4.2H_2O$	Gorazda et al., 2012
6	Lab scale, direct crystallization	Synthetic wastewater		MAP 96.8%	Hao et al., 2008
7	Lab scale Acidic leaching + precipitation	Fly ash of municipal solid waste	70%	$Ca_3(PO_4)_2$, $AlPO_4$, $Fe_3(PO_4)_2$, $MgHPO_4$	Kalmykova and Fedje, 2013
8	Jar test	Liquor of thermally pre-treated waste activated sludge: 650 mg P/L	80%	MAP and some calcium and magnesium phosphates	Karabegovic et al., 2013
9	Lab scale, Anion exchange + crystallization	Eutrophic water: 1.3 mg PO_4/L		MAP 75.8%	Li et al., 2012
10	Field test Adsorption +	Municipal wastewater		Ca_3PO_4 16% P, low	Midorikawa et al., 2008

	precipitation	secondary effluent: Total P: 0.1-2.1 mg P/L		content of hazardous elements	
11	Lab scale	Anaerobic sludge digestion liquor (ASDL) and synthetic model liquor (s-ASDL	69% for ASDL and 73% for sASDL		Okano et al., 2013
12	Lab scale, direct crystallization	Swine waste biogas digester effluent: 42 mg PO_4/L	97%	MAP	Perera et al., 2007
13	Lab scale, direct precipitation	Sewage sludge ash	78%	Calcium phosphate, aluminum phosphate	Petzet et al., 2012
14	Lab scale, direct crystallization	Swine wastewater	97%	MAP	Song et al., 2007
15	Lab scale, direct crystallization	Sewage sludge ash extraction	97.2%	MAP 97%, P availability 94%, low contents of heavy metals	Xu et al., 2012

2.4.3 MAP crystallization process

A. Formation, characteristics and practical applications

(i) MAP formation

MAP crystallization has been investigated with different WWTPs products, such as swine wastewater (Perera et al., 2007; Song et al., 2007), sludge liquor (Karabegovic et al., 2013; Okano et al., 2013), sewage sludge ash (Gorazda et al., 2012; Petzet et al., 2012; Xu et al., 2012), fly ash of municipal solid waste incineration residues (Kalmykova and Fedje, 2013), membrane concentrate (Bradford-Hartke, 2012), anaerobic digester concentrate (Garcia-Belinchón et al., 2013), cola beverage (Foletto et al., 2013), municipal wastewater secondary effluent (Midorikawa et al., 2008), household domestic wastewater (Ebie et al., 2008), eutrophic water (Li et al., 2012), synthetic wastewater (Hao et al., 2008). However, from an economic point of view, only side stream or process water with phosphorus level greater than 50 m/L is appropriate for this purpose (Perera et al., 2007). It is reported that the formation of

MAP requires P: Mg: N molar ratio of 1: 1: 1 and alkaline pH medium of 8-10 (Cornel and Schaum, 2009). The additional condition is a low concentration of TSS (Jia, 2014). MAP is produced via the following chemical reaction (Huchzermeier, 2011).

$$Mg^{2+} + NH_4^+ + HPO_4^{2-} + 6H_2O \rightarrow MgNH_4PO_4.6H_2O\downarrow + H^+ \quad (2.4)$$

(ii) MAP characteristics

Struvite (magnesium ammonium phosphate, MAP) is a soft phosphate mineral with formula $MgNH_4PO_4.6H_2O$. The molar weight of MAP is about 245.41 g/mol. With a specific gravity of 1.7, MAP exhibits high settle ability, and thus can be easily separated from wastewaters. The solubility of MAP is influenced by pH, temperature, and ionic strength. MAP is slightly soluble in neutral and alkaline mediums, but readily soluble in the acid condition (Liu et al., 2013). The minimal solubility of MAP occurs at pH above 8.5 (Nieminen, 2010). The maximal solubility of MAP is in the temperature range of 20-30 °C (Lanning, 2008). At the temperature >50 °C, MAP crystals become unstable and may lose the attached water molecules to form dittmarite (Wu and Bishop, 2004). Depending on the category of wastewaters, the recovered MAP may have different colors, such as white, yellow or brownish, light gray (Huchzermeier, 2011). MAP crystals are observed in the form of needles (Fig.2.8). The sizes of MAP crystals produced at lower phosphate concentration were a little larger (80-100 µm) than those yielded at higher phosphate concentration (60-80 µm) (Li et al., 2012). In a study performed by Foletto et al. (2013), MAP crystals had a particle size 0.25µm, surface area 6.59 m^2/g.

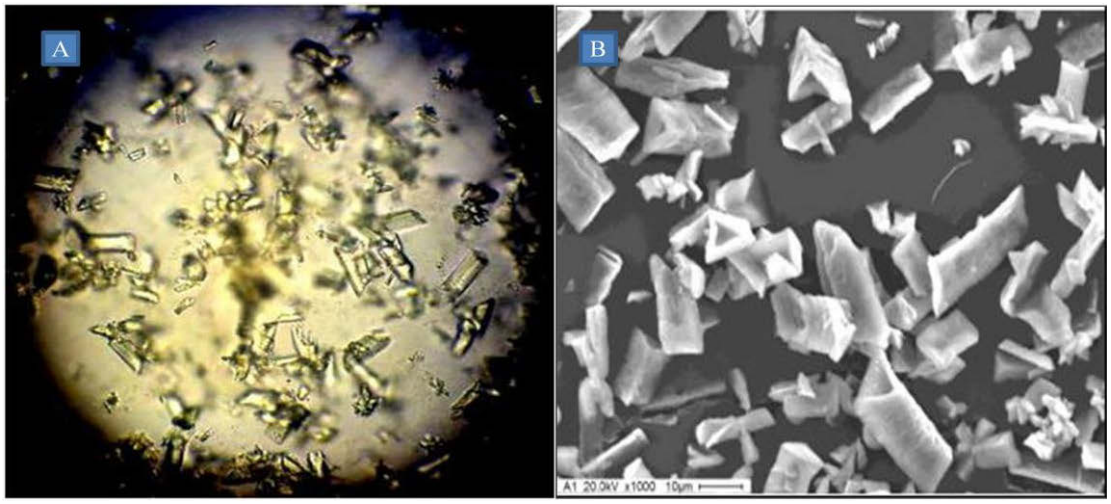

Figure 2.8 A. Photomicrograph of a MAP liquor (adapted from Yetilmezsoy et al., 2011), and B. SEM image of MAP recovered from dairy manure filtrate (adapted from Huchzermeier, 2011)

(iii) MAP practical applications

MAP can be applied directly as a fertilizer in agriculture because it contains both nitrogen (NH_4^+) and phosphorus (PO_4^{3-}) as primary nutrients (Ackerman, 2012). As a slow release fertilizer, MAP can be used at high rates without any risk of damaging plant roots (Diwania et al., 2007). It can also mitigate phosphorus leaching and thus protect aquatic medium from eutrophication (Garcia-Belinchón et al., 2013). It was reported that the hog manure derived MAP had the same agronomic effect on biomass yield of canola plants as pure MAP (Ackerman, 2012). Due to the presence of NH_4^+ in its composition, MAP is rarely utilized as a raw material in the electro-thermal process (Nieminen, 2010). In addition, MAP can be used as a component of fire resistant material, cement, detergent, cosmetics and animal feed (Jia, 2014; Lanning, 2008). Despite the dominant advantages, MAP has not been used widely so far. The impurity of MAP is a barrier to its application. High levels of heavy metals in phosphorus recovered from municipal solid waste incineration fly ash prevent it from being used directly in arable lands (Kalmykova and Fedje, 2013). Another obstacle is the public perception that MAP is produced from wastewater containing hazardous components such as heavy metals and/or pathogens, and thus it should not be used for crops. As an example, although five hundred tons of MAP was generated from wastewater of a potato processing plant in Kruiningen, the Netherlands each year, farmers were scared of using it as fertilizer for their potato fields (Lanning, 2008). Transportation across the borders may also present problems since MAP is considered as waste in some countries (Jeanmaire and Evans, 2001). Besides, MAP is more soluble in acid than alkaline mediums, raising the question of its effectiveness in alkaline soils (Ackerman, 2012).

B. Factors affecting MAP formation

It was found that MAP crystallization is controlled by several factors. Considering influential factors provides a chance for optimizing the process (Ackerman, 2012). This section will investigate in detail the effect of operating parameters on MAP crystallization.

(i) Solution pH

It is reported that solution pH is one of the most important factors influencing the MAP crystallization (Lanning, 2008; Liu et al., 2013; Xu et al., 2012). The effects of solution pH are as follows.

❖ Influence of pH on the availability of MAP component ions

Lower pH seems to be better for the availability of MAP component ions. At high pH values, both NH_4^+ and Mg^{2+} can be lost from the solution, making them unavailable for MAP crystallization (Ackerman, 2012). In an open system, a significant volatilization of NH_3 occurs at pH ≥ 9.3 (Hao et al., 2008; Lanning, 2008; Liu et al., 2013; Perera et al., 2007). Mg^{2+} is removed from solution in the form of $Mg(OH)_2$ when pH value reaches 10.7 (Ali and Schneider, 2008; Wang et al., 2005). Approximately 98% of orthophosphate is present as HPO_4^{2-} at pH 9.0 (Huchzermeier, 2011). The minimum solubility of MAP occurs at pH > 8.5 (Nieminen, 2010). Taking into consideration all these things, the ideal pH range for MAP crystallization should be 8.5 < pH ≤ 9.3. Lanning (2008) noted that pH should not be raised too high during MAP recovery because the effluent would then require neutralization before being discharged into the environment. In particular, if wastewater has a high buffer capacity, large amounts of chemicals need to be consumed for pH adjustment, and thus boosting up the cost of reclaimed MAP. For that reason, extremely high pH seems to be a challenge to MAP crystallization.

❖ Influence of pH on MAP purity

The pH increment was shown to reduce MAP content in reclaimed products. Hao et al. (2008) reported that MAP percentage decreased from 96.8 to 15.5% with increasing pH from 7.0 to 10.5, respectively. However, pH above 10.5 led to the complete disappearance of MAP in the precipitate. Li et al. (2012) showed that the MAP purity reduced from 81.3 to 3.9% with increase of pH from 9 to 11. These results are supported by Wang et al. (2005) who revealed that precipitation at pH > 8.7 yielded other compounds than MAP.

Since pH plays a critical role in MAP crystallization, a majority of studies on MAP crystallization has dealt with the determination of the optimal pH values (Table 2.9). It was done to optimize the recovery process in term of phosphorus removal efficiency and MAP purity. It seemed to be that synthetic wastewaters required lower optimal pH values than real wastewaters. Specifically, the ideal pH for MAP crystallization with synthetic wastewater was in the range of 7-7.5 (Hao et al., 2008). On the other hand, the best pH values for MAP crystallization were 8.5-9.5 with dairy manure (Huchzermeier, 2011), 9 with swine waste biogas digester effluent (Perera et al., 2007), 9.5 with cola beverage (Foletto et al., 2013), and 9.5-10.5 with swine wastewater

(Song et al., 2007). This can be ascribed to the effect of co-existing ions in the real wastewaters. These results will be used as references, when the present study examines the effect of pH on MAP recovery from municipal wastewater.

Table 2.9 Optimum pH for MAP crystallization from wastewater

No	Type of wastewater	Optimal pH	P recovery	Reference
1	Synthetic wastewater	8.5	98%	Çelen et al., 2007
2	Cola beverage	9.5	97%	Foletto et al., 2013
3	Anaerobic digester concentrate	7.3-8.2	60-81%	Garcia-Belinchón et al., 2013
4	Synthetic wastewater prepared by tap water	7.0-7.5		Hao et al., 2008
5	Synthetic wastewater	9.0-9.5		Jia, 2014
6	Digested swine manure concentrate	9.0	81%	Jordaan et al., 2010
7	Liquor of thermally pre-treated waste activated sludge	9.2	80%	Karabegovic et al., 2013
8	Eutrophic water	< 8.0		Li et al., 2012
9	Swine waste biogas digester effluent	9.0	97%	Perera et al., 2007
10	Synthetic wastewater	8.7	70.3%	Pastor et al., 2010
11	Synthetic swine wastewater	9.5-10.5	97%	Song et al., 2007
12	Sewage sludge ash extraction	10.0	97.2%	Xu et al., 2012

It is interesting to note that MAP crystallization may also affect the solution pH value. Lanning (2008) suggested that MAP formation resulted in the acidification of the solution since HPO_4^{2-} ions were reduced to PO_4^{3-}ions and released H^+ ions. Huchzermeier (2011) observed that solution pH decreased rapidly during the first 5-10 minutes which might be associated with MAP formation, and then gradually increased until equilibrium was established. Therefore, pH can be employed as an indicator for crystallization reaction completion. Also, continuous pH monitoring and subsequent adjustment is required throughout the process.

(ii) Magnesium (Mg^{2+}) supplementation

Magnesium is one of the three component ions for MAP crystallization. The theoretical Mg: N: P molar ratio for MAP crystallization is 1:1:1. However, most types of wastewater have low concentrations of Mg^{2+} as compared to that of NH_4^+ and PO_4^{3-}.

Therefore, it is necessary to add Mg^{2+} into wastewaters to ensure favorable MAP formation (Huchzermeier, 2011). The molar ratio of Mg: NH_4^+: PO_4^{3-} is supposed to be a critical factor influencing the MAP crystallization (Lanning, 2008; Liu et al., 2013; Xu et al., 2012).

❖ Magnesium sources

Different sources of magnesium have been tested for MAP crystallization, such as $MgCl_2.6H_2O$ (Foletto et al., 2013; Garcia-Belinchón et al., 2013; Li et al., 2012; Perera et al., 2007; Song et al., 2007; Xu et al., 2012), $MgSO_4.7H_2O$ (Hao et al., 2008), and MgO (Karabegovic et al., 2013; Lanning, 2008). The scientists have tried to search for the appropriate Mg^{2+} source, which can bring about high yield of MAP and has an acceptable price. Kumar and Pal (2013) tested three combinations which were $MgCl_2.6H_2O$ + $NaH_2PO_4.12H_2O$; $MgSO_4.7H_2O$ + $Ca(H_2PO_4)_2.H_2O$; MgO + H_3PO_4 and concluded that $MgCl_2.6H_2O$ + $NaH_2PO_4.12H_2O$ showed the best performance in terms of ammonium removal. Similarly, Jia (2014) applied two combinations which were $MgCl_2.6H_2O$ + KH_2PO_4 and MgO + H_3PO_4 and found that the more efficient removal of ammonium was attained from the combination of $MgCl_2.6H_2O$ + KH_2PO_4. Lanning (2008) compared two different sources of MgO and observed that chemical grade powdered MgO was better than industrial grade MgO concerning the MAP precipitation. According to Nieminen (2010), $MgCl_2.6H_2O$ and $MgSO_4.7H_2O$ are readily soluble in water and thus are the most common precipitants at both lab-scale and full-scale applications. On the other hand, MgO and $Mg(OH)_2$ are insoluble in water and require a longer time for disassociation. To become active, these compounds need to be used with fine particle size and vigorous agitation. Consequently, MgO and $Mg(OH)_2$ can hardly be employed for industry. Nevertheless, $MgCl_2.6H_2O$ and $MgSO_4.7H_2O$ are more expensive than MgO and $Mg(OH)_2$ (Table 2.10). To diminish the cost of MAP crystallization, seawater is proposed to be used as an alternative source of Mg^{2+} provided that WWTPs are adjacent to the coast (Liu et al., 2013). Besides, $MgCl_2$ can increase the acidity of the solution (Lanning, 2008).

Table 2.10 Mg sources for MAP crystallization (adapted from Liu et al., 2013)

Compound	Required Mg^{2+} input (kg/kg MAP)	Cost ($/kg MAP)
Magnesium (Mg)	0.10	3.12
Magnesium chloride hexahydrate ($MgCl_2.6H_2O$)	0.83	6.50
Magnesium sulfate heptahydrate ($MgSO_4.7H_2O$)	1.00	5.52
Magnesium oxide (MgO)	0.16	3.22
Magnesium hydroxide ($Mg(OH)_2$)	0.24	1.88

❖ Mg: P molar ratio

Table 2.11 summarizes studies on MAP crystallization from wastewaters performed with varying Mg: P molar ratios. It appears to be that an extra Mg^{2+} source, indicated by Mg: P molar ratio higher than 1, is usually added to ensure high phosphorus removal. Liu et al. (2013) explained that depending on solution pH, four types of phosphate magnesium salts might be formed, namely $MgNH_4PO_4.6H_2O$, $MgHPO_4.3H_2O$, $Mg_3(PO_4)_2.22H_2O$, $Mg_3(PO_4)_2.8H_2O$. Thus, the real amount of added Mg^{2+} would be higher than the theoretical value. However, the overuse of magnesium salts would induce undesirable impacts, such as increase in chemical cost, precipitation of $Mg(OH)_2$ at strong alkaline condition, and excessive amount of residual Mg^{2+} and Cl^- ions in the effluent (Huchzermeier, 2011). Consequently, there would be a need to remove excessive Mg^{2+} in the effluent before discharging it into the environment (Lanning, 2008).

Table 2.11 Effect of Mg: P molar ratio on P recovery efficiency

No	Type of wastewater	Mg source	Mg: P molar ratio	P recovery efficiency	Reference
1	Synthetic wastewater	$MgCl_2.6H_2O$	2:1	98%	Çelen et al., 2007
2	Cola beverage	$MgCl_2.6H_2O$	1:1	97%	Foletto et al., 2013
3	Anaerobic digester centrate	$MgCl_2.6H_2O$	1.3-2.5:1	60-81%	Garcia-Belinchón et al., 2013
4	Synthetic wastewater	$MgSO_4.7H_2O$	1.2:1		Hao et al., 2008
5	Synthetic wastewater	$MgCl_2.6H_2O$	1.3:1.1	99.9%	Jia, 2014
6	Digested swine manure centrate	$MgCl_2.6H_2O$	1.6:1	81%	Jordaan et al., 2010
7	Liquor of waste activated sludge	MgO	1.2:1	80%	Karabegovic et al., 2013
8	Eutrophic water	$MgCl_2.6H_2O$	1.2:1		Li et al., 2012
9	Synthetic wastewater	$MgCl_2.6H_2O$	1.1:1	70.3%	Pastor et al., 2010
10	Swine waste biogas digester effluent	$MgCl_2.6H_2O$	1:1	97%	Perera et al., 2007
11	Swine wastewater	$MgCl_2.6H_2O$	1.4:1	97 %	Song et al., 2007
12	Sewage sludge ash extraction	$MgCl_2.6H_2O$	1.6:1	97.2%	Xu et al., 2012

(iii) Chemical addition sequence and rate

Different feeding sequences have been examined by researchers. Hao et al. (2008) proposed that the optimum MAP crystallization from synthetic wastewater could be achieved by the addition of $NaH_2PO_4.2H_2O$ into the mixture of $MgSO_4.7H_2O$ and NH_4Cl, followed by pH adjustment. On the contrary, Xu et al. (2012) found that the best feeding sequence for MAP precipitation from sewage sludge ash was by adding $MgCl_2.6H_2O$ into the phosphorus solution, followed by pH adjustment and subsequent NH_4Cl supplement. Kim et al. (2007) tested eight chemical feeding sequences and found that the addition of magnesium and phosphate at the same time, followed by a pH altering chemical yielded the best MAP crystallization. They believed that an increase in pH prior to addition of phosphate might lead to the formation of $Mg(OH)_2$, and thus reducing Mg availability for MAP crystallization. Similarly, calcium phosphate was formed instead of MAP if the magnesium addition was the sequent stage of phosphate

feeding. Regarding the effect of chemical addition rate, Jia (2014) observed that feeding rate had limited impact on the phosphorus recovery.

(iv) Presence of calcium (Ca^{2+})

High levels of Ca^{2+} in wastewater may hinder MAP formation, due to the reaction of Ca^{2+} with orthophosphate to form various calcium phosphate compounds, such as $CaHPO_4.2H_2O$ (brushite), $CaHPO_4$ (monetite), $Ca_8H_2(PO_4)_6.5H_2O$ (octa calcium phosphate), $Ca_3(PO_4)_2$ (tricalcium phosphate), $Ca_5(PO_4)_3OH$ (hydroxylapatite), $Ca_3(PO_4)_2nH_2O$ (amorphous tricalcium phosphate) (Ackerman, 2012; Hao et al., 2008; Song et al., 2007). It was observed that the percentage of pure MAP reduced from 85 to 61 and 38% with elevating Ca: P molar ratio from 0.5:1 to 1:1 and 2:1, respectively (Wang et al., 2005). These results agreed well with findings by Ackerman (2012) who noted that the Ca: P molar ratio above 2 could reduce MAP content in the precipitation to zero. It is because calcium may block active sites and compete with magnesium for orthophosphate (Huchzermeier, 2011). Likewise, Moerman et al. (2009) reported that no MAP was formed in a full-scale MAP reactor in Europe, when Ca: P molar ratio in anaerobically digested potato wastewater was as high as 2.36. In an attempt to abate the effect of Ca^{2+} on MAP precipitation in liquid dairy manure, Shen et al. (2011) used acidification followed by addition of EDTA and oxalate. However, high costs and side effects of chemicals were worth considering. Ackerman (2012) suggested conducting precipitation at a low pH medium (pH 6.8) to prevent calcium phosphate formation from hog manure. The author indicated that Ca^{2+} level in municipal sludge dewater liquor was usually small and could not pose a problem to MAP formation. Conversely, animal wastewater often contained high concentrations of Ca^{2+} and thus required proper treatment prior to MAP recovery.

(v) Alkalinity

Huchzermeier (2011) reported that in the high alkalinity medium, carbonate (CO_3^{2-}) might complex with magnesium (Mg^{2+}) and ammonium (NH_4^+) to form magnesium carbonate ($MgCO_3$), magnesium bicarbonate ($MgHCO_3$), and ammonium bicarbonate (NH_4HCO_3). These processes occupy two MAP component ions (Mg^{2+} and NH_4^+) which would otherwise be available for MAP precipitation. As a result, the MAP formation is reduced, and thus the supplement of Mg^{2+} is necessary. In contrast, Song et al. (2007) noted that CO_3^{2-} has a minor effect on morphology and purity of MAP.

(vi) Total suspended solids (TSS)

According to Lanning (2008), high levels of organic matters in the form of TSS might be a challenge to MAP formation as well. The author explained that the complexation of organics with MAP component ions would lead to a decrease in availability of MAP component ions and an increase in MAP solubility. Additionally, high contents of TSS could make it hard to separate MAP from organic matters. Huchzermeier (2011) stated that TTS ≥ 1000 mg/L might hinder the MAP formation. Thus, the pre-treatment of wastewater for the reduction of TSS before MAP crystallization was needed. Nieminen (2010) observed that TSS ≤ 150-200 mg/L reduced the impurities in the recovered phosphorus products. Although Ostara Pearl® technology could operate at TSS level up to 3000-4000 mg/L, the level of TSS below 1000 mg/L was recommended. The long settling time could be a solution for the problem with high TSS (Ackerman, 2012; Lanning, 2008).

(vii) Ionic strength (IS)

Ionic strength has been found to play a significant role in MAP formation. When Mg^{2+}, NH_4^+, and pH altering chemicals are introduced, IS value is increased. The activity of MAP component ions is decreased, due to the increase in electrostatic interaction between ions in the solution. Huchzermeier (2011) reported that IS around 0.196 M in anaerobically digested dairy manure filtrate weakened the activity of Mg^{2+}, NH_4^+, and PO_4^{3-} by 68%, 25%, and 92%, respectively.

(viii) Carbonate anion (CO_3^{2-})

Lanning (2008) reported that CO_3^{2-} had an adverse impact on MAP formation. That is because the presence of CO_3^{2-} led to the increase in ionic strength, and thus impeding the MAP crystallization reaction. As a result of the reaction between HCO_3^- and Mg^{2+}, $MgHCO_3^+$ was formed, and this reduced the activity of Mg^{2+} ions. Le Corre et al. (2005) found that CO_3: Mg ≥ 1:1 might result in the formation of other compounds rather than MAP. On the contrary, Song et al. (2007) reported that CO_3: Mg molar ratio of 0.5-2 could hardly affect the phosphorus removal and MAP purity.

(ix) Reaction temperature

It is well-documented that the precipitation was enhanced at lower temperatures. However, in reality, most of the studies have been performed at the ambient temperature (Ackerman, 2012). As a result of reducing temperature from 25 to 15 °C, the total phosphorus removal was increased from 27.1 to 37.8% (Adnan et al., 2003).

Conversely, Jia (2014) revealed that increasing temperature from 25 to 35 °C had a marginal effect on the phosphorus removal and MAP crystals mass. They explained this by minor variations in the activity of MAP component ions in this range of temperature. Increasing temperature was found to reduce MAP crystals size. It was reported that the MAP crystals size was reduced from 30 to 14 μm, when temperature was elevated from 25 to 35 °C (Jia, 2014). Likewise, Rouff (2013) reported that a temperature increment from 25 to 300 °C led to a decline in MAP crystals size, from 1 mm to < 25 μm. The temperature also affects the MAP purity. Rouff (2013) discovered that MAP was dominant at 25 °C, while newberyite and magnesium pyrophosphate were prevailing at 100 °C and 300 °C, respectively. Hence, they concluded that 25 °C was a desirable temperature for MAP formation.

(x) Other process parameters

Other operating parameters that can affect the MAP crystallization process include the presence of citrate, reaction time, mixing rate and existence of metals or sulfate. Citrate may adversely influence MAP formation as it can bind with Mg^{2+}. It was reported that, the presence of 1 μM citrate hampered MAP production up to 80% and yielded smaller MAP crystals (Lanning, 2008). Regarding the effect of reaction time, Diwania et al. (2007) found that the longer reaction time often resulted in the bigger sizes of MAP crystals. The less soluble the chemicals were, for example MgO versus $MgCl_2$, the longer the crystallization time was required (Lanning, 2008). Concerning the effect of the mixing rate, Suzuki et al. (2002) found that lower mixing velocity led to smaller MAP crystal size. On the other hand, Lanning (2008) reported that high mixing rate would reduce the crystal size. Sulfate (SO_4^{2-}) and metals (Al^{3+}, Fe^{2+}, and Fe^{3+}) were confirmed to be influential factors in MAP formation. However, their impacts are not discussed in detail in this thesis.

C. Case studies on MAP recovery at full scale

Up to this time, MAP has been successfully recovered on an industrial scale using different technologies (Table 2.12). The MAP crystallization processes from wastewater include Ostara Pearl® in Canada, Phosnix in Japan, and AirPrex in Germany. The wet chemical technology, recovering phosphorus from sludge by dissolution of phosphorus and crystallization of MAP, is the Seaborne process in Germany (Cornel and Schaum, 2009; Nieminen, 2010).

The full-scale Ostara Pearl® process was developed by the University of British Columbia, Canada, and it holds a U.S. Patent 7622047 B2. It can recover 85% of phosphorus and 10-15% of ammonium from sludge liquor as MAP by using NaOH for pH adjustment and $MgCl_2$ for MAP crystallization. The phosphorus concentration as low as 10 mg/L can be processed, but the feasible limit is 20-30 mg/L and the preferable level is ≥ 60 mg/L. The process was in use in Edmonton, Canada in 2007, in Oregon, United States in 2009 and in Virginia and Pennsylvania, United States in 2010. The Edmonton plant produces 500 kg MAP/day. The recovered product is named Crystal Green®, having N: P formula of 5: 28, and also containing 10% Mg.

The full-scale Phosnix process was developed by Unitika Ltd. Environmental and Engineering Divison, Japan. The process (1000 m^3/d) can recover phosphorus (80-90%) from phosphorus-rich sludge liquor (100-150 mg/L) as MAP (approximately 100 kg/d). NaOH and $Mg(OH)_2$ are used for pH adjustment and MAP crystallization, respectively. MAP granules have the size of 0.5-1.0 mm. As shown in Table 2.12, the recovered MAP by the Phosnix process has the same percentage of component elements as the pure MAP. The recovered MAP is sold to fertilizer companies at the price of 250 €/t. The process has been in operation in the Lake Shinji Eastern Clarification Centre, Japan since 1998 and Osaka South Ace Centre, Japan since 2010 (Nieminen, 2010).

The AirPrex procedure was developed by Berliner Wasserbetriebe, Germany. It is utilized at Waßmannsdorf WWTP, Germany. The process can recover phosphorus (98%) as MAP from digester sludge liquor (300 mg P/L) using air stripping of CO_2 to adjust pH and $MgCl_2$ to induce MAP crystallization. The process has been in operation since 2010 and can produce 2.5 t MAP/day. The recovered MAP with quality meeting the German fertilizer ordinance is used as raw material in fertilizer production. The cost of recovered MAP is estimated to be 50 €/ton, equivalent to 400 €/t phosphorus (Nieminen, 2010).

The Seaborne process is the first full-scale implementation of the wet chemical technology, which is suitable for recovering phosphorus from sludge. It was developed by Seaborne Environmental Research Laboratory, Germany. The process was installed at Gifhorn WWTP in 2003 and put into operation in 2005. It includes three major steps, namely acid leaching, removal of heavy metals, and MAP precipitation. H_2SO_4, NaOH and $Mg(OH)_2$ are employed for acid leaching, pH adjustment, and MAP crystallization, respectively. The influent phosphorus concentration of the process is 600 mg/L. The recovered products contain $MgNH_4PO_4$, $Mg_3(PO_4)_2$, $Ca_3(PO_4)_2$, $(NH_4)_3PO_4$,

$MgHPO_4.3H_2O$, $CaHPO_4.nH_2O$, and $(NH_4)_2HPO_4$. The precipitates are not crystalloid, the crystal content occupies only 10%, and around 90% is amorphous. The cost of recovering phosphorus by this process is nearly 46 €/kg phosphorus. Due to the significant chemical costs, low influent flow, and intricate design, the process is not yet feasible and is considered as a big pilot process.

Table 2.12 Industrial scale processes for P recovery as MAP (adapted from Nieminen, 2010)

Full scale process	Developer	Location	Start	Feed material	Feed material flow (m^3/d)	P level in influent (mg P/L)	P level in effluent (mg P/L)	Method	Chemical	P production (kg/d)	Price of recovered (€/t P)
Ostara Pearl®	University of British Columbia/ Ostara	Edmonton	2007	Liquid	500	100-900	Not found	Crystallization	NaOH, $Mg(OH)_2$	500	N/A
Phosnix	Unitika Ltd.	Shimane Prefecture, Japan	1998	Liquid	500	100-110	10	Crystallization	NaOH, $Mg(OH)_2$	500-550	N/A
AirPrex	Berliner Wasserbetriebe	Waßmannsdorf, Berlin, Germany	2010	Sludge liquor	2000	300	< 5	Crystallization	$MgCl_2$ Rockaway PX 60 N Flocculent Praestol® 40560	2500	390
Seaborne	Seaborne Environmental research laboratory	Gifhorn, Germany	2005	Sludge	110	600 (P_{total})	5-6 (P_{total})	Acid leaching, crystallization	H_2SO_4, Na_2S, NaOH, MgO, Flocculent Praestol® K 255 L	680	40,000

Note: N/A – Not available.

Table 2.13 The percentage of Mg, N, and P in the recovered and pure MAP (adapted from Nieminen, 2010)

Element	Theoretical value from chemical formula (%)	MAP from Oxley Creek (%)	MAP from Phosnix (%)
Mg	9.9	9.1	9.9
N (NH_4)	5.7 (7.4)	5.1	5.9
P (PO_4)	12.6 (38.7)	12.4	12.6
6 H_2O	44	39	-

D. Economic evaluation

Despite many studies on MAP crystallization from wastewater around the world, very little work has been done in the literature on the cost-benefit analysis of the process so far. Jia (2014) compared the cost of phosphorus removal between MAP crystallization and coagulation coupled with activated sludge. Taking into consideration the operation cost and MAP sale profit, the author revealed that the latter process was 7 times more expensive than the former one. Garcia-Belinchón et al. (2013) conducted economic evaluation of MAP recovery at full scale in WWTPs with three options of phosphorus removal technologies. They found that MAP crystallization was not economically viable in the case of using anaerobic digestion and physicochemical removal techniques. Conversely, the process could be an economical option with bio-P removal and the investment costs might be recovered after a period of 5-10 years. Xu et al. (2012) analyzed the cost-benefit of MAP production from sludge ash. The costs included HCl consumption for phosphorus extraction, cation exchange resin consumption for heavy metals elimination while the benefit comes from MAP sale. The authors claimed that the profit of the process exceeded 5 $/kg sludge ash.

2.4.4 Barriers to phosphorus recovery

Until now, phosphorus recovery was still an un-established process. The high cost appears to be the main obstacle to expanding this technology (Lanning, 2008). At present, recycled phosphorus is not competitive with the mineral source, in term of the price (Cornel and Schaum, 2009). Tyagi and Lo (2013) claimed that the recovered phosphorus was 22 times more costly than mined phosphorus. Bottini and Rizzo (2012) reported that the expenditures for phosphorus recovered from sludge liquor using ion exchange method coupled with crystallization and mined phosphorus were 8.2 and

0.652 €/kg, respectively. Taking the annual increase in the mined phosphorus cost (0.012 €/ per kg per annum) into consideration, the phosphorus recovery from sludge liquor was expected to be beneficial in the next 10-15 years. Molinos-Senante et al. (2011) revealed that the cost of phosphorus recovered from wastewater varied between 2 and 8 €/kg P while that of rock phosphate ranged from 35 to 50 $/ton. They concluded that unless environmental benefits were taken into account, phosphorus recovery would not be economically viable. Sartorius et al. (2012) predicted that phosphorus recovery would become an established process in the next 20 years in developed countries. Another reason for limiting the broad application of MAP crystallization is the quality of reclaimed phosphorus products (Sartorius et al., 2012). High levels of heavy metals in phosphorus recovered from municipal solid waste incineration fly ash prevent them from being used directly in arable lands (Kalmykova and Fedje, 2013). In addition, due to the improper public perception that MAP is a waste product, people tend to avoid using it as fertilizer for their crops (Lanning, 2008).

2.5 PHOSPHORUS REMOVAL AND RECOVERY BY ADSORPTION AND CRYSTALLIZATION USING AGRICULTURAL WASTE/BY-PRODUCTS (AWBs) BASED ADSORBENTS

2.5.1 Justification of using AWBs based adsorbents for phosphorus removal

AWBs have several properties that make them attractive as the substrate for developing phosphorus adsorbents. To begin, AWBs are abundant, low-priced, and non-toxic. In addition, AWBs usually have chemical stability and high reactivity. Particularly, AWBs have appropriate chemical composition (cellulose, hemicelluloses) with a large number of active hydroxyl groups. Consequently, AWBs can easily be involved in chemical reactions for the preparation of functional groups of adsorbents, for example metal loading, polymerization, graft reaction (Xu et al., 2010b). It provides a foundation for AWBs to be converted into some functional polymers (Benyoucef and Amrani, 2011a). Specifically, the -OH groups can combine with alkoxyamine ligands, and hence enhancing their anion exchange abilities (Karthikeyan et al., 2002).

The use of AWBs as phosphorus adsorbents is novel and is drawing increasing attention (Gibbons, 2009). This practice may result in many benefits. Firstly, it can protect surface water from eutrophication. Secondly, there are huge amounts of AWBs produced worldwide annually, posing a challenge to solid waste disposal. Thus, the

recycling of AWBs as phosphate adsorbents not only provides a viable solution to reduce waste materials in a cheap and eco-friendly way but also adds value to AWBs (Anirudhan et al., 2006; Eljamal et al., 2013; Ismail, 2012; Tshabalala et al., 2004). It also fits well with the principle 'use of renewable resources' of Green Chemistry (Srivastava and Goyal, 2010). In addition, the production of anion exchange resins from abundant, cheap and renewable AWBs may help reduce the cost of phosphorus treatment (Liu et al., 2013). Moreover, by converting phosphorus in wastewater into fertilizers, this practice can generate revenues (Huang et al., 2010; Peng et al., 2012). Also, the successful exploitation of phosphorus from wastewater will diminish the use of mineral phosphorus, and hence will save the global phosphorus rock resource. Clearly, the use of AWBs based adsorbents for phosphorus decontamination may provide a sustainable, efficient and profitable solution for phosphorus pollution management.

2.5.2 Modification of AWBs for efficient phosphorus removal

A. Significance

There is a growing trend in using AWBs as substrates for the development of phosphate adsorbents. Nevertheless, little work has been done on the ability of natural AWBs to adsorb phosphorus. Whereas some natural AWBs can hardly remove phosphorus from aqueous solutions, others exhibit very low sorption abilities as compared to commercial adsorbents. The lack of efficiency in the phosphate removal of original AWBs can be explained by the abundant availability of negatively charged functional groups (for example −OH, −COOH) as well as the absence of positively charged functional groups (for example $–NH_2$) on the surface of raw AWBs (Mallampati and Valiyaveettil, 2013). For these reasons, AWBs need to be modified to improve their phosphate sorption abilities. According to Biswas (2008), the feasibility of a phosphorus adsorption process is controlled by the preparation of adsorbents. Besides, modification of AWBs was found to increase the strength of lignocelluloses materials, and hence mitigating the release of organic matter into aqueous solutions (Anirudhan et al., 2006).

Methods of modifying AWBs for better phosphate removal can be grouped into (i) cationization (for example metal loading, grafting with ammonium type chemicals), (ii) anionization (for example surface coating with sulfate), (iii) activation (for example thermal, chemical and steam activation) (Fig. 2.9). This section aims to gain insight into

each method of modification, with respect to the principle, procedure, influential factors, application, and limitations of each method. Although this literature review referred to all existing methods of modification, it mainly focused on the two most common methods, namely metal loading and quaternization. It is expected that this study will enrich the fundamental theory and promote the practical application of modified AWBs based adsorbents in the future.

B. Metal loading method

(i) Background

It was reported that metal (for example Fe, Al, Mn) oxides in some low-cost materials played important roles in their phosphate removal abilities (Liu et al., 2013; Penn et al., 2007). It suggests a solution to improve the phosphate uptake of AWBs based adsorbents, which is the saturation of AWBs with metal salts. It is desirable that the metal treated AWBs with highly positive charges can effectively sequester phosphate anions (Cheng et al., 2013). Likewise, since Zr^{4+} exhibited an excellent affinity for PO_4^{3-} ions, Zr^{4+} loaded polymers could be a good choice for phosphate decontamination (Ruixia et al., 2002).

(ii) Procedure

The cationization of AWBs is indented to improve their PO_4^{3-} retention via electrostatic interaction. The process is implemented by reacting AWBs with metal salts. Due to the abundance of negatively charged functional groups (for example −OH, −COOH) on their surfaces, AWBs can naturally adsorb metals. Nevertheless, to further boost their metal sequestering ability, it is necessary to graft AWBs with carboxyl (−COOH) groups or modify AWBs with bases before metal loading (Eberhardt and Min, 2008). The metal loading procedure is proposed as follows.

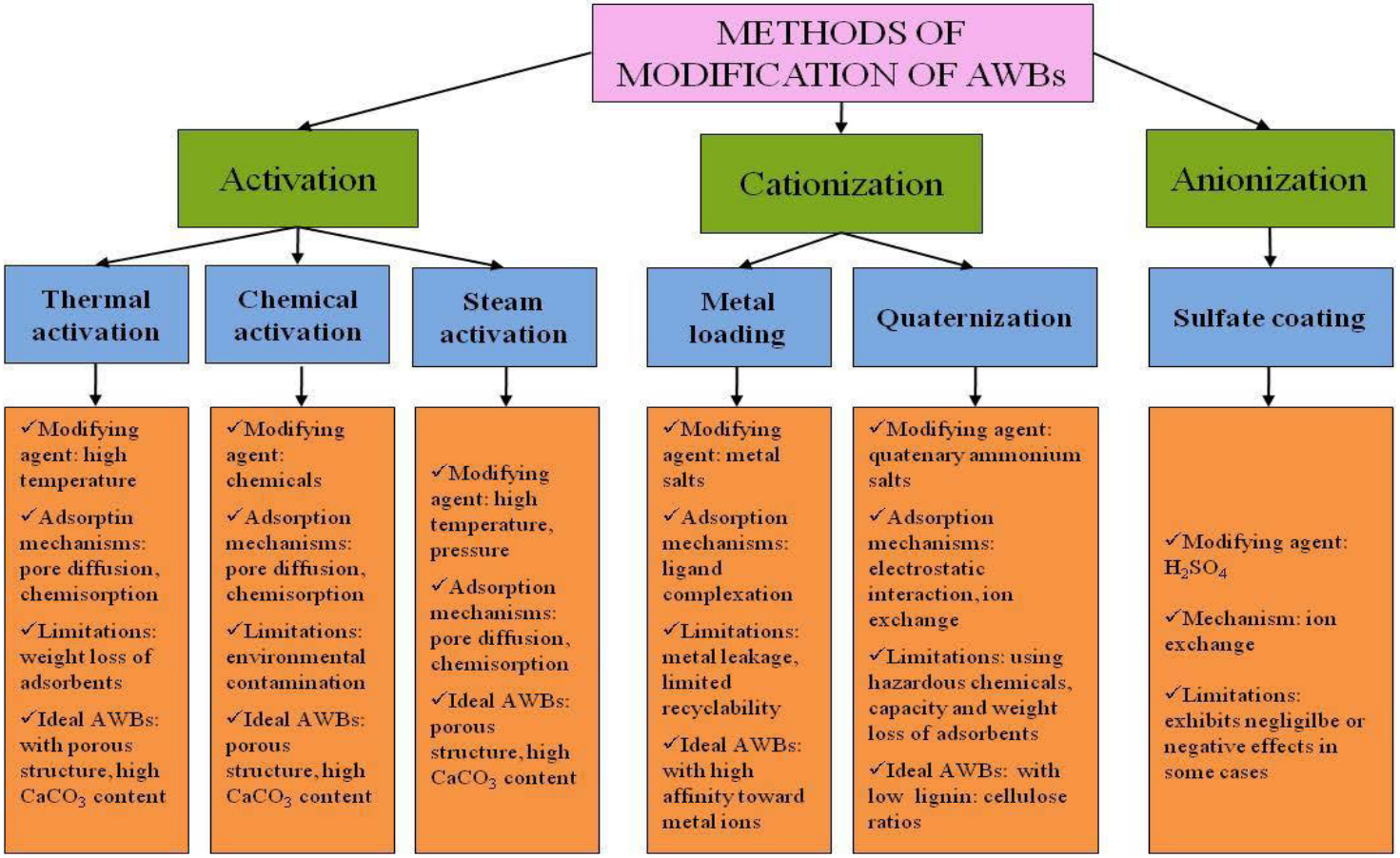

Figure 2.9 Methods of modifying AWBs for better P removal

❖ Grafting carboxyl groups onto AWBs

The carboxylic (−COOH) group is considered the most important functional group for metal sorption by AWBs (Min et al., 2004). Therefore, one of the well-known methods to improve metal sorption ability is through incorporation of carboxylic (−COOH) groups into AWBs. Nada and Hassan (2006) introduced three ways to incorporate carboxylic (−COOH) groups into sugarcane bagasse to prepare cationic exchange resins. That is etherification using mono chloroacetic acid (Eq. 2.5), esterification using succinic anhydride, and oxidation using sodium chlorite. They discovered that carboxymethylated bagasse displayed the highest cationic exchange ability and thermal stability over that of succinylated and oxidized bagasse.

$$Poly–OH + Cl–CH_2–COOH \rightarrow Poly–O–CH_2–COOH \quad (2.5)$$

Carvalho et al. (2011) confirmed the efficacy of the etherification method by reporting that the maximum Fe^{2+} adsorption capacity of sugarcane bagasse fibers rose from 16.0 to 75.4 mg/g (371.25%) after the reaction with mono chloroacetic acid. As a consequence, the phosphate removal percentage of carboxymethylated sugarcane bagasse fibers rose 3% when compared to the raw material. Similarly, Eberhardt and Min (2008) revealed that, the pre-treatment with carboxymethyl cellulose (CMC) augmented the phosphate uptake capacity of Fe^{2+} impregnated wood particles from 2.05 to 17.38 mg/g (748%). They attributed the higher phosphate uptake capacity to additional binding sites to complex iron ions, which were formed by chemical reaction of wood particles with anionic polymer. Evidently, the integration of carboxylic (−COOH) groups into AWBs prior to their reactions with metal salts significantly increases their metal adsorption capacities.

❖ Base treatment (saponification)

Another method to enhance the metal sorption ability of AWBs is through base treatment. Min et al. (2004) examined the efficacy of base treatment on the Cd^{2+} sorption by juniper fiber. It was found that base treatment enhanced the maximum Cd^{2+} adsorption capacity almost 3.2 times (from 9.18 to 29.54 mg/g). They explained that (−OH) ions derived from NaOH changed ester in the wood fiber to carboxylate, which played a significant role in binding Cd^{2+} to AWBs.

$$R–COO–R' + H_2O \rightarrow R–COO^- + R'–OH \quad (2.6)$$

Equally, the base treatment (saponification) was used prior to metal loading in many studies conducted by Biswas (2008), Han et al. (2005), Mallampati and Valiyaveettil (2013). Han et al. (2005) claimed that treatment of juniper mats with 0.5

M NaOH improved their cationic exchange capacity, and hence enhanced the binding ability of Fe irons. As a result, the capture of PO_4^{3-} ions onto Juniper mats was strengthened. Mallampati and Valiyaveettil (2013) saponified apple peels with NaOH before impregnation with Zr^{4+} salt. They assumed that the base treatment broke up ester bonds and produced more (–OH) groups, which were responsible for metal binding onto AWBs.

❖ Deposition of metal ions onto AWBs

It is well-recognized that metals can attach to AWBs via cationic binding sites on the surface of AWBs, for example hydroxyl (−OH) groups, carboxylic (−COOH) groups (Han et al., 2005; Min et al., 2004). Besides, Shin et al. (2005) claimed that ion exchange mechanism might be responsible for the La^{3+} attachment to juniper bark fiber. This assumption is supported by Powder X-ray diffraction (XRD) patterns, indicating that after La^{3+} treatment, the height of the Ca peak declined as compared to the reference peak. In contrast, Ca^{2+} concentration in the solution increased. Based on obtained data, they concluded that La^{3+} was retained by replacing some of Ca^{2+} in the bark as follows:

$$La^{3+} + H_2O \leftrightarrow LaOH^{2+} + H^+ \quad (2.7)$$

$$LaOH^{2+} + H_2O \leftrightarrow La(OH)_2^+ + H^+ \quad (2.8)$$

$$Bark - C_2O_4^{2-}Ca^{2+} + 2\ La(OH)_2^+ \rightarrow bark - C_2O_4^{2-}[La(OH)_2^+]_2 + Ca^{2+} \quad (2.9)$$

(iii) Influential factors

The efficacy of AWBs metal loading is found to rely on the type and concentration of loading metals, as well as the method of metal loading. Wang et al. (2012) reported that the maximum phosphate adsorption capacity of AC/N-Fe(II) (14.12 mg/g) was greater than AC/N-Fe(III) (8.73 mg/g). The authors ascribed this to the higher intraparticle diffusion and binding energy of AC/N-Fe(II) in comparison with AC/N-Fe(III). Shin et al. (2005) revealed that the increase in $La(NO_3)_3.6H_2O$ concentration from 0.01 to 0.1 M led to a rise in phosphate capture ability of La^{3+} loaded juniper bark fiber, from 20.05 to 33.35 mg/g. Etherification was found to be more efficient than oxidation and esterification in deposition of four heavy metals, such as Cu, Fe, Ni, Cr onto carboxymethylated bagasse (Nada and Hassan, 2006).

(iv) Application and limitations

Table 2.14 summarizes 12 studies on metal loaded AWBs based phosphate adsorbents, which have been conducted in the period from 2002 to 2013. Whereas

100% research focuses on the adsorption capacity of adsorbents, the research on desorption and recovery represents 55% and 0%, respectively. The dynamic adsorption studies represent 33.33%. Some metal loaded AWBs based adsorbents had very high adsorption and desorption efficiency with potential reusability, such as Zr^{4+} loaded orange waste gel (Biswas, 2008), Fe^{2+} treated sugarcane bagasse (Carvalho et al., 2011), Zr^{4+} loaded apple peels (Mallampati and Valiyaveettil, 2013). Unfortunately, these potential bio-adsorbents have not been applied, in combination with precipitation/ crystallization for phosphorus recovery. Biswas (2008) claimed that the phosphate could be efficiently extracted from incinerated sewage sludge ash (ISSA) using 0.05 M H_2SO_4 or 0.1 M HCl. Because of the high selectivity of Zr^{4+} loaded orange waste gel, the extracted phosphorus was separated from other contaminants, such as Ca, Fe, and Al. The adsorbed phosphorus could be quantitatively eluted using NaOH 0.2 M. That paved the way for the recovery of phosphorus from ISSA. Köse and Kivanç (2011) proposed a procedure, whereby the eluted phosphorus from calcined waste eggshell was recovered as calcium phosphate. Desorption and recovery efficiencies of phosphate were found to be 37.6% and 37.72%, respectively. It seems clear that, metal loaded AWBs may hold promise for phosphorus recovery from wastewater. However, their application for this purpose is still in the initial stage of development, and thus being an un-established process. To promote practical application of metal loaded AWBs as phosphate adsorbents, comparisons between metal loaded AWBs and commercially available adsorbents in term of the price are necessary. However, this kind of information is particularly rare in the literature. Biswas et al. (2007) predicted that the metal loaded orange waste gel would be cheaper than commercial adsorbents provided that the water treatment plant was adjacent to a juicing factory. The lack of information on the cost - benefit analysis of the process can be considered as a significant research gap, which needs to be filled in future research.

While metal loaded AWBs have been demonstrated to be potential phosphate adsorbents, the metal leakage is a major limitation, hindering their actual application. The significant detachment of loaded metals during their performance is undesirable (Shin et al., 2005). The amount of metal retained on AWBs determines the phosphate adsorption capacity of AWBs. Thus, the high metal leakage may lead to the loss of phosphate adsorption capacity after several cycles of operation (Eberhardt and Min, 2008). Besides, the quality of aqueous solutions treated with metal loaded adsorbents can deteriorate, owing to excessive levels of metals. Another detrimental effect is an

increase in the cost of water treatment. The reason is that the spent adsorbents need to be repeatedly treated with metal salts to ensure the stable sorption capacity (Shin et al., 2005).

The common metal solutions used for cationization of AWBs consist of Zn^{2+}, Fe^{2+}, Fe^{3+}, La^{3+}, Ce^{3+}, and Zr^{4+}. Among these elements, La and Fe were found to be detached vigorously during their performance. Shin et al. (2005) reported that 85% loaded La was leaked at pH 2.5 in the case of removing phosphate by La treated juniper bark. To avoid problems associated with La detachment, the authors suggested using the biosorbent at neutral pH. Similarly, Biswas et al. (2007) discovered the La detachment during desorption test with HCl 0.4 M, when La loaded orange waste gel was employed as a phosphate adsorbent. These findings agree well with a previous study implemented with La loaded activated carbon fiber (Zhang et al., 2011). In the same way, both Han et al. (2005) and Nguyen et al. (2013) revealed that Fe^{3+} ions were vigorously detached from acid mine drainage treated juniper bark and iron-loaded okara during their performance. On the contrary, the Zr leakage was found to be trivial in the studies conducted by Biswas (2008), Mallampati and Valiyaveettil (2013), Ohura et al. (2011). High affinity and selectivity for the phosphate, combined with the stable chemical property make Zr attractive among various loading metals. However, high cost is a major factor limiting the widespread application of Zr for cationization of AWBs. Since each of the existing loading metals has its own merits and demerits, the search for sustainable, cost-effective loading metals is going on.

Table 2.14 P adsorption performances of various metal loaded AWBs based adsorbents

No	Adsorbent	Modifying agent	Mechanism	Side effect	Phosphate uptake capacity (mg/g)	Desorption efficiency (%)	Type of reactor	Reference
1	Orange waste gel	$Ca(OH)_2$ + 0.01 M La(III)-/ Ce(III)-/ Fe(III)-solutions	Ligand exchange reaction	La(III) was eluted during desorption test	42.72 for all 3 types of gels	0.4 M HCl (85%)	BSR + PBR (with La(III)-loaded SOW gel only)	Biswas et al., 2007
2	Orange waste gel	$Ca(OH)_2$ + 0.1 M $ZrO_2Cl.8H_2O$	Polynuclearcomplexation	No significant leakage of Zr(IV)	175 (322 at opt pH)	BSR 0.2 M NaOH (95%) PBR HCl (<40%) NaCl (0%)	BSR + PBR	Biswas, 2008
3	Bagasse fibers	Monochloroacetic acid + $FeCl_2$ 0.9%, 1.8%, 3.6%, and 5.3%			152	-	-	Carvalho et al., 2011
4	Wood particles	Carboxymethyl cellulose (CMC) 4% + $FeCl_2$ 12%	Complexation	Fe release during sorption increased with decreasing particle sizes – No detailed data	17.38		BSR	Eberhardt and Min, 2008
5	Juniper fiber	Acid mine drainage (AMD)		Iron release was found	7.08	-	BSR + PBR (synthetic WW) + Field (real WW)	Han et al., 2005
6	Coir pith	$Fe(NO_3)_3.9H_2O$	Ligand exchange reaction	No information on Fe(III) leakage during performance	70.92 (BSR) 68 (PBR)	-	BSR + PBR (sewage)	Krishnan and Haridas, 2008
7	Apple peels	NaOH + 0.1 M $ZrO_2Cl.8H_2O$	Electrostatic interaction	No release of Zr(IV) during adsorption	20.35	Distilled water pH 12 (>70%)	BSR	Mallampati and Valiyaveettil, 2013
8	Eggshell	$FeCl_3.2H_2O$	Diffusion is not	No information	14.49	-	BSR	Mezenner and

		5 mg/L	only rate – controlling step	on Fe(III) leakage				Bensmaili, 2009
9	Coir pith AC	$ZnCl_2$	Chemisorption + ion exchange		5.1	Distilled water pH 2 (30%) pH 11 (50%) pH 3-11 (<10%)	-	Namasivayam and Sangeetha, 2004
10	Okara	NaOH + 0.25 M $FeCl_3$	-	Vigorous leakage of Fe during adsorption and desorption tests	14.66	Distilled water pH 2,4,6,8,10 (<20%) Distilled water pH 12, 0.25 M NaOH, 0.1 M HCl (>94%)	BSR	Nguyen et al., 2013
11	Juniper fiber	0.1 and 0.01 M $La(NO_3)_3.6H_2O$	Ion exchange + complexation + precipitation	Significant desorption of La(III) occurred under acidic condition (pH<4.5)	20.045 (La/JB01) 33.35 (La/JB02)	-	BSR	Shin et al., 2005
12	Sawdust	N,N'-methylenebisacrylamide Acrylamide oxydisulfate Ethylenediamine $FeCl_3.6H_2O$	Ligand exchange	q_{max} reduced 8.9% after 3 cycles Weight loss 3% after NaOH treatment	28.79	NaOH 0.1 M (96.8%)	BSR(synthetic and real wastewaters)	Unnithan et al., 2002

Notation: BSR - batch stirred reactor; PBR -packed bed reactor.

C. Quaternization method

(i) Synthetic reactions and quaternized products

Quaternization of AWBs is intended to produce anion exchange resins for phosphorus removal. It can be implemented by treatment of AWBs with various quaternary ammonium compounds.

Quaternary ammonium compounds provide amino groups for grafting into the structure of AWBs (Wang et al., 2010). Various quaternary ammonium compounds can be utilized, such as poly-allylamine hydrochloride (PAA •HCl) (Karthikeyan et al., 2004, 2002; Tshabalala et al., 2004), 3 chloro -2- hydroxypropyl trimethyl ammonium chloride (De Lima et al., 2012; Karthikeyan et al., 2002), trimethylammonium chloride (Marshall and Wartelle, 2004; Wartelle and Marshall, 2006), dimethylamine (Anirudhan et al., 2006; Zhang et al., 2012), triethylamine (Xu et al., 2011a, 2011c, 2010b), urea (Benyoucef and Amrani, 2011b; Karachalios, 2012).

Due to the poor interactivity between cellulose and quaternary ammonium compounds, cross-linking agents were used to convert cellulose into more active cellulose ether. The epoxy cellulose ether then was grafted with different amines (Karachalios, 2012; Marshall and Wartelle, 2004).This procedure has been employed in a majority of studies on quaternization by Anirudhan et al. (2006); Wang et al. (2010); Xu et al. (2011b, 2011c, 2010b, 2009). In addition, a cross-linking step has been found to prevent the loss of carboxylated components from lignocellulosic materials (Nada and Hassan, 2006). The most commonly used cross-linking reagent is epichlorohydrin. However, in some cases, choline chloride derivative (Karachalios, 2012), N-(3-chloro-2-hydroxypropyl) (Marshall and Wartelle, 2004; Wartelle and Marshall, 2006), ethylenediamine (Xu et al., 2011a, 2011c) can be used alternatively.

Because epichlorohydrin and quaternary ammonium compounds do not dissolve each other, some organic solvents are employed, such as N, N-Dimethylformamide (DMF) (Anirudhan et al., 2006; Xu et al., 2011a, 2011c, 2010b; Zhang et al., 2012) and methanol (Xu et al., 2010a).

Occasionally, pyridine (Anirudhan et al., 2006; Xu et al., 2010a; Zhang et al., 2012), and imidazole (Karachalios, 2012) are used as catalysts to open the ring of the epoxide group in the base medium (Xu et al., 2010a).

Another method to make the reaction between cellulose and quaternary ammonium compounds occur is to synthesize an aminated intermediate first, which can

efficiently react with cellulose later. Xu et al. (2010a) utilized this two-step process to synthesize quaternized wheat straw. In the first step, epichlorohydrin was reacted with triethylamine in methanol to yield the aminated intermediate. In the second step, wheat straw was reacted with the intermediate in the presence of pyridine to produce aminated wheat straw. Equally, in an earlier study, Tshabalala et al. (2004) proposed a reaction pathway for synthesis of pine bark anion exchanger. This procedure included two steps: Initially, poly-allylamine hydrochloride (PAA•HCl) was reacted with epichlorohydrin (EPI) to form epoxy - PAA•HCl as the aminated intermediate. Next, quaternized pine bark was developed by reacting the epoxy - PAA•HCl with bark polyphenol. As a result, a network of fixed cationic sites of quaternary ammonium, with mobile chloride ions as anion exchangers, was formed on the bark surface. In the same way, the quaternization of coconut shell fibers was achieved by epoxide formation, followed by reaction between the epoxide and lignin cellulose materials (De Lima et al., 2012).

Karachalios (2012) claimed that the major problem with the quaternization process was the use of toxic solvents or reagents. For that reason, the author proposed to utilize a mixture of choline chloride derivative and urea, in the presence of imidazole for quaternization of wood residues. The advantage of this procedure was the use of non-hazardous reagents and bi-functional compounds that played the role of both reagent and solvent.

It can be noted that, among various quaternary ammonium compounds used for amination reactions, urea appears to be the best. The reason for this is, remarkably high adsorption capacities were attained with all sorbents modified with urea, for example sawdust (116.25 mg/g) and wood residues (205.63 mg/g) (Benyoucef and Amrani, 2011b; Karachalios, 2012). Particularly, when the same substrate was used to prepare cationized adsorbents, urea modified sorbent showed a phosphate adsorption capacity (205.63 mg/g) far superior to that of PAA•HCl modified sorbent (25.65 mg/g) (Karachalios, 2012; Karthikeyan et al., 2004). Apparently, urea was much better than PAA•HCl in promoting the phosphate removal capacity of quaternized AWBs. Another promising ammonium quaternary salt was 2-hidroxypropyltrimethyl ammonium chloride, which resulted in exceptionally high adsorption capacity of coconut shell fibers (200 mg/g) (De Lima et al., 2012). The results verify the potential of quaternization in enhancing the phosphate sorption capacity of AWBs.

(ii) Influential factors

The quaternization of AWBs is influenced by the nature and dosage of raw biomaterials, as well as the volume of modifying agents. Wartelle and Marshall (2006) developed anion exchange resins from 12 types of AWBs. Comparing their phosphate adsorptive properties, they discovered that the lignin content of AWBs determined the efficacy of quaternization. Specifically, AWBs with lower lignin: cellulose ratio could react more efficiently with N-(3-chloro-2-hydroxypropyl) trimethylammonium chloride (CHMAC) and yield better anion exchange resins. Xu et al. (2010a) found that, reaction temperature, reaction time and dosage of epoxy propyl-triethyl-ammonium-chloride intermediate were influential factors to the quaternization of wheat straw. The results showed that the maximum phosphate removal was achieved at the following conditions: reaction temperature: reaction time: intermediate dosage = 55 °C: 3 h: 35 ml. Wang et al. (2010) examined the effect of sorbent dosage, temperature and volume of modifying agents on the phosphate removal of modified giant reed. The results of single-factor experiments indicated that the optimum conditions for quaternization of giant reed were Giant reed: epichlorohydrin: DMF (N,N-dimethylformamide): EDA (ethylenediamine triethylamine) = 4 g: 10 ml: 5 ml: 2 ml: 10ml at 60-70 °C. Based on the results of orthogonal experiments, they concluded that, the dosage of EDA was a critical factor, influencing the preparation of quaternized giant reed.

(iii) Applications and limitations

The summary in Table 2.15 deals with 14 original research papers on removal of phosphate using quaternized AWBs based adsorbents. While the majority of studies deal with the removal capacity of adsorbents, the studies on desorption and recovery account for 57.14% and 0%, respectively. The column mode studies represent 21.43%, although they are important in reference to the real application. A large portion of studies has been performed at the lab-scale. It is evident that the application of quaternized AWBs is still limited. It can be partially explained by the reasons mentioned below.

The recyclability of the quaternized adsorbents plays a significant role in their practical application (Xu et al., 2011b). Hence, the capacity and weight loss of adsorbents during adsorption and desorption tests are undesirable. Unfortunately, these effects were occasionally found to be significant. Anirudhan et al. (2006) conducted a stability analysis of modified banana stem for four cycles. They discovered a capacity

loss of around 12%. Karachalios (2012) revealed a decline of 5.92% in the ability of quaternized wood residues, after five consecutive operation cycles. Notably, De Lima et al. (2012) observed a complete loss of adsorption capacity of modified coconut shell fibers when the modified adsorbent was treated with HCl. The authors attributed this to the physical ruin of the adsorbent by HCl. A weight loss of 12-18% of the quaternized wheat straw was reported by Xu et al. (2011c) after using 1M HCl as an elution solution. They attributed this to the damage of cellulose/hemi-cellulose structure, which resulted from the corrosion of HCl. Conversely, Anirudhan et al. (2006), Karachalios (2012) found minor or negligible loss of capacity and weight. It indicates the significance of selecting the appropriate substrates and elution solutions to enhance the recyclability of quaternized AWBs.

It should be kept in mind that the removal of phosphate using AWBs based adsorbents has an advantage of being environmentally friendly. Therefore, the use of hazardous solvents and quaternizing agents was considered as a major drawback of the process (Abdul and Aberuagba, 2005; Karachalios, 2012). Xu et al. (2010b) claimed that the formation of large amounts of odoriferous wastewater prevented the wide application of pyridine as a catalyst in the synthesis of quaternized AWBs adsorbents. In the same way, the utilization of neutral salts with high concentrations for desorption of phosphorus may increase the salinity in arable lands, once phosphorus desorbed by this way was recovered and applied as fertilizers (Loganathan et al., 2014).

Cost is an important indicator for the comparison of adsorbents (Saka et al., 2012). However, this kind of information could be hardly detected in the literature. According to Wartelle and Marshall (2006), the synthesis cost of quaternized corn stover was from 44 to 59 times lower than that of Whatman QA 52, a commercially available adsorbent, depending on whether the quaternizing agent was recycled or not. Therefore, further work should focus on this field of study.

D. Other modification methods

The other modification methods, such as thermal activation, steam activation, chemical activation and sulfate surface coating, are introduced in Table 2.16.

(i) Thermal activation

Thermal activation is a process of carbonization or calcinations of organic matters using high temperature. Huang et al. (2010) used high temperatures to activate oyster shells for better phosphate removal. They discovered that thermal activation

substantially improved the phosphate capture of oyster shells. Natural oyster shell could not remove any phosphorus from 80 mL wastewater with the phosphorus level of 20 mg/L. Nevertheless, the removal percentage of 100% was achieved after 3-4 days by oyster shells activated at 500 °C. The authors explained the inefficient phosphorus removal of oyster shell in natural form by the attachment of the nacreous layer and the organic mucous membrane to microscopes, which prevented phosphate from being adsorbed onto the porous structure. Although the thermal activation boosted the phosphorus removal of oyster shells, the weight loss of oyster shells was reported as a side effect. The authors ascribed the weight loss of 1.57% at the temperature 700 °C to the volatility of water and combustion of organic matter. However, they suggested that the decomposition of $CaCO_3$ would be responsible for the weight loss of 42.37% in the temperature range of 700-900 °C. This effect is undesirable since a higher amount of raw oyster shells and more energy are required to produce a certain amount of activated oyster shells. The similar decomposition of $CaCO_3$ into CaO and increasing surface area were noticed, when waste eggshells were calcinated at 800 °C (Köse and Kivanç, 2011). This is the unique research in the literature, which referred to the recovery of phosphorus by means of adsorption onto AWBs (Table 2.16). Desorption efficiency of 37.6% was achieved with 0.5 M NaOH solution. CaO was used to precipitate the eluted phosphorus as $Ca_3(PO_4)_2$ with the recovery efficacy of 37.72%. It seems to be that high desorption percentage does not guarantee the success of phosphorus recovery, but the poor desorption ability is likely to reduce the potential recovery of phosphorus. Another study on thermal activation was conducted by Peng et al. (2012), in which fast pyrolysis was applied to produce biomass char from pine sawdust. It was shown that the pyrolysis temperature and holding time were primary factors, affecting the phosphate adsorption capacity of biomass char. The phosphate adsorption capacity of biomass char (15.11 mg/g) was attributed to high carbon content, and porous structure, which resulted from pyrolysis (Table 2.16).

(ii) Steam activation

Steam activation is a selective oxidation process of carbonaceous compounds with the presence of air at low temperature/steam, and CO_2/blue gas at high temperature. Namasivayam et al. (2005) employed high-pressure steam (234 °C and 3.0 MPa) to activate oyster shells. It was revealed that natural oyster shells did not adsorb phosphate. In contrast, 24 g of activated oyster shells could lower the phosphate concentration in 1 L of synthetic wastewater from 50 to 7 mg/l in 7.7 days. The authors assumed that

phosphate was adsorbed onto activated oyster shells as amorphous calcium phosphate, which later was converted into thermodynamically more stable hydroxyapatite. However, Ca^{2+} was detected in the aqueous solutions during adsorption performance of activated oyster shells. Similarly, Abdul and Aberuagba (2005) utilized a steam oxidation process (450 °C, 10 bars) to prepare activated charcoals from three kinds of AWBs. The sorption capacities for different pollutants of activated charcoals were attributed to the developed pore structure and large internal surface area. Among various types of charcoals, corncob proved to be the best. It was ascribed to the contribution of other mechanisms in addition to pore diffusion in the phosphate removal of corncob. They concluded that, not only a method of activation but also the raw materials can affect the adsorption features of activated AWBs.

(iii) Chemical activation

Chemical activation is a process of carbonization or calcination, in which inorganic chemicals are employed to degrade and dehydrate the organic compounds. According to Abdul and Aberuagb (2005), the overuse of chemicals in the chemical activation may cause environmental contamination or equipment erosion, and thus preventing this method from extensive application. Kumar et al. (2010) used carbon, prepared from coir pith at 600 °C and activated by H_2SO_4, for phosphate removal from aqueous solutions. It was found that H_2SO_4 treated coir pith activated carbon was a cost-effective phosphate adsorbent. The high phosphate adsorption capacity of coir pith activated carbon (7.74 mg/g) was validated by high BET surface area and pore size, which were reported to be 727.4 m^2/g and 18.79 Å, respectively.

(iv) Sulfate surface coating

Another method to improve the phosphate adsorption capability of AWBs is sulfate surface coating. Choi et al. (2012) prepared phosphate adsorbents by coating sulfate ions onto zeolite, hydrotalcite, and activated alumina surfaces. They found that the surface coating led to a dramatic increase (2272%) in the phosphate adsorption capacity of zeolite. They explained this by ion exchange between PO_4^{3-} in the solution and SO_4^{2-} on the surface of zeolite. Conversely, a minor improvement (1.47%) or negative effect (-14.83%) were reported for activated alumina and hydrotalcite, respectively. The diverse impacts of sulfate surface coating could be responsible for its limited utility in the literature.

Table 2.15 P adsorption performances of different quaternized AWBs based adsorbents

No	Adsorbent	Modifying agent	Mechanism	Side effect	Phosphate uptake capacity (mg/g)	Desorption solution and efficiency (%)	Type of reactor	Reference
1	Banana stem	DMA, DMF, EPI,Pyridin	Ion exchange	Capacity loss of <12% after 4 cycles	72.46 (BSR)	NaOH 0.1 M (98.6%)	BSR	Anirudhan et al., 2006
2	Aleppo pine sawdust	Urea	Chemisorption		116.25 BSR		BSR	Benyoucef and Amrani, 2011b
3	Coconut shell fibers	Ammonium quaternary salt (2-hidroxypropyltrimethyl ammonium chloride)		Less reuse and recyclability	200		BSR	De Lima et al., 2012
4	Wood agricultural residues	Chlorocholine chloride, Imidazole,Urea	Ion exchange	Reduced in q_m after 5 cycles	67.1	0.2 M NaOH (99.8%)	BSR	Karachalios, 2012
5	Cationized pine wood and bark	PAA•HCl	Ion exchange + Lewis acid base interactions		44.65 (bark) 26.03 (wood)		BSR	Karthikeyan et al., 2004
6	Soybean hulls	N-(3-chloro-2-hydroxypropyl) trimethylammonium chloride, NaOH			60.8 (BSR)			Marshall and Watelle, 2004
7	Cationized milled pine bark	EPI, PAA•HCl	-	-	12.65	-	-	Tshabalala et al., 2004
8	Wheat straw	EPI, ETC, TEA Methanol, Pyridine	Ion exchange		45.7 BSR	0.1 M NaCl 0.1 M HCl	PSR + BPR	Xu et al., 2010a

9	Wheat residue	EDA, EPI, DMF, TEA	Ion exchange	Minor loss in q_{max}after 10 cycles	171 BSR 66.3 BPR	HCl 0.1 M NaCl 0.1 M	PSR + BPR	Xu et al., 2010b
10	Giant reed	DMF, EDA, TEA	Ion exchange	Slight weight (1-3%) and adsorption capacity loss	54.67	0.1 M HCl, NaCl, NaOH (100%)	BPR	Xu et al., 2011a
11	Cotton stalk (CS) and wheat stalk (WS)	DEA; EPI; TMA	Electrostatic attraction	Weight loss (5%)	51.54 (AC-CS) 60.61 (AC-WS) for BSR 41.9 (AC-CS) 49.05 (AC-WS) for BPR	0.1 M NaCl, HCl	PSR + BPR	Xu et al., 2011b
12	Wheat straw	DMF, EDA, EPI, TEA	Ion exchange	Weight loss (12-18%)	16.5-52.4 BSR	1 M HCl	PSR	Xu et al., 2011c
13	Giant reed	DMF, EDA, EPI, TEA	Physical adsorption		19.89 BSR		BSR	Yue et al., 2010
14	Sugarcane bagasse	DMA, DMF, EPI, Pyridine	Chemical process		21.3	0.05 M NaOH (95.6%)	BSR	Zhang et al., 2012

Notation:

BSR - batch stirred reactor; PBR -packed bed reactor.

DEA - Diethylenetriamine; DMA - Dimethylamine; DMF - N,N-dimethylformamide.

EDA - Ethylenediamin; EPI - Epichlorohydrin; ETC - Epoxypropyltriethylammonium chloride.

PAA•HCl - Polyallylamine hydrochloride.

TEA - Triethylamine; TMA – Trimethylamine.

Table 2.16 P adsorption performances of diverse AWBs based adsorbents prepared by other modifying methods

Adsorbent	Modifying agent	Mechanism	Side effect	Phosphate uptake capacity (mg/g)	Desorption solution and efficiency (%)	Recovery efficiency	Type of reactor	Reference
THERMAL ACTIVATION								
Activated alumina	Sulfate coating	Anion exchange	-	49.67	-	-	BSR	Choi et al., 2012
Hydrotalcite	Sulfate coating	Anion exchange	-	22.22	-	-	BSR	Choi et al., 2012
Zeolite	Sulfate coating	Anion exchange	-	111.49	-	-	BSR	Choi et al., 2012
Oyster shells	100÷900 ^{o}C	Physical and chemical sorption	Weight loss of 1.57% at 700^{o}C and 42.37% at 700-930 ^{o}C	-	-	-	BSR	Huang et al., 2010
CHEMICAL ACTIVATION								
Calcined waste eggshell*	Calcination, 800 ^{o}C	Electrostatic interaction	Unsuccessful regeneration	23.02	37.6% (0.5M NaOH) 0.7% (0.5 M NaCl)	$Ca_3(PO_4)_2$ (37.72%)	BSR	Köse and Kivanç, 2011
Coir pith	600 ^{o}C 98% H_2SO_4	Physical and chemical sorption	-	7.74	70.1% (HNO_3) 61.4% (Acetone) 19.2% (Water)	-	BSR	Kumar et al., 2010
STEAM ACTIVATION								
Oyster shell	234^{o}C and 3.0 MPa	Chemical sorption	Release of Ca^{2+}	-	-	-	BSR	Namasivayam et al., 2005
ANIONIZATION								
Pine sawdust char	Fast pyrolysis	Pore diffusion	-	15.11	-	-	BSR	Peng et al., 2012

Notation: BSR - batch stirred reactor; PBR - packed bed reactor

* The only AWBs based adsorbent in the literature was employed for phosphate recovery

Table 2.17 Comparison of various modification methods for development of AWBs based P adsorbents

No	Methods	Advantages	Disadvantages
1	Thermal activation	No consumption of chemicals Ideal for AWBs with porous structure, high content of $CaCO_3$	High energy consumption Special equipment requirement Significant weight loss of adsorbents
2	Chemical activation	High efficiency Ideal for AWBs with porous structure, high content of $CaCO_3$	Large consumption of chemicals Environmental contamination Equipment erosion
3	Steam activation	Minimization of chemical use Ideal for AWBs with porous structure, high content of $CaCO_3$	Special equipment is needed
4	Metal loading	Simple operation High efficiency High selectivity toward phosphate anions Ideal for AWBs with high affinity toward loading metals Wide application	High cost of loading metal Limited stability and reusability of biosorbents due to metal detachment during operation Environmental contamination caused by leaked metals Extra operational cost due to metal reloading requirement
5	Quaternization	High efficiency High regeneration of adsorbents Ideal for AWBs with low lignin: cellulose ratios Wide application	Complicated process Secondary pollution by toxic solvents or quaternizing reagents Less selectivity toward PO_4^{3-} anions Weight and capacity loss of adsorbents after several cycles of operation
6	Sulfate coating	Efficacy depends on adsorbents Limited application	Simplicity

2.5.3 Process fundamentals and applications

A. Adsorption mechanisms

Understanding the adsorption mechanisms is necessary for optimizing the adsorption process. Various information (pH profile, desorption, kinetic, activation energy) and techniques (FTIR, XRD, TEM) are required to clarify the adsorption mechanism, due to its complex nature. The mechanisms for adsorption of phosphorus onto AWBs based adsorbents have been reported to include ion exchange, ligand exchange, surface precipitation and diffusion.

(i) Ion exchange

Ion exchange is considered as physical adsorption (electrostatic attraction). It is associated with very fast, weak and reversible adsorption, which occurs through outer-sphere complex. It replaces any ion on the surface of an ion exchanger by a chemically equal number of another ion while preserving the electro neutrality of the ion exchanger (Loganathan et al., 2014). The ion exchange was found to be the dominant adsorption mechanism in many studies on phosphorus removal using AWBs, such as banana stem (Anirudhan et al., 2006); wood residues (Karachalios, 2012); giant reed (Xu et al., 2011a). A typical method to predict the type of adsorption is based on the activation energy (E) magnitude. While E value in the range of 8-16 kJ/mol represents the chemical adsorption, the E value lower than 8 kJ/mol stands for physical adsorption. The E values for the sorption of P onto modified wheat residue, modified sawdust, and calcined waste eggshell were found to be 3.39, 3.08, 8.04 kJ/mol, respectively. It implies that physical adsorption might be the prevailing sorption mechanism in these cases (Benyoucef and Amrani, 2011b; Köse and Kivanç, 2011; Xu et al., 2009). Based on the effect of pH, Anirudhan et al. (2006) concluded that the removal of phosphorus using quaternized banana stem could mainly be attributed to ion exchange between Cl^- of quaternary mine group and HPO_4^{2-}/ $H_2PO_4^-$ in the solution as follows:

$$2BS{-}CH_2{-}N^+H(CH_3)_2Cl^- + HPO_4^{2-} \rightarrow [BS - CH_2 - N^+H(CH_3)_2]_2HPO_4^{2-} + 2Cl^- \quad (2.10)$$

$$BS{-}CH_2{-}N^+H(CH_3)_2Cl^- + H_2PO_4^- \rightarrow BS{-}CH_2{-}N^+H(CH_3)_2\ H_2PO_4^- + Cl^- \quad (2.11)$$

Similarly, Xu et al. (2011a) proposed that the ion exchange could be an important pathway for the remediation of P by modified giant reed. The replacement of chloride ions in the amine groups of quaternized giant reed by phosphate ions in the solution could occur as follows:

$R'-N^+(CH_2CH_3)_{3...}Cl^- + H_2PO_4^- \rightarrow R'-N^+(CH_2CH_3)_3...H_2PO_4^- + Cl^-$ (2.12)

From FTIR results, De Lima et al. (2012) suggested that the modification of coconut shell fibers with ammonium quaternary salt led to the integration of $-NH_2$ groups into the material. Thus, the removal of P using quaternized coconut shell fibers occurred mainly via electrostatic interactions between $-NH_2$ groups and PO_4^{3-} anions.

(ii) Ligand exchange

Ligand exchange is considered as chemical sorption, which is characterized by fast, strong and less reversible adsorption with reduced zero-point charges. It may happen through inner sphere complex, when PO_4^{3-} anions create a covalent chemical bond with a metallic cation on the surface of AWBs. It leads to the liberation of other anions, which were formerly attached to the metallic cation (Loganathan et al., 2014). This mechanism was reported for the case of decontaminating P using natural and iron impregnated coir pith (Krishnan and Haridas, 2008). The authors suggested that in the pH range of 2.0-3.5, the ligand exchange occurred between $H_2PO_4^-$ ions and surface OH^- groups to form inner-sphere complexation as follows:

$CP-OH + H_2PO_4^- \rightarrow CP-(H_2PO_4 + H_2O$ (2.13)

$CP-Fe(OH) + H_2PO_4^- \rightarrow CP-Fe(H_2PO_4) + H_2O$ (2.14)

From the effect of pH, Biswas et al. (2007) concluded that the adsorption of P onto metal loaded orange waste (SOW) gels was possibly due to a ligand exchange mechanism between PO_4^{3-} ions in the solution and OH^- ions coordinated with the metal ions on the orange waste gels (Figs. 2.10 & 2.11). The authors suggested that loaded metal ions could be easily converted into hydrated forms, for example $[Ln(H_2O)_n]^{3+}$, $[Zr_4(OH)_8(H_2O)^{16}]^{8+}$ and $[Zr_8(OH)_{20}(H_2O)_{24}]^{12+}$ species with the abundant amount of OH^- ions and H_2O molecules. The H_2O molecules were deprotonated by releasing H^+ ions to form OH^- ions, which could be replaced by PO_4^{3-} ions via ligand exchange mechanism.

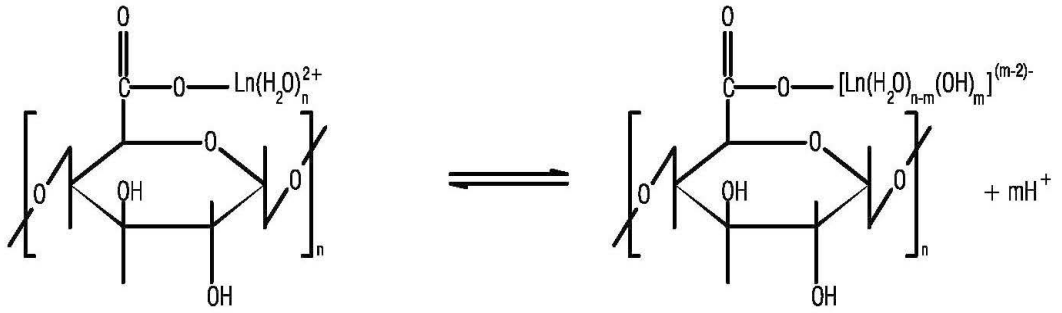

Figure 2.10 Formation of exchangeable hydroxyl ions during hydrolysis, where m =1 or 2; Ln stands for La^{3+}, Ce^{3+}, Fe^{3+} (adapted from Biswas et al., 2007)

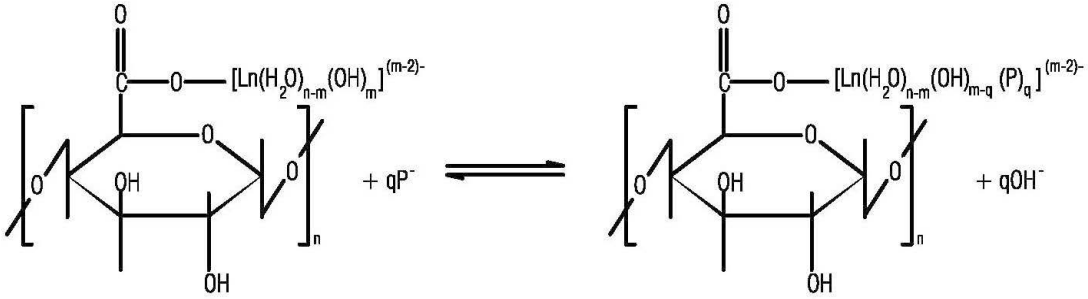

Figure 2.11 Ligand exchange reaction, where q = 1 or 2 and P represents phosphate anion (adapted from Biswas et al., 2007)

(iii) Surface precipitation

When the concentration of components of the precipitate surpasses the solubility product of the precipitate, the precipitation of P with metallic ions may take place on the surface of AWBs. This mechanism is described as fast and hardly reversible adsorption. With the help of XRD and FTIR results, Shin et al. (2005) verified the contribution of surface precipitation to the PO_4^{3-} binding onto La^{3+} loaded bark fiber. Based on kinetic studies, Namasivayam et al. (2005) concluded that the removal of P by oyster shell powder was probably due to the precipitation of P as calcium phosphate.

(iv) Intra-particle diffusion

This process is known as physical sorption, which takes place inside pores and cavities of AWBs. It is characterized by irreversible and very slow adsorption, which may last from several days to months (Loganathan et al., 2014). It is well recognized that if intraparticle diffusion mechanism prevails, a plot between the PO_4^{3-} adsorption capacity and the square root of the contact time should be a straight line passing through the origin. The relationship attained in a study by Karachalios (2012) was non-linear. That clearly indicated that intraparticle diffusion could not play a significant role in the

sorption of PO_4^{3-} onto quaternized wood residues. Based on TEM results, Riahi et al. (2009) suggested that intraparticle diffusion led to the accumulation of PO_4^{3-} into internal cells of date palm fibers.

(v) Co-existing mechanisms

It is quite common that the adsorption process can occur via several co-existing mechanisms. Tshabalala et al. (2004) observed a reduction in PO_4^{3-} uptake with increasing ionic strength and presence of SO_4^{2-}, NO_3^- anions. For that reason, they suggested that ion exchange and Lewis acid-base interactions might be responsible for the retention of PO_4^{3-} ions onto cationized milled wood residues. From P surface loading and spectroscopic analysis results, Shin et al. (2005) claimed that ion exchange and surface precipitation could contribute to the elimination of P by La^{3+} treated juniper bark fiber. Similarly, physical and chemical sorption mechanisms are found to co-exist in the studies conducted by Benyoucef and Amrani (2011b); Mezenner and Bensmaili (2009); Huang et al. (2010). In a more recent study, Karachalios (2012) proposed that the adsorption process of PO_4^{3-} onto quaternized pine bark residues resulted from both boundary layer and intraparticle diffusion mechanisms.

B. Desorption mechanisms

Desorption plays an important role in the reusability of the adsorbent and recovery of phosphorus. It was found that the loaded phosphorus can be desorbed by distilled water, salts, acids, and bases (Table 2.18).

In an attempt to reduce the cost of desorption chemicals and mitigate adverse impacts on the environment, some researchers have used distilled water as a desorption solution. Namasivayam and Sangeetha (2004) investigated the potential of eluting phosphorus from $ZnCl_2$ activated coir pith carbon by distilled water. The authors found that desorption was favored at pH 2 (30%) and pH 11 (50%) while it was suppressed in the pH range of 3-11 (<10%). The high desorption ability at pH values 2 and 11 could be explained by the dissociation constants of phosphate and the dominant phosphate species at different pH values. At pH 2, unionized H_3PO_4 species are dominant. These phosphate species have poor affinity for the sorbent, and thus provide favorable conditions for phosphorus desorption. At pH 11, more OH^- ions are available in the solution, leading to a stronger competition with HPO_4^{2-} and PO_4^{3-} for binding sites. Consequently, desorption was efficient at pH 11. Nevertheless, the maximum desorption efficiency was the relatively low (50%). The author explained that though

PO_4^{3-} ions were retained via both ion exchange and chemisorptions mechanisms, only PO_4^{3-} ions captured by the ion exchange mechanism could be desorbed. On the other hand, Mallampati and Valiyaveettil (2013) observed a relatively high desorption capacity (90%) in a very short time (10 min.), when distilled water with pH 12 was employed in the case of desorbing phosphorus from Zr^{4+} loaded apple peels. The successful desorption at high pH value was explained by the replacement of PO_4^{3-} on apple peel surface by OH^- anions in the solution.

Another means for phosphorus desorption is using neutral salts, for example NaCl, KCl. In some studies, the use of these salts at different concentrations resulted in exceptionally high desorption efficiencies, such as 99.8% for 0.2 M NaCl from quaternized wood residues (Karachalios, 2012); 95,4% for 0.1 M NaCl from wheat straw anion exchanger (WS-AE) (Xu et al., 2010b); 100% for 0.1 M NaCl from modified giant reed (Xu et al., 2011a). Conversely, very poor desorption capacities could be detected in other studies, for example 0.7% for 0.5 M NaCl from calcined waste eggshell (Köse and Kivanç, 2011); 11.2% and 13% for 0.01 M for KCl from granular date stones and palm surface fibers, respectively (Ismail, 2012). Loganathan et al. (2014) suggested that neutral salts would work well as desorption solutions just in the case of weak and reversible sorption, whereby ion exchange was an important pathway for the phosphorus removal (Karachalios, 2012; Xu et al., 2010a). In contrast, for strong and less reversible sorption, which was controlled by ligand exchange, surface precipitation or chemisorptions mechanisms, the efficacy of these salts was usually limited (Ismail, 2012; Köse and Kivanç, 2011). The higher concentrations of neutral salts seem to favor desorption. A rise in the concentration of NaCl from 0.001 to 0.1 M increased the phosphorus desorption efficiency of modified giant reed by 48.7% (Xu et al., 2011a). However, the use of neutral salts at high concentrations for desorption will increase the salinity of arable lands once the desorbed phosphorus was recovered and applied as fertilizers (Loganathan et al., 2014). The advantage of eluting phosphorus using neutral salts is the minor loss of the uptake capacity and mass of the adsorbent after several cycles of operation. Karachalios (2012) reported that the adsorption capacity was decreased by only 5.59% after five cycles of adsorption-desorption using 0.2 M NaCl. Likewise, Xu et al. (2010b) revealed that using 0.1 M NaCl as a desorption solution led to the reduction of 9.58% in the phosphorus uptake capacity of the adsorbent. The slight weight loss (1-3%) was reported when 0.1 M NaCl

was used for eluting phosphorus from modified giant reed (Xu et al., 2011a). The stability of the adsorption capacity and mass of the adsorbents enable their reusability.

To further improve the desorption efficiency of phosphorus, acids or bases are often used to substitute for distilled water and neutral salts. Among various acids and bases used for this purpose, NaOH and HCl are most commonly used. They usually demonstrated extremely high desorption efficiencies. For example, the desorption efficiency was reported to be 97.1% for 0.1 M NaOH (Anirudhan et al., 2006); 85% for 0.4 M HCl and 95% for 0.2 M NaOH (Biswas, 2008); 97.5% for 0.1 M HCl (Xu et al., 2010a); 100% for 0.1 M NaOH and HCl (Xu et al., 2011a); 95.6% for 0.05 M NaOH (Zhang et al., 2012). High efficacy of acids or bases could be explained by the low affinity of H_3PO_4 (in acidic medium), HPO_4^{2-} and PO_4^{3-} (in alkaline medium) toward binding sites on AWBs surface. Another reason for that was the stronger competition in alkaline medium between OH^- ions and PO_4^{3-} for binding sites on AWBs. It is worth mentioning studies conducted by Ismail (2012) and Zhang (2012), where the adsorption was controlled by the chemisorptions mechanism. While 0.01 M KCl exhibited inadequate desorption (11.2-13%), satisfactory elution was observed for 0.05 M NaOH (95.6%). This provides strong evidence that bases are superior to neutral salts for phosphorus desorption in the case of strong sorption. Both Xu et al. (2011a) and Zhang et al. (2012) found that, higher concentration of NaOH promoted desorption. This was probably due to a stronger competition between OH^- ions and PO_4^{3-} for binding sites. Though HCl and NaOH were proven to be effective eluents, their application could result in some side effects. The loss in the adsorption capacity was shown to be 12% for 0.1 M NaOH (Anirudhan et al., 2006) or 10.53% for 0.1 M HCl (Xu et al., 2010a). Particularly, the complete loss of the adsorption capacity of modified coconut shell fibers was recorded after the second cycle of reuse. This could be ascribed to the physical ruin of the adsorbent (De Lima et al., 2012). Xu et al. (2011c) revealed a weight loss of 12-18% as a result of using 1 M HCl as a desorption solution. They attributed this to the corrosion of the cellulose/hemicellulose structure. In addition, Biswas (2008) reported the release of La^{3+} during desorption when 0.4 M HCl was employed as an eluant. In view of practical application, these effects are undesirable as they may reduce the stability and thus restrict reusability of AWBs based adsorbents. Thus, these factors need to be taken into consideration when the exploration of appropriate desorption solutions was made.

Table 2.18 Desorption of P from spent AWBs based adsorbents

No	AWBs based adsorbent	Desorption solution	Desorption efficiency	Remark	Reference
1	Quaternized banana stem	0.1 M NaOH	Cycle 1: 97.1% Cycle 4: 90.7%	No weight loss. Capacity loss < 12%.	Anirudhan et al., 2006
2	Zr(IV) loaded saponified orange waste (SOW) gel	NaCl HCl 0.2 M NaOH	For NaCl: 0% For HCl:<40% For 0.2 M NaOH:95%	0.2 M NaOH exhibited very high desorption ability without remarkable release of loaded Zr(IV)	Biswas, 2008
3	La(III) loaded SOW gel	0.4 M HCl	85%	La(III) was leaked	Biswas et al., 2007
4	Modified coconut shell fibers	HCl	Cycle 1: 50% Cycle 2: 40% Cycle 3: 40%	Significant loss of P adsorption capacity and removal efficiency	De Lima et al., 2012
5	Granular date stones (GDS) Palm surface fibers (PSF)	0.01 M KCl	GDS: 10-11.2% PSF: 12.1-13%	Low desorption ability	Ismail, 2012
6	Quaternized pine bark residues	0.2 M NaCl	99.8%	Minor loss (5.59%) in phosphate sorption capacity after 5 uninterrupted sorption-desorption cycles	Karachalios, 2012
7	Calcined waste eggshell	0.5 M NaOH 0.5 M NaCl	For 0.5 M NaOH: 37.6% For 0.5 M NaCl: 0.7%		Köse and Kivanç, 2011
8	Zr(IV) loaded apple peels	Distilled water at different pH values (2-12)	For acidic pH: minimum desorption For pH 12: 90%	No Zr(IV)detachment at various pH values	Mallampati and Valiyaveettil, 2013
9	$ZnCl_2$ activated coir pith carbon	Distilled water at different pH values (2-11)	For pH 2: ~ 30% For pH 11: 50%	Low desorption ability	Namasivayam and Sangeetha, 2004

			For pH 3-11:<10%		
10	Zr(IV) loaded SOW	0.2 M NaOH	93%	No Zr(IV) leakage	Ohura et al., 2011
11	Fe(III) loaded carboxylatedpolyacrylami degrafted sawdust	NaOH Na_2SO_4 NH_4NO_3-HNO_3 HCl NaCl	For NaOH: 96.8% For Na_2SO_4: 73.6% For NH_4NO_3-HNO_3: 50.8% For HCl: 36.8% For NaCl: 34.5%	Adsorption capacity reduced by 8.9% after 3 cycles, desorption efficiency decreased from 98.2% (Cycle 1) to 92.8% (Cycle 3). 3% weight loss with 0.1 M NaOH	Unnithan et al., 2002
12	Quaternized giant reed	0.1 M HCl 0.1 M NaCl 0.1 M NaOH	For 0.1 M HCl: 100% For 0.1 M NaCl: 100% For 0.1 M NaOH: 100%	Minor weight loss (1-3%)	Xu et al., 2011a
13	Quaternized wheat straw	0.1 M HCl 0.1 M NaCl	For 0.1 M NaCl: 86.6-95.4% For 0.1 M HCl: 87.4-97.5%	Marginal reduction in the adsorption capacity (10.53%)	Xu et al., 2010a
14	Quaternized cotton stalk (CS) and wheat stalk (WS)	0.1 M HCl 0.1 M NaCl	For 0.1 M HCl: CS: 93.1-98.4%; WS: 93.7-98.9% For 0.1 M NaCl: CS 92.3-97.1%; WS 95.0-98.2%	5% weight loss for HCl 0.1M	Xu et al., 2011b
15	Quaternized wheat straw (WS)	1 M HCl	For medium cost resin: 98-100%	12-18% weight loss	Xu et al., 2011c
16	Modified sugarcane bagasse	0.05 M NaOH	95.6%		Zhang et al., 2012

In some studies, the desorption efficiency was extremely poor, for example 11.2-13% (Ismail, 2012); 0.7-37.6% (Köse and Kivanç, 2011); 11-13% (Riahi et al., 2009). In these cases, it was recommended to use phosphorus bearing AWBs based adsorbents as fertilizers or soil conditioners in acid soils, due to their high contents of nutrients (P, Ca, Mg) (Loganathan et al., 2014). However, from a phosphorus recovery point of view, appropriate AWBs based phosphorus adsorbents should be easily desorbed and regenerated. It is one of the most important criteria when the selection of potential AWBs based adsorbents is made.

C. Factors affecting P adsorption performance

(i) Solution pH

The solution pH can affect the dissociation of phosphate species, the chemical state of binding sites, and the affinity of phosphate species towards binding sites. The pH profile is useful for elucidating sorption mechanisms, optimizing the adsorption process, and selecting proper desorption solutions. Hence, a majority of studies on phosphorus adsorption using AWBs based adsorbents have been devoted to determining the ideal pH values.

AWBs based adsorbents tend to sequester PO_4^{3-} anions effectively in a specific pH range while extremely acidic or alkaline medium is found to suppress the process. Yue et al. (2010) found that the pH range of 4-9 favored the adsorption of PO_4^{3-} onto modified giant reed. However, the pH value below 4 or above 9 was found to hinder the process. The authors explained this by dissociation constants of phosphate, dominant phosphate species in the solution, and the affinity of phosphate ions towards binding sites. The dissociation constants of H_3PO_4, $H_2PO_4^-$ and HPO_4^{2-} are 2.12, 7.21 and 12.67, respectively (Biswas, 2008). Consequently, the presence of phosphate species in the solution might vary, depending on the solution pH value. In the pH range of 4-9, $H_2PO_4^-$ and HPO_4^{2-} species were dominant. Due to their strong affinity toward binding sites, the sorption of phosphate was enhanced. In contrast, at pH below 4, the H_3PO_4 and HPO_4^{2-} species were most common. Their inferior affinities toward binding sites led to the unsuccessful decontamination of phosphate. In the same way, at pH above 9, HPO_4^{2-} and PO_4^{3-} species were prevalent. The weak affinity of these species for the active adsorption sites combined with strong competition between OH^- ions and PO_4^{3-} ions for adsorption sites hampered the process. Similarly, the effective pH range was found to be 5-7 for modified banana stem (Anirudhan et al., 2006); 7-10 for metal loaded orange

waste gel (Biswas, 2008); 3.5-6.0 for quaternized pine bark residues (Karachalios, 2012); 3-10 for $ZnCl_2$ activated coir pith carbon (Namasivayam and Sangeetha, 2004); 3-11 for modified sugarcane bagasse (Zhang et al., 2012); 4-9 for modified giant reed (Yue et al., 2010), etc. This trend more or less agrees with the findings reported by Riahi et al. (2009) and Ismail (2012). They both found that an increase in the pH led to a decrease in the phosphate uptake. The authors explained this phenomenon by stronger repulsion force in the alkaline medium. The optimum pH values were found to be low, for example 2 or 3 in the work performed by Jeon and Yeom (2009); Krishnan and Haridas (2008); Mallampati and Valiyaveetttil (2013). On the other hand, the best pH values were found to be high, for example 7.5 or 10 in the studies by Benyoucef and Amrani (2011a), Biswas (2008) and Jyothi et al. (2012). The former result was explained by the dominance of $H_2PO_4^-$ species and their affinity for binding sites in acidic medium (Mallampati and Valiyaveetttil, 2013). In contrast, the latter finding was ascribed to the possible existence of natural compounds and metal ions, such as Ca, Mg, Fe, Al, Cu, Zn inside these AWBs, which had strong affinity toward HPO_4^{2-} in alkaline medium (Jyothi et al., 2012). In some studies, the pH had a minor effect on the sorption of phosphorus in a wide range, for example 4-10 for crab shells (Jeon and Yeom, 2009), 5.0-10.5 for oyster shell powder (Namasivayam et al., 2005), 2-7.5 for scallop shells (Yeom and Jung, 2009). Especially, De Lima et al. (2012) claimed that pH could hardly affect the sorption of PO_4^{3-} onto coconut fiber. The results showed that many AWBs based adsorbents are highly effective in a wide pH range. This property represents an appreciable advantage of AWBs derived adsorbents over conventional adsorbents for PO_4^{3-} removal.

(ii) Initial P concentration

There was a typical trend that the phosphorus uptake capacity increased, while the phosphorus removal efficiency decreased as the initial concentration of phosphorus augmented. Mezenner and Bensmaili (2009) claimed that the phosphorus removal of iron hydroxide eggshell waste decreased from 95 to 64% with increasing initial concentration of phosphorus from 2.8 to 110 mg/L. A similar tendency was reported for sugarcane bagasse by Zhang et al. (2012). The authors explained this by a higher ratio of PO_4^{3-} molecules to the active binding sites at the higher PO_4^{3-} initial concentration. For a given dose of AWBs, the amount of binding sites is a constant. Thus, an increase in initial concentration of PO_4^{3-} led to the decline in its percentage removal.

Riahi et al. (2009) reported that the PO_4^{3-} adsorption capacity of date palm fibers increased from 1.45 to 5.85 mg/g as the initial phosphate concentration increased from 10 to 110 mg/L. These results were consistent with those reported by Anirudhan et al. (2006), Kumar et al. (2010), Mezenner and Bensmaili (2009), Xu et al. (2009) Yue et al. (2010), and Zhang et al. (2012). Both Kumar et al. (2010) and Yue et al. (2010) attributed this to the stronger driving force to convey PO_4^{3-} ions from solution to the surface of the adsorbent at the greater PO_4^{3-} initial concentrations. Higher initial phosphorus concentration led to the augmented availability of PO_4^{3-} ions in the solution. As a result, the interaction between binding sites and PO_4^{3-} ions was enhanced, thus improving the phosphorus uptake capacity of the adsorbent (Mezenner and Bensmaili, 2009; Riahi et al., 2009).

(iii) Adsorbent dose

The general trend is that the phosphate removal efficiency increases with a rise in the adsorbent dosage to a particular level then remains constant or reduces slightly with further increase in the adsorbent dose. The better PO_4^{3-} removal efficiency at higher AWBs dose was explained by more adsorption sites and larger surface area available at higher dose of AWBs (Köse and Kivanç, 2011; Xu et al., 2009; Zhang et al., 2012). The reduction in the PO_4^{3-} removal efficiency when the AWBs dose exceeded the optimum dose could be attributed to the higher resistance to mass transfer, particle aggregation and repulsive forces between binding sites (Ismail, 2012; Mezenner and Bensmaili, 2009; Riahi et al., 2009). An increase in the dose of AWBs also results in an increase in the phosphorus uptake capacity. Riahi et al. (2009) found that the PO_4^{3-} uptake increased from 3.75 to 4.69 mg/g as date palm fiber dose increased from 2 to 6 g/L. However, further increase in adsorbent dose suppressed the sorption process. This can be explained by poor interaction between PO_4^{3-} ions and the adsorbent as a result of the roll up of fibers at excessive doses. In view of practical application, for the same removal efficiency, the lower the adsorbent dose, the better the efficacy of AWBs is. For the purpose of referencing, PO_4^{3-} removal efficiency and the corresponding dose of AWBs in various adsorption systems were introduced as follows: 79.8% - 1 g/L of modified sugar baggese (Zhang et al., 2012); 92.5% - 2 g/L of modified wheat residue (Xu et al., 2009); 85-87% - 5 g/L of date palm wastes (Ismail, 2012); 99.6%-10 g/L of calcined waste eggshell (Köse and Kivanç, 2011; 98% - 16 g/L of modified giant reed (Yue et al., 2010).

(iv) Adsorbent particle size

Chen et al. (2012) found that PO_4^{3-} uptake capacity increased with a decrease in oyster shell diameter from 590 to 180 μm. Similarly, Yeom and Jung (2009) revealed that 100 mg PO_4^{3-}/L could be removed entirely by 1 g of scallop shells of 0.045 mm diameter in 3 h, whereas it was scarcely eliminated by that of 3 mm in 80 h. In the same way, Jeon and Yeom (2009) found that crab shells particles <1 mm in diameter showed a removal percentage >85%, whereas only 50% was attained by the particles 3.35 mm. These results proved that the smaller size of the adsorbents favored the phosphorus adsorption processes. However, for the prevention of a clogging problem in a packed bed reactor, the optimum particle size needs to be identified and applied.

(v) Co-existing anions

Examining the effects of co-existing ions is necessary to enhance the practical application of the adsorbents. Namasivayam and Sangeetha (2004) reported that Cl^-, NO_3^-, MoO_4^{2-}, VO_3^- slightly affected the PO_4^{3-} removal by $ZnCl_2$ activated coir pith carbon. Equally, Biswas et al. (2007) revealed that the addition of Cl^-, CO_3^{2-}, SO_4^{2-} did not affect the adsorption of PO_4^{3-} onto La^{3+} loaded orange waste gel significantly. In a later study, Biswas (2008) revealed that Cl^- (0.56 mM), CO_3^{2-} (0.33 mM), SO_4^{2-}(0.42 mM) hardly affected the sorption of PO_4^{3-} (0.20 mM). Köse and Kivanç (2011) claimed that the supplementation of SO_4^{2-}, NO_3^- and NH_4^+ with the concentrations ranging from 10 to 50 mg/L had minor influences on the retention of PO_4^{3-} onto calcined waste eggshell. Jyothi et al. (2012) discovered that such foreign anions as Cl^-, SO_4^{2-}, NO_3^-, F^- and CO_3^{2-} with the same concentration as that of PO_4^{3-} hardly interfered with the sorption of PO_4^{3-} by thermally modified barks/stems and their ashes of *Ficusreligiosa, Cassiaauriculata, Punicagranatum* and *Calotropis gigantean*. The adsorption of PO_4^{3-} by AWBs was not strongly affected by the presence of co-anions, implying the high applicability of AWBs derived adsorbents in the real wastewater. On the other hand, Namasivayam and Sangeetha (2004) found that the presence of ClO_4^- , SeO_3^{2-} and SO_4^{2-} with the same concentrations as that of PO_4^{3-} hampered the removal of PO_4^{3-} ions. Likewise, Karachalios (2012) claimed that SO_4^{2-} was superior to NO_3^- in competing with PO_4^{3-} for binding sites. The higher Cl^- concentrations resulted in the lower PO_4^{3-} uptake. It is interesting to note that the presence of divalent cationic ions, for example Ca^{2+}, Mg^{2+}, Cu^{2+}, Zn^{2+}, Fe^{2+} and Ni^{2+} with the concentration 10 times greater than that of PO_4^{3-}, boosted the PO_4^{3-} extraction by thermally activated barks/ stems and their

ashes of *Ficusreligiosa,Cassiaauriculata, Punicagranatum* and *Calotropis gigantean* (Jyothi et al., 2012). The positive effect of divalent cationic ions on the adsorption suggests a way to improve the PO_4^{3-} adsorption capacity of these adsorbents, which is metal loading.

(vi) Natural organic matter (NOM)

Boyer et al. (2011) found that NOM impeded phosphate removal of engineered and low-cost adsorbents by occupying adsorption sites or complexing metal ions.

(vii) Contact time

The contact time is an indicator of the adsorption speed. Therefore, it is a key factor in evaluating the efficacy of AWBs based adsorbents (Eljamal et al., 2013). In many cases, the adsorption was found to be rapid, reaching equilibrium in approximately 1 h. The equilibrium time was reported to be 20 min for quaternized wood residues (Karachalios, 2012), 25 min for modified giant reed (Yue et al., 2010), 40 min for modified sawdust (Benyoucef and Amrani, 2011a) and 60 min for natural date palm wastes (Ismail, 2012) and sugarcane bagasse (Zhang et al., 2011). In contrast, the longer contact time was necessary for the equilibrium to be reached by other AWBs. It was shown to be 15 h for La^{3+}, Ce^{3+} and Zr^{4+} loaded SOW gels (Biswas, 2008), 12 h for iron impregnated coir pith (Krishnan and Haridas, 2008), and 6 h for Zr^{4+} loaded apple peels (Mallampati and Valiyaveettil, 2013). The short contact time means that AWBs do not have to be kept in reactors for a long time, and thus space can be saved. It can be considered as an advantageous feature of potential AWBs, from a practical application point of view.

(viii) Temperature

Normally, the adsorptive removal of PO_4^{3-} by AWBs based adsorbents is temperature sensitive. Some adsorption processes are endothermic while others have an exothermic nature. Mezenner and Bensmaili (2009) found that the retention of PO_4^{3-} by iron hydroxide eggshell was enhanced with a rise in the temperature from 20 to 45 °C. From the positive ΔH (81.84 kJ/mol), they concluded that the adsorption was endothermic. It was assumed that, higher temperature was responsible for the better solubility of iron hydroxide eggshell compound, and this produced more iron and calcium hydrolysis complexes. Consequently, the phosphate precipitation was enhanced. Similar observation was noted by Benyoucef and Amrani (2011b), Boujelben et al. (2008), Chen et al. (2012), Kumar et al. (2010), Peng et al. (2012), Yeom and

Yung (2009). It was explained by the enlargement of pore sizes (Benyoucef and Amrani, 2011b), the better dissolution of PO_4^{3-} ions and more efficient intra-particle diffusion at higher temperature (Kumar et al., 2010). On the contrary, Yue et al. (2010) observed that the phosphorus uptake by modified giant reed declined from 19.89 to 17.79 mg/g as the temperature increased from 20 to 60 °C, indicating the exothermic nature of the adsorption process. From negative values of ΔG and ΔH, Karachalios (2012) concluded that the adsorption of PO_4^{3-} by quaternized pine bark residues was exothermic. These results were in harmony with those reported by Köse and Kivanç (2011) and Xu et al. (2009). They explained that the higher temperature resulted in stronger leakage of PO_4^{3-} ions from AWBs surface into the solution (Xu et al., 2009). Particularly, the change in the temperature from 15 to 45 °C hardly affected the sorption of PO_4^{3-} onto crab shell (Jeon and Yeom, 2009).

D. P removal by AWBs based adsorbents

(i) P removal by AWBs in the natural form

Natural AWBs have received far less attention for being used as phosphate adsorbents than their modified counterparts. Up to date, only a few reports exist on the use of raw AWBs for phosphorus decontamination, for example Ismail (2012), Jeon and Yeom (2009), Krishnan and Haridas (2008), Riahi et al. (2009), Yeom and Yung (2009), Zhang et al. (2012). Table 2.19 reports phosphate adsorption capacities of natural AWBs and commercial adsorbents for comparison purpose. Among existing raw AWBs, crab shell displayed the highest PO_4^{3-} adsorption capacity (108.9 mg/g) (Jeon and Yeom, 2009). This value is higher than those obtained with most of the commercial adsorbents (3.36-60 mg/g). It was assumed that not only calcium carbonate but also proteins and cellulose-like backbone of the crab shells played significant roles in the PO_4^{3-} retention. Another reason is that the initial phosphorus concentration of the synthetic wastewater used for the adsorption test was very high (up to 2000 mg/L). The extremely good adsorption capacity placed crab shell among the best AWBs currently available for PO_4^{3-} removal, in term of the adsorption capacity. In contrast, other natural AWBs displayed the adsorption capacity for phosphate in the range between 1.10 and 26.66 mg/g. These values are substantially lower than those of many common commercial adsorbents (31.74-131.77 mg/g). Obviously, with very few exceptions, the phosphorus removal by natural AWBs was not efficient enough for practical application. It can be explained by the fact that as lignocellulosic materials, natural

AWBs contain a large number of negatively charged functional groups (-OH, -COOH) on their surfaces. Consequently, raw AWBs are supposed to be less effective in decontaminating anionic contaminants than cationic ones (Mallampati and Valiyaveetttil, 2013). Because of the lack of efficacy, the use of natural AWBs for decontaminating PO_4^{3-} from wastewater is still limited.

Table 2.19 The maximum phosphate adsorption capacity of natural AWBs and commercial adsorbents

Adsorbent	Adsorption capacity (mg PO_4/g)	Reference
NATURAL AWBS		
Palm surface fibers	26.05	Ismail, 2012
Granular date stones	26.66	Ismail, 2012
Crab shells	108.9	Jeon and Yeom, 2009
Coir pith	4.35	Krishnan and Haridas, 2008
Date palm fibers	13.33	Riahi et al., 2009
Scallop shells	23.00	Yeom and Jung, 2009
Sugarcane bagasse	1.10	Zhang et al., 2012
COMMERCIAL ADSORBENTS		
Duolite A-7	31.74	Anirudhan et al., 2006
Dowex	40.23	Anirudhan and Senan, 2011
Zirconium loaded Muromac	131.77	Biswas, 2008
Zirconium ferrite	39.84	Biswas, 2008
Zr-MCM 41	3.36	Jutidamrongphan et al., 2012
Zirconium ferrite	27.73	Jutidamrongphan et al., 2012
Whatman QA-52	14.26	Marshall and Wartelle, 2004
Amberlite IRA-400	32.24	Marshall and Wartelle, 2004
Aluminium oxide	34.57	Peleka and Deliyanni, 2009
Hydrotalcite	60.00	Peleka and Deliyanni, 2009

(ii) P removal by AWBs in the modified form

Since natural AWBs typically exhibit very low affinity for phosphorus, they need modification to be efficient in eliminating phosphorus from wastewaters (Mallampati and Valiyaveettil, 2013). This section will investigate the phosphorus adsorption of AWBs based adsorbents, which are developed by different modification methods.

❖ Metal loaded AWBs based adsorbents

Table 2.14 presents the phosphorus adsorption capacity of various metal loaded AWBs. Krishnan and Haridas (2008) found that impregnation of coir pith with Fe^{3+}

solution enhanced the phosphate retention ability of coir pith from 5 to 6 times. Supporting the Eberhardt and Min's (2008) argument that the phosphate adsorption capacity of modified wood particles was governed by the amount of loaded Fe^{2+}, Carvalho et al. (2011) reported that the phosphate adsorption capacity of Fe^{2+} impregnated sugarcane bagasse increased 2.25 times as compared to the reference. These results are in line with those by Shin et al. (2005), who observed that the phosphate uptake by raw juniper bark was marginal, whilst that of La^{3+} treated juniper bark was 22.14 mg/g. Clearly, the cationization of AWBs considerably improved their phosphate sorption capacities.

The maximum phosphorus adsorption capacity (q_{max}) of metal loaded AWBs in the literature varies in a wide range (2.05-174.68 mg/g). It can be ascribed to the difference in the nature, composition of AWBs, and the concentration of loading metals. In the literature, the metal loaded AWBs (with the q_{max} value higher than 50 mg/g) with the most potential are Fe^{2+} treated carboxymethylated sugarcane baggage fiber (152 mg/g) and saponified Zr^{4+} loaded SOW gel (172 mg/g) (Biswas, 2008; Carvalho et al., 2011). These two metal loaded adsorbents are even better than several commercial adsorbents listed in Table 2.19, in term of the q_{max}. It is a sound evidence for the influence of metal loading on improving phosphorus adsorption capacity of AWBs.

❖ Quaternized AWBs based adsorbents

The adsorption performance of quaternized AWBs is presented in Table 2.15. In all cases, quaternized AWBs exhibit higher phosphate adsorption capacities than their raw counterparts. Zhang et al. (2012) reported that the phosphate uptake capacity of quaternized sugarcane bagasse (MSBG) and raw sugarcane bagasse (SBG) was 21.30 and 1.1 mg/g, respectively. They explained the higher adsorption capacity of MSBG by its higher zeta potential (32 mV), as compared to that of SBG (-22 mV). Due to electrostatic interactions, the positive zeta potential of MSBG favored the retention of PO_4^{3-} while the negative zeta potential of SBG hampered the adsorption process. Similarly, Xu et al. (2011a) claimed that amino grafted giant reed demonstrated an excellent phosphate adsorption capacity (54.67 mg/g), as compared with raw giant reed (0.863 mg/g). Xu et al. (2009) also found that the phosphate removal of modified wheat residue (92.5%) was considerably higher than that of raw wheat residue (4.8%). Equally, Anirudhan et al. (2006) discovered that the phosphate removal percentage of quaternized banana stem was 99.7%, whilst it was 73.9% for raw banana stem (BS). This indicated that quaternized banana stem was more efficient than raw banana stem in

phosphate elimination. The authors attributed the superior phosphate removal of quaternized banana stem to the strengthened stability of constitutive units, which led to the enhanced access of phosphates to the binding sites.

Quaternized AWBs based adsorbents are compared with commercial adsorbents, in term of phosphate adsorption capacity, to evaluate their applicability. A comparative study between quaternized soybean hulls and a commercial adsorbent (QA52) showed that quaternized soybean hulls (0.64 mmol/g) were better than QA52 (0.46 mmol/g) in phosphorus elimination (Marshall and Wartell, 2004). Since both of these adsorbents are mainly composed of cellulose, the comparison provides a foundation for the replacement of high-cost, commercial, cellulose-based resins by low-cost, natural AWBs based sorbents in remediation of phosphate pollution. Anirudhan et al. (2006) compared the quaternized banana stem and a commercial anion exchanger, Duolite A-7. It was revealed that quaternized banana stem demonstrated two-fold higher phosphate adsorption capacity than Duolite A-7. Although the difference in experimental conditions may hinder the direct comparison among adsorbents, quaternized AWBs usually exhibit equal to or even higher adsorption capacities (45.7-205.63 mg/g) than well-known commercial adsorbents (3.36-131.77 mg/g). The excellent phosphate adsorption capacity makes quaternized AWBs based adsorbents attractive for practical application. In view of searching potential AWBs for quaternization, Wartelle and Marshall (2006) recommended the use of AWBs with low lignin: cellulose ratio, because of their high affinity for quaternizing reagents. These results highlight the potential of improving the phosphate uptake capacity of AWBs by quaternization.

The promising quaternized AWBs, with $q_{max} \geq 50$ mg PO_4/g, include wheat straw (Xu et al., 2011c), cotton stalk and wheat stalk (Xu et al., 2011b), giant reed (Xu et al., 2011a; Yue et al., 2010), corn stover (Wartelle and Marshall, 2006), banana stem (Anirudhan et al., 2006), sawdust of Aleppo pine (Benyoucef and Amrani, 2011a), green coconut shell fibers (De Lima et al., 2012), wood residues (Karachalios, 2012). It seems to be that, quaternization can result in better phosphate adsorption capacities of modified AWBs, as compared to metal loading.

❖ <u>AWBs based adsorbents prepared by other modifying methods</u>

Thermal activation is shown to be efficient in boosting the phosphorus removal of AWBs. Huang et al. (2010) found that preheating oyster shell in the temperature range of 100-400 °C improved its adsorption capacity for PO_4^{3-} ions. While natural oyster shells could hardly remove any PO_4^{3-} from 80 mL wastewater with PO_4^{3-} concentration

of 20 g/L, the removal efficiency of preheated oyster shells reached up to 100% after 3 or 4 days. This is attributed to the increase in the pore size and surface area. Peng et al. (2012) found that better PO_4^{3-} uptake was achieved for pine sawdust char produced at the higher pyrolysis temperature. The maximum adsorption capacity of pine sawdust char is comparable to Whatman QA-52 and higher when compared with Zr-MCM 41.

E. Phosphorus recovery by adsorption coupled with crystallization

Although phosphorus recovery as MAP or calcium phosphate is widely known, only a few reports exist on the use of adsorption for this purpose. Ebie et al. (2008) investigated the phosphorus recovery in decentralized advanced Johkasou by adsorption onto Zr^{4+}. The two-step desorption process with NaOH 7% resulted in a phosphorus desorption efficiency up to 95%. The phosphorus recovery rate of 95.6% was attained by crystallization. The recovered phosphorus product ($Na_{3.25}(OH)_{0.25}PO_4.12H_2O$) had high purity (> 95%) and acceptable levels of hazardous elements, for example As, Hg, Pb, Cd, Ni. The tests on germination rate and fertilizer response showed that recovered phosphorus was as good as Na_2HPO_4, a chemical fertilizer. Similarly, Midorikawa et al. (2008) utilized a high-speed adsorbent for phosphorus recovery from municipal wastewater secondary effluent. Due to the exceptionally high removal percentage (99.5%) and desorption efficiency (97%) of this adsorbent, phosphorus was successfully separated. $Ca(OH)_2$ was added to precipitate eluted phosphorus as calcium phosphate. With 16% phosphorus and very low levels of toxic substances, the recovered product could be used as a replacement for phosphorus ore and fertilizer.

The works on phosphorus recovery using adsorption onto AWBs followed by crystallization are scarce. A large proportion of studies are limited to desorption and reusability of AWBs. Biswas (2008) claimed that phosphorus could be efficiently extracted from incinerated sewage sludge ash (ISSA) using 0.05 M H_2SO_4 or 0.1M HCl. Due to the selective adsorption onto Zr^{4+} loaded orange waste gel, the extracted phosphorus was separated from other contaminants, for example Ca, Fe, Al. The adsorbed phosphorus could be easily eluted using 0.2 M NaOH. That paves the way to the phosphorus recovery from ISSA. In another study conducted by Köse and Kivanç (2011), calcined waste eggshell was used for adsorption of phosphorus from wastewater. By addition of solid CaO, phosphorus in desorption solution could be recovered as calcium phosphate with the recovery rate of 37.72%. These studies show that adsorption may hold a promise for phosphorus recovery from wastewater but has not been fully exploited. Based on previous studies with conventional adsorbents, the procedure for the removal and recovery of phosphorus from wastewaters by adsorption coupled with crystallization is depicted in Fig.2.12.

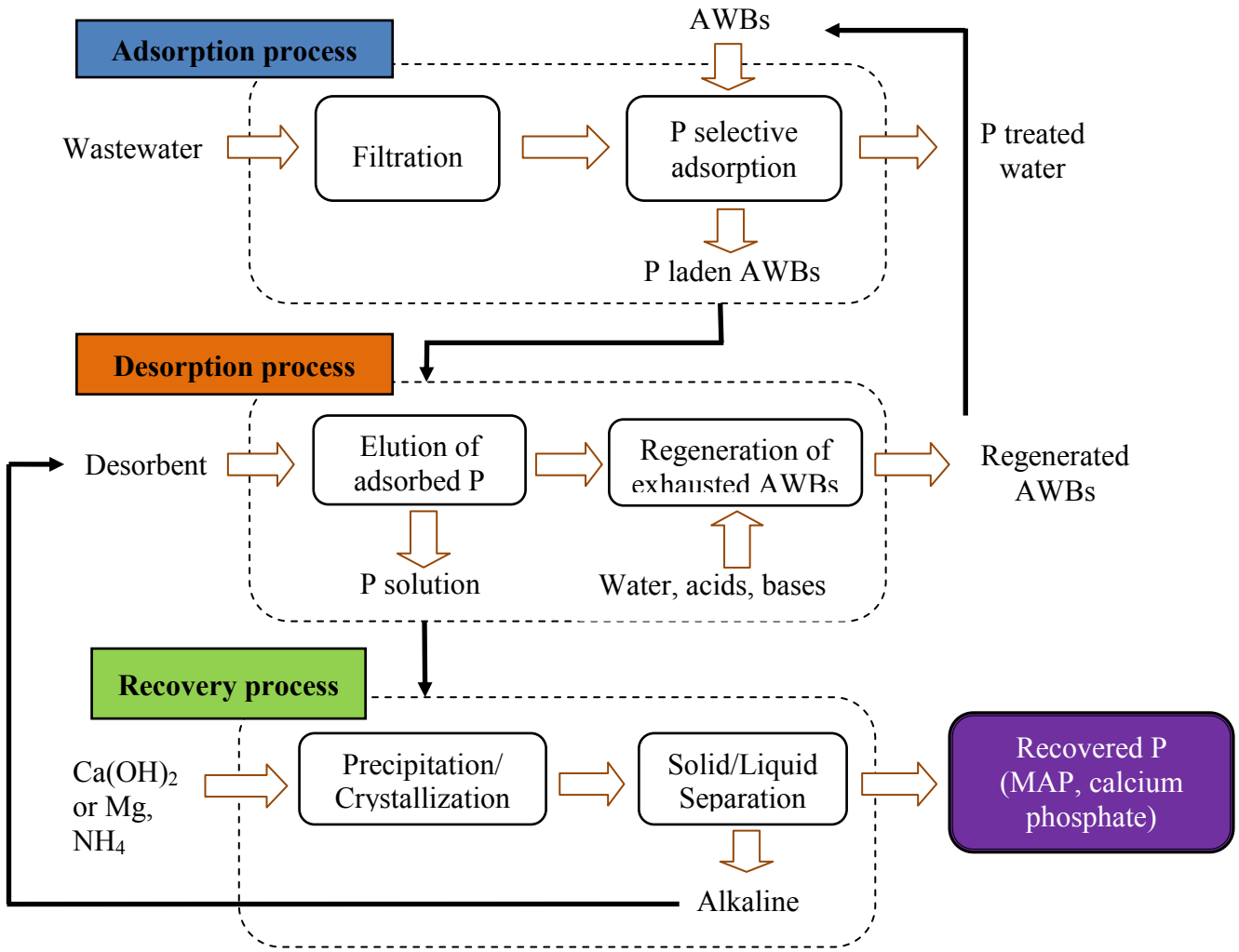

Figure 2.12 P recovery from wastewaters via adsorption onto AWBs based adsorbents and crystallization

2.6 SOYBEAN BY-PRODUCT (OKARA) AS A CHOICE MEDIUM

Okara is a byproduct of soy beverage and tofu production (Fig.2.13). It has a white color and is quite similar to wet sawdust in its texture and form (Fig.2.14). Okara is also named soybean milk residue, soy pulp, soy fines, bean mash, bean curd dreg (English), le okara (French), das okara (German), tofuzha or douzha (Chinese), tofukasu (Japanese), bejee (Korean), sepal (Filipino), ampastahu (Indonesian), tauhu tor (Thai). The production of every 1,000 L of soy beverage can result in 250 kg of okara (Soy 20/20, 2005). Accordingly, vast amounts of okara are generated worldwide annually. In Japan about 800,000 tons, in Korea approximately 310,000 tons, and in China nearly 2,800,000 tons are yielded from soymilk and tofu industries per annum (Li et al., 2012). As okara contains 50% fiber (cellulose, hemicellulose, and lignin), 25% protein, 10% lipid, and other nutrients, it is usually used as animal feed, fermentation substrate, fertilizer, pet food, food production. However, fresh okara degrades very quickly (less than 2 days) even under refrigeration. As a result, okara needs to be dried or frozen for further use in food. However, this is costly because of intensive energy consumption and special equipment requirement. Therefore, at present okara is mostly dumped or burned as waste (Li et al., 2012). It can cause an environmental burden and thus requires a proper disposal.

Okara was chosen for investigation in this study because of its insolubility in water, non-toxicity, low cost, easy acquiring and abundant availability, enough for large scale application. In this research, okara is defined as “low-cost” material since the only cost relevant to this material is transportation, and there is a plentiful supply of this material. As a by-product of food processing process, okara is very clean and can be used directly for modification. Additionally, okara has phosphorus inside (396-444 mg P/100 g dry matter), giving a platform for the phosphorus recovery from both raw okara and wastewater (Li et al., 2012). Moreover, due to the existence of large amounts of hydroxyl and carboxyl groups on its cell walls, okara can easily and efficiently get involve in chemical modification reactions (Benyoucef and Amrani, 2011b). Up until this time, some types of soybean by-product were used as environmentally friendly materials for water treatment, such as soybean hulls (Marshall and Wartelle, 2004), lees materials (Adachi et al., 2005), bean dregs (Li, 2009), and okara (Gao et al., 2015). It was found that these materials exhibited good sorption abilities to organochlorine compounds, benzene, heavy metals, and reactive dye. Nevertheless, to the best of the

author's knowledge, the use of okara for the removal and recovery of phosphorus has not been reported in the previous studies.

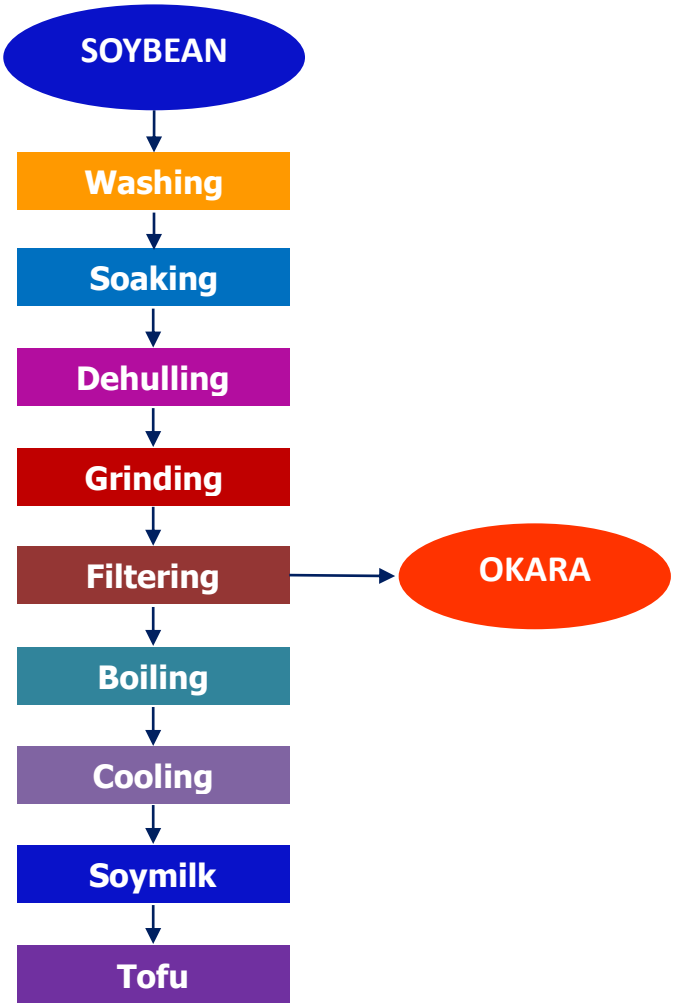

Figure 2.13 Okara as a by-product of the tofu and soymilk production processes

Figure 2.14 Image of fresh soybean by-product (okara)

2.7 CONCLUSION AND RESEARCH GAPS

2.7.1 Major findings from literature review

The removal and recovery of phosphorus from wastewater have received considerable attention in recent years. From this literature review, numerous findings were achieved:

- Phosphorus is essential for the development of living organisms and agricultural production. However, it is a non-renewable resource and is at a risk of being exhausted in the near future. From another perspective, the excessive amount of phosphorus in the water medium is mainly responsible for eutrophication, inducing environmental damage, and threatening the biodiversity of ecosystems. Thus, the elevated level of phosphorus needs to be eliminated and recovered from wastewater for preventing eutrophication, saving the phosphate rock reserve, protecting engineered systems from MAP scale, and meeting the stringent regulations.
- Municipal wastewater may represent a valuable recyclable phosphorus resource, due to large amounts generated worldwide and the lack of toxic substances, such as heavy metals. The concentration of soluble and reactive phosphorus in municipal wastewater is in the range of 5-20 mg/L. It is far too low compared to the minimum concentration (50 mg/L) to ensure the successful recovery of phosphorus. This low concentration can be considered as the major challenge to the phosphorus recovery from municipal wastewater and is expected to be overcome with a pre-concentration method. The composition of municipal wastewater changes considerably with time and location, depending on influent quality and processing levels at WWTPs. As a result, the feasibility of MAP recovery from municipal wastewater needs case-by-case testing and process optimization.
- The phosphorus can be eliminated from wastewater by numerous methods. Though chemical precipitation and biological treatment are most commonly used processes, they often suffer from inefficiency for the treatment of diluted wastewater or un-sustainability by producing non-recyclable phosphorus products. In contrast, adsorption has significant advantages, such as simple operation, low cost, high efficiency. In particular, it is documented that adsorption can pre-

concentrate phosphorus in aqueous solution to a very high level, and thus can facilitate the phosphorus recovery.

- There is a growing trend to use AWBs based adsorbents for phosphorus removal. It has been shown that in the most cases, AWBs based adsorbents in the natural form can hardly remove phosphorus. Thus, modification plays a significant role in the preparation of phosphorus adsorbents from AWBs. Of modifying methods, metal loading and quaternization are the usual methods of choice. The main problems that currently exist with AWBs based adsorbents are lack of mechanical strength, inefficiency in the continuous adsorption at high flow rate and limited reusability.
- To date, the majority of the studies using AWBs based adsorbents for phosphorus removal have been performed in the batch mode. The major concerns with the batch mode experiments are the small volume of treated water and the difficulty in scaling-up. The existing batch studies have mainly focused on influential factors, isotherms, kinetics, mechanisms, and desorption. Only a small percentage of adsorption tests with AWBs based adsorbents have been carried out in the lab-scale rapid small-columns.
- Phosphorus can be recovered from many products of WWTPs, such as wastewater, sludge or ash. Consequently, technologies for phosphorus recovery can be divided into crystallization/precipitation, wet-chemical and thermo-chemical, respectively. Despite the fact that wet-chemical and thermo-chemical can yield better recovery efficiency than crystallization/precipitation, they are less preferred due to extensive consumption of chemicals and energy as well as the requirement of special equipment. Of the precipitating products, calcium phosphate and magnesium ammonium phosphate (MAP) are most favored. Up to now, most of the studies on phosphorus recovery have been performed directly from wastewater by crystallization/precipitation. The major hindering effect to this process is likely attributed to low phosphorus concentration in municipal wastewater. Much attention has been paid to the technical feasibility, such as process optimization and product characterization. The research on economic feasibility is at the initial stage, indicating that without taking the environmental benefits into consideration, the current phosphorus recovery process is economically unfeasible. In view of phosphorus recovery, both recovery efficiency and recovered product purity are significant.

2.7.2 Research gaps

Although much work has been implemented on the removal and recovery of phosphorus from municipal wastewater using AWBs based adsorbents, there are still significant research gaps as follows.

- It is desirable to develop a sustainable technology that can both remove and recover phosphorus from wastewater in reusable forms. Specifically, to make the phosphorus recovery from municipal wastewater viable, there is a need to search for a method that can pre-concentrate phosphorus to a high level before the phosphorus recovery.
- The additional studies are required to develop innovative, cost-effective, and sustainable phosphorus adsorbents from AWBs. When the selection of adsorbents is made, more attention should be paid to reusability, selectivity, and hydraulic conductivity properties of the adsorbents, which play a vital role in practical application. This verifies the significance of developing a set of criteria for the selection of potential phosphorus AWBs based adsorbents.
- Despite the fact that modification can considerably enhance the adsorption capacity for phosphorus of AWBs, it cannot be denied that some modifying chemicals are toxic and expensive. Up until now, there is still lack of information in literature about recycling of modification chemicals to reduce the cost of adsorbent development while mitigating negative impacts on the environment. Moreover, the cost of developed adsorbents needs to be compared with that of commercial adsorbents to confirm the feasibility of the modification method.
- Despite numerous studies on the removal of phosphorus using AWBs derived adsorbents around the world, the literature is insufficient about their usage in the real wastewater under continuous operating conditions, particularly at pilot-scale and full-scale. Hence, further research on this aspect would be necessary for promoting the industrial application of AWBs based adsorbents.
- A minority of studies have investigated the phosphorus recovery from desorption solution, where the phosphorus level is tens or hundreds of times higher than that in feed solution. Further work should be done to improve the purity of recovered phosphorus. Additionally, agronomic studies would be necessary to confirm the applicability of recycled products. Moreover, the cost-benefit analysis of the whole process should be evaluated in the future research.

- Overall, it is clear from the literature survey that the feasibility of removing and recovering phosphorus from municipal wastewater by adsorption coupled with crystallization has not adequately been clarified yet.

UNIVERSITY OF TECHNOLOGY, SYDNEY

CHAPTER 3

EXPERIMENTAL INVESTIGATIONS

3.1 MATERIALS

3.1.1 The soybean by-product (okara)

The homemade okara was obtained from soybean milk production at home with Lumina glass blender (Model No BL-805C). Every 4 liters of soybean milk made could produce 1 kg of fresh okara. The virgin okara was washed with tap and distilled water on a 300 µm sieve to remove residual soy milk. It was subsequently dried in the oven at 105 °C for 24 h and kept in desiccators for chemical modification. The home made okara was used to produce iron loaded okara (ILO), combined iron and zirconium loaded okara (IZLO), and zirconium loaded okara (ZLO), which were utilized for the batch experiments.

The industrial okara was collected from Nhu Quynh tofu and soy milk workshop, Yagoona, NSW, Australia (Fig.3.1). The fresh okara consists of 80% humidity. The raw okara was dried in the oven at 105 °C for 24 h to keep it for a long use. After that, it was cooled down to the ambient condition and kept in a glass bottle for further chemical treatments. The dried okara has the particle size of 150-1000 µm and the density of 0.23-3.65 g/cm^3. The industrial okara was employed to prepare ZLO, which was used in the characterization and column tests.

Figure 3.1 Collecting soybean by-product (okara) from Nhu Quynh tofu and soy milk workshop

3.1.2 The raw municipal wastewater

The raw municipal wastewater was sampled from Sydney Olympic Park Wastewater Treatment Plant in Burwood, Australia (Fig.3.2). The physicochemical characteristics of the raw municipal wastewater were as follows: pH 7.6, COD 158 mg/L, TSS 167 mg/L, PO_4-P 5.5 mg/L, NO_3-N 3.6 mg/L, NO_2-N 0.19 mg/L, NH_4-N 51 mg/L, Cl^- 108.1 mg/L, Mg^{2+} 9.2 mg/L, Ca^{2+} 30.55 mg/L, Cu^{2+} 0.1 mg/L, Pb^{2+} 0.35

mg/L, Fe^{3+} 0.25 mg/L, Cd^{2+}, Zn^{2+}, and Zr^{4+} were non-detectable. After being settled for 24 h, the raw municipal wastewater was screened through a 150 µm stainless steel sieve. Afterwards, the municipal wastewater is ready for the adsorption tests.

Figure 3.2 Collecting raw municipal wastewater at Sydney Olympic Park Wastewater Treatment Plant using a refrigerated sampler

3.1.3 Chemical reagents

The chemicals used in this work were of analytical grade. The stock solution of phosphorus (1000 mg/L) was prepared by dissolving 4.58 g of disodium hydrogen phosphate (Na_2HPO_4) in a 1000 ml of Milli-Q water. The working solutions of phosphorus (10, 25, 50, 100, 125, 200, 250, 400, 500mg P/L) were prepared by diluting the stock solution (1000 mg P/L) with Milli-Q water accordingly (100, 40, 20, 10, 8, 5, 4, 2.5, 2 times). The pH of the synthetic solutions was adjusted using NaOH or HCl solutions of different concentrations to ensure a minimal change in the volume of the solution. The solutions of 0.05 M and 0.2 M NaOH, 0.1 M HCl and 0.25 M Zr^{4+} were produced by liquefying proper amounts of sodium hydroxide (NaOH), hydrochloric acid (HCl), and zirconyl chloride octahydrate ($ZrOCl_2.8H_2O$) in the Milli-Q water.

3.2 METHODS

3.2.1 Development of the metal loaded adsorbents

A. Preparation of metal loaded adsorbents

The initial investigation showed that raw okara was inefficient in phosphorus removal. Thus, a chemical modification of okara was made to improve its phosphorus removal efficiency. In this study, three categories of metal loaded okara were prepared, including iron (Fe^{3+}) loaded okara (ILO), iron/zirconium (Fe^{3+}/Zr^{4+}) loaded okara (IZLO), and zirconium (Zr^{4+}) loaded okara (ZLO). The procedures for the development of these adsorbents are as follows.

To prepare single metal loaded okara (ILO and ZLO), the dried raw okara was first stirred with 0.05 M NaOH to enhance its metal capture ability (solid/liquid ratio = 1 g/20 ml, contact time = 120 rpm, temperature = 298 K, and contact time = 24 h). The wet NaOH treated okara was then washed with tap and distilled water until pH of the washing solution was almost neutral. Next, the washed NaOH treated okara was dried in the oven at 105 °C for 24 h. After being cooled down to the ambient temperature, the dried NaOH treated okara was kept in the plastic bags for the further treatment. In the next step, the dried NaOH treated okara was saturated with 0.25 M metal solutions (Fe^{3+} or Zr^{4+}), then washed and dried at the same conditions as described above. This procedure led to the deposition of metal ions onto okara (Mallampati and Valiyaveettil, 2013). Due to the presence of cationic ions (Fe^{3+} or Zr^{4+}) on the surface of adsorbents, it was expected that ILO and ZLO could efficiently sequester phosphorus from aqueous solutions. The metal loaded okara (ILO and ZLO) was stored in plastic bags for being used as phosphorus adsorbents in this study.

To prepare combined metal loaded okara (IZLO), the dried raw okara was pretreated with 0.05 M NaOH and then loaded with 0.25 M $FeCl_3$ as mentioned above. Next, the dried NaOH/$FeCl_3$ treated okara was stirred with 0.25 M Zr^{4+} at the same conditions as mentioned above. After carefully washing with tap water and then with distilled water to remove free Zr^{4+} ions, the material was dried in the oven at 105 °C for 24 h and cooled down to the room temperature.

B. Selection of the potential adsorbent

(i) Adsorption test

The adsorption experiments were carried out with three developed adsorbents as follows: 0.5 g of each adsorbent (particle size of 150-300 μm) was taken into conical

flasks of 250 mL containing 50 ml of different phosphorus solutions (10, 25, 50, 100, 125, 200, 250, 400, 500 mg P/L). The pH of the solutions was kept natural (7.6-7.8). The samples were shaken at the speed of 120 rpm, room temperature for 24 h to ensure the equilibrium could be fully reached. After the equilibrium time, the samples were filtered through Whatman™ 1822–047 Grade GF/C filter paper (diameter: 4.7 cm and pore size: 1.2 μm). The filtrate was taken for phosphorus analysis. The phosphorus adsorption capacity (mg/g) was calculated from the difference between initial and equilibrium phosphorus concentrations as follows:

$$q = \frac{(C_o - C_e)*V}{m} \quad (3.1)$$

where C_o and C_e are the initial and equilibrium phosphorus concentrations in the solution (mg/L), respectively; V is the volume of the solution (L); and m represents the dry weight of the metal loaded okara powder (g). The maximum phosphate adsorption capacities of three developed adsorbents were calculated from Langmuir equation.

(ii) Desorption and regeneration tests

After adsorption, the spent adsorbent (0.5 g) was separated from the solution by filtration through Whatman™ 1822–047 Grade GF/C filter paper (diameter: 4.7 cm, pore size: 1.2 μm). The phosphorus bearing adsorbent was washed with tap and then with distilled water to eliminate unbound phosphorus. The solid was then collected into 5 conical flasks of 250 mL, containing 50 ml of 5 elution solutions including 0.2 M NaOH, 0.05 M NaOH, pH 12 distilled water, 0.1 M NaCl, and 0.1 M HCl. All samples were agitated on an orbital shaker at the speed of 120 rpm, room temperature for 24 h. After that, the solid was removed from the solution by filtration again. The filtrates were used to evaluate the desorbed phosphorus amounts. Based on the desorption results, the best desorption solution was determined and applied in the generation studies.

After desorption with the selected desorption solution, the exhausted adsorbents were repeatedly used for other four continuous adsorption - desorption cycles, with or without activation by 100 mL of 0.1 M HCl. The reusability of the adsorbents was evaluated based on the phosphorus removal percentage.

(iii) Metal leaching test

To evaluate the metal leakage from metal loaded okara during adsorption and desorption tests, the suspensions obtained from these processes were filtered through Whatman™ 1822-047 Grade GF/C filter paper (diameter: 4.7 cm, pore size: 1.2 μm).

The filtrates were then used for metal analysis. The metal bleeding was evidenced by the presence of loading metals in the filtrates.

C. Effect of metal loading conditions on P uptake capacity of ZLO

In an attempt to identify the optimum metal loading condition, ZLO was first developed at three different modification conditions including A) 0.05 M NaOH + 0.25 M $ZrOCl_2.8H_2O$, B) 0.05 M NaOH + 0.5 M $ZrOCl_2.8H_2O$, and C)) 0.5 M NaOH + 0.5 M $ZrOCl_2.8H_2O$. The isotherm tests were then carried out with the three developed adsorbents at same adsorption conditions as follows: adsorbent particle size = 300-425 μm, initial P concentration range = 10-500 mg/L, dose = 10 g/L, shaking speed = 120 rpm, temperature = 298 K, contact time = 24 h. Based on the experimental isotherm data, the maximum adsorption capacities of ZLO-A, ZLO-B, and ZLO-C were calculated using Langmuir equation.

D. Recycling of the loading metal (Zr^{4+}) solution

The original 0.25 M Zr^{4+} solution was used to produce ZLO-1 at the following conditions: solid/liquid ratio = 1 g/20 mL, stirring speed = 120 rpm, temperature = 298 K and contact time = 24 h. To prepare a recycled Zr^{4+} solution, the distilled water was firstly added into the spent Zr^{4+} solution to make the volume remain unchanged (1 L). The above solution was then supplemented with 7.242 g of $ZrOCl_2.8H_2O$ to compensate for the amount of Zr adsorbed (2.05 g), which was calculated based on the mass of NaOH treated okara (50 g) and its Zr adsorption capacity (40.44 mg/g). The recycled Zr^{4+} solution was used to prepare ZLO-2 under the same conditions as those applied to ZLO-1.

In the next step, ZLO-1 and ZLO-2 were investigated in an adsorption test using four different particle sizes (1000-600, 600-425, 425-300, 300-150 μm). The adsorption conditions were as follows: initial P concentration = 50 mg/L, adsorbent dose = 8 g/L, shaking speed = 120 rpm, temperature = 298 K, and contact time = 24 h. The particle size resulted in the least difference in P removal percentage between ZLO-1 and ZLO-2 was recycled for other nine times. The P removal percentage was used to evaluate the Zr^{4+} recycling feasibility.

E. Characterization of the selected adsorbent (ZLO)

(i) Physical properties

This study investigates such physical characteristics of ZLO as density, porosity, and permeability. The density can be divided into particle density and bulk density. The

particle density can be determined by dividing the total mass of the solid particles by their total volume. The bulk density can be defined as the density of a unit of soil including air spaces. Porosity indicates to the proportion of the bulk volume not occupied by solids (Okochi, 2013).

The ZLO particle density was calculated according to the following equation (Okochi, 2013):

$$\rho_p = \frac{\rho_w(m_{s+f}-m_f)}{(m_{s+f}-m_f)-(m_{s+f+w}-m_{f+w})} \quad (3.2)$$

where ρ_p = ZLO particle density (g/cm^3), ρ_w = water density (g/cm^3), m_{s+f} = mass of ZLO + volumetric flask (g), m_f = mass of empty flask (g), m_{s+f+w}= mass of ZLO + volumetric flask + ultrapure water (g), and m_{f+w}= mass of filled volumetric flask + ultrapure water (g).

The bulk density was determined by the following equation (Okochi, 2013):

$$\rho_b = \frac{m}{V_b} \quad (3.3)$$

where ρ_b = ZLO bulk density (g/cm^3), m = mass of ZLO (g), and V_b= baker volume (cm^3)

The porosity was calculated via the following equation (Okochi, 2013):

$$\eta = \left(1 - \frac{\rho_b}{\rho_p}\right) \times 100 \quad (3.4)$$

where η = porosity (%), ρ_p = ZLO particle density (g/cm^3), ρ_b = ZLO bulk density (g/cm^3).

The permeability coefficient of ZLO was determined using Darcy's Law (http://www.ajdesigner.com/phppermeameter/permeameter_equation_permeability_coefficient.php). The experiment design is illustrated in Fig.3.3.

$$K = \frac{Q\Delta L}{A\Delta h} \quad (3.5)$$

where K is the permeability coefficient (m/day), Q is the porous medium flow rate (m^3/s), ΔL is the length change (m), A is the cross sectional area (m^2), ΔH is the pressure head change (m).

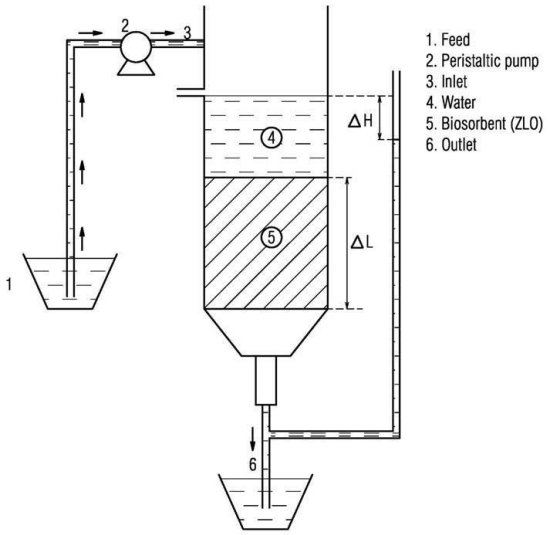

Figure 3.3 Experiment design to determine the permeability coefficient of ZLO

(ii) Chemical properties

The morphology of ZLO was examined by S4800-NIHE SEM, Hitachi (Japan). The EDS analysis of ZLO was implemented by an Energy Dispersive Spectroscopy (EDS) detector (JOEL JSM-7600F FE-SEM). The FTIR pattern of ZLO was acquired by a Nicolet 6700 FTIR Spectrometer.

Phosphorus inside okara was determined using a procedure described by Vietnam standards TCVN 8551:2010, Plants - Method for sampling and preparing the sample, which was issued on 29 December 2010, at the Decision of 2945/QĐ-BKHCN. The concentration of phosphorus in the obtained solution was then determined spectrophotometrically by molybdenum blue method on Spectroquant® NOVA 60.

The quantity of Zr present in ZLO was estimated suing a procedure adapted from Boujelben et al. (2008). Firstly, 1 g of ZLO was mixed with 10 mL of concentrated HNO_3 (70%, density 1.42 g/cm^3) at 50 °C and shaken for 30 min. The mixture was then added with 20 mL of 0.1 M HNO_3 and shaken for another 1 h. After that, the suspension was filtered through Whatman™ 1822-047 Grade GF/C filter paper (diameter: 4.7 cm, pore size: 1.2 μm), and the filtrate was used for Zr^{4+} analysis.

3.2.2 Phosphorus removal by ZLO in batch mode experiments

A. Effects of process parameters

(i) Effect of the solution pH

The effect of solution pH on the phosphorus adsorption by ZLO was evaluated by varying the solution pH from 2 to 12, while maintaining other process parameters constant. 0.5 g of ZLO was added to 50 mL of phosphorus solution of 50 mg/L in a

series of 250 mL Erlenmeyer flasks. The parafilm covered flasks were put on a shaker at 120 rpm, 298 K for 24 h to attain equilibrium. The suspensions were filtered through Whatman™ 1822-047 Grade GF/C filter paper (diameter: 4.7 cm, pore size: 1.2 μm) and filtrates were used for phosphorus measurement.

(ii) Effect of the adsorbent dose

To determine the effect of adsorbent dose on the phosphorus removal by ZLO, the experiment was performed at several adsorbent doses (1, 2, 3, 5, 7, 10, 12 g/L). Different amounts of ZLO (0.05-0.6 g) were placed into a series of flasks filled with 50 mL of phosphorus solution of 50 mg/L at natural pH. The flasks were agitated on a shaker at 120 rpm, 298 K for 24 h. The sampling and analytical procedures were similar to those described for investigating the effect of pH. For a real application purpose, the experiment was repeated at different phosphorus concentrations (5, 10, 25 mg/L).

(iii) Effect of the adsorbent particle size

The adsorbent particle size effect on phosphorus removal of ZLO was investigated by varying the ZLO particle size (1000-600 μm and 300-150 μm). The initial P concentrations used were 50, 100, 200, 300, 400, 500, and 600 mg/L. Other parameters such as ZLO dose (10 g/L), shaking speed (120 rpm), and the reaction temperature (298 K) were kept unchanged.

(iv) Effect of co-anions

The influence of typical foreign anions, such as sulfate (SO_4^{2-}), nitrate (NO_3^-), chloride (Cl^-) and carbonate (CO_3^{2-}) on the adsorption of phosphate (PO_4^{3-}) was investigated. The KCl, KNO_3, K_2CO_3 and Na_2SO_4 salts were used to prepare the corresponding foreign anion solutions. 1 g of ZLO was added into a flask containing 50 mL of phosphorus solution, which was mixed with one foreign anion separately or four foreign anions simultaneously. The molar concentration of each co-existing anion in the combined solution was 10 fold higher than that of phosphorus. The experiment was performed at the initial phosphorus concentration of 100 mg P/L (~ 3 mmol PO_4/L), original pH, 298 K, and agitation speed of 120 rpm for 24 h, in the presence of single or multi foreign anions. The control experiment was conducted under the same conditions, in the absence of foreign anions. The ability of foreign anions to compete with PO_4^{3-} for binding sites on ZLO was calculated using the following equation (Shin et al., 2005).

$$\text{Efficiency of competing anion (\%)} = \left(1 - \frac{\text{P adsorbed in the presence of anion}}{\text{P adsorbed when added alone}}\right) * 100 \qquad (3.6)$$

B. Adsorption isotherm study

The isotherm study was performed by mixing 0.5 g ZLO of the mixed particle sizes (150-1000 µm) with 50 mL solution of various phosphorus concentrations (10, 25, 50, 100, 150, 200, 300, 400, and 500 mg/L) in a series of conical flasks. The initial pH values were kept natural. The suspensions were shaken at 120 rpm, 298 K for 24 h in a thermostatic shaker to ensure the equilibrium was fully reached. After filtration through Whatman™ 1822-047 Grade GF/C filter paper (diameter: 4.7 cm, pore size: 1.2 µm), the filtrates were analyzed to determine phosphorus concentrations. The adsorption isotherm data were fitted to Langmuir, Freundlich, and Temkin models.

C. Adsorption kinetic study

Phosphorus adsorption kinetics by ZLO was examined by conducting experiments at a given initial phosphorus concentration and adsorbent dose. The pH of solutions was kept neutral. The adsorption reaction was facilitated at 120 rpm and 298 K, using a thermostatic shaker. At the different intervals (0.25, 0.5, 0.75, 1.0, 1.5, 2, 3, 4, 5, 6 h), the samples were taken and filtered through Whatman™ 1822–047 Grade GF/C filter paper (diameter: 4.7 cm, pore size: 1.2 µm). The filtrates were analyzed to determine phosphorus concentrations. For comparison purpose, experiment were repeated for different initial phosphorus concentrations (5, 10, 25, 50 mg/L) with corresponding optimal doses (2, 3, 7, 10 g/L) or a given dose (10 g/L) of the adsorbent. The data were fitted to three common kinetic models including Pseudo-first order, Pseudo-second order, and Intra-particle diffusion.

D. Adsorption thermodynamic study

The impact of temperature on phosphorus retention by ZLO was evaluated by performing experiments at 298, 308, and 318 K. The amounts of 0.5 g ZLO were added to several 250 mL Erlenmeyer flasks containing 50 mL of solution of different phosphorus concentrations (10-500 mg/L). The pH of suspensions was kept as natural. After being covered with parafilm, to keep the reaction temperature at 298, 308, and 318 K, the flasks were shaken at 120 rpm in a thermostatic shaker. At the end of the contact time (24 h), the suspensions were filtered through Whatman™ 1822-047 Grade GF/C filter paper (diameter: 4.7 cm, pore size: 1.2 µm), and the filtrates were analyzed to identify the phosphorus concentration.

E. Desorption and regeneration studies

After adsorption, the spent adsorbent (0.5 g) was separated from the solution by filtration through Whatman™ 1822-047 Grade GF/C filter paper (diameter: 4.7 cm, pore size: 1.2 μm). The phosphorus bearing adsorbent was washed lightly with tap water and then with distilled water to eliminate unbound phosphorus. The desorption was performed with five categories of elution solutions, including 0.2 M NaOH, 0.05 M NaOH, pH 12 distilled water, 0.1 M NaCl, and 0.1 M HCl. The solid was placed into five conical flasks of 250 mL, containing 50 ml of each elution solutions. The mixtures were agitated on an orbital shaker at the speed of 120 rpm, room temperature for 24 h. After that, the solid was removed from the solution by filtration again. The filtrates were used to measure the desorbed phosphorus concentration. Based on the desorption results, the best elution solution was selected and applied for generation studies.

After desorption test, the exhausted adsorbent was repeatedly utilized for other four adsorption - desorption cycles, with or without being activated by 100 mL of 0.1 M HCl. The phosphorus removal percentage was used to determine the reusability of the adsorbent.

F. Calculation of the batch adsorption parameters

The batch isotherm and kinetic parameters are usually determined by linear regression method in Microsoft Excel. However, different results can be obtained from various types of linear isotherm and kinetic equations. It leads to a difficulty in comparing several studies in the case of lacking information on the type of equations applied. Conversely, the use of nonlinear regression method in Curve Expert Professional 2.0.4 brings a unique result and thus overcomes the above limitations of the conventional calculation.

3.2.3 Phosphorus removal by ZLO in column mode experiments

A. Lab scale reactor

(i) Adsorption tests with synthetic solution

The column adsorption tests were conducted in glass mini-columns of 120 cm height and 1.75 cm inner diameter. To begin with, ZLO was stirred thoroughly with distilled water to enable the swelling and removing air bubbles. In the next step, it was packed into a column using the "slurry method" (Zach-Maor et al., 2011). The column was first filled with glass beads (~11 cm) at the bottom to produce an even flow. It was then packed with wet ZLO, followed by another layer of glass beads (~11 cm) and a

piece of sponge to prevent ZLO from seeping out with the effluent. The column was packed with a certain amount of ZLO (5, 10, 15 g) to achieve the desired bed height (11.5, 23 and 34.5 cm). The feed solution containing various phosphorus concentrations (5.5, 10.2, and 15.5 mg/L), was percolated through the column in the upward direction at different flow rates (12, 20, and 28 mL/min) by peristaltic pumps. Effluent samples were collected at definite intervals of time in 14 mL plastic tubes for determination of the phosphorus concentration.

(ii) Adsorption test with the real municipal wastewater

The ability of ZLO packed bed column for phosphorus removal from municipal wastewater was evaluated with the same mini-column as above. Municipal wastewater secondary effluent was collected from Sydney Olympic Park Wastewater Treatment Plant. Prior to the adsorption test, the municipal wastewater was settled for 24 h, filtered using a 150 μm sieve, and used for column adsorption tests without any pH alterations. The wastewater was percolated through the column from the bottom at the flow rate of 12 mL/min. The concentrations of phosphorus and major quality parameters of the solutions before and after passing through the column were determined according to standard procedures.

(iii) Desorption and regeneration tests with real municipal wastewater

Desorption and regeneration tests were performed with the same mini-columns as in adsorption. 0.2 M NaOH was chosen as desorption solution while 0.1 M HCl was used for regeneration since these solutions were proven to be effective in the previous batch experiments (Nguyen et al., 2014a). Prior to desorption, phosphorus loaded ZLO was rinsed with 300 mL distilled water at a flow rate of 12 mL/min to remove residual phosphorus. 0.2 M NaOH solution was then pumped upward through the column at a flow rate of 12 mL/min until the phosphorus concentration of the effluent reached 5 mg/L. The desorbed ZLO column was washed with 1000 mL of distilled water at a volumetric flow rate of 36 mL/min. Next, it was reactivated with 1000 mL of 0.1 M HCl at a flow rate of 12 mL/min. After that, it was washed with 1000 mL of distilled water at a flow rate of 36 mL/min. The regenerated ZLO column was reused for the next cycle of adsorption - desorption. Three cycles were continuously implemented.

B. Semi-pilot scale reactor

(i) Adsorption test with real municipal wastewater

The dynamic adsorption test was conducted using a large scale glass column (4.5 cm internal diameter × 120 cm height). The raw municipal wastewater was collected from Sydney Olympic Park Wastewater Treatment Plant, Australia. After being settled for 24 h and screened with a 150 μm sieve, the wastewater was percolated through the column in the upward direction at a flow rate of 53 mL/min using a peristaltic pump (Masterflex® Console Drive, Model No. 77521-47, Cole-Parmer Instrument Company). The column was backwashed every 24 h in the upward direction at a flow rate of 200 mL/min for 30 min each time to prevent column clogging. The effluent samples were collected at pre-determined intervals in 14 mL plastic tubes for the analysis of phosphorus concentration.

(ii) Desorption test with real municipal wastewater

After adsorption, the ZLO packed bed column was rinsed with the tap water at a flow rate of 53 mL/min for 1 h to remove the residual phosphorus from adsorption test. The elution test was then carried out using 0.2 M NaOH at a flow rate of 13.5 mL/min for 5 h. The effluent samples were collected in a 14 mL plastic tube for measurement of phosphorus and other quality parameters. After desorption, the exhausted ZLO bed was taken out of the column and impregnated into 1 L of 0.1 M HCl for 3 h for activation. After being washed with the distilled water, the activated ZLO was packed into the column again for the next adsorption cycle. The column experimental set-up is shown in Fig.3.4 as the follows:

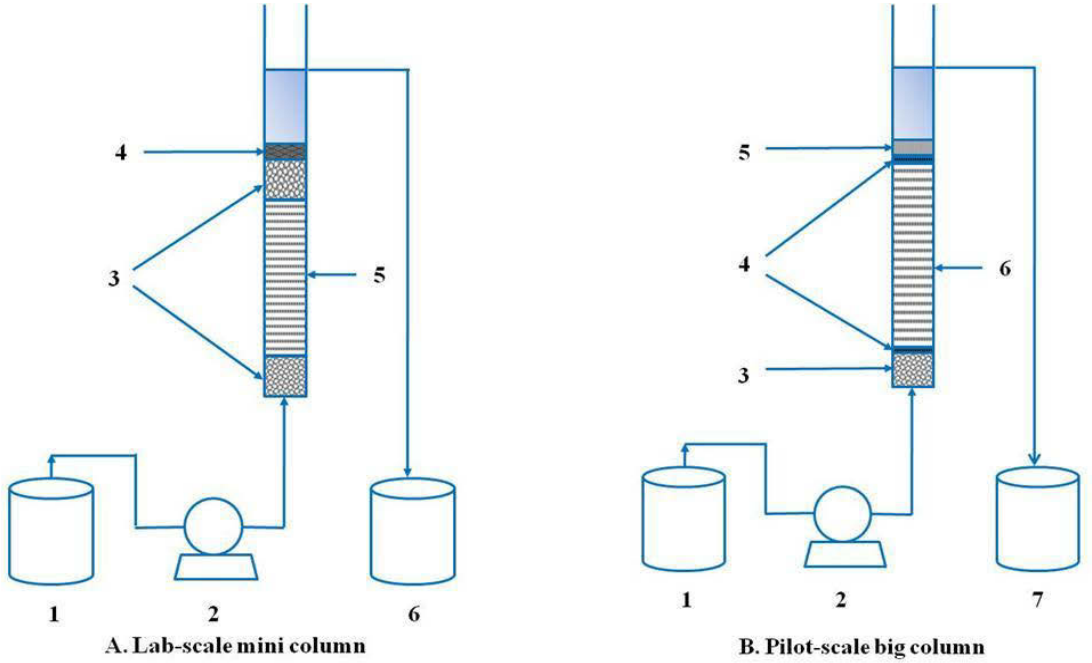

Figure 3.4 Design of the fixed-bed column tests

A. Lab-scale mini column: 1. Feed tank, 2. Peristaltic pump, 3. Glass beads, 4. Sponge pad, 5. ZLO bed, 6. Effluent storage tank

B. Semi-pilot scale big column: 1. Feed tank, 2. Peristaltic pump, 3. Glass beads, 4. Stainless steel sieve, 5. Sponge pad, 6. ZLO bed, 7. Effluent storage tank

C. Column scale-up calculations

Step 1: Estimate superficial velocity for the full-scale column:

$$v_{LC} = v_{SC} = \frac{Q_{SC}}{A_{SC}} = \frac{12\ cm^3 mL^{-1}}{2.4\ cm^2} = 4.99\ cm/min$$

$$v_{LC} = 4.99\ cm/min$$

Step 2: Estimate bed depth for the full-scale column:

$$\frac{D_{SC}}{H_{SC}} = \frac{D_{LC}}{H_{LC}} \rightarrow H_{LC} = D_{LC} = \frac{H_{SC}}{D_{SC}} * D_{LC} = \frac{23\ cm}{1.75\ cm} * 4.5\ cm = 59.14\ cm$$

$$H_{LC} = 59.14\ cm$$

Step 3: Estimate bed volume for the full-scale column:

$$V_{BLC} = A_{LC} * H_{LC} = \pi r_{LC}^2 * H_{LC} = 3.14 * (4.5/2)^2\ cm^2 * 59.14\ cm = 940.10\ cm^3$$

$$V_{BLC} = 940.10\ cm^3$$

Step 4: Estimate adsorbent weight for the full-scale column:

$$d_{LC} = \frac{m_{LC}}{V_{LC}} \rightarrow m_{LC} = V_{LC} * d_{LC} = V_{LC} * d_{SC} = V_{LC} * \frac{m_{SC}}{V_{SC}} = 940.10\ cm^3 * \frac{10\ g}{55.29\ cm^3} = 170\ g$$

$$m_{LC} = 170\ g$$

Step 5: Estimate volumetric flow rate for the full-scale column:

$v_{LC} = \frac{Q_{LC}}{A_{LC}} \rightarrow Q_{LC} = v_{LC} * A_{LC} = v_{LC} * \pi r_{LC}^2$ = 4.99 cm/min * 3.14* $(4.5/2)^2$ cm^2 = 79.32 cm^3/min = 79.32 mL/min = 4.76 L/h

Q_{LC} =4.76 L/h

Step 6: Estimate empty bed contact time (EBCT) for the full-scale column:

$EBCT_{LC} = \frac{H_{LC}}{v_{LC}} = \frac{59.14\ cm}{4.99\ cm/min}$ = 11.85 min

$EBCT_{LC}$ = 11.85 min

Step 7: Estimate service time at 10% breakthrough for the full-scale column:

$t_{LC} = \frac{H_{LC}N_o}{C_o v_{LC}} - \frac{1}{K_b C_o} \ln(\frac{C_o}{C_b} - 1)$ = 31.50 h

where, C_o = 5.5 mg P/L, C_b = 0.55 mg P/L, v = 4.99 cm/min, H = 59.14 cm, N_o and K_b values previously determined from BDST model at 10% breakthrough were 16.69 mg/L and 0.0897 L/(mg h), respectively (Table 6.3).

t_{LC}= 31.50 h

Step 8: Estimate treated water volume at 10% breakthrough for the full-scale column:

$V_{WLC} = Q_{LC} * t_{LC}$ = 4.76 L/h * 31.50 h = 149.94 L

V_{WLC} = 149.94 L

Step 9: Estimate adsorbent exhaustion rate for the full-scale column:

$AER = \frac{m_{LC}}{V_{WLC}} = \frac{170\ g}{149.94\ L}$ = 1.14 g/L

AER = 1.14 g/L

D. Calculation of breakthrough curve parameters

To evaluate the adsorption performance of a column, it is necessary to analyze the breakthrough curve. It can be done by calculating breakthrough curve parameters.

The breakthrough time (t_b) and treated volume at breakthrough time (V_b) are determined as the time and volume when the outlet phosphorus concentration (C_t) reached 10% of the inlet phosphorus concentration (C_t/C_o = 0.1). Similarly, the exhaustion time (t_s) and treated volume at exhaustion time (V_s) are defined as the time and volume when the outlet phosphorus concentration (C_t) reached 90% of the inlet phosphorus concentration (C_t/C_o = 0.9).

The total amount of phosphorus adsorbed onto ZLO column, q_{total} (mg) and the dynamic adsorption capacity, q_e (mg/g) are calculated according to the following equations (Paudyal et al., 2013; Sharma and Singh et al., 2013):

$$q_{total} = \frac{Q}{1000} \int_{t=0}^{t=total} C_{ad} dt \quad (3.7)$$

$$q_e = \frac{q_{total}}{M} \quad (3.8)$$

where t_{total}, Q, M, and C_{ad} are the total time for the column to reach saturation (min), volumetric flow rate (mL/min), the amount of ZLO packed in the column (g), and the difference in the phosphorus concentration at the initial time and the t time caused by adsorption (mg/L), respectively.

The eluted amount of phosphorus (EAP) is calculated by the following equation (Awual and Jyo, 2011):

$$EAP\ (mg/g) = (1/m) \sum_{q=1}^{n2} C_q V_q \quad (3.9)$$

where C_q, V_q, and n2 are the effluent phosphorus concentration, volume of the q-th fraction, and number of the last fraction in the desorption experiment.

The mass transfer zone (MTZ), which is defined as the length of the adsorption zone in the column, can be obtained from the following equation (Bulgariu and Bulgariu, 2013):

$$MTZ = H \frac{(t_s - t_b)}{t_s} \quad (3.10)$$

where MTZ represents the length of the mass transfer zone (cm); H is the bed height (cm); t_b is the breakthrough time (min); t_s is the exhaustion time (min).

The empty bed contact time (EBCT) in the column (min) is achieved from the ratio of bed volume (mL) to the flow rate (mL/min) as follows (Ohura et al., 2011):

$$EBCT = \frac{Bed\ volume}{\text{Flow rate}} \quad (3.11)$$

3.2.4 Recovery of phosphorus as MAP

A. MAP synthesis

The phosphorus source used for MAP crystallization in this work was the desorption solution. The MAP crystallization tests were performed to evaluate the effect of solution pH (9.0, 9.5, and 10.0). Three different P: N: Mg molar ratios (1:1:1, 1:1.5:1.5, and 1:2:2) were investigated. In addition, the MAP crystallization was evaluated using different chemical sources (NH_4Cl + $MgCl_2.6H_2O$ and $(NH_4)_2SO_4$ + $MgSO_4.7H_2O$). The influence of reaction temperature (8 °C and 22 °C) on the MAP crystallization was also examined.

The crystallization reactor in this study was a glass baker with a volume of 2 L. The changeable composition of municipal wastewater may lead to the unstable composition of desorption solution. To ensure a constant concentration of phosphorus

when investigating effects of crystallization conditions, desorption solution was accumulated to an adequately large volume, and then was divided equally. The agitation was conducted by a magnetic stirrer (S.E.M. ISAJ Pty Ltd, No 579, Australia) with a paddle of 7.5 cm length 2.5 cm width, and 30 cm height. The weights of magnesium and ammonium salts were determined from the phosphorus concentration in the desorption solution, based on the P: Mg: N molar ratio. Desorption solution was vigorously stirred at 200 rpm for 0.5 h to remove the dissolved CO_2. The pH of desorption solution was adjusted to around 8 using H_2SO_4 98% to prevent NH_3 evaporation or Mg precipitation. To avoid the formation of magnesium phosphate, NH_4Cl was added to desorption solution before $MgCl_2.6H_2O$. The solution was stirred slowly to dissolve NH_4Cl and $MgCl_2.6H_2O$ completely. Afterwards, the pH of solution was raised to the expected value for MAP crystallization using 5 M NaOH. The mixture was stirred at 200 rpm for 30 min, followed by settling for another 30 min. After that, the mixture was used for determination of the residual phosphorus, magnesium, and ammonium. Ultimately, the suspension was filtered through 1.2 μm filter paper and washed with Milli-Q water seven times to eliminate the residual salts like NH_4Cl. The precipitate was dried in the oven at 40 °C for 24 h.

B. Evaluation of the harvested MAP

(i) Crystal characterization

The elemental analysis of the harvested precipitate was conducted by the dissolution method (Hao et al., 2008; Perera et al., 2007). Accordingly, 0.2 g of the precipitate was dissolved in 10 mL of 32% hydrochloric acid and then diluted to 1 L with Milli-Q water. The mixture was stirred continuously at 200 rpm for 1 h prior to the analysis of Mg^{2+}, NH_4^+-N, and PO_4^{3-}-P.

The crystal structure of the recovered precipitate was characterized by Siemens D5000 X-ray Diffractometer (XRD). The morphology of the harvested precipitate was examined by Zeiss Evo LS15 SEM (Germany). The FTIR pattern of the reclaimed precipitate was recorded on an IRAffinity-1 Fourier Transform Infrared Spectrophotometer, Shimadzu Corporation (Japan).

(ii) MAP purity evaluation

In this study, the MAP purity was evaluated by a method adapted from Hao et al. (2008). This method also includes two major steps as suggested by Hao et al. (2008), which are (1) dissolution of the precipitate followed by (2) elemental analysis of the

obtained solution. However, considering the fact that ammonium (NH_4^+) compound used for the crystallization reaction may be left in the harvested precipitate, this study suggested that MAP purity should be determined according to the minimum molar number of MAP components.

(iii) The P-bioavailability

The P-bioavailability of the recovered precipitate was evaluated by its solubility in the 2% citric acid (Nur, 2014). The solution was prepared by dissolving 0.3 g of the precipitate with 100 mL of 2% citric acid in a glass flask. The flask was placed on a flat shaker at a speed of 120 rpm for 2 h at room temperature. After filtration with 1.2 µm filter paper, the solution was utilized for phosphorus measurement.

3.2.5 Analytical methods and instruments

Phosphate (PO_4-P), nitrate (NO_3-N), nitrite (NO_2-N), and ammonium (NH_4-N) were analyzed spectrophotometrically using Spectroquant® NOVA 60, Merck (Germany). Chloride (Cl^-) was measured using 790 Personal IC, Metrohm (USA). Magnesium (Mg^{2+}), calcium (Ca^{2+}) zirconium (Zr^{4+}) and heavy metals were determined by 4100 MP-AES Spectrometer (Microwave Plasma-Atomic Emission Spectrometry), Agilent Technologies (USA). The pH and conductivity were measured by Hach HQ40d Multi meter. The chemical oxygen demand (COD) analysis was carried out with Hach DR/2000 Spectrophotometer. The total organic carbon (TOC) measurement was conducted using Multi N/C 3100, Analytik Jena AG. The total suspended solid (TSS) determination was done in accordance with the standard method. The images of instruments used in this study are given as follows.

Figure 3.5 Analytical instruments: a) SA7 vortex mixer and b) Spectroquant® NOVA 60, Merck, Germany

Figure 3.6 Analytical instruments: a) Zeiss Evo LS15 SEM, Germany, b) IRAffinity-1 Fourier Transform Infrared Spectrophotometer, Shimadzu Corporation, Japan, and c) Siemens D5000 X-ray Diffractometer

Figure 3.7 Analytical instruments: a) 790 Personal IC, Metrohm, USA, and b) 4100 MP-AES Spectrometer, Agilent Technologies, USA

3.2.6 Statistical analysis

Experiments were implemented in triplicate, and the data represented the mean values. The highest deviation was limited to 5%. The error bars indicating the standard deviation were shown in figures wherever possible.

3.3 GENERAL EXPERIMENTAL PROCEDURE

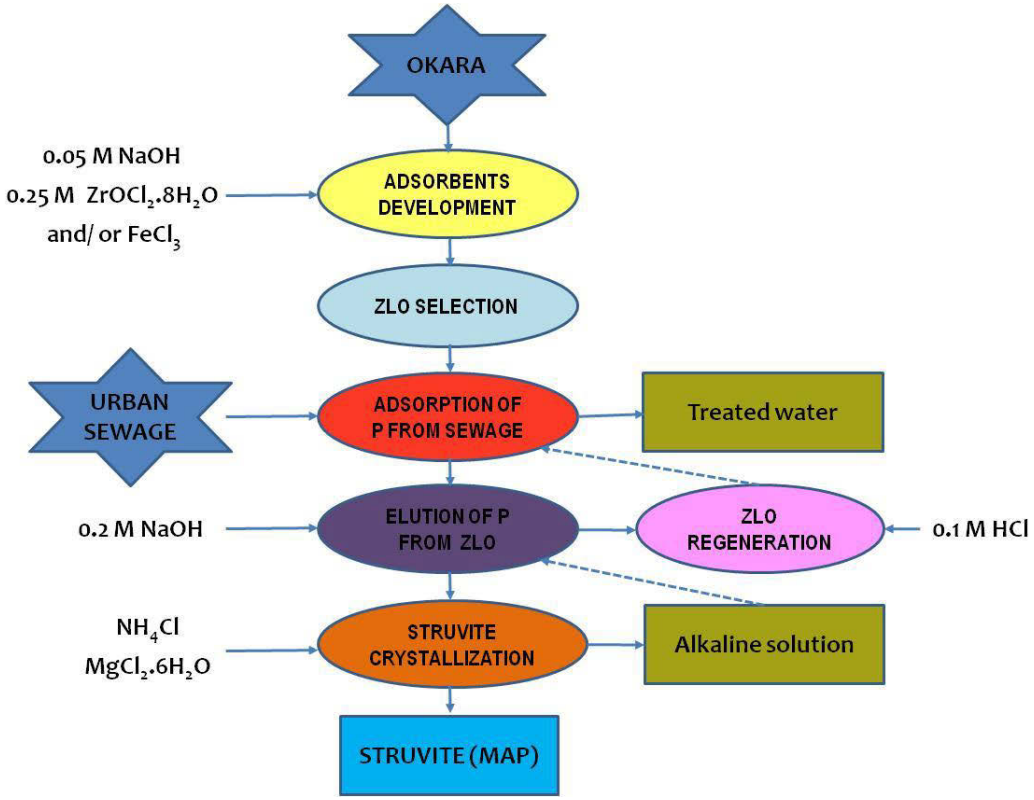

Figure 3.8 Diagram of P recovery from municipal wastewater by adsorption onto ZLO coupled with crystallization as MAP

UNIVERSITY OF TECHNOLOGY, SYDNEY

CHAPTER 4

DEVELOPMENT OF METAL LOADED OKARA AS PHOSPHORUS ADSORBENTS

4.1 INTRODUCTION

4.1.1 Research background

The success of adsorption process relies on the selection of a proper adsorbent. The most important criteria for selecting an adsorbent are adsorption capacity, reuse, local availability, compatibility, kinetics and cost (Gupta, 2011). The adsorbent characterized by low-cost and high adsorption capacity should be selected to meet both economic and technical requirements (Zhang et al., 2014).

The agricultural by-products in natural forms have very poor phosphorus adsorption capacities. However, the adsorption capacity of these materials can be improved by activation or surface modification. The activation consists of chemical activation or physical activation. The physical activation is carried out by oxidation of the material at high temperatures while chemical activation involves the carbonization followed by activation. After the activation, the porous structure of the materials has been improved by increasing the pore volume. Surface modification can significantly improve the adsorption capacity of an adsorbent by incorporating functional groups on the surface of the material. This can be done via metal loading (Biswas, 2008; Carvalho et al., 2011; Mallampati and Valiyaveettil, 2013) or quaternization (Benyoucef and Amrani, 2011a; De Lima et al., 2012; Karachalios, 2012; Zhang et al., 2012). The grafted functional groups play a role of adsorption sites for sequestering phosphate from aquatic medium (Krishnan and Haridas, 2008).

Previous studies have showed that the compounds of multi valence metals have a high affinity for anions, including phosphate (Ruixia, 2002). In addition, metal loading method is quite simple and efficient (Nguyen et al., 2014b). Hence, in the recent time, the development of phosphorus adsorbents from agricultural by-products using metal loading method has received considerable attention from adsorption researchers. The metal loaded phosphorus adsorbents include Fe^{3+} loaded sawdust (Unnithan et al., 2002), Zn^{2+} loaded coir pith activated carbon (Namasivayam and Sangeetha, 2004), La^{3+} loaded juniper fiber (Shin et al., 2005), Fe^{3+} loaded coir pith (Krishnan and Haridas, 2008), Zr^{4+}, La^{3+}, Ce^{3+}, and Fe^{3+} loaded orange waste gels (Biswas, 2008), Fe^{3+} loaded egg shell (Mezenner and Bensmaili, 2009), Zr^{4+} loaded apple peels (Mallampati and Valiyaveettil, 2013), Fe^{2+} loaded bagasse fiber (Carvalho et al., 2011). The prevailing adsorption mechanism for these metal loaded adsorbents is the formation of an inner-sphere complex between phosphate ions and the loaded metals (Boyer et al.,

2011). To date, several phosphorus adsorbents have been developed from AWBs using metal loading method. However, there are still lack of adsorbents that meet the following criteria: (1) owing an adequate mechanical strength, (2) retaining the adsorption capacity after several cycles of operation, and (3) efficiently removing phosphate in the column mode with the space velocity of more than 50 h^{-1} (Awual and Jyo, 2011).

4.1.2 Objectives of Chapter 4

This study aims to develop innovative, cost-effective and green phosphorus adsorbents from the soybean by-product (okara) using metal loading method. Okara was loaded with single or combined metal (Fe^{3+}, Fe^{3+}/Zr^{4+}, and Zr^{4+}) solutions to form positively charged functional groups. With the presence of these binding groups, metal loaded okara is expected to eliminate efficiently phosphate from wastewater. Of three developed adsorbents, the most potential one was selected, considering adsorption capacity, desorption and regeneration abilities, and metal leaching. The modification method was then further optimized. Finally, the selected adsorbent was characterized using SEM-EDS, FTIR, elemental analysis, and other methods. A major part of Chapter 4 was published in the two following papers:

3) **Nguyen, T.A.H.,** Ngo, H.H., Guo, W.S., Zhang, J., Liang, S., Tung, K.L., 2013. Feasibility of iron loaded 'okara' for biosorption of phosphorus in aqueous solutions. *Bioresour. Technol.* 150, 42-49.
4) **Nguyen, T.A.H.,** Ngo, H.H., Guo, W.S., Nguyen, T.V., Zhang, J., Liang, S., Chen, S.S., Nguyen, N.C., 2014. A comparative study on different metal loaded soybean milk by-product 'okara' for biosorption of phosphorus from aqueous solution. *Bioresour. Technol.* 169, 291-298.

4.2 SELECTION OF THE POTENTIAL ADSORBENT FROM THREE DEVELOPED METAL LOADED ADSORBENTS

In this study, three categories of metal loaded okara were developed, namely iron-loaded okara (ILO), iron/zirconium-loaded okara (IZLO), and zirconium-loaded okara (ZLO). Among them, the best adsorbent was selected using the major selection criteria, which included high adsorption capacity, high desorption and regeneration abilities, and

marginal metal leaching level. These properties of ILO, IZLO, and ZLO are evaluated in detail as follows.

4.2.1 Phosphate adsorption capacity

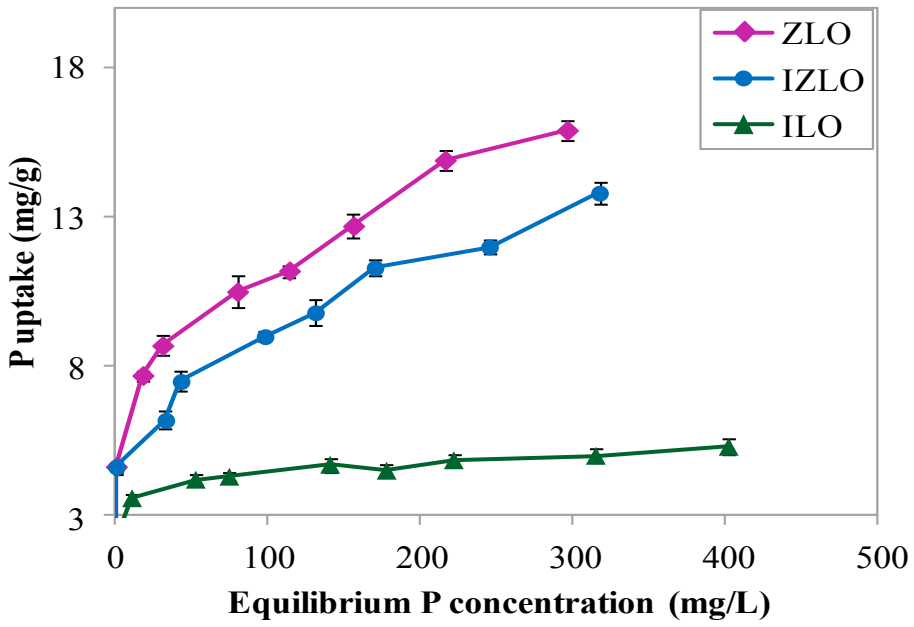

Figure 4.1 Isotherm of P adsorption by ILO, IZLO, ZLO (Adsorbent particle size = 150-300 µm, pH = 7.6 ÷ 7.8, C_i = 10 ÷ 500 mg P/L, adsorbent dose = 10 g/L, shaking speed = 120 rpm, temperature = 298 K, contact time = 24 h. The standard deviation values = 0.04÷0.52 mg/g for sample size N = 3)

The maximum PO_4^{3-} adsorption capacity (q_m) of ILO, IZLO, and ZLO was determined from Langmuir equation. It was found that ZLO had the highest q_m value (47.88 mg/g), followed by IZLO (40.86 mg/g) and ILO (16.39 mg/g). The q_m value of the natural okara was 2.45 mg/L. The results indicate that the phosphate adsorption capacities of ZLO, IZLO, and ILO were increased 19.54, 16.68 and 6.69 times, respectively compared to the natural okara. Evidently, loading of the natural okara with multi valence metals, such as Fe^{3+} and Zr^{4+}, was an efficient means to enhance its PO_4^{3-} sequestering ability. Table 4.1 summarizes the q_m values of various biosorbents for the comparison purpose. Table 4.1 reveals that IZLO and ZLO possessed relatively high q_m values, which were favorably comparable to most of the biosorbents in the literature. Biswas et al. (2008, 2007) claimed that, the adsorption of phosphate by metal loaded biosorbents was possibly due to a ligand exchange mechanism, which occurred between PO_4^{3-} ions in the solution and OH^- ions coordinated with the metal ions deposited on the biosorbents. They suggested that, loaded metal ions could be readily converted into

hydrated forms, such as $[Ln(H_2O)_n]^{3+}$, $[Zr_4(OH)_8(H_2O)_{16}]^{8+}$, and $[Zr_8(OH)_{20}(H_2O)_{24}]^{12+}$ species, with the abundant amounts of OH^- ions and H_2O molecules. During the hydrolysis, H_2O molecules were deprotonated by releasing H^+ ions to form exchangeable OH^- ions, which could be replaced by PO_4^{3-} ions via the ligand exchange mechanism. From the data obtained, it is proved that among three developed adsorbents, ILO displayed a far too low adsorption capacity of PO_4^{3-} compared to IZLO and ZLO. Thus, only IZLO and ZLO will be further investigated in the next desorption and regeneration tests.

Table 4.1 Comparing ILO, IZLO, and ZLO with other metal loaded adsorbents in the literature in term of PO_4^{3-} adsorption capacity

Bio-adsorbents	Initial concentration (mg PO_4/L)	pH	Adsorbent dose (g/L)	Max. adsorption capacity (mg PO_4/g)	Reference
Zr^{4+} loaded orange waste gels		7.0	1.67	175	Biswas et al., 2008
Fe^{2+} impregnated bagasse fiber	2-10	-	-	152	Carvalho et al., 2011
Fe^{2+} treated aspen wood fiber	-	4.8	2	4.3	Eberhardt et al., 2006
Fe^{2+} modified wood	0-100		4	17.38	Eberhardt and Min, 2008
Mine drainage treated juniper fiber	30.64	6.4	2-20	7.08	Han et al., 2005
Al^{3+} loaded skin split waste	47.5-285	7.0	1	21.65	Huang et al., 2009
Fe^{3+} loaded skin split waste	47.5-285	7.0	1	72	Huang et al., 2009
Fe^{3+} impregnated coir pith	20-200	3.0	2	70.92	Krishnan and Haridas, 2008
Zr^{4+} loaded apple peels	5-200	2-6	10	20.35	Mallampati and Valiyaveettil, 2013
Iron hydroxide eggshell	7-140	7.0	7.5	14.49	Mezenner and Bensmaili, 2009
Zn^{2+} activated coir pith carbon	10-40	3-10	6	5.10	Namasivayam and Sangeetha, 2004
Fe^{3+} loaded sawdust	9.50-23.75	2.5	2	28.79	Unnithan et al., 2001
Fe^{3+} loaded okara (ILO)	10-500	7.6-7.8	10	16.39	This study
Fe^{3+}/Zr^{4+}loaded okara (IZLO)	10-500	7.6-7.8	10	40.86	This study
Zr^{4+} loaded okara (ZLO)	10- 500	7.6-7.8	10	47.88	This study

4.2.2 Desorption and regeneration abilities

Desorption of phosphorus from an adsorbent paves the way to the recovery of this finite resource. Meanwhile, the regeneration of the adsorbent gives a change to reduce the cost of water treatment and minimize the adverse impacts on the environment. Therefore, desorption and regeneration abilities of an adsorbent are crucial to its practical application and need to be thoroughly examined.

Five desorption solutions were tested with ZLO to determine the best solution. The extremely low desorption percentage (<1%) for phosphorus was observed with both 0.1 M HCl and 0.1 M NaCl solutions. The distilled water with pH 12 and 0.05 M NaOH exhibited better desorption results, which were 49.45% and 70.76%, respectively. The highest desorption percentage, reaching up to 97.8%, was achieved with 0.2 M NaOH. The result was consistent with a previous study conducted by Unnithan et al. (2001), reporting that desorption efficiency of 96.8% was attained with 0.1 M NaOH. The high efficacy of NaOH can be explained by the replacement of PO_4^{3-} anions adsorbed on ZLO by OH^- ions from NaOH solution. The results also suggested that ion exchange might be a dominant mechanism for the adsorption of PO_4^{3-} onto ZLO.

Due to the most satisfactory result with ZLO, 0.2 M NaOH was employed in the regeneration tests with both IZLO and ZLO. Fig.4.2 represents the regeneration results of non-activated ZLO and IZLO, which were not subjected to any treatment after desorption tests. It was well observed that the adsorption and desorption performances of both ZLO and IZLO were dropped dramatically from the second cycle. After five cycles, the phosphorus adsorption and desorption efficiencies of ZLO were reduced by 46.74% and 68.30%, respectively. The corresponding values for IZLO were 42.93% and 64.83%. The desorption efficiency of ZLO and IZLO in the fifth cycle was just around 25%, which was too low for any application. It can be assumed that as a result of desorption of phosphorus from ZLO and IZLO with 0.2 M NaOH, the pH of the adsorption solution in the next cycle was increased. Due to unfavorable pH condition, the retention of PO_4^{3-} by these adsorbents was hindered.

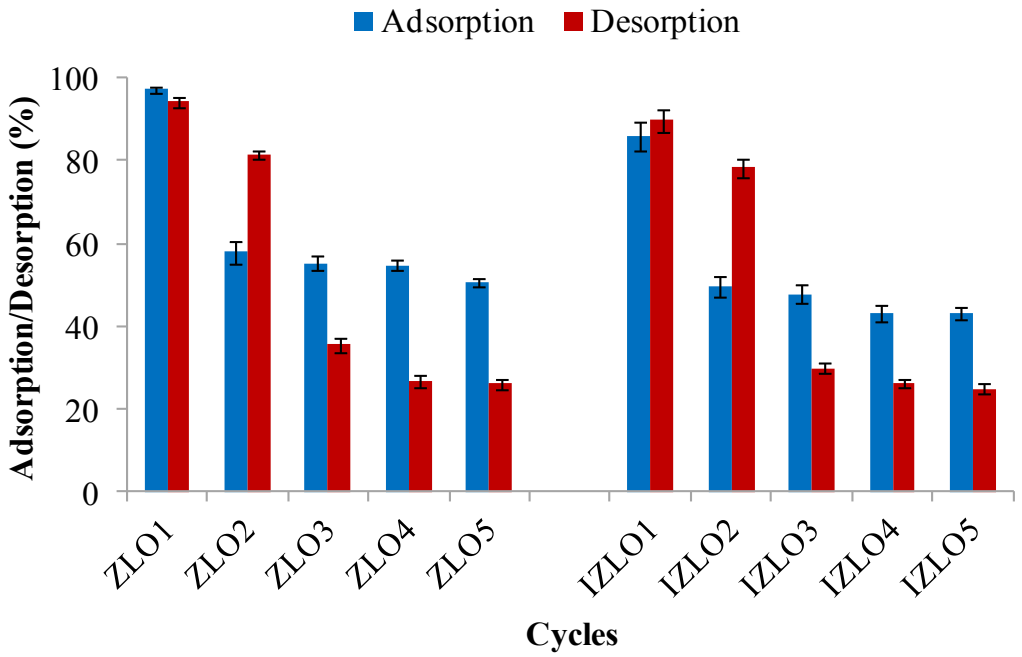

Figure 4.2 The P adsorption and desorption efficiencies of non-activated ZLO and IZLO in 5 consecutive cycles (C_i = 50 mg P/L, adsorbent dose = 10 g/L, shaking speed = 120 rpm, temperature = 298 K, contact time = 24 h. The standard deviation values = 0.70÷3.49% for sample size N = 3)

The above assumption was examined by conducting regeneration tests with 0.1 M HCl activated ZLO and IZLO (Fig. 4.3). As can be seen in Fig. 4.3, the adsorption and desorption performances of activated ZLO and IZLO were significantly improved compared to their non-activated counterparts. After five cycles, the phosphorus adsorption and desorption efficiencies of ZLO were reduced by only 12.46% and 7.40%, respectively. The corresponding values for IZLO were 21.91% and 17.45%. The pH values of the adsorption solutions with activated ZLO and IZLO were around 7.5, whereas those with non-activated ZLO and IZLO were above 10. The results validate the hypothesis that low efficiencies of non-activated ZLO and IZLO in the next adsorption cycle resulted from the use of a concentrated base (0.2 M NaOH) for the previous desorption cycle. Based on this, it would seem that 0.2 M NaOH can be used for desorption of phosphorus from ZLO and IZLO provided that the spent adsorbents be activated with 0.1 M HCl before the next adsorption cycle. Due to a significant reduction in the efficiency of IZLO after five cycles of adsorption-desorption, IZLO cannot repeatedly be used for a long time. On the contrary, the phosphorus adsorption and desorption efficiencies of ZLO remained about 85% after five consecutive cycles of

operation. The result indicates a high reusability of ZLO for phosphorus elimination from aqueous solutions.

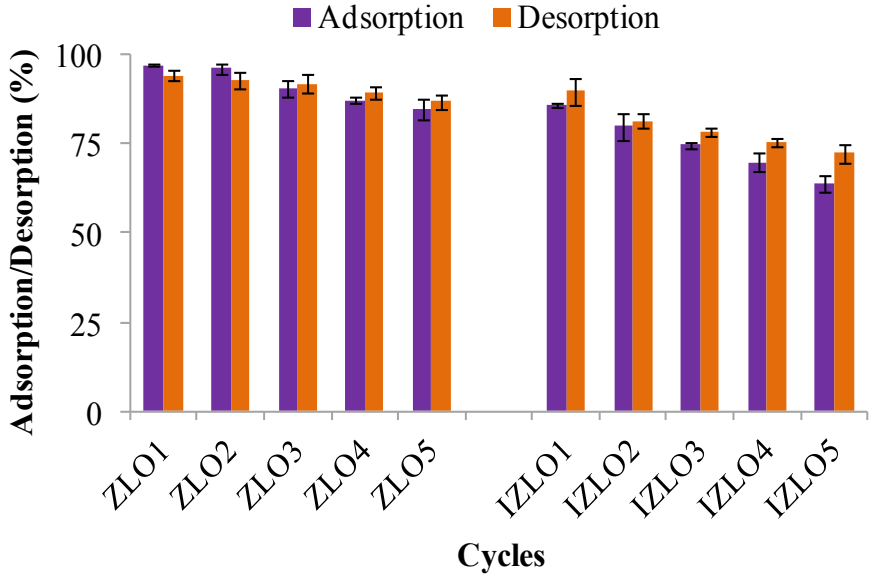

Figure 4.3 The P adsorption and desorption efficiencies of activated ZLO and IZLO in 5 consecutive cycles (C_i = 50 mg P/L, adsorbent dose = 10 g/L, shaking speed = 120 rpm, temperature = 298 K, contact time = 24 h. The standard deviation values = 0.29 ÷ 3.97% for sample size N = 3)

4.2.3 Metal leaching from metal loaded adsorbents during adsorption and desorption tests

The leakage of metal, which was earlier loaded on an adsorbent, is evidence for the instability of the adsorbent. It was found that, there was no Zr bleeding from ZLO during adsorption and elution tests. The result provides strong evidence that ZLO is chemically stable and durable. A similar observation was noticed for Zr^{4+} in the case of IZLO. The results were in harmony with previous studies reporting that Zr^{4+} could hardly be detached from Zr^{4+} loaded adsorbents during their performance (Biswas et al., 2008; Mallampati and Valiyaveettil, 2013; Ohura et al., 2011). On the other hand, the release of Fe^{3+} from ILO during adsorption and desorption was found to be 1.59 mg/g and 3.30 mg/g, respectively. The corresponding values for IZLO were 0.54 mg/g and 0 mg/g. The result of Fe^{3+} detachment from ILO during adsorption test (1.59 mg/g) was quite similar to 1.65 mg/g previously reported by Eberhardt and Min (2008) for Fe^{2+} treated wood particles. Based on the results obtained here, ZLO was proven to be most stable and durable among three developed adsorbents. The vigorous leakage of metals

from ILO and IZLO may be a critical factor, limiting the extensive application of these adsorbents.

4.2.4 Selection of the best adsorbent among three developed ones

ZLO offered the highest adsorption capacity, which was equal or even better than several biosorbents reported in the literature. Additionally, ZLO could be recycled at least five times without a significant reduction in the phosphorus adsorption and desorption efficiencies. Moreover, Zr leakage from ZLO was not observed during its performance. As there is no need to reload ZLO with Zr after several cycles of adsorption - desorption, the cost of ZLO preparation may be minimized. The absence of Zr in the effluent convinces that the use of ZLO as a phosphorus adsorbent will not pose any risk to aquatic creatures. Conversely, the use of IZLO and ILO as phosphorus adsorbents suffered from significant limitations, such as a notable metal leakage, a fast drop in adsorption and desorption efficiencies after many cycles of operation. As a final remark, among three developed metal loaded adsorbents, ZLO was the best choice for the elimination of phosphorus from aqueous solutions.

4.3 EFFECTS OF THE METAL LOADING CONDITIONS ON THE PHOSPHATE ADSORPTION CAPACITY OF ZLO

This study examines effects of the concentration of NaOH and Zr^{4+} solution on the PO_4^{3-} adsorption capacity of ZLO. The adsorbents were prepared at three different modification conditions as follows: ZLO-A: 0.05 M NaOH + 0.25 M Zr^{4+}, ZLO-B: 0.05 M NaOH + 0.5 M Zr^{4+}, and ZLO-C: 0.5 M NaOH + 0. 5 M Zr^{4+}. The isotherm study was conducted with ZLO-A, ZLO-B, and ZLO-C at the same adsorption condition to compare their PO_4^{3-} adsorption capacities. Fig.4.4 shows the P uptake by these adsorbents. It can be seen from the figure that ZLO-C exhibited the highest P adsorption capacity (19.61 mg/g), followed by ZLO-B (16.95 mg/g) and ZLO-A (15.13 mg/g). The P adsorption capacity of ZLO-B increased by 12.03% as compared to that of ZLO-A. It can be attributed to the acceleration of Zr^{4+} concentration by 2 times. Likewise, the P uptake capacity of ZLO-C was improved by 29.61% compared to ZLO-A. This may result from the augmentation of the concentrations of NaOH and Zr^{4+} solutions 10 and 2 times, respectively. Vázquez et al. (2012) suggested that NaOH increased the hydrolysis, swelling and dissolving some components of adsorbents. The additional OH^- groups increased the binding between NaOH treated okara and positively charged Zr^{4+}

metal ions. The larger the amount of Zr^{4+} deposited on the surface of ZLO, the more the positively charged sites are available, thus enabling the retention of PO_4^{3-} anions. The superior adsorption capacity of ZLO-C can be explained by higher electrostatic interactions between cationic Zr^{4+} ions and PO_4^{3-} anions (Long et al., 2014). The adsorption capacity of ZLO-C was 19.61 mg P/g (~ 60.09 mg PO4/g), which was higher than that of many other AWBs derived adsorbents. It was well observed that the higher the concentration of NaOH and Zr^{4+} applied, the better the phosphate adsorption capacity of ZLO could be obtained. The results indicated that both NaOH and Zr^{4+} played important roles in boosting the PO_4^{3-} capture ability of ZLO. However, considering the economic and technical feasibility, the optimum metal loading condition was selected to be 0.05 M NaOH + 0.25 M Zr^{4+} solution. Thus, ZLO produced at this modification condition will be used in the next experiments.

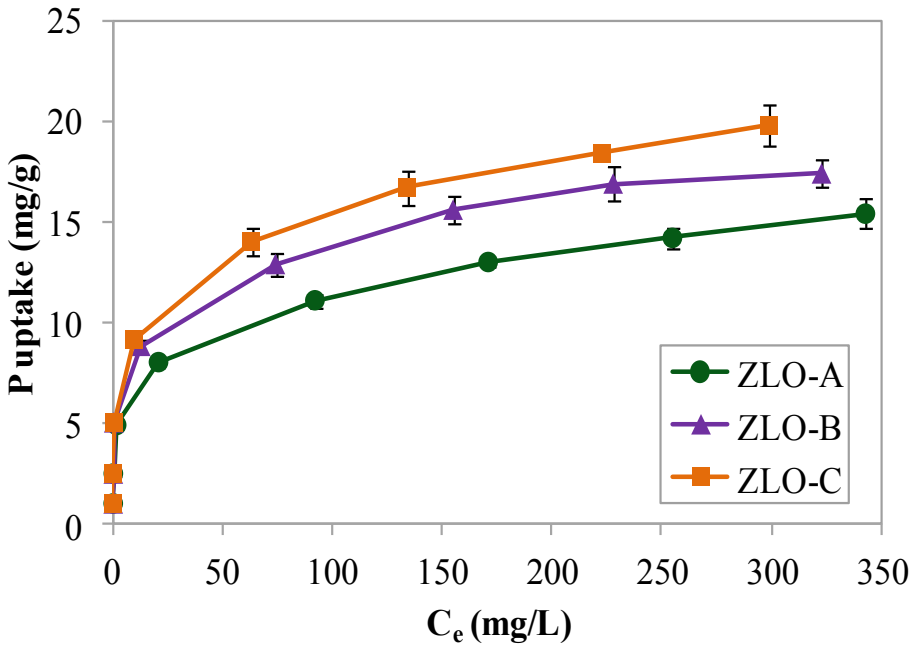

Figure 4.4 Effect of metal loading conditions on the P uptake of ZLO (ZLO particle size = 300-425 µm, pH = 7 ÷ 7.5, C_i = 10 ÷ 500 mg P/L, ZLO dose = 10 g/L, shaking speed = 120 rpm, temperature = 298 K, contact time = 24 h. The standard deviation values = 0.04-0.98 mg/g for sample size N = 3)

4.4 RECYCLING OF THE LOADING METAL (Zr^{4+}) SOLUTION

The recycling of Zr^{4+} solution was conducted by maintaining the volume of Zr^{4+} solution a constant, while compensating for the Zr^{4+} deficiency caused by Zr^{4+} adsorption onto okara and ZLO washing with the tape water. The additional

$ZrOCl_2.8H_2O$ salt was calculated based on the Zr adsorption capacity of NaOH-treated okara (300-150 μm) and the quantity of NaOH-treated okara employed.

To evaluate the feasibility of Zr^{4+} recycling, this study made a comparison in the P removal percentage between ZLO-1 and ZLO-2, which were prepared with the original and the recycled Zr^{4+} solutions, respectively (Table 4.2). As is shown by the table, ZLO-2 exhibited the same P removal percentage as ZLO-1 for the smallest particle size (300-150 μm). This finding proved that the amount of Zr^{4+} added to the cycle 2 was equal to the amount of Zr^{4+} adsorbed in the cycle 1. It also indicated that the Zr^{4+} reduction caused by washing Zr^{4+} loaded okara with the tap water was negligible. However, ZLO-2 demonstrated considerably higher P removal percentages than ZLO-1 for the larger particle sizes (1000-600, 600-425, 425-300 μm). It is recognized that the Zr^{4+} adsorption capacity of NaOH-treated okara is conversely proportional to its particle size. It means that the large particle sizes (1000-600, 600-425, 425-300 μm) of NaOH-treated okara will adsorb less Zr^{4+} ions than the small particle size (300-150 μm) to produce ZLO-1. Thus, when the addition of Zr^{4+} was implemented based on the Zr adsorption capacity of the small particle size (300-150 μm), the added Zr^{4+} was greater than Zr^{4+} adsorbed by large particle sizes (1000-600, 600-425, and 425-300 μm). Consequently, higher P removal percentages of ZLO were obtained with large particle sizes. The results demonstrated that the current recycling of Zr^{4+} solution, which calculated the additional amount of $ZrOCl_2.8H_2O$ based on the Zr adsorption capacity of the particle size range of 300-150 μm, was only applicable to this particle size range. Thus, the particle size range of 300-150 μm was used to produce ZLO with Zr^{4+} solution, which was recycled up to 10 times. The P removal percentages of ZLO-1 to ZLO-10 are displayed in Fig.4.5 for comparison purpose. It is evident from the figure that the repeated utilization of Zr^{4+} up to 10 times seemed to cause a minor loss (9.13%) in the P removal percentage of the recycled ZLO. The results proved that it was viable to recycle Zr^{4+} solution up to 10 times as long as the $ZrOCl_2.8H_2O$ addition was made based on the Zr adsorption capacity of the particular particle size applied.

Table 4.2 Comparison of the P removal percentage between ZLO-1 and ZLO-2

Particle size (μm)	1000-600	600-425	425-300	300-150
ZLO-1	87.24%	91.22%	94.06%	97.28%
ZLO-2	92.54%	94.79%	95.11%	97.11%

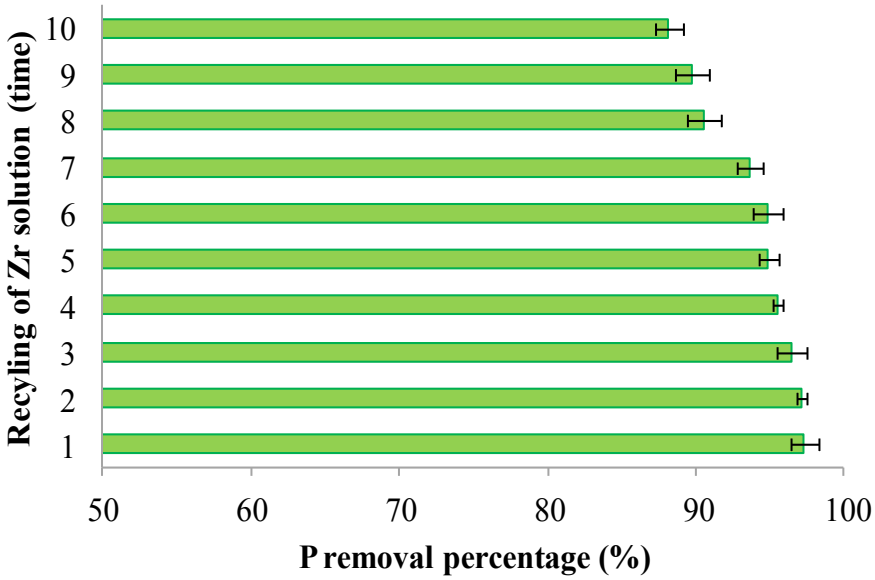

Figure 4.5 Comparison of the P removal percentage of ZLO prepared with Zr^{4+} recycled up to 10 times (The standard deviation values = 0.35-1.19% for sample size N = 3)

4.5 CHARACTERIZATION OF THE SELECTED ADSORBENT (ZLO)

4.5.1 Physical properties

The applicability of ZLO not only depends on the adsorption capacity, desorption ability and reusability but also relies on the physical characteristics of the material. The particle size distribution of ZLO is given in Fig.4.6. The figure shows that though ZLO had a wide range of particle sizes (75-1000 μm), the majority (70.45%) of ZLO was retained on the larger sieves (300-1000 μm). The result implies that ZLO may have a good permeability, owing to relatively large voids produced when used in a fixed-bed column. The experimental result showed that ZLO had a permeability coefficient of 0.0079 m/s. Because of minimized water clogging, the real application of ZLO is likely to be enhanced.

As 600-425 μm was the most common particle size, the main physical characteristics of ZLO of this particle size was investigated. It was found that, ZLO had a particle density of 1.15 g/cm^3, a bulk density of 0.36 g/cm^3, and a porosity of 68.70%. According to Okochi (2013), these parameters of the electric ARD furnace steel slag, another phosphorus adsorbent, were 3.732 g/cm^3, 1.861 g/cm^3 and 50.14%, respectively. It is evident that ZLO possessed a relatively low density but a high

porosity. As a result, ZLO is appropriate for being applied in the packed bed column mode experiments in the upward direction.

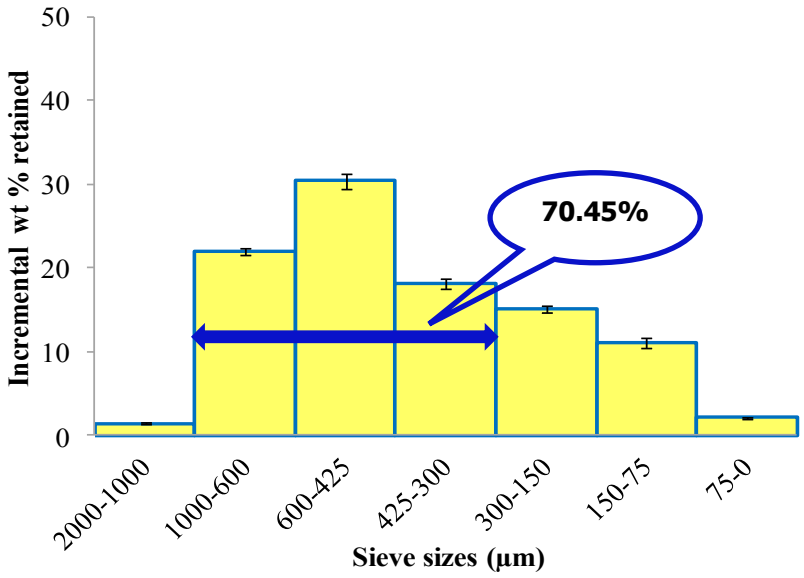

Figure 4.6 Particle size distribution of ZLO (The standard deviation values = 0.07-0.88% for sample size N = 3)

4.5.2 Chemical properties

A. SEM analysis

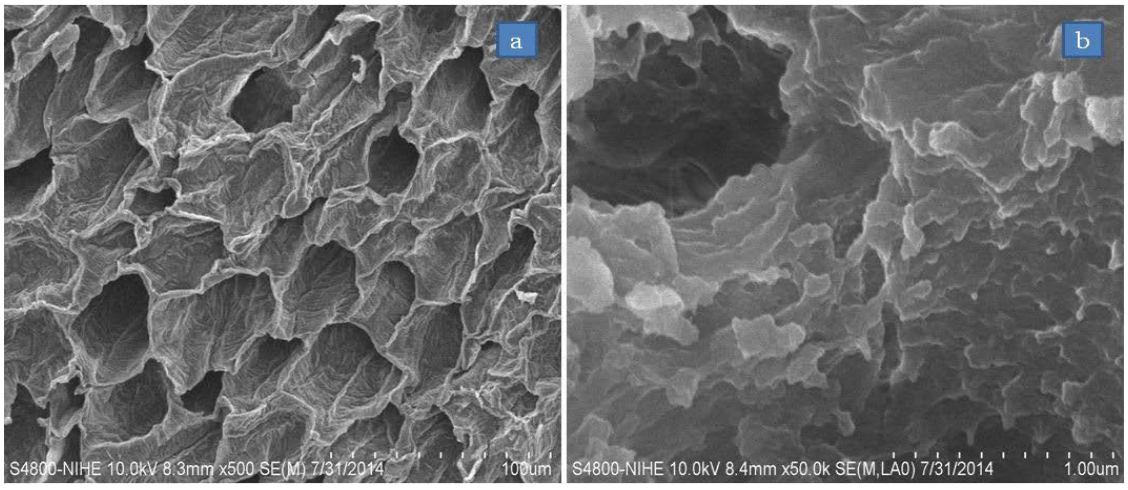

Figure 4.7 SEM images of a) raw okara and b) zirconium loaded okara (ZLO)

The morphological characteristics of ZLO before and after adsorption of phosphorus were acquired by a scanning electron microscope (SEM) (S4800-NIHE, Hitachi, Japan). The SEM images of ZLO are displayed in Fig.4.7. The figure shows that natural okara had a porous structure like a beehive. The average diameter of a hole was around 35 µm. The result is an indicator of a good adsorbent as the porous structure will increase the surface area of okara as well as the diffusion of zirconium into okara.

Meanwhile, ZLO was observed with many particles on its surface and inside of the holes. In addition, the holes were narrowed to the average diameter of only 1.2 μm. This can be attributed to the zirconium deposition, occurring both on the surface and inside the holes of okara. The phosphorus retention onto metal loaded adsorbents may occur via ion exchange (Shin et al., 2005), ligand exchange (Biswas et al., 2007), surface precipitation (Namasivayam et al., 2005) or a combination of these mechanisms. The SEM results confirm that ZLO has high porosity and permeability, as previously suggested by physical properties analysis.

B. EDS analysis

The EDS spectra of natural okara, ZLO, and phosphorus loaded ZLO were recorded using Energy Dispersive Spectroscopy (EDS) detector (JOEL JSM-7600F FE-SEM) and illustrated in Fig. 4.8. The figure shows that like other bio-materials, the natural okara, ZLO, and phosphorus loaded ZLO mainly composed of C, O, and N. The EDS spectrum a) indicated that the natural okara contained phosphorus inside, which accounted for approximately 1.7%. This peak intensity was found to increase noticeably in the EDS spectrum b). A new insight was gained that the peaks of Zr and P occurred at the same position. Due to the overlap of the peaks of these two elements, it was impossible to determine any change in the peak of Zr separately. However, based on the change in the intensity of the combined peak of P and Zr, the change in the chemical composition the adsorption material can be figured out. It was observed that the intensity of the combined peak of ZLO was increased when compared to that of the natural okara. This can be attributed to the deposition of Zr^{4+} onto okara, which resulted from Zr^{4+} metal loading reaction. The intensity of the combined peak of phosphorus loaded ZLO was higher than that of ZLO. This may result from the retention of PO_4^{3-} onto ZLO after adsorption process. These assumptions were further confirmed by the fact that the total weight (%) of P and Zr in the natural okara, ZLO, and phosphorus loaded ZLO increased from 1.7 to 15, and then to 21.3%, respectively. The EDS results clearly demonstrate that Zr^{4+} deposited on the okara played a role of binding sites in adsorption of PO_4^{3-} by ZLO.

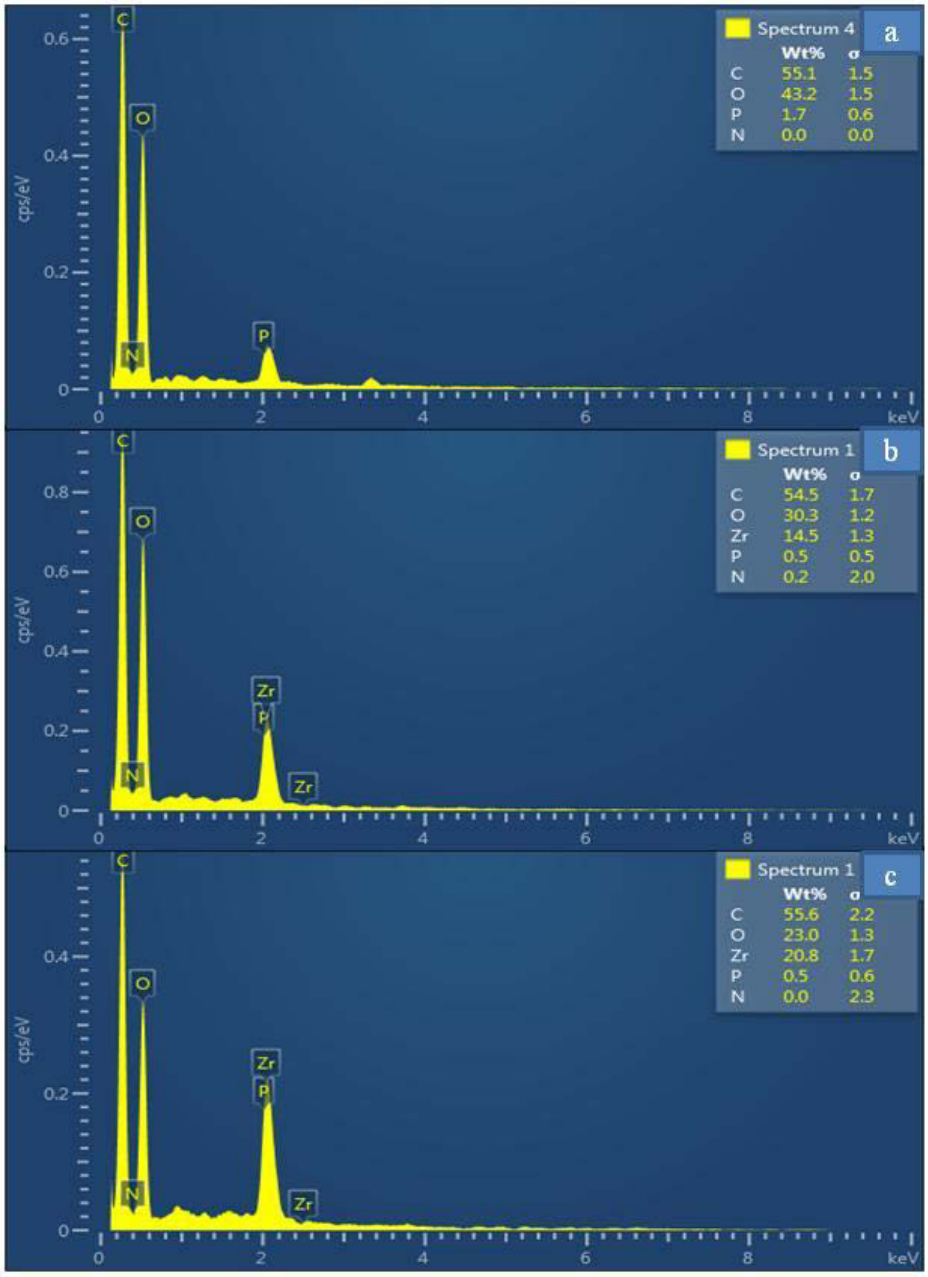

Figure 4.8 EDS spectra of a) natural okara, b) ZLO, and c) phosphorus loaded ZLO

C. FTIR analysis

The FTIR analysis of the natural okara, ZLO before and after phosphorus adsorption was carried out using a Thermo Nicolet 6700 FTIR spectrometer. The spectra are illustrated in Fig.4.9. The FTIR spectrum of natural okara shows the presence of several functional groups, indicating its complex nature. The peaks at 3445.7 cm^{-1} and 669.7 cm^{-1} are attributed to O-H groups in alcohols and phenols. A broad adsorption band in the wave range of 3009.8-2854.4 cm^{-1} can be assigned to O-H groups in carboxylic acids. The width of this band indicates the existence of strong hydrogen bonds. The peak appearing at 1239.1 cm^{-1} arises from P-H phosphine and

phosphoramide compounds. The vibrations at 1161.0 cm^{-1} and 1053.6 cm^{-1} are expressive of P=O in phosphate. These results verify the presence of phosphorus inside natural okara. The peaks at 1558.0 cm^{-1}, 1541.7 cm^{-1}, and 1522.0 cm^{-1} can be ascribed to N-H in amide.

Table 4.3 reveals a change in the functional groups between the natural okara and ZLO. The shifting of adsorption peaks, which corresponded to O-H groups from 3445.7 to 3735.3 cm^{-1}, from 669.7 to 659.7 cm^{-1} and from 3009.8 to 3007.0 cm^{-1} was observed. This implied the involvement of O-H groups in the Zr^{4+} loading reaction. In addition, the shifting of adsorption bands, which corresponded to P=O in phosphoramide, phosphine, and phosphate was noticed. This is possibly because these functional groups were affected by the treatment of okara with 0.05 M NaOH. These findings were supported by Volesky (2007), who stated that hydroxyl, phosphonate, and phosphodiester groups were principal functional groups, which played a vital role in the biosorption.

The comparison of FTIR spectra between ZLO and phosphorus loaded ZLO demonstrated an evident shift of the adsorption peaks, from 3735.3 to 3647.4 cm^{-1}, from 1059.6 to 1095.5 cm^{-1}, and from 659.7 to 669.7 cm^{-1}. The change of these bands can be an indication for the attachment of PO_4^{3-} to ZLO during the adsorption process.

It is inferred from the obtained FTIR results that O-H groups were responsible for the reaction of okara with Zr^{4+}. The presence of Zr^{4+} on the surface of ZLO enabled the retention of PO_4^{3-} onto ZLO. Thus, the electrostatic interaction can be a mechanism for phosphate adsorption onto ZLO.

Table 4.3 Functional groups of okara, ZLO, and P loaded ZLO

Functional groups	Wave number (cm^{-1})		
	Okara	ZLO before P adsorption	ZLO after P adsorption
O-H (usually broad) (alcohols & phenols) and N-H (1^o amines), 2 bands	3445.7	3735.3	3647.4
O-H (very broad) (carboxylic acids & derivatives)	3009.8	3007.0	3009.7
O-H (very broad) (carboxylic acids & derivatives) and CH_3, CH_2, CH II or III bands (alkanes)	2925.5	2925.8	2925.6
O-H (very broad) (carboxylic acids & derivatives) and CH_3, CH_2, CH II or III bands (alkanes)	2854.4	2854.5	2854.4
C=O (esters)	1745.5	1745.6	1745.6
C=O (amide I band)	1649.2	1649.8	1650.3
NH_2 scissoring (1^o amines)	1558.0	1559.3	1558.6
N-H (2^o-amide) II band	1541.7	1541.8	1541.8
N-H (2^o-amide) II band	1522.0	1522.4	1522.4
CH_3 & CH_2 deformation (alkanes)	1458.0	1457.8	1458.8
P=O (phosphoramide) and P-H bending (phosphine) and C-N (amines)	1239.1	1237.7	1237.8
P=O (phosphate) and C-N (amines)	1161.0	1161.7	1161.6
P=O (phosphate) and C-N (amines)	1053.6	1059.6	1095.5
= C-H & = CH_2 (alkenes)	889.9	890.4	890.4
O-H bend (alcohols & phenols) and C-H deformation (alkynes) and	669.7	659.7	669.7

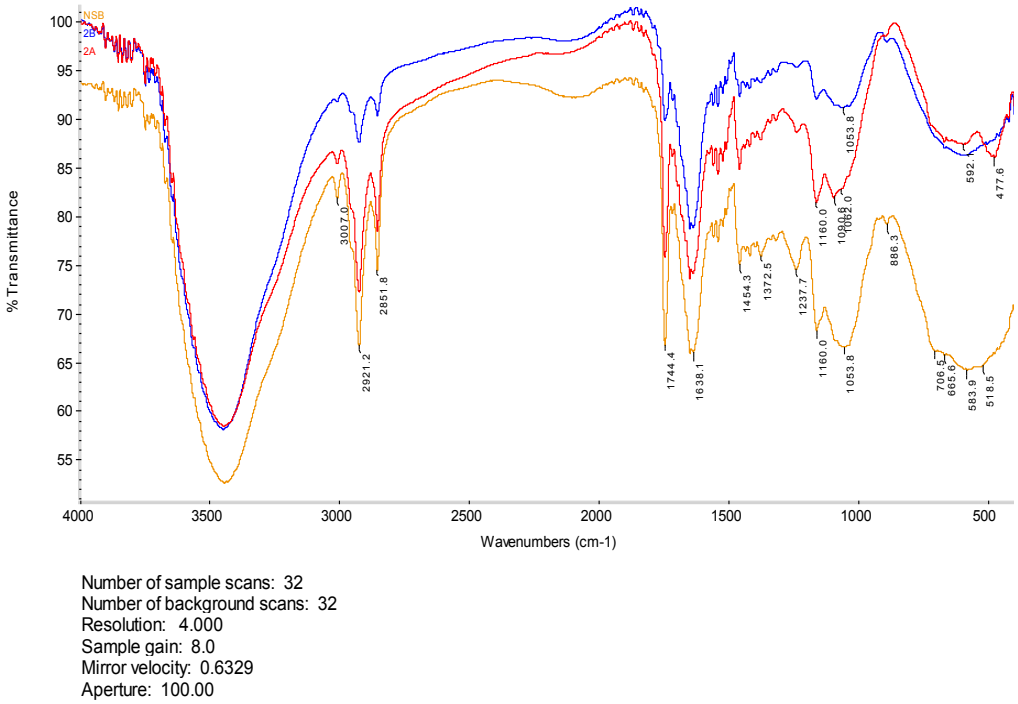

Figure 4.9 FTIR spectra of NSB) natural okara, 2B) ZLO before P adsorption, and 2A) ZLO after P adsorption

D. Elemental analysis

While SEM and FTIR methods provide the qualitative information on the chemical composition of an adsorbent, the dissolution method followed by elemental analysis can quantitatively determine the chemical constituents of the adsorbent.

According to Li et al. (2012), the soybean milk residue (okara) had some phosphorus inside, which varied from 400 to 440 mg P/g dry okara. This finding is important to the practical application as it can enable the recovery of phosphorus from both the natural okara and wastewater. Bearing this in mind, this work evaluated the phosphorus constituent in the natural okara. It was found that the natural okara in this study contained 200-250 mg P/ 100 g dry okara. This result is lower than that described above. This can be attributed to the difference in the type of soybean and the processing procedures between these two studies. However, this is a sound proof for the presence of P in the natural okara, as the previous FTIR and EDS result seemed to suggest.

The ability to sequester PO_4^{3-} from aqueous solutions of a metal loaded adsorbent largely depends on the amount of the loaded metal (Carvalho et al., 2011). Thus, this study investigated the content of zirconium in ZLO to evaluate the efficacy of the metal loading process and the affinity of ZLO for PO_4^{3-} ions. The elemental analysis result indicated that 1 g of ZLO contained 40.44 mg of zirconium. The result is relatively small when compared to the previous study performed by Ohura et al. (2011). The authors reported that Zr^{4+} loaded saponified orange waste (Zr-SOW) exhibited Zr^{4+} uptake capacity of 154.7 mg/g. This can be explained by the dissimilarity in the composition of okara and orange waste when used as substrates for the development of phosphorus adsorbents. However, the elemental analysis data verified the presence of Zr in ZLO, which agreed perfectly with the previous EDS analysis result.

4.6 CONCLUSION

Among three developed adsorbents, ZLO proved to be superior to IZLO and ILO, with respect to adsorption, desorption, regeneration and metal leaching.

Considering the technical and economic feasibility, the optimum metal loading conditions was selected to be a combination of 0.05 M NaOH and 0.25 M $ZrOCl_2.8H_2O$.

Recycling of Zr^{4+} solution as metal loading reagent could be implemented up to 10 times, without any significant loss of the P removal percentage of the recycled ZLO.

The loaded Zr^{4+} cationic ions were responsible for the retention of PO_4^{3-} anionic ions onto ZLO. In addition, the physical properties of ZLO appeared to favor its application in the column mode experiments.

UNIVERSITY OF TECHNOLOGY, SYDNEY

CHAPTER 5

ADSORPTION OF PHOSPHORUS FROM SYNTHETIC WASTEWATER BY ZIRCONIUM LOADED OKARA: BATCH STUDY

5.1 INTRODUCTION

Phosphorus is essential to the development of plants, animals and the industrial manufacture (Choi et al., 2012; Karachalios, 2012; Mezenner and Bensmaili, 2009). However, due to the over-exploitation, the global phosphate rock reserve can be exhausted in the next 50-100 years (Cooper et al., 2011; Eljamal et al., 2013). In another perspective, the phosphorus concentration in the aqueous medium above 0.02 mg/L can cause eutrophication. As a consequence, the water quality is deteriorated, and the life of aquatic creatures is threatened (Ismail, 2012; Jyothi et al., 2012). Therefore, the excessive amounts of phosphorus need to be removed from the aquatic medium to protect water bodies from this undesirable phenomenon, and to pave the way for the phosphorus recovery as well.

Numerous technologies have been developed for phosphorus pollution treatment, including chemical precipitation, biological processes, electrodialysis, reverse osmosis, ion exchange, and adsorption (Biswas et al., 2008; Boujelben et al., 2008; Xu et al., 2011a). Of these, adsorption is usually a method of choice, because of being simple, effective, applicable, appropriate for the decontamination of low levels of phosphorus, favorable to the phosphorus recovery (Loganathan et al., 2014). Nevertheless, the drawbacks of commercial adsorbents (for example, high cost, and non-renewability) prevent the adsorption from widespread use in developing countries.

In an attempt to diminish the cost of treatment, there is an emerging trend to use agricultural wastes/by-products (AWBs) as phosphorus adsorbents (Zhang et al., 2012). The recycling of AWBs as phosphorus adsorbents helps the environment by reducing waste in a green way (Ismail, 2012). Moreover, it gives a chance to add values to AWBs, and to develop attractive, economical alternative to existing treatment methods (Peng et al., 2012). Nevertheless, due to the lack of binding sites for anions, AWBs need to be cationized. This can be done via metal impregnation or quaternization reaction to remove efficiently phosphorus (Han et al., 2005; Mallampati and Valiyaveettil, 2013). Whereas many articles have confirmed the efficacy of different phosphorus - AWBs based adsorbent systems, the search for novel, efficient, and sustainable adsorbents is going on.

Among various methods of modification for the development of phosphorus adsorbents, metal loading seems to be favored due to the simplicity and effectiveness. Of different loading metals, Zr^{4+} is usually a metal of choice because of a strong affinity for phosphate, high selectivity, large surface area, and chemical stability (Biswas,

2008). However, the high cost of Zr^{4+} is the primary challenge, limiting the wide application of Zr^{4+} in cationization of AWBs.

In the Chapter 4, by comparing three developed adsorbents, ZLO was determined as a promising adsorbent because of its high adsorption capacity, desorption ability, and reusability. As the next stage, this Chapter extensively investigated ZLO in the batch mode, with respect to influential factors, isotherms, kinetics, thermodynamics, desorption, and regeneration. To that end, the effect of principal process parameters, such as solution pH, adsorbent dose, adsorbent particle size, foreign anions, initial phosphorus concentration, contact time, and temperature were evaluated. The maximum phosphate adsorption capacity of ZLO was determined from isotherm study. The kinetic study was conducted to identify the rate of the adsorption process. The experimental isotherm, kinetic, and thermodynamic data were analyzed using nonlinear regression method in Curve Expert Professional 2.0.4. The elution and regeneration tests were designed to evaluate the reusability of ZLO as well. Chapter 5 also validates the nature and mechanisms of phosphate sorption by ZLO. Additionally, it provides essential information for designing and operating the phosphorus - ZLO adsorption system in the future. Hence, this work has both theory and practical values.

A main part of Chapter 5 was published in the following paper:

5) "**Nguyen, T.A.H.**, Ngo, H.H., Guo, W.S., Zhou, J.L., Wang, J., Liang, H., Li, G., 2014. Phosphorus elimination from aqueous solution using 'zirconium loaded okara' as a biosorbent. *Bioresour. Technol.* 170, 30-37".

5.2 FACTORS AFFECTING THE BATCH ADSORPTION

The effects of initial phosphorus concentration, contact time, and temperature are investigated later in isotherm, kinetic, and thermodynamic studies, respectively. Therefore, this section only focuses on influences of solution pH, adsorbent dose, adsorbent particle size, and co-anions.

5.2.1 Solution pH

The solution pH can affect the chemical state of binding sites on ZLO, the dissociation of phosphate species in aqueous solutions, and the affinity of phosphate species towards binding sites. Evidently, pH plays an important role in the phosphate adsorption, and hence requiring case-by-case examination. The effect of solution pH on

the phosphorus removal by ZLO is shown in Fig.5.1. It was found that, the phosphate removal by ZLO was most favored in the pH range of 2-6, with the efficiency higher than 98%. This can be attributed to the dominance of $H_2PO_4^-$ and HPO_4^{2-} species in the acidic medium. Due to their strong affinity for binding sites, the phosphate capture was boosted by replacement of OH^- ions from ZLO surface (Mallampati and Valiyaveettil, 2013). The augmentation in the solution pH from 2 to 11 led to the decrease of the phosphate removal by almost 10%. This is ascribed to the high competition for the binding sites between phosphate species and OH^- anions in the alkaline medium (Ismail, 2012; Riahi et al., 2009). Notably, a dramatic decline in the phosphate removal percentage (40%) was caused by an increase in the solution pH from 11 to 12. This might have happened that, at pH >11, HPO_4^{2-} and PO_4^{3-} species were prevalent. Their vigorous competition with OH^- anions in the alkaline medium resulted in their weak affinity for adsorption sites (Benyoucef and Amrani, 2011a; Biswas et al., 2008; Zhang et al., 2012). Bearing the facts in mind, it can be concluded that, except pH 12, the pH range of 2-11 demonstrated a minor effect on the phosphorus retention by ZLO. Due to the high effectiveness in a broad pH range, ZLO has an appreciable advantage over other biosorbents when used in the reality. These results fit well with the findings reported by Xu et al. (2011a) and Zhang et al. (2012). They revealed that optimal pH values for the phosphate sorption onto giant reed and sugarcane bagasse were of 5-10 and 4-11, respectively.

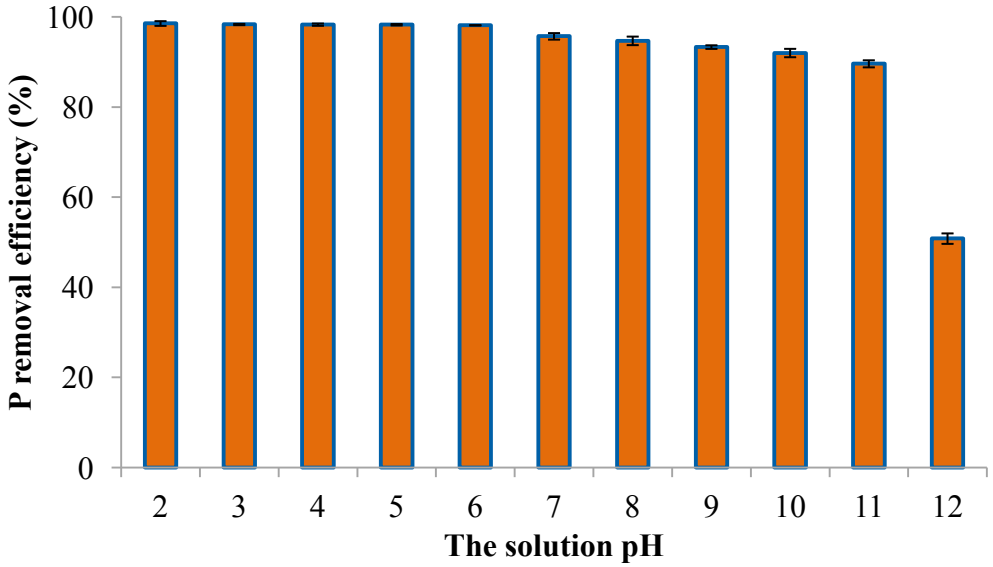

Figure 5.1 Effect of the solution pH on P adsorption onto ZLO (C_i = 50 mg P/L, ZLO dose = 10 g/L, shaking speed = 120 rpm, conctact time = 24 h, temperature = 25 °C. The standard deviation values = 0.05-1.16% for sample size N = 3)

5.2.2 The adsorbent dose

Fig.5.2 shows the influence of the ZLO dose on the retention of phosphorus by ZLO. As shown in Fig.5.2, the extent of phosphorus removal increased from 62.5 to 100% with increasing ZLO dose from 1 to 2 g/L, at the initial phosphorus concentration of 5 mg P/L. Similarly, the phosphorus decontamination by ZLO was enhanced by 62.63%, 79.35%, and 84.50% with an elevation of the ZLO dose from 1 to 3 g/L, respectively. The enhanced phosphorus removal percentage at higher ZLO dose can be ascribed to more adsorption sites or larger total surface area (Yue et al., 2010; Zhang et al., 2012). However, the removal percentage remains constant with further increase in ZLO dose. The result can be explained by the resistance to the mass transfer of phosphorus from solution to ZLO surface (Ismail, 2012; Mezenner and Bensmaili, 2009). Therefore, for different initial phosphorus concentrations of 5, 10, 25, 50 mg/L, the optimal ZLO doses were determined as 2, 3, 7, 10 g/L, respectively. In view of the practical application, for the same level of phosphorus removal, the lower the dose is required, the more efficient the adsorbent is. In the light of this, the results obtained in this study are even better than those reported by Yue et al. (2010). The authors claimed that, 98% of phosphorus was removed with the modified giant reed at the dose of 16 g/L, for the initial phosphorus concentration of 50 mg/L.

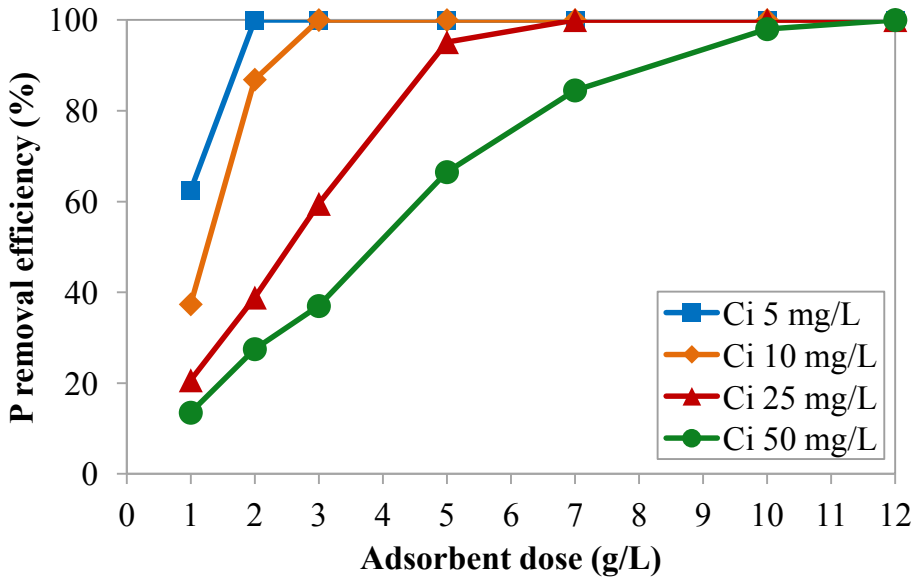

Figure 5.2 Effect of biosorbent dose on P adsorption onto ZLO (C_i = 5, 10, 25, 50 mg P/L, shaking speed = 120 rpm, contact time = 24 h, reaction temperature = 25 °C, ZLO dose = 1, 2, 3, 5, 7, 10, 12 g/L)

5.2.3 The adsorbent particle size

The effect of ZLO particle size on the P removal by ZLO is shown in Fig.5.3. As the figure shows, the higher P removal percentages were achieved by ZLO of smaller particle size (300-150 µm) for all kinds of the initial P concentration. The results proved that the smaller the adsorbent particle size, the higher the P removal efficiency of an adsorbent could be acquired. The increase in P removal efficiency at smaller particle size can be attributed to the larger adsorption surface area (Okochi, 2013). Similar observations were reported by Chen et al. (2012) and Yeom and Jung (2009). Though small particle size is found to facilitate the P adsorption, it can also be responsible for the column clogging. Thus, the optimum adsorbent particle size should be determined prior to applying the adsorbent in a column mode experiment.

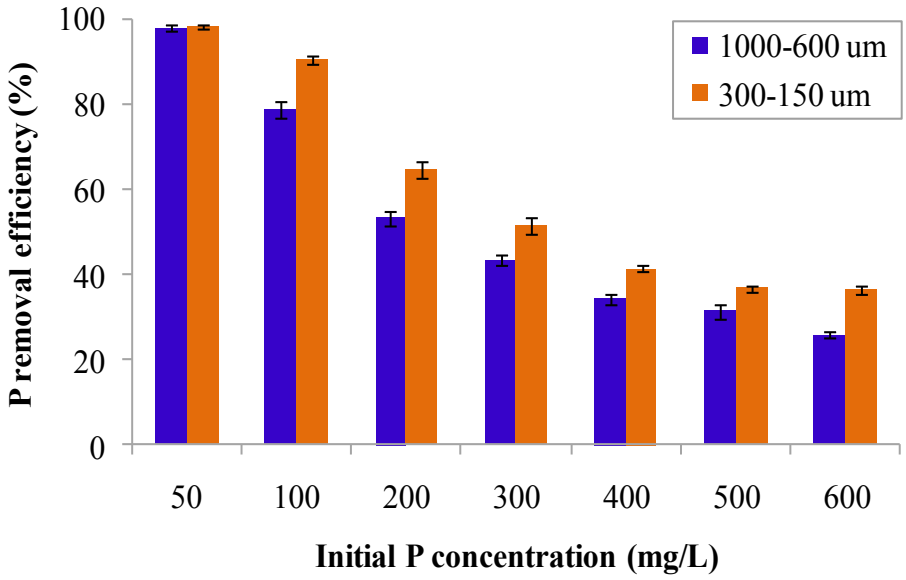

Figure 5.3 Effect of the biosorbent particle size on P removal percentage of ZLO (C_i = 50, 100, 200, 300, 400, 500, 600 mg P/L, ZLO dose = 10 g/L, shaking speed = 120 rpm, temperature = 298 K, contact time = 24 h. The standard deviation values = 0.45-2.12% for sample size N = 3)

5.2.4 Foreign anions

The real wastewater usually contains many kinds of anions that may hinder the sorption of PO_4^{3-} anions. Thus, this Chapter investigates the effect of co-existing anions on the sorption of phosphate onto ZLO to elucidate its practical application. A series of adsorption experiments were set up with the presence of SO_4^{2-}, NO_3^-, Cl^-, and CO_3^{2-} individually and collectively. The concentration of coexisting anions was 10 times higher than that of PO_4^{3-} anion in the mol ratio. The experiment was conducted at the

initial P concentration of 100 mg/L (~ 3 mmol), ZLO dose of 20 g/L, orbital shaking rate of 120 rpm, temperature of 298 K, and contact time of 24 h.

The efficiency of competing anions is presented in Fig. 5.4. The efficiency of competing anions was in the order CO_3^{2-} (23.60%) > SO_4^{2-} + NO_3^- + Cl^- + CO_3^{2-} (18.88%) > SO_4^{2-} (2.42%) > NO_3^-(1.36%) > Cl^- (0.48%). The results indicated that among various co-existing anions, only CO_3^{2-} considerably affected the PO_4^{3-} retention by ZLO. The results suggested that to maximize the performance of ZLO, it should not be applied in the wastewater with high levels of CO_3^{2-} anions. Otherwise, the dissolved carbonate salts need to be converted into the precipitated carbonate salts or the gas carbon dioxide before phosphate adsorption. This can be done via pH adjustment with NaOH and HCl, respectively. Since ZLO works efficiently in a wide range of pH between 2 to 11, the above pH alteration will not interfere with the phosphate adsorption. This result was just converse to that reported by Biswas et al. (2008). The authors observed that the competing effect of CO_3^{2-} in the case of removing PO_4^{3-} by Zr^{4+} loaded orange waste was minor. The disagreement in the results between these studies can be explained by the difference in the composition of orange waste and okara. The low competing efficiencies of other anions revealed that the affinity of ZLO for these anions was smaller than that for PO_4^{3-} anions. The marginal interference of SO_4^{2-}, NO_3^-, and Cl^- can also be found in the work conducted by Biswas et al. (2008, 2007) and Jyothi et al. (2012). The results showed the potential of using ZLO for the decontamination of phosphorus in the real wastewater.

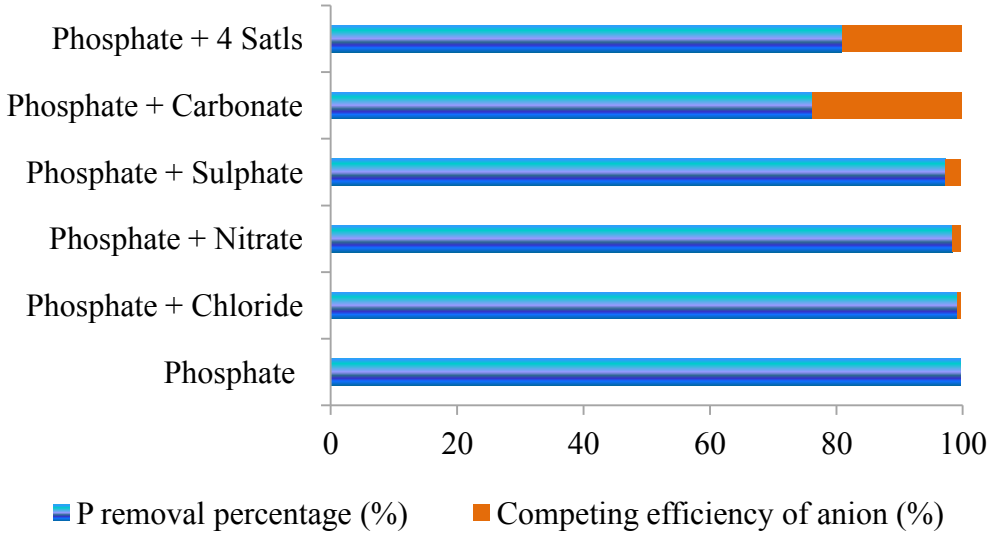

Figure 5.4 Effect of the competing anions on P adsorption onto ZLO (C_i = 100 mg P/L, ZLO dose = 20 g/L, contact time = 24 h, shaking speed = 120 rpm, reaction temperature = 298 K)

5.3 ADSORPTION ISOTHERMS

Isotherm study provides information on the adsorption capacity of an adsorbent. It also helps to identify suitable isotherm models that can be applied in the system design (Benyoucef and Amrani, 2011b; Biswas et al., 2008; Mezenner and Bensmaili, 2009). Hence, it is considered as the first step for the practical application of the adsorbent (Quintelas et al., 2013).

Table 5.1 The maximum adsorption capacity of ZLO for PO_4^{3-} in comparison with various biosorbents and commercial adsorbents

Adsorbent	Type of adsorbent	q_{max} (mg/g)[(1)]	Reference
Dowex	Commercial	40	Anirudhan and Senan, 2011
Hydrotalcite	Commercial	60	Anirudhan and Senan, 2011
Aleppo pine sawdust	Modified	116	Benyoucef and Amrani, 2011a
Orange waste gel	Modified	175	Biswas et al., 2008
Zirconium ferrite	Commercial	40	Biswas et al., 2008
Zirconium loaded MUROMAC	Commercial	132	Biswas et al., 2008
Orange waste gel	Modified	43	Biswas et al., 2007
Sugar cane bagasse fiber	Modified	152	Carvalho et al., 2011
Coconut shell fibers	Modified	200	De Lima et al., 2012
Aspen wood	Modified	17	Eberhardt and Min, 2008
Palm surface fibers	Natural	26	Ismail, 2012
Granular date stones	Natural	26	Ismail, 2012
Wood residues	Modified	206	Karachalios, 2012
Coir pith	Natural	4	Krishnan and Haridas, 2008
Coir pith	Modified	71	Krishnan and Haridas, 2008
Apple peels	Modified	20	Mallampati and Valiyaveettil, 2013
Eggshell	Modified	11	Mezenner and Bensmaili, 2009
Aluminum oxide	Commercial	35	Peleka and Deliyanni, 2009
Pine sawdust char	Modified	15	Peng et al., 2012
Date palm fibers	Natural	13	Riahi et al., 2009
Posidoniaoceanica (L.) fibers	Natural	7	Wahab et al., 2011
Cotton stalk	Modified	52	Xu et al., 2011b
Wheat stalk	Modified	61	Xu et al., 2011b
Giant reed	Modified	61	Yue et al., 2010
Sugarcane bagasse	Modified	21	Zhang et al., 2012
ZLO[(2)]	Modified	44	This study
ZLO[(3)]	Modified	59	This study

Notation:

(1) q_{max} values were round off to the none decimal number

(2) the adsorbent prepared from the homemade okara

(3) the adsorbent prepared from the industrial okara

This study found that, the absorbed phosphorus amount (q_e) increased with growing equilibrium phosphorus concentrations (C_e) and got level off later. This can be ascribed to the less available phosphorus binding sites at higher equilibrium phosphorus concentrations (Benyoucef and Amrani, 2011b). Based on the stable values of q_e at the plateau section of the plot of q_e and C_e, the maximum adsorption capacity of ZLO at 298 K was determined to be 14.4 mg P/g (~44.13 mg PO_4/g). Similarly, the q_m of ZLO at 308 and 318 K were found to be 14.70 mg P/L (~45.05 mg PO_4/g) and 15.10 (~46.27 mg PO_4/g), respectively. These results are equal to or even better than those of many biosorbents and commercial adsorbents listed in Table 5.1. In a previous study, Biswas et al. (2008) explored that the phosphate retention by Zr^{4+} loaded orange waste (SOW) gels was possibly due to the ligand exchange mechanism, which occurred between PO_4^{3-} ions in the solution and OH^- ions coordinated with the Zr^{4+} ions loaded on the SOW gels. The authors explained that loaded Zr^{4+} ions could be easily converted into hydrated forms, such as $[Zr_4(OH)_8(H_2O)_{16}]^{8+}$, and $[Zr_8(OH)_{20}(H_2O)_{24}]^{12+}$ species, with the abundant amounts of OH^- ions and H_2O molecules. During the hydrolysis, H_2O molecules were deprotonated by releasing H^+ ions to form exchangeable OH^- ions, which could be replaced by PO_4^{3-} ions. It is evident that, zirconium plays a crucial role in the PO_4^{3-} removal by Zr^{4+} loaded orange waste (SOW) gel. However, the amount of Zr^{4+} deposited on the adsorbent depends on the binding ability, and thus the nature of the orange waste. Similarly, the superior phosphate adsorption capacity of ZLO to other adsorbents can be ascribed to the strong binding ability of okara for Zr^{4+} and high affinity of Zr^{4+} for PO_4^{3-} anions.

To determine isotherm parameters and the most suitable isotherm model, the experimental data obtained at 298, 308, and 318 K were fitted with Langmuir, Freundlich, and Temkin models, using the Curve Expert Professional 2.0.4. Langmuir model stands for monolayer adsorption, assuming that adsorption takes place at a specific number of adsorption sites, each site is occupied by one adsorbate molecule, all sites are the same, and there is no interaction between adsorbed molecules. Langmuir isotherm model in the nonlinear form (Kumar et al., 2010) is given by the Eq. (5.1):

$$q_e = \frac{q_m K_L C_e}{1 + K_L C_e} \quad (5.1)$$

where q_m (mg/g) is the maximum mass of phosphates adsorbed per unit weight of ZLO when the surface of ZLO is entirely covered by monolayer of phosphate ions, K_L (L/mg) is Langmuir constant associated with the affinity of binding sites on ZLO

surface to the phosphate ions, q_e (mg/g) is the quantity of phosphate adsorbed onto 1 g of ZLO under equilibrium condition, C_e (mg/L) is the equilibrium phosphate concentration.

The Langmuir isotherm is characterized by the separation factor (R_L) (Mallampati and Valiyaveettil, 2013) and is expressed by the Eq. (5.2).

$$R_L = \frac{1}{1+ K_L C_i} \quad (5.2)$$

where K_L (L/mg) represents Langmuir constant and C_i indicates the initial concentration of phosphorus.

The Freundlich model represents non-ideal adsorption, with multi adsorption sites and heterogeneous surfaces. It is based on the assumption that active binding sites are occupied first, and the binding ability declines with an increase in the site occupation. Freundlich isotherm model in the nonlinear form (Boujelben et al., 2008) is expressed by the Eq. (5.3):

$$q_e = K_f(C_e)^{1/n} \quad (5.3)$$

where K_f (L/g) and n are Freundlich constants, indicating the adsorption capacity and adsorption intensity, respectively.

Temkin isotherm model (Benyoucef and Amrani, 2011b) in nonlinear form can be expressed in the Eq. (5.4):

$$q_e = q_m \ln (K_T C_e) \quad (5.4)$$

where q_m represents the adsorption capacity and K_T is indicator for the adsorption intensity, respectively.

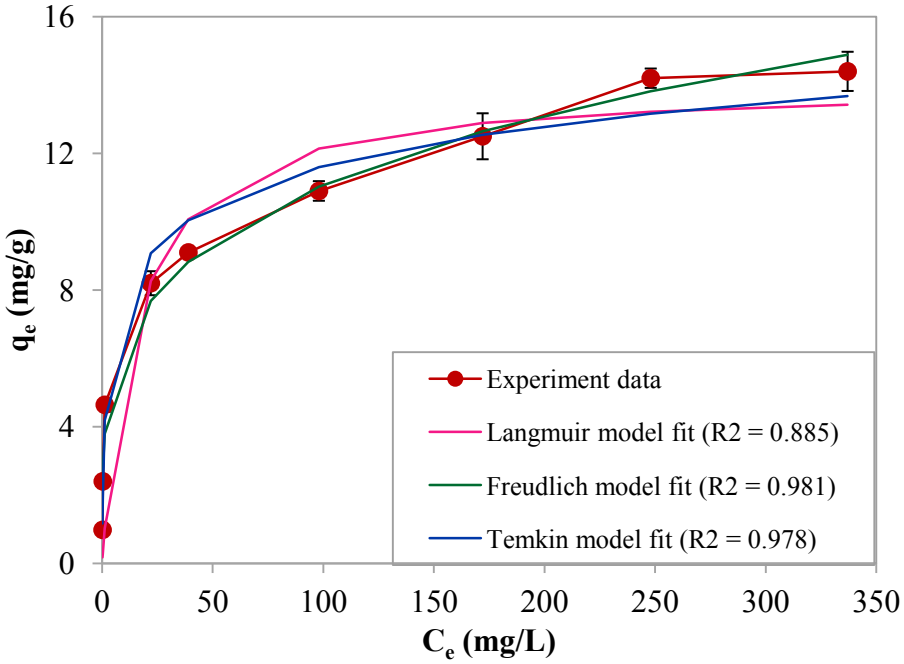

Figure 5.5 The fitting of isotherm models to P adsorption onto ZLO (biosorbent particle size = 150-1000 µm, pH = 7 ÷ 7.5, C_i = 10÷500 mg P/L, ZLO dose = 10 g/L, contact time = 24 h, shaking speed = 120 rpm, reaction temperature = 298 K. The standard deviation values = 0.10-0.67 mg/g for sample size N = 3)

The isotherm parameters of three models obtained at 298, 308, and 318 K are listed in Table 5.2. The fitting curves to three models are presented in Fig.5.5. As shown in Table 5.2, the correlation coefficients (r^2) achieved at 298 K for Langmuir, Freundlich, Temkin models were 0.885, 0.981, and 0.978, respectively. According to the r^2 values, both Freundlich and Temkin models yielded satisfactory fit to the experimental data. Compared with Freundlich model, Langmuir exhibited much poorer fit, as shown by a substantially lower value of r^2. The results suggest the heterogeneous surface of ZLO and the multilayer nature of the adsorption. These results are consistent with earlier reports on Aleppo pine sawdust (Benyoucef and Amrani, 2011b), aspen wood fiber (Eberhardt et al., 2006), and biomass char (Peng et al., 2012). It can be noted that, the values of n>1 indicate the favorable adsorption. This is supported by the value of Langmuir separation factors (R_L), which was in the range of $0 < R_L < 1$ for all cases. Furthermore, both K_F and n were observed to reach the highest values at 318 K. This showed that an increase in temperature boosted the adsorption capacity and the affinity of ZLO for PO_4^{3-}anions. Hence, this adsorption process had an endothermic nature.

In the Chapter 5, the focus has been placed on homemade okara derived ZLO. However, the maximum phosphate adsorption capacity of the industrial okara originated ZLO was also estimated using the same procedure, for a comparison purpose (Table 5.1). It is evident from the table that industrial ZLO exhibited a significantly higher adsorption capacity for PO_4^{3-} (59 mg/g) than the homemade ZLO (44 mg/g). This can be interpreted that due to the difference in the processing technology, the industrial okara seemed to be smaller in the particle size than the homemade okara. As a result, the manufacturing okara could adsorb Zr^{4+} better than the homemade okara. Since the industrial ZLO contained more Zr^{4+} ions, which were responsible for PO_4^{3-} capture, it might sequester PO_4^{3-} more efficiently than the homemade ZLO.

Table 5.2 Isotherm and kinetic parameters by non-linear regression method for P adsorption onto ZLO

Isotherm parameters	Temperature (K)			Kinetic parameters	Initial P concentration (mg/L)		
	298	308	318		10	25	50
1. Langmuir				1. Pseudo−first order			
$q_{m,\,exp.}$ (mg P g^{-1})	14.400	14.700	15.100	$q_{e,\,exp.}$ (mg g^{-1})	1.060	2.560	4.540
$q_{m,\,cal.}$ (mg P g^{-1})	14.039	14.608	15.321	$q_{e,\,cal.}$ (mg g^{-1})	1.055	2.479	4.232
K_L (L mg^{-1})	0.065	0.069	0.062	K_{1p} (h^{-1})	5.852	2.194	1.221
R_L(at Ci 50−500 mg/L)	0.030−0.235	0.028−0.225	0.031−0.244	r^2	0.9997	0.980	0.975
r^2	0.885	0.894	0.894	2. Pseudo−second order			
2. Freundlich				$q_{e,\,exp.}$ (mg g^{-1})	1.060	2.560	4.540
K_F (L g^{-1})	3.630	4.080	4.371	$q_{e,\,cal.}$ (mg g^{-1})	1.091	2.718	4.916
n	4.124	4.383	4.513	K_{2p}(g mg^{-1} h^{-1})	13.345	1.224	0.3005
r^2	0.981	0.977	0.978	r^2	0.993	0.997	0.989
3. Temkin				3. Intraparticle diffusion			
q_m (mg P g^{-1})	1.684	1.661	1.608	k_p(mg g^{-1} $h^{-0.5}$)	0.275	0.884	1.465
K_T	10.003	15.149	24.891	C	0.577	0.842	1.226
r^2	0.978	0.982	0.974	r^2	0.439	0.758	0.879

5.4 ADSORPTION KINETICS

The kinetic study provides information on the adsorption rate, which is essential for system design and real application (Ismail, 2012; Peng et al., 2012). Furthermore, it helps to reveal the adsorption mechanisms (Mallampati and Valiyaveettil, 2013; Mezenner and Bensmaili, 2009). Consequently, the kinetic study of the phosphorus adsorption from aqueous solutions plays an important role in the treatment of phosphorus pollution.

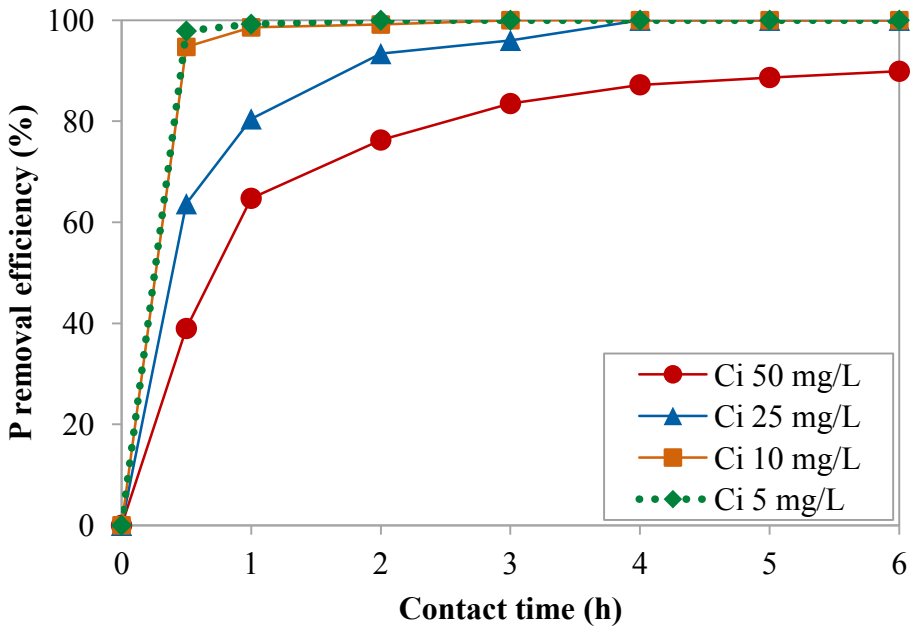

Figure 5.6 Kinetic curves of P adsorption onto ZLO at different initial P concentrations and a given ZLO dose

The kinetics for P adsorption onto ZLO at various initial P concentrations (5, 10, 25, 50 mg/L) and a given biosorbent dose (10 g/L) is shown in Fig.5.6. It can be seen that, the adsorption rate was very fast in the beginning, and then slowed down and reached equilibrium. After the first 0.5 h, almost 40%, 60%, 90% and 95% of P was captured by ZLO at initial P concentrations of 50, 25, 10, 5 mg/L, respectively. The result suggested that the lower the initial P concentration was, the faster the adsorption equilibrium could be reached.

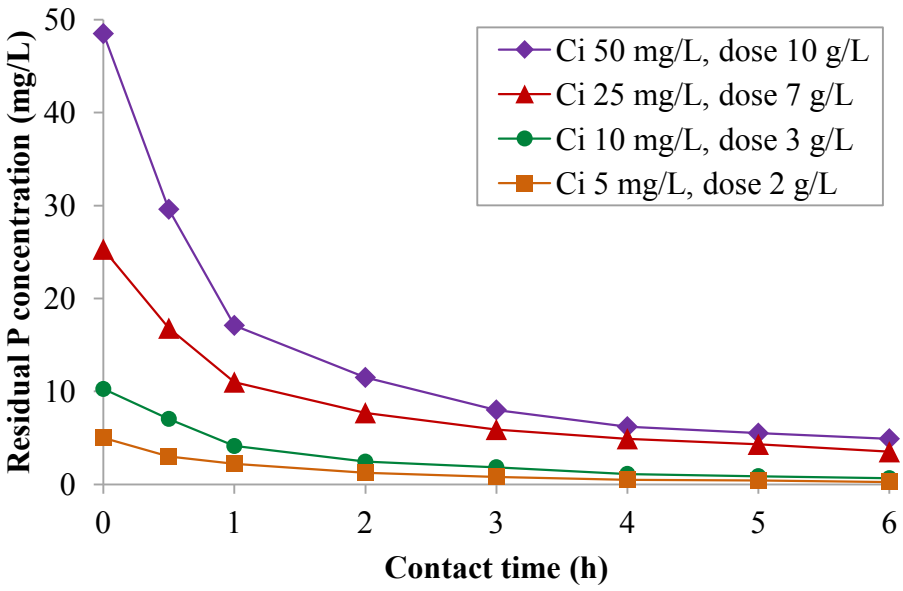

Figure 5.7 Kinetic curves of P adsorption onto ZLO at different initial P concentrations and optimal ZLO doses

Kinetic curves of several initial P concentrations (5, 10, 25, 50 mg/L) and optimal ZLO doses (2, 3, 5, 7 g/L) are presented in Fig.5.7. As can be seen from the figure, 2, 3, 4, and 5 h was necessary to ensure the equilibrium was completely reached, respectively. At the initial P concentration of 10 mg/L, 3 h was required to remove 80% P with ZLO dose of 3 g/L (Figs. 5.6 and 5.7). However, when the ZLO dose was increased to 10 g/L, the P removal efficiency reached 95% in only 0.5 h. This means that the reaction time could be shortened by applying higher doses. It would be useful for designing a fix bed column experiment and a large-scale application.

To date, numerous mathematical models have been applied in the kinetic study. Nevertheless, only appropriate models could satisfy experimental data and explain rational sorption mechanisms (Benyoucef and Amrani, 2011a). In this work, the experimental data were fitted to three well-known kinetic models to explore main adsorption mechanisms as well as to predict the adsorption rates. The Pseudo-first order and Pseudo-second order models based on equilibrium adsorption capacity (Behnamfard and Salarirad, 2009) can be expressed by the following equations:

$$q_t = q_e[1 - \exp(-k_{1p}t)] \quad (5.5)$$

$$q_t = \frac{k_{2p}q_e^2 t}{1 + q_e k_{2p} t} \quad (5.6)$$

The Weber-Morris diffusion model (Benyoucef and Amrani, 2011a; Ismail, 2012; Kumar et al., 2010) is given by the Eq. (5.7):

$$q_t = k_p t^{0.5} + C \quad (5.7)$$

where q_t is the amount of phosphorus adsorbed at time t (mg/g), q_e is the adsorption capacity at equilibrium (mg/g), k_{1p} is the pseudo-first order rate constant (h^{-1}), k_{2p} stands for the pseudo-second order rate constant (g/mg/h), k_p indicates the intra-particle diffusion rate constant ($mg/g/h^{0.5}$), C (mg/g) is concerned with the boundary layer thickness, and t is the contact time (h). The kinetic model parameters were determined by nonlinear regression method, using Curve Expert Professional 2.0.4. The results are presented in Table 5.2. As the table shows, the experimental q_e values were all higher than corresponding results calculated by Pseudo-first order model. The result demonstrated that the Pseudo-first order model could not predict well the kinetic data. Additionally, the experimental data followed the Pseudo-first order and Pseudo-second order models with correlation coefficients equal to or higher than 0.975 and 0.989, respectively. Clearly, Pseudo-second order model was more satisfactory than Pseudo-first order model in describing the experimental data. On the contrary, exceptionally low correlation coefficients (0.439-0.879) were achieved with Weber-Morris diffusion model. In term of the correlation coefficient (r^2), the fitness of three investigated kinetic models to experimental data was in the following order: Pseudo-second order > Pseudo-first order > Weber-Morris diffusion (Fig.5.8). This finding implied that the chemisorptions might be a significant pathway, while intra-particle diffusion could not be the governing mechanism for the adsorption of phosphate by ZLO (Zhang et al., 2012). These results agreed well with those reported by Mallampati and Valiyaveettil (2013) and Peng et al. (2012) in the cases of removing phosphate by apple peels and biomass char, respectively.

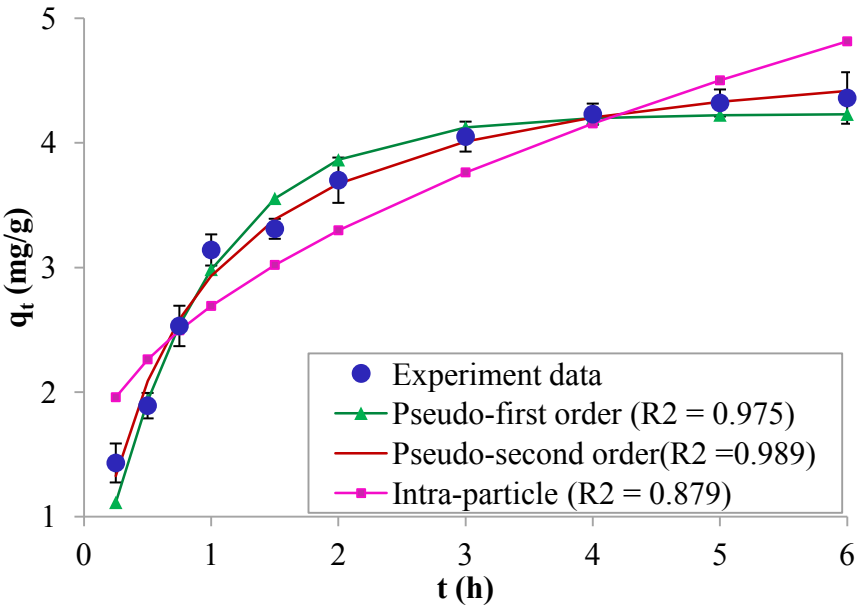

Figure 5.8 The fitting of kinetic models to P adsorption onto ZLO (C_i = 50 mg P/L, ZLO dose = 10 g/L, shaking speed = 120 rpm, temperature = 298 K. The standard deviation values = 0.08-0.21 mg/g for sample size N = 3)

It is worth pointing that, the rate constants of pseudo-first order and pseudo-second order models (k_{1p}, k_{2p}) decreased, whereas the rate constant of Weber-Morris diffusion model (k_p) increased with increasing initial P concentration. This is supported by Fig. 5.6, which displays that the adsorption was faster at lower initial phosphorus concentration. Similar trends can be detected in the work performed by Mezenner and Bensmaili (2009). The authors attributed the latter trend to the intensifying diffusion in the solid caused by higher driving force. Table 5.2 also demonstrates that, the enhanced initial P concentration led to the increase of C values.

5.5 ADSORPTION THERMODYNAMICS

The thermodynamic parameters for the adsorption of phosphorus onto ZLO were calculated from experimental data by using the following equations (Mezenner and Bensmaili, 2009):

$$\Delta G° = -RT\ln K_d \quad (5.8)$$

$$\ln K_d = -\frac{\Delta H°}{RT} + \frac{\Delta S°}{R} \quad (5.9)$$

where K_d is the distribution coefficient of the adsorption process; $\Delta G°$, $\Delta H°$, and $\Delta S°$ are the changes in Gibbs free energy (J/mol), enthalpy (J/mol) and entropy (J/mol/K),

respectively; T is the absolute temperature (K); and R is the gas constant (8.314 J/mol/K).

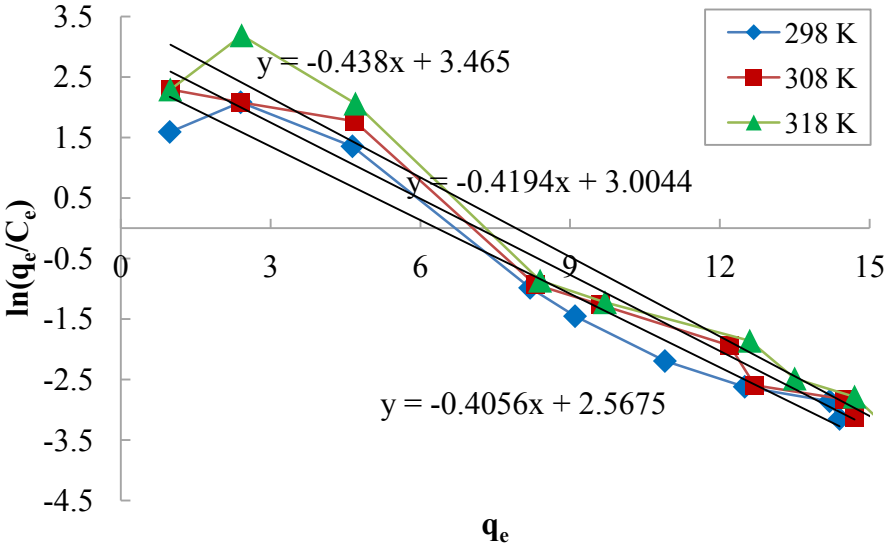

Figure 5.9 Thermodynamic analysis for P adsorption onto ZLO (C_i = 10÷500 mg P/L, ZLO dose = 10 g/L, shaking speed = 120 rpm, contact time = 24 h, temperature = 298, 308, 318 K): A plot of $\ln(q_e/C_e)$ versus q_e

Initially, K_d at a specific temperature was obtained by plotting $\ln(q_e/C_e)$ versus q_e, using linear regression type. The intercept of the plot represents the value of K_d (Benyoucef and Amrani, 2011a) (Fig.5.9). Next, $\Delta G°$ was calculated with the Eq. (5.8). Eventually, $\Delta H°$ and $\Delta S°$ were determined from the slope and intercept of the plot of $\ln K_d$ versus 1/T, using Eq. (5.9).

Table 5.3 Thermodynamic parameters for P adsorption onto ZLO

T (K)	$q_{max, exp.}$ (mg PO_4/g)	K_d	$\Delta G°$ (J/mol)	$\Delta H°$ (J/mol)	$\Delta S°$ (J/mol/K)	R^2
298	44.13	2.567	-2336	11814	47	0.999
308	45.05	3.004	-2817			
318	46.27	3.465	-3286			

Table 5.3 represents thermodynamic parameters at different temperatures. The values of $\Delta G°$ at 298, 308, and 318 K were -2163, -2675, and -3132 J/mol, respectively. The negative values of $\Delta G°$ suggested that the adsorption of phosphorus onto ZLO be spontaneous and feasible. The $\Delta G°$ declined from -2163 to -3132 J/mol when temperature increased from 298 to 318 K, indicating an enhancement in phosphorus uptake at higher temperatures. This can be ascribed to the activation of ZLO surface by

the temperature (Benyoucef and Amrani, 2011a). The positive ΔH° confirmed endothermic nature of the process (Kumar et al., 2010; Peng et al., 2012). The positive value of ΔS° reflected high affinity of ZLO for PO_4^{3-} anions, and increasing randomness at the solid-liquid interface during the adsorption process (Kumar et al., 2010; Mezenner and Bensmaili, 2009).

5.6 DESORPTION AND REGENERATION STUDIES

This study investigates five desorption solutions, including 0.1 M NaCl, 0.1 M HCl, 0.05 M NaOH, 0.2 M NaOH, and the distilled water with pH 12. Of these, 0.1 M NaCl and 0.1 M HCl solutions showed very poor desorption efficiencies (<1%). Better desorption efficiencies were achieved with pH 12 distilled water (49.45%) and 0.05 M NaOH (70.76%). The best desorption solution was found to be 0.2 M NaOH, with the desorption efficiency reached up to 94.25%. The successful desorption can be explained by the replacement of PO_4^{3-} anions adsorbed onto ZLO by OH^- ions in the desorption solution. The desorption results revealed that ion exchange might be a leading mechanism for the adsorption of PO_4^{3-} by ZLO. This result was in line with an earlier study conducted by Unnithan et al. (2002), reporting that 98.2% of adsorbed phosphorus could be eluted with 0.1 M NaOH. In this study, 0.2 M NaOH was the best desorption solution, and thus it has been selected for the regeneration test. The results of ZLO regeneration are shown in Fig. 5.10.

In the case of non-activation of ZLO after desorption, after five continuous cycles of adsorption - desorption, the phosphorus adsorption and desorption efficiencies of ZLO were dropped by 46.74% and 68.30%, respectively. Desorption efficiency of ZLO in the fifth cycle was limited to 26%, which was too low for any application. The inefficient regeneration can be explained by the fact that using 0.2 M NaOH for desorption led to an increase in the pH value of the adsorption solution in the next cycle. Due to the unfavorable pH medium, the uptake of PO_4^{3-} in the next cycle was sharply declined. This assumption was confirmed by the pH value of the adsorption solution from the second cycle on, which was found to be above 10.

In the case of activating the desorbed ZLO by 0.1 M HCl, the activated ZLO exhibited the same adsorption and desorption efficiencies as the virgin adsorbent. After five cycles of operation, the adsorption and desorption efficiencies of ZLO decreased by only 12.46% and 7.40%, respectively. Thus, it is possible to reuse ZLO and reduce the adsorbent preparation cost. Apparently, activation of the desorbed adsorbent with an

acid solution significantly enhanced the adsorption and desorption efficiencies in the next cycle. A similar observation was noted by Ebie et al. (2008), who used 1% H_2SO_4 for the activation of zirconium as a phosphorus adsorbent. From the obtained results, it is inferred that 0.2 M NaOH can be used as a long-term desorption solution, provided that the desorbed ZLO is activated with 0.1 M HCl before the next adsorption cycle. The phosphorus adsorption and desorption efficiencies of ZLO remained about 85% after five consecutive adsorption-desorption cycles. This indicates the high reusability of ZLO.

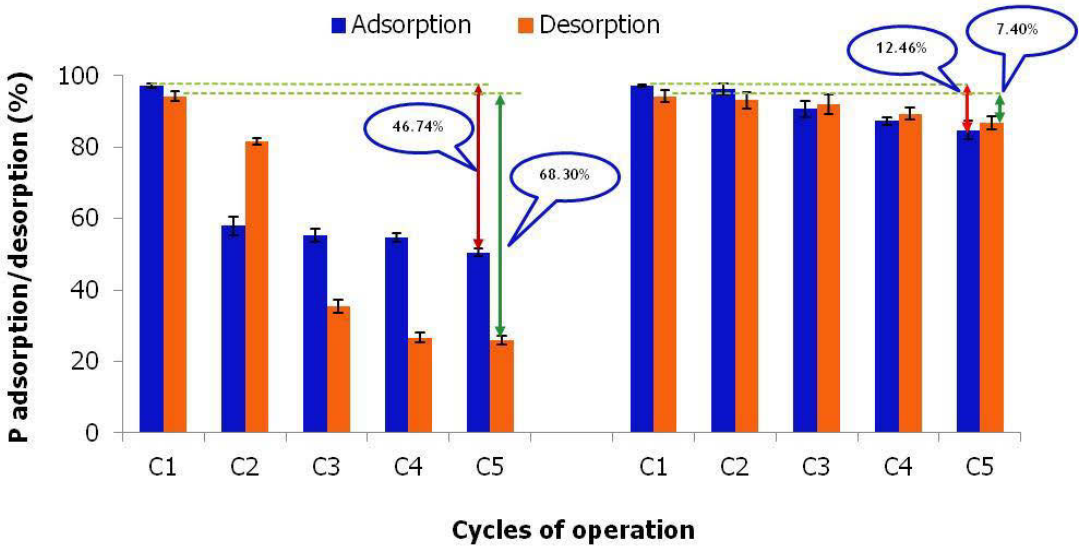

Figure 5.10 Comparison of adsorption/desorption efficiencies ater 5 consecutive cycles between non-activated ZLO and activated ZLO (The standard deviation values = 0.29-2.76% for sample size N = 3)

5.7 CONCLUSION

Chapter 5 deals with the adsorption of PO_4^{3-} from aqueous solutions by ZLO in the batch mode experiments. The effects of pH, adsorbent dose, adsorbent particle size, co-anions, initial phosphorus concentration, contact time, and temperature on the adsorption process were examined. Though adsorption was most favored in the pH range of 2-6, ZLO worked well in a wide range of pH from 2 to 11. The optimal doses for the P sorption at initial P concentrations of 5, 10, 25, and 50 mg/L were 2, 3, 7, and 10 g/L respectively. The presence of common anions, such as sulfate, nitrate and chloride hardly interfered with the adsorption performance of ZLO. The maximum adsorption capacity of ZLO was around 59 mg PO_4/g adsorbent at 298 K. The

phosphate removal was fast, reaching 95% in 30 min. The Freundlich model best fitted the equilibrium data. The Pseudo-second model was most suitable for describing the adsorption kinetics, implying the dominance of chemisorptions in the entire process. The negative value of $\Delta G°$, the positive value of $\Delta H°$, and the positive value of $\Delta S°$ revealed the feasible, spontaneous and endothermic nature of the process. The adsorbed phosphorus was efficiently eluted using 0.2 M NaOH with the desorption efficiency reached up to 94.25%. ZLO could repeatedly be used for at least five consecutive cycles of adsorption - desorption with a reduction in the adsorption and desorption efficiencies of 12.46% and 7.40%, respectively. Overall, ZLO exhibited high capability for phosphorus elimination from the aquatic medium. The significant advantages of ZLO can be listed as wide effective pH range, minimum interference of foreign anions, reasonably high adsorption capacity, fast kinetics, and good reusability. These results would be beneficial for the development of a cheap, efficient and green phosphorus adsorbent from a plentiful AWB - okara.

UNIVERSITY OF TECHNOLOGY, SYDNEY

CHAPTER 6

ADSORPTION OF PHOSPHORUS FROM SYNTHETIC AND MUNICIPAL WASTEWATER BY ZIRCONIUM LOADED OKARA: COLUMN STUDY

6.1 INTRODUCTION

Phosphorus is not only an essential macro nutrient of living organisms and a fundamental material of many industries but also one of the major environmental concerns (Awual and Jyo, 2011). As a result of overexploitation of phosphate rocks, the global reserve for phosphorus can be depleted in only 100-250 years (Bottini and Rizzo, 2012; Ohura et al., 2011). In another perspective, the phosphorus concentration in receiving water medium above 0.02 mg/L can cause eutrophication (Mallampati and Valiyaveetttil, 2013). Thus, the elimination of phosphorus from effluents before discharging into aquatic medium is mandatory (Kalmykova and Fedje, 2013). The removal of phosphorus from water and wastewater can be achieved with several methods, such as membrane filtration, reverse osmosis (Greenlee et al., 2009), coagulation, precipitation, crystallization (Ackerman, 2012; Jia, 2014), adsorption/ion exchange (Biswas, 2008; Nur et al., 2014a; Okochi, 2013), magnetic separation, biological treatment, and constructed wetland (Martín et al., 2013). Of these, adsorption is considered as an attractive option, owing to simple operation, low cost, steady phosphorus removal, and the potential for phosphorus recovery (Zhang et al., 2014).

Recently, there is a growing trend in using low-cost adsorbents for phosphorus elimination to reduce the cost of water treatment. In this context, several AWBs have been tested as phosphorus adsorbents, e.g. apple peels, orange waste gel, bagasse, coir pith, and wood particles (Mallampati and Valiyaveettil, 2013; Biswas, 2008; Carvalho et al., 2011; Krishnan and Haridas, 2008; Eberhardt and Min, 2008). However, the biomaterials derived adsorbents often suffer from lack of mechanical strength, inefficiency in column adsorption with high flow rate, and limited reusability (Awual and Jyo, 2011). Till date, a majority of the studies on adsorptive removal of phosphorus from water and wastewater have been performed in the batch mode experiments (Nur et al., 2014a). The primary concern with batch experiment is that only a small quantity of wastewater can be treated (Damte, 2006). Though adsorption capacity acquired from batch equilibrium isotherm provides information about effectiveness of phosphorus - adsorbent system, it is impossible to apply the result to continuous flow fixed-bed column, where the contact time is usually shorter than the equilibrium time (Kumar and Bandyopadhyay, 2006). In contrast, the dynamic adsorption systems have significant advantages, such as large volume of treated water, easy scale-up from lab-scale processes, simple and continuous operation, and reduced requirement of adsorbents (Damte, 2006; Kumar et al., 2011; Long et al., 2014; Okochi, 2013). Besides, the

column breakthrough curve provides information on dynamic adsorption capacity (Zach-Maor et al., 2011). Until this present work, little information is available on the sustainable use of agricultural by-products based adsorbents for phosphorus removal from real wastewater in the continuous flow fixed-bed column adsorption systems (Bottini and Rizzo, 2012; Li et al., 2013; Paudyal et al., 2013). Therefore, attentions should be continuously paid to these aspects to promote the practical application of agricultural by-products derived adsorbents.

Soybean by-product (okara) is considered as a potential material for the development of phosphorus adsorbent, due to the abundant availability, low cost, simple processing, and unique physical characteristics. A vast amount of okara is generated worldwide, especially in Asian countries. Though okara can be used for other purposes, it usually causes environmental burden, due to the fast decay. Therefore, the utilization of okara for water treatment not only helps dispose of okara in a green way but also add value to this AWB. The idea of developing okara into phosphorus adsorbent is based on the formation of active binding sites for anions by loading okara with Zr^{4+} solution. In the Chapter 5 on the batch mode experiments, ZLO was proven to be a promising phosphorus adsorbent, due to high efficiency, selectivity and reusability (Nguyen et al., 2014a). The general objective of Chapter 6 was to develop a continuous phosphorus removal process that is applicable to households by using ZLO as an adsorbent. The specific objectives were as follows:

- To investigate the effect of different operating variables (flow rate, bed depth, feed concentration, adsorbent particle size, influent pH) on the performance of ZLO packed bed column and to estimate the dynamic adsorption capacity of ZLO;
- To examine the possibility of using common mathematical models (Adams-Bohart, Thomas, Yoon-Nelson, BDST) for predicting the breakthrough curves of phosphorus adsorption onto ZLO packed bed column;
- To evaluate desorption, regeneration and reuse properties of ZLO column;
- To explore the actual application of ZLO packed bed column in treating the real municipal wastewater; and
- To scale-up the ZLO packed bed column adsorption system.

A major part of Chapter 6 was published in the following paper:

6) **Nguyen**, **T.A.H.,** Ngo, H.H., Guo, W.S., Pham, T.Q., Li, F.M., Nguyen, T.V., Bui, X.T., 2015. Adsorption of phosphate from aqueous solutions and sewage using zirconium loaded okara (ZLO): Fixed-bed column study. *Sci. Total Environ.* 523, 40-49.

6.2 LABORATORY SCALE BIOREACTOR

6.2.1 Removal phosphorus from synthetic solution

A. Effect of column design parameters

(i) Effect of flow rate

The effect of the flow rate on phosphorus adsorption by ZLO was explored with various flow rates (12, 20, and 28 mL/min) and a constant bed height (23 cm), initial phosphorus concentration (5.5 mg/L). The breakthrough curves for the column were determined by plotting the C_t/C_o (C_t and C_o are the phosphorus concentration of effluent and influent, respectively) against the time and depicted in Fig.6.1. As the figure shows, the shorter breakthrough time occurred at higher flow rate. It can be explained by the fact that a larger volume of water elapsed through the bed at higher flow rate. As a consequence, more PO_4^{3-} anions contacted with the binding sites of ZLO, making them get saturated more quickly. Similarly, higher adsorption capacity was attained at lower flower rate. It is probably because lower flow rate resulted in more residence time of the phosphorus ions in the column. Since phosphate ions had longer contact time with ZLO, equilibrium can be reached before PO_4^{3-} ions moved out of the column (Jain et al., 2013). According to Damte (2006), the longer contact time led to a more efficient diffusion of PO_4^{3-} ions into ZLO particles, and thus better adsorption capacity was achieved. These findings agree with the previous studies conducted by Awual and Jyo (2011), and Paudyal et al. (2013).

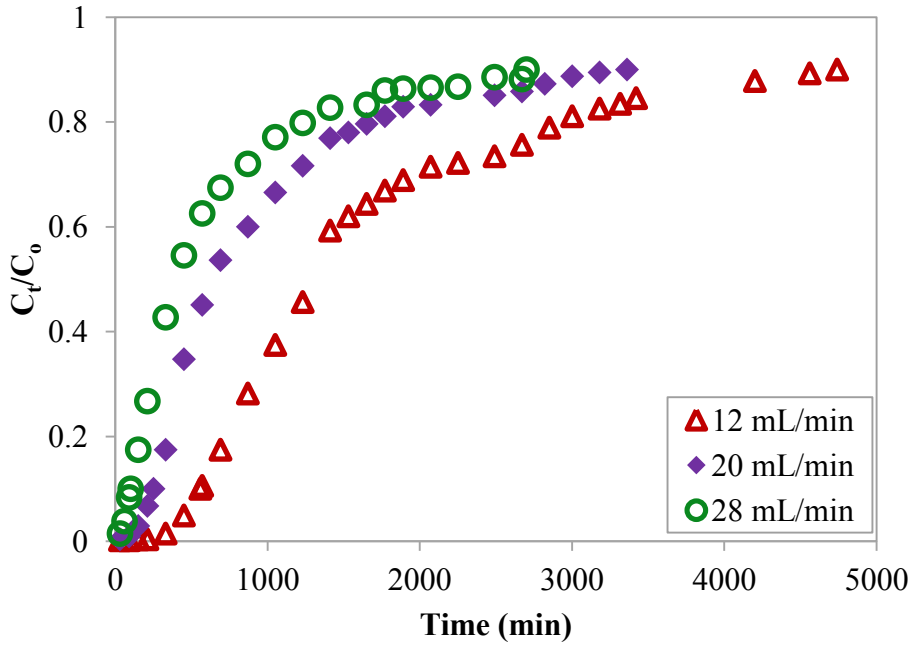

Figure 6.1 Effect of flow rate on the breakthrough curve of P adsorption onto ZLO (natural pH, particle size = 1 mm-600 µm, C_i = 5.5 mg P/L, bed height = 23 cm)

(ii) Effect of initial phosphorus concentration

It is reported that influent phosphorus concentration can also affect the breakthrough curve (Awual and Jyo, 2011). Fig.6.2 illustrates the breakthrough curves for varying feed phosphorus concentrations (5.5, 10.2, and 15.5 mg/L), given bed height (23 cm) and flow rate (12 mL/min.) The breakthrough time was 558, 380, and 254 min. for influent phosphorus concentration of 5.5, 10.2, and 15.5 mg/L, respectively. Equally, the exhaustion time declined with a rise in phosphorus initial concentration, from 4740 min. (5.5 mg/L) to 3030 min. (10.2 mg/L) to 1590 min. (15.5 mg/L). It is evident from Fig.6.2 that the higher the influent phosphorus concentration was, the faster the breakthrough and exhaustion took place. Higher retention rate and thus, earlier saturation might result from greater concentration gradient and smaller mass transfer resistance at a higher phosphate concentration (Mohammed and Rashid, 2012; Paudyal et al., 2013). A similar tendency was reported by Zhang et al. (2014) in case of removing phosphate using activated laterite. The dynamic adsorption capacity of ZLO for phosphorus increased, from 11.93 to 14.28 mg/g with the elevating phosphorus inlet concentration, from 5.5 to 15.5 mg/L. These results are in line with those reported by Awual and Jyo (2011) for the elimination of phosphorus by polymeric anion exchangers.

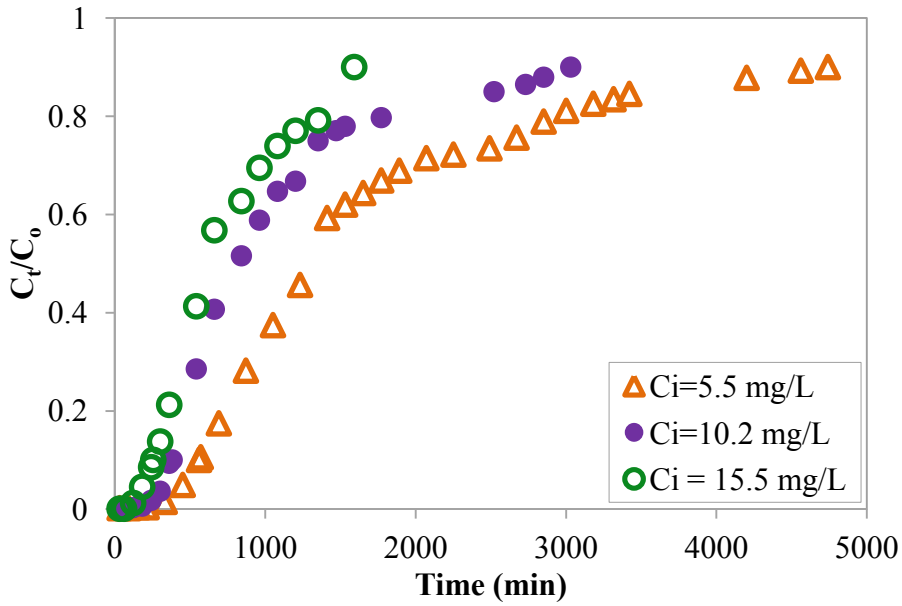

Figure 6.2 Effect of influent P concentration on the breakthrough curve of P adsorption onto ZLO (natural pH, particle size = 1 mm-600 µm, flow rate = 12 mL/min, bed height = 23 cm)

(iii) Effect of bed height

Fig.6.3 described the effect bed height on the breakthrough curve of phosphorus adsorption onto ZLO column. As can be seen from Fig.6.3, shorter breakthrough time or steeper breakthrough curve occurred at low bed height. Specifically, the breakthrough time (at C_t/C_o 10%) was 1000, 558, and 160 min. for 34.5, 23 and 11.5 cm bed height, respectively. Likewise, the exhaustion time (at C_t/C_o 90%) declined from 6600 to 2160 min when bed height reduced from 34.5 to 11.5 cm. The phosphorus uptake capacity of ZLO was 12.12 and 10.41 mg/g for the bed height of 34.5 and 11.5 cm, respectively as listed in Table 6.1. The result suggested that reducing bed height led to a fall in phosphorus uptake capacity of ZLO. Jain et al. (2013) attributed this to the fewer adsorption sites at lower bed height. Conversely, Paudyal et al. (2013) explored that lessening the bed height led to an augmentation of the adsorption capacity of Zr^{4+}-DOJR for fluoride. The authors ascribed this to the greater channeling effect at the higher bed depth and proposed to mitigate this effect by increasing the column diameter.

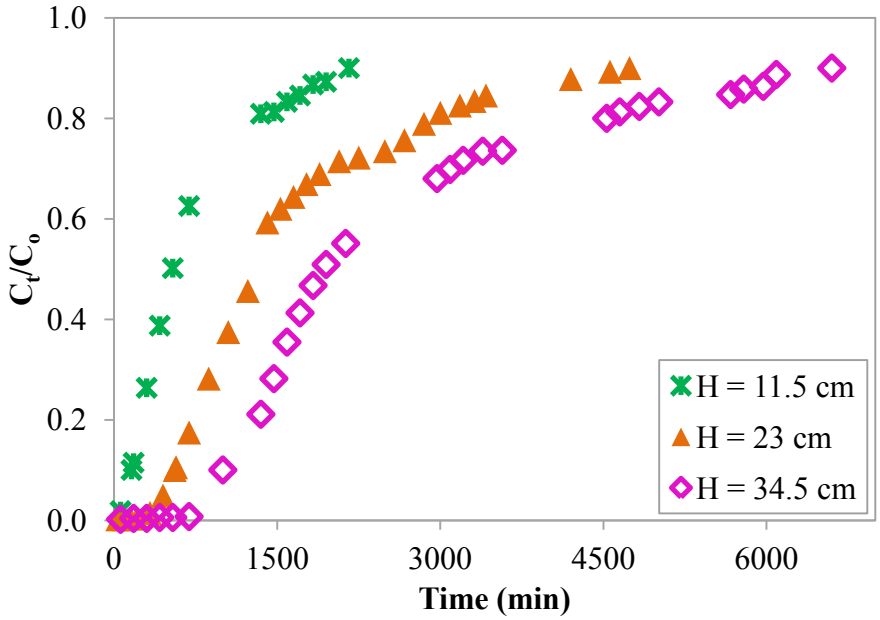

Figure 6.3 Effect of bed height on the breakthrough curves of P adsorption onto ZLO (natural pH, particle size = 1 mm-600 µm, flow rate = 12 mL/min, C_i = 5.5 mg P/L)

(iv) Effect of influent pH

The solution pH is a critical influencing factor to the dynamic adsorption process since it can affect the ionic state of the functional groups and phosphate species as well (Chen et al., 2012b). The effect of influent pH on PO_4^{3-} removal by ZLO column was examined at pH values of 3 and 8, while maintaining the same initial P concentration (5.6 mg/L), bed height (23 cm), and flow rate (12 mL/min). It is clear from Fig.6.4 that the breakthrough time increased from 550 to 1099 min. with decreasing pH from 8 to 3. It implied that the breakthrough happened more slowly at pH 3. As a result, pH 3 was chosen as the optimal pH for phosphorus adsorption on ZLO column. These findings agreed well with those of the batch adsorption tests reported in the previous paper (Nguyen et al., 2014b). It can be explained by the electrostatic interaction between anionic phosphates species with cationic functional groups on the surface of ZLO. In the acidic medium (pH 3), $H_2PO_4^-$ and HPO_4^{2-} species were dominant, which were powerfully retained onto ZLO (Mallampati and Valiyaveettil, 2013). Nevertheless, in alkaline medium (pH 8), the competition between hydroxyl ions with phosphate anions for binding sites led to the decline in phosphate adsorption onto ZLO column. The phosphorus uptake by ZLO packed bed column at pH 3 and pH 8 was 16.43 and 12.26 mg/g, respectively (Table 6.1). These results are in good agreement with those reported by Awual and Jyo (2011) and Biswas (2008) showing that lower pH can result in better

phosphate adsorption. Although phosphorus adsorption by ZLO was more efficient at pH 3, in the subsequent experiments, the natural pH of the synthetic solution and municipal wastewater (7.5-8.0) was used to evaluate the actual application of ZLO.

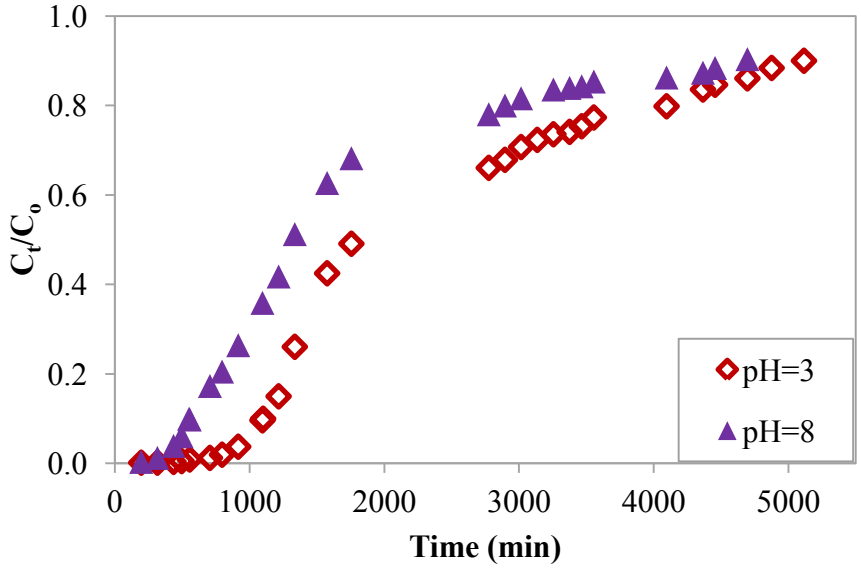

Figure 6.4 Effect of pH on the breakthrough curve of P adsorption on ZLO (bed height = 23 cm, flow rate = 12 mL/min, influent P concentration = 5.6 mg/L, and particle size = 1 mm-600 µm)

(v) Effect of adsorbent particle size

Fig.6.5 depicted the effect of adsorbent particle size on the breakthrough curve of phosphate adsorption onto ZLO. It was shown that, the use of smaller ZLO particle size resulted in longer breakthrough time and higher phosphorus uptake capacity. Specifically, as a result of reducing ZLO particle size from 1000-600 to 300-150 µm, the breakthrough occurred more slowly 178 min. while the phosphorus uptake capacity boosted by 43.52%. Apparently, the smaller particle size of ZLO facilitates the phosphorus adsorption from aqueous solutions. The larger surface area may be responsible for higher adsorption capacity with smaller particle size. This finding is supported by that of earlier batch adsorption system with ZLO. A similar observation was reported by Okochi (2013) for the removal of phosphorus from storm water using electric ARC furnace steel slag. Unfortunately, the use of the particle size of 300-150 µm resulted in the column clogging during desorption test with 0.2 M NaOH. To solve this problem, the column should be packed with a mixture of different particle sizes instead of individual particle size. By this way, it is expected to enhance the adsorption capacity of ZLO while reduce the column clogging.

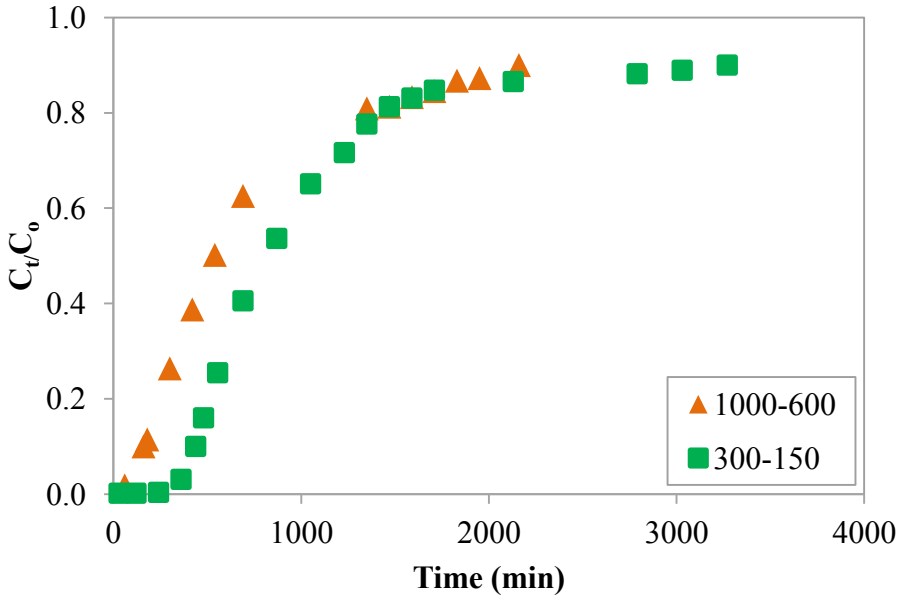

Figure 6.5 Effect of particle size on the breakthrough curve of P adsorption onto ZLO (natural pH, bed heights = 11.5 cm and 9 cm, flow rate = 12 mL/min, influent P concentration = 5.5 mg/L)

Table 6.1 Breakthrough curve parameters for P adsorption onto ZLO at different operating conditions

pH	P_S (mm)	Q (mL/min)	Z (cm)	C_o (mg/L)	t_b (min)	V_b (L)	q_b (mg/g)	R_b (%)	t_s (min)	V_s (L)	q_s (mg/g)	R_s (%)	AER (g/L)	MTZ (cm)
Natural	1-0.6	12	23	5.5	558	6.70	3.59	97.58	4740	56.88	11.93	38.12	1.49	20.29
Natural	1-0.6	20	23	5.5	250	5.00	2.67	96.87	3360	67.20	11.87	32.12	2.00	21.29
Natural	1-.0.6	28	23	5.5	100	2.81	1.48	96.23	2700	75.60	11.84	28.47	3.56	22.15
Natural	1-0.6	12	23	5.5	558	6.70	3.59	97.58	4740	56.88	11.93	38.12	1.49	20.29
Natural	1-0.6	12	23	10.2	380	4.56	4.54	97.74	3030	36.36	14.09	37.99	2.19	20.12
Natural	1-.0.6	12	23	15.5	254	3.05	4.58	97.11	1590	19.08	14.28	48.30	3.28	19.33
Natural	1-0.6	12	11.5	5.5	160	1.92	2.03	95.96	2160	25.92	10.41	36.50	2.60	10.65
Natural	1-0.6	12	23	5.5	558	6.70	3.59	97.58	4740	56.88	11.93	38.12	1.49	20.29
Natural	1-.0.6	12	34.5	5.5	1000	12.00	4.31	97.58	6600	79.20	12.12	41.74	1.25	29.27
Natural	1-0.6	12	11.5	5.5	160.2	1.92	2.03	95.96	2160	25.92	10.41	36.50	2.60	10.65
Natural	0.3-0.15	12	9	5.5	438	5.26	5.68	98.24	3270	39.24	14.97	34.69	0.95	7.79
3	1-0.6	12	23	5.6	1100	13.20	7.25	98.14	5118	61.38	16.43	47.81	0.76	18.05
8	1-0.6	12	23	5.6	550	6.60	3.62	97.85	4698	56.34	12.26	38.86	1.51	20.30

Notation: P_S - Particle size (mm); Q- Volumetric flow rate (mL/min); Z - bed depth; C_o - initial P concentration (mg/L); t_b,V_b - the service time and treated volume at 10% breakthrough point; t_s, V_s- the service time and treated volume at 90% saturation point; q_b, q_s - the amount of phosphorus captured per unit of dry weight of ZLO at 10% breakthrough point and 90% saturation points, respectively; R_b, R_s- the removal percentage of phosphorus at 10% breakthrough and 90% saturation points, respectively; AER - adsorbent exhaustion rate; MTZ - mass transfer zone.

B. Breakthrough curve modeling

The prediction of the breakthrough curve is essential for designing a continuous adsorption system. The relation between concentration and time provides insights into the adsorbent affinity, adsorbent surface properties, and adsorption pathways (Foo et al., 2013). For that reason, several mathematical models have been developed for this purpose. This study investigates the dynamic adsorption behavior of ZLO using Adams-Bohart, Thomas, Yoon-Nelson, and BDST models.

(i) Adam's-Bohart model

Adams-Bohart model assumes that equilibrium is not instant, and the adsorption rate is controlled by external mass transfer (Quintelas et al., 2013). This model is appropriate for analyzing the initial part of the breakthrough curve (C_t/C_o = 0-0.5) (Long et al., 2014; Sharma and Singh, 2013). The equation of Adams-Bohart model is expressed as follows:

$$ln\frac{C_t}{C_0} = K_{AB}\,C_0 t - K_{AB}\,N_0\frac{Z}{F} \quad (6.1)$$

where C_o and C_t (mg/L) are the influent and effluent phosphorus concentration, K_{AB} (L/mg min) is the kinetic constant, N_o (mg/L) is saturation concentration of the column, Z (cm) is the bed depth, F (cm/min) is the linear velocity achieved by dividing the flow rate (cm^3/min) by the column section area (cm^2).

The constants K_{AB} and N_o of the Adams-Bohart model can be estimated from the linear plot of $ln(C_t/C_o)$ against t. As can be seen in Table 6.2, the adsorption capacity of the bed (N_o) decreased from 1.26 to 0.78 mg/L with increasing flow rate (Q) from 12 to 28 mL/min. Conversely, N_o value expanded from 1.34 to 1.74 mg/L when bed height rose from 11.5 to 34.5 cm. The increase in initial phosphorus concentration from 5.5 to 15.5 mg/L led to a growth in N_o value, from 1.26 to 1.71 mg/L. The kinetic constant (k_{AB}) declined from 127 to 54.55 L/(mg min) with increasing bed height (Z) from 11.5 to 34.5 cm. On the contrary, the k_{AB} value extended from 109.09 to 272.73 L/(mg min) with growing flow rate (Q) from 12 to 28 mL/min. The results suggest that, better adsorption performance of the column, characterized by higher adsorption capacity (N_o) and lower kinetic constant (k_{AB}), can be achieved with higher initial phosphorus concentration (C_o) and bed height (Z), but lower feed flow rate (Q) (Bulgariu and Bulgariu, 2013). Based on the correlation coefficients, Adams-Bohart model provided a relatively good fit to the phosphorus - ZLO adsorption system.

(ii) Thomas model

Thomas model is developed on the assumption that (1) the adsorption is not limited by chemical interactions but by mass transfer at the interface and (2) the experimental data follows Langmuir isotherms and second-order kinetics (Foo et al., 2013). Unlike Adams-Bohart model, Thomas model is appropriate for depicting the whole breakthrough curve (Bulgariu and Bulgariu, 2013). Thomas model can be written in the linear form by the following equation (Paudyal et al., 2013):

$$\ln(\frac{C_0}{C_t} - 1) = k_{Th}\, q_o \frac{m}{Q} - k_{Th} C_o t \quad (6.2)$$

where k_{Th} stands for Thomas rate constant (mL/min mg), q_o is the adsorption capacity (mg/g), C_o is the inlet phosphorus concentration (mg/L), C_t is the outlet phosphorus concentration at time t (mg/L), m is the mass of adsorbent (g), Q is the feed flow rate (mL/min), and t is the filtration time (min). The values of k_{Th} and q_o were determined from the linear plot of $\ln(\frac{C_0}{C_t} - 1)$ against t and shown in Table 6.2.

As the flow rate increased (12 to 28 mL/min), the Thomas rate constant increased (0.098 to 0.140 mL/(min mg)), whereas the adsorption capacity reduced (3.29 to 0.31 mg/g). An increase in initial phosphorus concentration (5.5 to 15.5 mg/L) led to an elevation in both Thomas rate constant (0.098 to 0.129 mL/(min mg)) and adsorption capacity (3.29 to 12.21 mg/g). The increase in bed depth (11.5 to 34.5 cm) resulted in a decrease in the Thomas rate constant (0.182 to 0.076 mL/(min mg)), but a growth in uptake capacity (2.42 to 5.74 mg/g). Superior uptake capacity at the higher feed phosphorus concentration can be attributed to the larger concentration gradient and higher driving force (Paudyal et al., 2013). A similar trend was reported by Bulgariu and Bulgariu (2013), Long et al. (2014) and Samuel et al. (2013). In the most cases, the correlation coefficients of Thomas models were higher than 0.9. It indicates that Thomas model can be used to describe the phosphorus adsorption onto ZLO column. Also, the adsorption process was not regulated by internal and external diffusions (Chen et al., 2012a).

(iii) Yoon-Nelson model

Similar to Thomas model, Yoon-Nelson model can mitigate limitations of Adams-Bohart model during the later period of the breakthrough curve. The linear expression of Yoon-Nelson model is given by the following equation (Sharma and Singh, 2013):

$$ln(\frac{C_t}{C_0 - C_t}) = k_{YN} t - \tau k_{YN} \quad (6.3)$$

where k_{YN} is the Yoon-Nelson rate constant (min^{-1}), τ is the time required for 50% phosphorus breakthrough (min).

Table 6.2 represents Yoon-Nelson model parameters (k_{YN} and τ) which were calculated from the linear plot of $\ln[C_t/(C_o-C_t)]$ against t. It was found that k_{YN} increased (0.54 to 0.99 min^{-1}) while τ decreased (23.95 to 3.64 h) with an increase in the flow rate (12 to 18 mL/min). A similar trend occurred to k_{YN} and τ with the increasing influent phosphorus concentration. Sharma and Singh (2013) explained these results by the faster saturation of the column at higher flow rate and inlet phosphorus concentration. Nevertheless, τ was extended at higher bed depths. Similar trends were reported by Chen et al. (2012a) and Long et al. (2014). The τ values predicted by Yoon-Nelson model were quite similar to those obtained from experiments. Nevertheless, the investigation of correlation coefficients showed that Yoon-Nelson model was less satisfactory than Adams-Bohart and Thomas models in describing the phosphate-ZLO adsorption system.

(iv) Bed depth service time (BDST) model

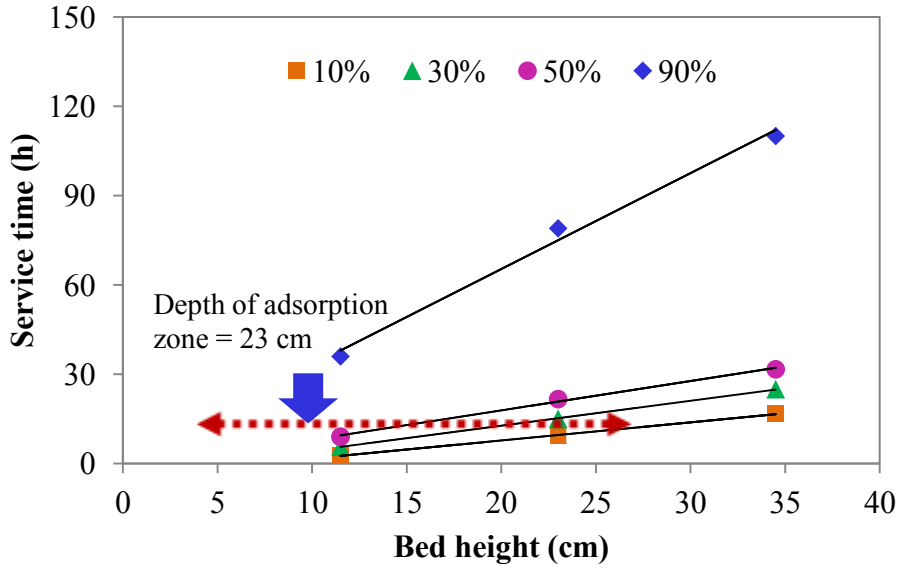

Figure 6.6 BDST model for 10%, 30%, 50%, and 90% breakthrough at different bed depths and constant inlet P concentration (5.5 mg/L) and flow rate (12 mL/min)

The BDST model is to represent the relationship between bed depth and service time. It is reported that BDST model can describe appropriately initial part (10-50%) of the breakthrough curve (Jain et al., 2013). The linear expression of BDST model is given by the following equation (Li et al., 2013; Paudyal et al., 2013):

$$t = \frac{ZN_o}{C_o v} - \frac{1}{K_b C_o} ln(\frac{C_o}{C_b} - 1) \quad (6.4)$$

where t is the service time of column (h), Z is the bed depth (cm), C_o is the inlet phosphorus concentration (mg/L), C_b is the outlet concentration at breakthrough point (mg/L), N_o is the column adsorption capacity (mg/L), K_b is the rate constant [L/(mg h)], v is the linear flow velocity and is calculated by dividing the flow rate by the area of column (cm/min).

Table 6.2 Adams-Bohart, Thomas and Yoon-Nelson model constants for P adsorption onto ZLO column

Conditions					Adams-Bohart			Thomas			Yoon-Nelson		
pH	P_S	Q	Z	C_o	k_{AB}	N_o	R^2	k_{Th}	q_o	R^2	k_{YN}	τ	R^2
Natural	1-0.6	12	23	5.5	109.09	1.26	0.928	0.098	3.29	0.982	0.54	23.95	0.890
Natural	1-0.6	20	23	5.5	200.00	0.99	0.934	0.136	1.75	0.903	0.96	10.62	0.825
Natural	1-.0.6	28	23	5.5	272.73	0.78	0.887	0.140	0.31	0.936	0.99	3.64	0.831
Natural	1-0.6	12	23	5.5	109.09	1.26	0.928	0.098	3.29	0.982	0.54	23.95	0.890
Natural	1-0.6	12	23	10.2	98.04	1.49	0.946	0.099	8.33	0.860	1.21	15.49	0.780
Natural	1-.0.6	12	23	15.5	83.87	1.71	0.790	0.129	12.21	0.963	2.00	10.94	0.963
Natural	1-0.6	12	11.5	5.5	127.00	1.34	0.871	0.182	2.42	0.984	1.00	7.77	0.971
Natural	1-0.6	12	23	5.5	90.91	1.52	0.928	0.098	3.29	0.982	0.54	23.95	0.890
Natural	1-.0.6	12	34.5	5.5	54.55	1.74	0.962	0.076	5.74	0.970	0.49	31.07	0.945
Natural	1-0.6	12	11.5	5.5	109.09	1.44	0.843	0.182	2.42	0.984	1.00	7.77	0.971
Natural	0.3-0.15	12	9	5.5	181.82	2.23	0.945	0.180	7.26	0.742	1.15	13.29	0.730
3	1-0.6	12	23	5.6	71.43	2.18	0.973	0.109	11.00	0.988	0.63	28.28	0.991
8	1-0.6	12	23	5.6	71.42	1.60	0.831	0.100	4.06	0.941	0.75	22.77	0.902

Notation: P_S, particle size (mm); Q, feed flow rate (ml/min); Z, bed height (cm); C_o, initial phosphorus concentration (mg/L); k_{AB}, Adams-Bohart model rate constant (L/mg min)x10^{-5}; N_o, saturation concentration (mg/L)x10^3; k_{Th}, Thomas model rate constant (mL/mg min)x10^{-3}; q_o, equilibrium phosphorus sorption capacity (mg/g); k_{YN}, Yoon-Nelson model rate constant (1/min)x10^{-3}; τ, the time required for 50% breakthrough (min).

From the plots of time versus bed depth (Fig.6.6), the BDST parameters, namely N_o and K_b, are calculated as follows (Zach-Maor et al., 2011):

$$m = \text{slope} = \frac{N_o}{C_o v} \rightarrow N_o = mC_o v \quad (6.5)$$

$$C = \text{intercept} = -\frac{1}{K_b C_o}\ln\left(\frac{C_o}{C_b} - 1\right) \rightarrow K_b = -\frac{1}{C * C_o}\ln\left(\frac{C_o}{C_b} - 1\right) \quad (6.6)$$

Setting t = 0 and solving Eq. (6.4) for Z produces the following equation (Kumar and Bandyopadhyay, 2006):

$$Z_o = \frac{v}{K_b N_o} ln\left(\frac{C_o}{C_b} - 1\right) \quad (6.7)$$

where Z_o (cm) is called the critical bed depth, which is the minimum bed depth required to yield the desired effluent concentration (C_b).

Table 6.3 represents BDST model constants (N_o, K_b) and corresponding critical bed depth (Z_o) for various breakthrough points (10%, 30%, and 50%) at a constant initial P concentration (5.5 mg/L) and flow rate (12 mL/min). The high correlation coefficients (R^2 >0.995) demonstrated that BDST model could efficiently depict the phosphate - ZLO dynamic adsorption system.

Table 6.3 BDST model constants for P adsorption on ZLO

Breakpoint (%)	m (h/cm)	C (h)	N_o (mg/L)	K_b (L/mg h)	Z_o(cm)	R^2
10	0.608	-4.555	16.69	0.0897	7.33	0.999
30	0.840	-4.106	23.06	0.0973	4.89	0.999
50	0.985	-1.89	27.04	0.2114	1.92	0.995

The adsorption zone, known as the mass transfer zone (MTZ), can be defined as the adsorbent layer through which the effluent concentration changes from 10 to 90% of the influent concentration. MTZ is identified as the horizontal distance between these two lines in the BDST plot (Kumar and Bandyopadhyay, 2006). From Fig.6.6, MTZ in this study was estimated to be 23 cm. The Eq. (9) allows predicting the breakthrough time (t_b) for a new bed depth (Z) without conducting further experiments. The prediction utilizes N_o, K_b values determined at the same initial phosphorus concentration (C_o) and velocity (v). Table 6.4 represents the predicted and observed breakthrough times for varying bed depths. It was found that the breakthrough times calculated by BDST model were quite similar to those obtained from the experiment. It validates the applicability of BDST model to P - ZLO dynamic adsorption system.

Table 6.4 Prediction of breakthrough time for different bed depths by BDST model

Bed depth (cm)	10% breakthrough		50% breakthrough	
	Predicted t_b (h)	Observed t_b (h)	Predicted t_b (h)	Observed t_b (h)
11.5	2.44	2.67	9.44	9.00
23	9.43	9.30	20.77	21.67
34.5	16.42	16.67	32.09	32.50

C. Column adsorption capacity of ZLO

The dynamic adsorption capacity of ZLO for phosphorus at the breakthrough time and exhaustion time was calculated for different operating conditions (Table 6.1). The highest P adsorption capacity of ZLO at the exhaustion time was 16.43 mg/g, accounting for 85.44% its equilibrium adsorption capacity (19.93 mg/L). This maximum value was achieved for a bed height of 23 cm, flow rate of 12 mL/min and initial phosphorus concentration of 5.6 mg/L, particle size of 1000-600 µm, and influent pH of 3.

Table 6.5 indicates that ZLO is favorably comparable to most of the reported adsorbents in term of P adsorption capacity. The result shows that ZLO can effectively remove P in the continuous adsorption systems. The reasonably high adsorption capacity of ZLO column for phosphorus can be explained by the fact that Zr^{4+} loading resulted in the development of effective binding sites for phosphate anions on the surface of okara. Consequently, the retention of phosphate onto ZLO was strengthened.

Table 6.5 Comparing ZLO with various adsorbents in term of the P dynamic adsorption capacity

Adsorbent	Z (cm)	Q (mL/min)	C_o (mg/L)	pH	Temp. (^oC)	q_b (mg/g)	q_s (mg/g)	Reference
Diaion WA20	-	1.67	34.68	7	-	12.74	-	Awual and Jyo, 2011
La^{3+}-loaded SOW	-	0.12	20	7.5	30	-	13.63	Biswas et al., 2007
Zr^{4+}-loaded SOW	-	-	20	7	30		10	Biswas, 2008
Zr^{4+}-loaded SOW	-	-	20	3	30		36	Biswas, 2008
CP-Fe-I	-	6.1	16.32	-	30	-	22.19	Krishnan and Haridas, 2008
Purolite FerrIX A33E	19	13	20	7.2-7.6	room	12.5	-	Nur et al., 2014b
Purolite FerrIX A33E	12	13	5	7.2-7.6	room	4.1	-	Nur et al., 2014b
Zr^{4+}-loaded SOW	-	0.20	5.9		30	-	40.3	Ohura et al., 2011
Steel slag	7.5	7.92	-	6.0-7.4	room	-	0.7	Okochi, 2013
AC-WS	-	5	100	-	-	-	13.67	Xu et al., 2011b
AC-CS	-	5	100	-	-	-	16.01	Xu et al., 2011b
GR based resin	-	5	200	5.12	-	-	17.84	Xu et al., 2011a
Zr^{4+}-loaded okara	23	12	5.6	3	room	7.25	16.43	This study
Zr^{4+}-loaded okara	9	12	5.5	7.6	room	5.68	14.97	This study

Notation**:**

Z, bed depth (cm); Q, flow rate (mL/min); C_o, influent phosphorus concentration (mg/L); q_b, column adsorption capacity at breakthrough time (mg/g), q_s, column adsorption capacity at exhaustion time (mg/g)

6.2.2 Application of ZLO in treating municipal wastewater

A. Comparative study on adsorption performance of ZLO in synthetic and municipal wastewater

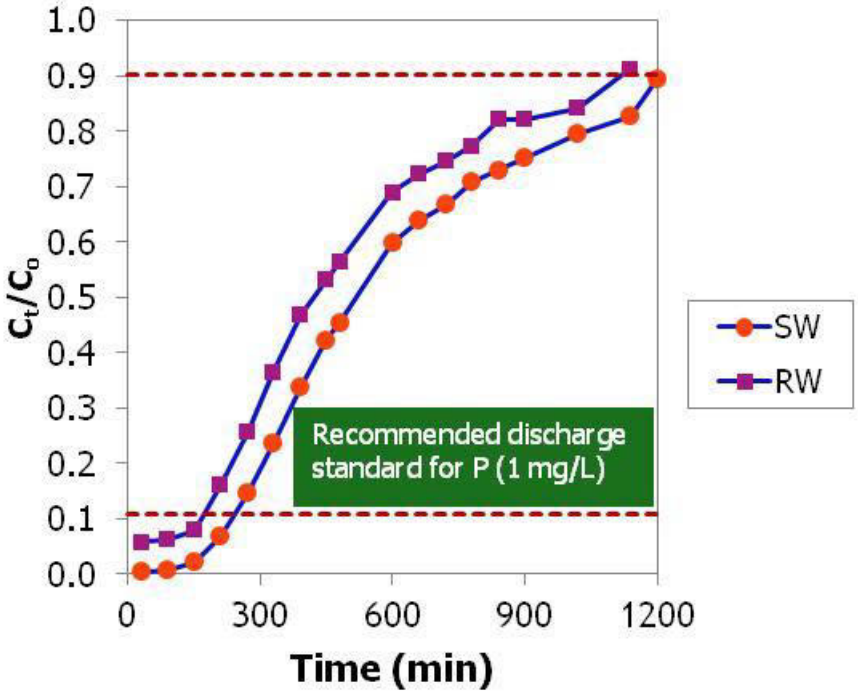

Figure 6.7 Breakthrough curves for P adsorption from synthetic and raw municipal wastewater by ZLO (Particle size >600 µm; bed depth = 21 cm, flow rate = 28 mL/min, inlet P concentration = 5.7 mg/L)

The application of ZLO in treating real wastewater was tested in a mini-column using the raw municipal wastewater, which was collected from Sydney Olympic Park Wastewater Treatment Plant. The municipal wastewater composition was determined as follows: pH 7.68, salinity 0.42‰, turbidity 87.9 NTUs, electrical conductivity 870 µS/cm, total suspended solids (TSS) 84 mg/L, ammonium (NH_4-N) 51 mg/L, nitrate (NO_3^--N) 3.60 mg/L, nitrate (NO_2^--N) 0.19 mg/L, orthophosphate (PO_4-P) 5.7 mg/L, total organic carbon (TOC) 22.05 mg/L, chemical oxygen demand (COD) 239 mg/L, chloride (Cl^-) 108.10 mg/L, calcium (Ca^{2+}) 30.55 mg/L, magnesium (Mg^{2+}) 9.2 mg/L, iron (Fe^{2+}) 0.25 mg/L, copper (Cu^{2+}) 0.1 mg/L, lead (Pb^{2+}) 0.35 mg/L, manganese (Mn^{2+}) 0.04 mg/L, nickel (Ni^{2+}) 0.02 mg/L, zinc (Zn^{2+}) and cadmium (Cd^{2+}) non-detectable. Obviously, the concentration of heavy metals was negligible in municipal wastewater. The municipal wastewater was settled for 24 h prior to adsorption test. Fig.6.7 shows the breakthroughs for phosphorus adsorption onto ZLO column using

synthetic solution and real municipal wastewater for comparison purpose. It was found that the phosphorus level of the municipal wastewater was lowered to the recommended discharge limit (1 mg/L) for a period of 210 min, using a column packed with only 10 g of ZLO. Comparing the phosphorus content of the municipal wastewater before and after passing through ZLO column showed that more than 90% phosphorus was eliminated from 5880 mL municipal wastewater in 210 minutes. The results proved that phosphorus from the municipal wastewater was successfully captured by ZLO column. The breakthrough time and the dynamic adsorption capacity of ZLO obtained with the municipal wastewater were quite similar to those with the synthetic solution. The results indicated that the effect of co-existing ions in the municipal wastewater on the continuous adsorption process was negligible. As a final remark, ZLO is capable of removing P from the real municipal wastewater in the dynamic adsorption system.

B. Successive adsorption-desorption cycles

(i) Adsorption of phosphate onto ZLO packed bed column

In order to investigate the reusability of ZLO in the reality, the adsorption tests of ZLO were repeated three times with real municipal wastewater. Fig.6.8 represents the breakthrough curves for three adsorption times of ZLO. From the figure, it is clear that there was no big difference among breakthrough curves for three adsorption times. For the first time, the breakthrough occurred at 60 min. while the exhaustion achieved at 1500 min. For the third time, the breakthrough time and exhaustion time were 90 min. and 1710 min., respectively. Despite a slight reduction in the uptake capacity (18.64%) and removal percentage at the exhaustion time (7.30%) after three adsorption times , the regenerated ZLO still had a high adsorption capacity, and thus it can be kept recycling.

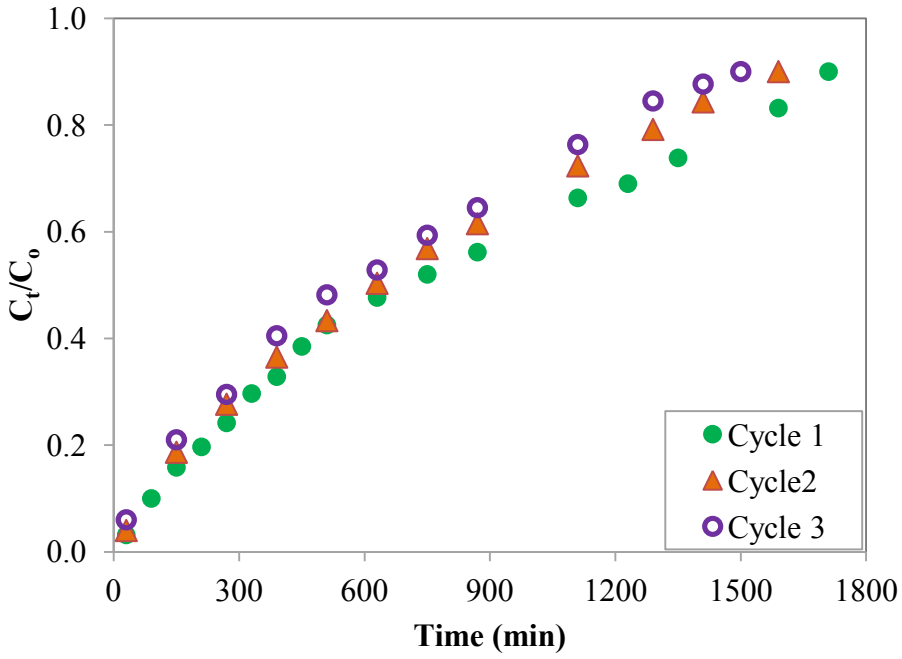

Figure 6.8 Breakthrough curves for P adsorption from municipal wastewater by ZLO in three cycles (C_i = 6.0 mg P/L, flow rate = 12 mL/min, bed depth = 10 cm, and particle size = 1mm-600 µm)

(ii) Elution of loaded phosphorus and regeneration of exhausted ZLO

Desorption and regeneration play a critical role in the sustainable use of the adsorbent (Jain et al., 2013; Xu et al., 2011b). In the earlier batch adsorption tests, the dilute alkaline solution (0.2 M NaOH) was proven to be the best desorption solution (Nguyen et al., 2014a). In the present study, 0.2 M NaOH was employed for eluting phosphorus from saturated ZLO column. Prior to desorption test, phosphorus saturated ZLO column was washed with an abundant amount of distilled water to eliminate unbound phosphate ions. In the first cycle, more than 70% of loaded phosphorus was eluted when 360 mL of 0.2 M NaOH was percolated through the column, which lasted for around 0.5 h. The effluent phosphorus concentration at 0.5 h was 112 mg/L, 18.67 times higher than the feed phosphorus concentration. Desorption process was almost completed within 2.75 h with the efficiency reached up to 92.16%, indicating that the adsorption of phosphorus onto ZLO column was revisable. After three cycles of operation, the desorption efficiency of ZLO column was still above 88% (Table 6.6, Fig.6.9), showing that ZLO column had efficient regeneration and reuse properties. The elution of phosphate from ZLO column might result from an ion exchange reaction, whereby OH- ions from NaOH displaced phosphate ions from ZLO surface. Nevertheless, after three cycles of adsorption-desorption, the weight loss of ZLO

column was found to be 8.7%. This is in line with the result by Xu et al. (2011b), who reported that the weight loss after three adsorption - desorption cycles of the cotton stalk and wheat stalk was about 5%. The authors suggested this weight loss might result from the corrosion of cellulose and hemicelluloses in these adsorbents, caused by HCl desorption solution. After several cycles of operation, ZLO may become inefficient in removing phosphorus from wastewater. By that time, it was recommended to recover loaded Zr^{4+} using strong acids while recycle the residual substrate as fertilizer (Paudyal et al., 2013).

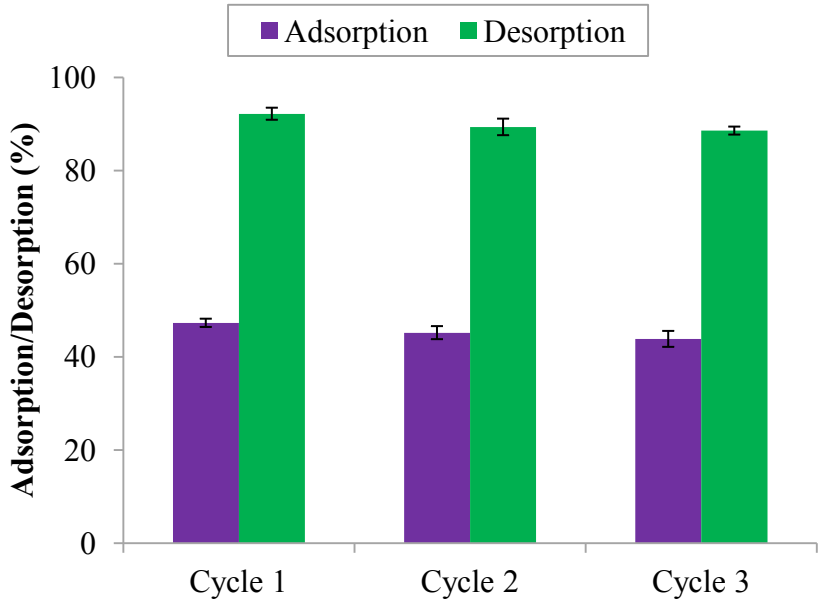

Figure 6.9 The performance of ZLO packed bed column in three successive cycles of adsorption - desorption (The standard deviation values = 0.86-1.77% for sample size N = 3)

Table 6.6 Parameters for three cycles of adsorption - desorption with raw municipal wastewater

Cycle No	Breakthrough time (min)	Exhaustion time (min)	Exhaustion uptake (mg/g)	Desorption efficiency (%)
1	90	1710	11.64	92.16
2	75	1590	10.34	89.33
3	60	1500	9.47	88.54

6.3 SEMI-PILOT SCALE BIOREACTOR

The application of data from lab-scale, small columns in designing a full-scale, large column may be ineffective. This can be attributed to several problems that may occur to a large column, such as non-uniform distribution of the flow, selective flow path or uneven packing. Besides, running a full-scale column typically takes a long time and is costly with respect to the adsorbent preparation (Damte, 2006). Thus, a semi-pilot scale study using a large column was carried out to envisage any challenges in pilot to full-scale reactor.

6.3.1 Adsorption of P from municipal wastewater by ZLO

The dynamic adsorption test at semi-pilot scale was examined with ZLO in a big column (4.5 cm x 120 cm) using real municipal wastewater. The raw municipal wastewater was collected from Sydney Olympic Park Wastewater Treatment Plant and had the average phosphorus concentration of 5.5 mg/L. The operating conditions of the big column adsorption test were presented in Table 6.7. The feed solution was pumped upward into the column, which was packed with 100 g of ZLO, at the flow rate of 53 mL/min.

Table 6.7 Operating conditions of the semi-pilot scale column adsorption test

Parameter	Unit	Value
ZLO weight (m)	g	100
ZLO bed height (Z)	cm	30
ZLO bed volume (BV)	cm^3	477
P initial concentration (C_o)	mg/L	5.5
Volumetric flow rate (Q)	cm^3/min	53
Superficial velocity (V_s)	cm/min	3.33
Empty bed contact time (EBCT)	min	9

Fig.6.10 shows the breakthrough curve for phosphorus adsorption onto ZLO column. It can be seen that the breakthrough occurred at 34.5 h while exhaustion was achieved at 109.7 h. The volume of treated water at 10% breakthrough was 109.71 L. The dynamic adsorption capacity of ZLO for phosphorus at the saturation time was 10.99 mg P/g ZLO, representing 70.34% its equilibrium adsorption capacity. The phosphate retention onto ZLO may occur due to electrostatic attraction between

phosphate anions in the solution and Zr^{4+} ions onto ZLO surface (Mallampati and Valiyaveettil, 2013).

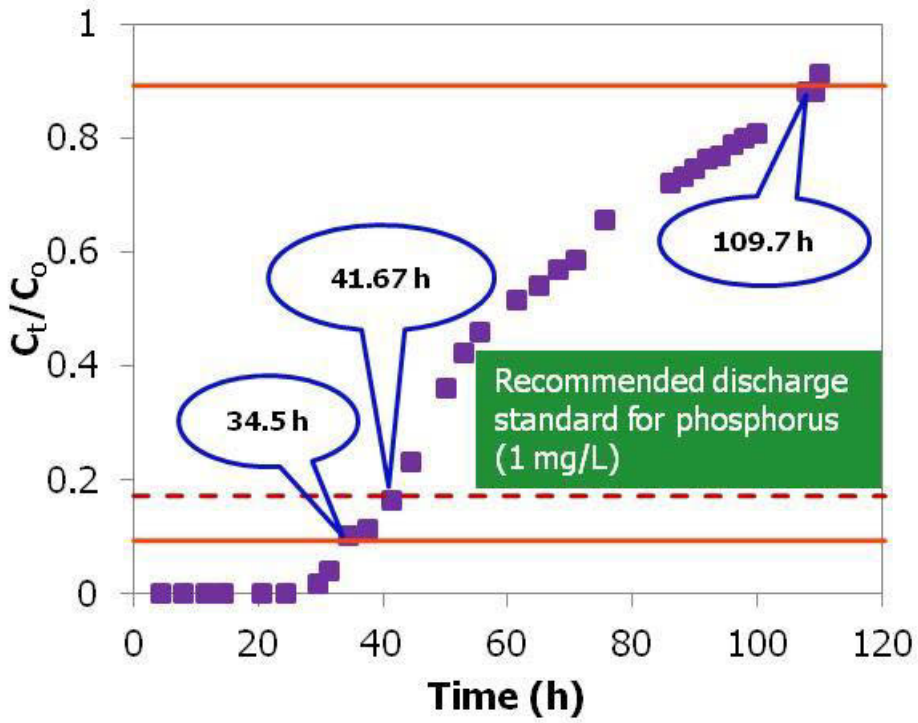

Figure 6.10 Breakthrough curve for P adsorption from municipal wastewater on ZLO column at semi-pilot scale (100 g ZLO; bed depth = 30 cm, flow rate = 53 mL/min, C_i = 5.5 mg P/L)

6.3.2 Desorption of P from ZLO

Desorption was performed by feeding 0.2 M NaOH solution through the bed in the upward direction. The flow rate of desorption was 13.24 mL/min, much lower than that of adsorption (53 mL/min). It is expected that, a low flow rate of desorption solution will result in a small volume and a high concentration of phosphorus in the effluent, and thus making phosphorus recovery cost-effective (Kumar and Brandyopadhyay, 2006). The concentration of phosphorus was measured at different intervals of time as illustrated in Fig.6.11. It was observed that desorption process was almost completed within 20 h, after which desorption was marginal. The phosphorus desorption efficiency at 20 h was 72.89%. The total volume and phosphorus concentration of the effluent at 20 h were 15.9 L and 50 mg/L, respectively. It is interesting to note that though desorption was finished at 20 h, almost 80% of the eluted phosphorus was attained at 5 h. The total volume and phosphorus concentration of the effluent at 5 h were 3.975 L and 156 mg/L, respectively. In view of phosphorus

recovery, it is desirable to attain the desorption solution with low volume and high concentration of phosphorus. Hence, it is highly recommended to finish desorption process by 5 h. At this time, the phosphorus concentration in desorption was 28.36 fold higher than that in the raw municipal wastewater. It was found that the desorption efficiency of the large column (72.89%) was far too low compared to that of mini column (92.16%). This can be explained by the fact that, desorption flow rate (12 mL/min) was the same as the adsorption flow rate (12 mL/min) for the mini-column, whereas desorption flow rate (13.24 mL/min) was much lower than adsorption flow rate (53 mL/min) for the large column. These findings are supported by Ebie et al. (2008), who stated that low desorption flow rate would result in low desorption efficiency but high effluent phosphorus concentration.

The ZLO packed bed column was repeatedly used for several times. The eluted ZLO was first taken out of the column. Next, the desorbed ZLO was washed with a large amount of tap water to remove residual OH^- ions. Then, the washed ZLO was dipped into 1 L of 0.1 M HCl for 3 h for activation. After that, the activated ZLO was washed with tap water again. Finally, the regenerated ZLO was packed into the column again for the next adsorption cycle. The alkaline solution is an anion exchange agent, which can displace phosphate anion from ZLO. The excessive amount of OH^- ions can lower the PO_4^{3-} adsorption capacity of ZLO, due to the competition for anion binding sites. Therefore, residual OH^- ions from 0.2 M NaOH need to be eliminated. Washing ZLO with tap water enables the removal of residual OH^- ions while activating ZLO with 0.1 M HCl helps produce the optimal pH condition for the next adsorption cycle. Similar desorption process has been reported by Damte (2006) for fluoride - aluminum hydroxide system, whereby 1% NaOH and 0.05 N H_2SO_4 were employed as elution and regeneration solutions, respectively.

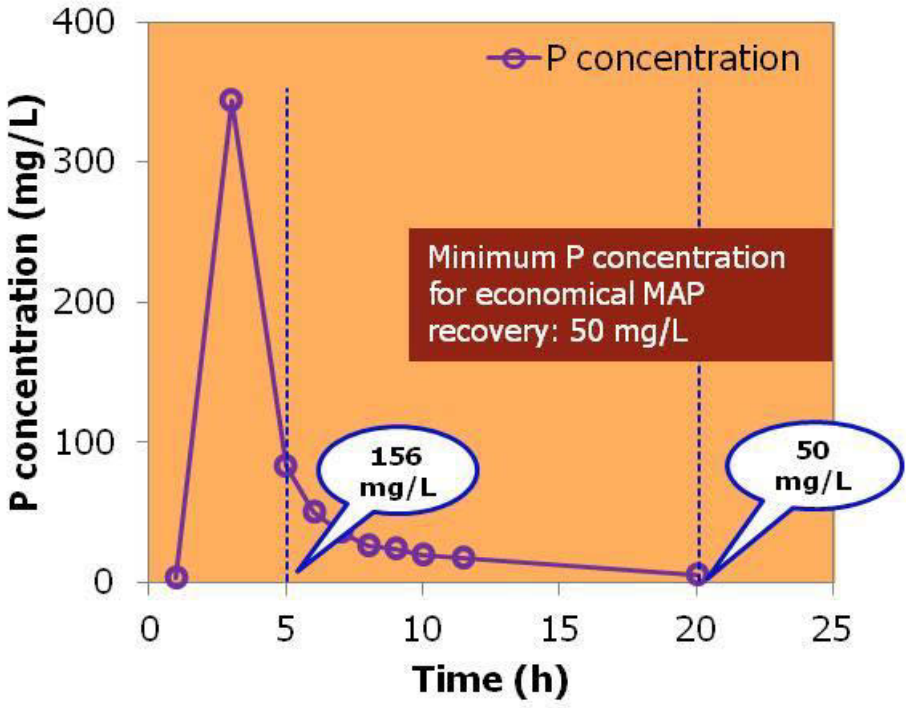

Figure 6.11 Desorption profile of ZLO column (100 g ZLO, desorption solution = 0.2 M NaOH, flow rate = 13.25 mL/min)

6.4 SCALE-UP OF THE COLUMN ADSORPTION SYSTEM

The significant advantage of the column adsorption system is easy scale-up, whereby data obtained from lab-scale columns can be used for predicting the performance of the pilot and the full-scale column. The scaling, which results in similar breakthroughs, is based on the similarity in mass transfer and hydrodynamic features between the small column and the large column. It can be done with the assumption that no change in the boundary conditions, dimensionless parameters, and mechanisms may occur while changing the size of the system (Okochi, 2013). According to Ohura et al. (2011), the scale-up of the dynamic adsorption system can be implemented properly based on the empty bed contact time (EBCT). Damte (2006) proposed that the superficial velocity of the large column should be the same as that of the small column when scaling the system. Although the internal diameter and the bed depth of the large column would increase, their ratio was expected to remain a constant. The service time of the large column can be predicted using BDST model parameters (K and N_o), which were determined from earlier small column tests. In the literature, the scale-up has been successfully applied for several fixed-bed column systems, such as phosphorus - ARC

furnace steel slag, fluoride - granular aluminum hydroxide (Damte, 2006; Okochi, 2013). The aim of scale-up in this work was to develop a phosphorus decontamination process, which is applicable to households. Based on the scale-up method proposed by Damte (2006), the design parameters for the full-scale column were determined as listed in Table 6.8. Detailed calculations can be found in the Section 3.2.3.2.

Table 6.8 Proposed full-scale column parameters

Parameters	Symbol	Unit	Small column	Large column	Scale-up ratio
Column design					
Inner diameter	D	cm	1.75	4.50	0.39
Column area	A	cm^2	2.40	15.90	0.15
Bed depth	Z	cm	23	59.14	0.39
Adsorbent weight	m	g	10	170	0.06
Operation					
Influent concentration	C_o	mg/L	5.5	5.5	1
Superficial velocity	V_S	cm/min	4.99	4.99	1
Volumetric flow rate	Q	L/h	0.72	4.76	0.15
Empty bed contact time	EBCT	min	4.61	11.85	0.39
Service time	t_b	h	9.3	31.50	0.30
Treated water volume	V_b	L	6.70	149.94	0.04
Adsorbent exhaustion rate	AER	g/L	2.17	1.14	1.90

Notation:

Service time and treated water volume were calculated at 10% breakthrough.

6.5. CONCLUSION

Chapter 6 investigated phosphorus removal by ZLO packed bed column. The results clearly demonstrated that it was feasible to eliminate phosphorus from aqueous solutions and real municipal wastewater using ZLO in a dynamic adsorption system.

The effect of column design parameters, such as flow rate, inlet phosphorus concentration, bed depth, ZLO particle size and influent pH was examined. The results revealed that lower flow rate, higher bed depth, smaller feed phosphorus concentration, smaller particle size, and lower influent pH facilitated the adsorption performance of the column, which was evidenced by longer service time and higher treated volume.

The highest dynamic adsorption capacity of ZLO for phosphorus was obtained at the flow rate of 12 mL/min, influent phosphorus concentration of 5.6 mg/L, bed depth

of 23 cm, ZLO particle size of 1000-600 μm, and influent pH of 3. It was estimated to be 16.43 mg P/g ZLO, accounting for 85.44% the equilibrium adsorption capacity (Table 6.1).

Both the BDST and Thomas model fitted well the experimental data. The BDST successfully described the linear relationship between bed depth and service time, with extremely high correlation coefficient (R^2 = 0.999) for 12 mL/min flow rate, 5.5 influent phosphorus concentration, 1000-600 μm particle size. The BDST model predicted accurately the breakthrough time for the change of bed depth. This model was used for scaling the process from a mini-column to a big column. Taking into account the results from Thomas model, it would seem that the dynamic adsorption capacity of ZLO column (q_o) increased with a lower flow rate, a higher bed depth, and a higher feed phosphorus concentration. In addition, the greater Thomas rate constant could be attained with the increasing flow rate, the elevating feed concentration, and the decreasing bed depth.

The loaded phosphorus could be eluted quantitatively (92.16%) with 0.2 M NaOH, and the exhausted ZLO could be efficiently generated with 0.1 M HCl. ZLO could repeatedly be used for at least three cycles with a minor reduction in the phosphorus uptake capacity (18.64%) and a marginal weight loss (8.7%).

In the semi-pilot scale test, the recommended discharge standard for P (1 mg/L) was conquered for duration of 41.67 h, corresponding to 132.5 L of treated water by the treatment of real municipal wastewater in a 100 g ZLO packed bed column.

UNIVERSITY OF TECHNOLOGY, SYDNEY

CHAPTER 7

RECOVERY OF PHOSPHORUS FROM MUNICIPAL WASTEWATER BY ADSORPTION COUPLED WITH CRYSTALLIZATION

7.1. INTRODUCTION

7.1.1 The significance of phosphorus removal and recovery

Phosphorus plays an important role in the development of living organisms. It is also a major material for many industries. However, phosphorus is a non-renewable resource. Due to the human activity, the global reserve of rock phosphate will not last for more than 140 years (Molinos-Senante et al., 2011). In addition, the excessive amount of phosphorus in the wastewater is responsible for eutrophication in receiving water bodies. Notably, given the Directive 91/271/EEC comes into effect in Europe, interest is growing in the reduction of phosphorus level in wastewater. Furthermore, the spontaneous precipitation of magnesium ammonium phosphate (MAP) is harmful to the operation of WWTP (Jia, 2014; Perera et al., 2007). Thus, phosphorus removal and recovery from wastewater is becoming urgent for sustainable development.

7.1.2 The phosphorus recovery technologies

Depending on the use of various products of WWTP (liquor, sludge, and ash) for phosphorus recovery, the corresponding technologies are precipitation/crystallization, wet-chemical technology, and thermo-chemical technology (Sartorius et al., 2012). The phosphorus recovery from sludge and ash has disadvantages of high cost and special equipment requirement for phosphorus leaching and thermal treatment (Bottini and Rizzo, 2012; Nieminen, 2010). In addition, high contents of heavy metals and pathogen in the sludge are major factors, limiting the direct application of sludge in phosphorus recovery (Karabegovic et al., 2013). As a result, there is a growing trend to reclaim phosphorus from wastewaters.

7.1.3 The advantages of MAP recovery process

Although phosphorus can be recovered by various processes, the phosphorus recovery as magnesium ammonium phosphate (MAP) is preferred. The reason is that the MAP crystallization allows the simultaneous elimination of both nitrogen and phosphorus from wastewater (Ackerman, 2012; Muster et al., 2013). Additionally, the use of MAP as a slow release fertilizer mitigates the nutrient leaching and thus preventing the surface water from eutrophication (Garcia-Belinchón et al., 2013; Molinos-Senante et al., 2011). Besides, the controlled MAP crystallization is believed to protect engineered systems from undesirable pipe blockage (Jia, 2014; Perera et al., 2007). To date, MAP crystallization process has been successfully applied at full-scale in Netherlands, Japan, Canada and the United States (Karabegovic et al., 2013).

7.1.4 Potential and challenges of P recovery from municipal wastewater

It is believed that municipal is a potential source for phosphorus recovery due to enormous volume regenerated worldwide and moderate level of heavy metals. The direct use of wastewater containing high levels of heavy metals is not appropriate for phosphorus recovery, due to the risk of forming metal phosphates instead of MAP at pH >4.5. Thus, metal ions need to be eliminated prior to MAP crystallization. This activity can add more cost to MAP production process (Bottini and Rizzo, 2012). For this reason, low level of heavy metals can be considered as a dominant advantage of municipal wastewater over other wastewaters when used for phosphorus recovery. However, the main challenge to the phosphorus recovery from municipal wastewater is the low phosphorus concentration (Schick et al., 2009). Meanwhile, it has been reported that adsorption is suitable for elimination of phosphorus from dilute solutions (Krishnan and Haridas, 2008; Zhang et al., 2011). In particular, adsorption can pre-concentrate phosphorus to high level (Li et al., 2012; Ohura et al., 2011). Hence, it is assumed that the combination of adsorption and crystallization may be a solution for MAP recovery from low phosphorus concentration wastewater such as the municipal wastewater (Ebie et al., 2008).

7.1.5 Research gaps

Until now, numerous methods are available for the decontamination of phosphorus from wastewater. However, most of them are either inefficient for the treatment of dilute wastewater or unsustainable relative to the formation of non-recyclable phosphorus products (for example, metal-phosphate) (de Bashan and Bashan, 2004). Thus, it is desirable to develop a technology that can both remove and recovery phosphorus in a sustainable form (Karabegovic et al., 2013).

Although agricultural by-products based adsorbents (AWBs) are widely used for phosphorus removal, their application in phosphorus recovery has rarely been reported.

So far, MAP has been successfully been recovered from many P-rich wastewaters, such as swine wastewater (Perera et al., 2007; Song et al., 2007), cola beverage (Foletto et al., 2013), eutrophic water (Li et al., 2012), sludge liquor (Karabegovic et al., 2013; Okano et al., 2013), membrane concentrate (Bradford-Hartke, 2012). However, the MAP recovery from desorption solution has barely been tested (Nur, 2014).

While the technical feasibility of the MAP recovery has received much attention of researchers, the economic feasibility is still under discussion (Garcia-Belinchón,

2013; Molinos-Senante et al., 2011). In the traditional method for economic evaluation of MAP recovery, the external effects (for example, environmental benefits) usually received far less attention than their internal counterparts (for example, equipment, operation cost, and MAP sale). As a consequence, inaccurate concluding remarks about the economic feasibility of the process might be made (Molinos-Senante et al., 2011).

7.1.6 Aims and scopes

In the previous work, ZLO was found to be efficient in removing phosphorus from real municipal wastewater. The goal of this study was to examine the feasibility of recovering phosphorus from municipal wastewater as MAP by adsorption combined with crystallization. To that end, the effect of solution pH, molar ratio, chemical type, and temperature on the crystallization process was investigated. The recovered MAP was characterized using XRD, SEM, FTIR and element analysis. The cost-benefit analysis of ZLO development and MAP recovery was conducted. This research is expected to provide a novel and viable technique for reclaiming phosphorus from municipal wastewater, and thus contributing to saving the global phosphate reserve.

7.2 CHARACTERISTICS OF PHOSPHORUS DESORPTION SOLUTION

According to Karabegovic et al. (2013), the characteristics of wastewater used for phosphorus recovery needs to be determined in advance. The particular attention should be paid to ionic composition and alkalinity because these factors may affect the purity of the precipitate and alkali requirement for pH adjustment. In this study, phosphorus was recovered from phosphorus desorption solution. The composition of desorption solution was summarized in Table 7.1 below.

The table shows that the dominant components of desorption solution were phosphorus, ammonium, nitrate, chloride, magnesium and calcium. The phosphorus concentration of the desorption solution was 156 mg/L, almost 28.36 times higher than that of raw municipal wastewater. Thus, it placed the desorption solution among the P-rich solutions currently used for phosphorus recovery. It also confirms the potential of adsorption in pre-concentrating phosphorus from the diluted wastewater. The concentration of NH_4^+ in desorption solution was quite high (9.4 mg/L). However, the molar ratio of NH_4^+ to PO_4^{3-} was still very low (1:7.45). It implied that there was still a need to use external source of ammoniums to ensure successful MAP crystallization. The level of NO_3^- in desorption solution was minor (2.7 mg/L). The Zr^{4+} ions could not

be found in desorption solution, proving that no Zr^{4+} bleeding from ZLO occurred during the desorption performance of ZLO. The levels of heavy metals in desorption solution were negligible. The results confirmed that ZLO did not adsorb heavy metals present in the raw municipal wastewater. Especially, the concentration of Ca^{2+} in desorption was quite high (12.9 mg/L). At Ca/Mg molar ratio > 0.5, Ca^{2+} can impede the MAP crystallization and MAP purity (Song et al., 2007). In this study, the Ca/Mg molar ratio when an external source of magnesium was added for MAP crystallization was limited to 0.03. Consequently, the presence of Ca^{2+} can hardly affect the MAP recovery. However, the availability of Ca^{2+} in desorption solution may lead to the formation of $CaSO_4$ instead of MAP if $(NH_4)_2SO_4$ and $MgSO_4.7H_2O$ are used (Li et al., 2012). This should be taken into account when the external sources of ammonium and magnesium are selected. The existence of Mg^{2+} in desorption solution is expected to favor the MAP crystallization. The concentration of TSS in desorption solution was 120 mg/L, which was far too low compared to the recommended level (1000 mg/L) for Ostara Pearl® technology (Garcia-Belinchón et al., 2013). The pH of desorption solution (12.63-13.25) was much higher than that of normal wastewaters (6.5-8.5) used for phosphorus recovery. As a result, to prevent NH_3 evaporation and/or Mg precipitation, the pH of desorption solution should be lowered < 8 before the chemical addition in the MAP production process. This can add more cost to MAP recovery process. Overall, while the high concentration of phosphorus is a significant advantage, the high pH can be cited as a principal limitation of desorption solution when applied for MAP recovery.

Table 7.1 Characteristics of the desorption solution (1)

Parameter	Unit	Value
pH		12.63
Chemical oxygen demand (COD)	mg/L	421
Total organic carbon (TOC)	mg/L	198.3
Total suspended solids (TSS)	mg/L	120
Nitrogen as ammonium (NH_4-N)	mg/L	9.4
Nitrogen as nitrate (NO_3-N)	mg/L	2.7
Nitrogen as nitrite (NO_2-N)	mg/L	n.d.
Orthophosphate (PO_4-P)	mg/L	156
Chloride (Cl^-)	mg/L	34.1
Ca^{2+}	mg/L	12.9
Mg^{2+}	mg/L	0.9
Cu^{2+}	mg/L	0.01
Zn^{2+}	mg/L	n.d.
Pb^{2+}	mg/L	n.d.
Cd^{2+}	mg/L	n.d.
Ni^{2+}	mg/L	n.d.
Fe^{2+}	mg/L	0.03
Zr^{4+}	mg/L	n.d.

Notation:

(1) The solution obtained after 5 hours of desorption.

n.d. = not detected.

7.3 FACTORS AFFECTING THE MAP RECOVERY

7.3.1 Solution pH

As mentioned in the Section 2.4.3, pH can significantly affect the MAP crystallization process via the availability of the MAP components as well as the MAP purity. The minimum solubility of MAP occurs at pH > 8.5 (Nieminen, 2010). Approximately 98% of orthophosphate is present as HPO_4^{2-} at pH 9.0 (Huchzermeier, 2011). In an open system, a significant volatilization of NH_3 may occur at pH ≥ 9.3 (Hao et al., 2008; Lanning, 2008; Liu et al., 2013; Perera et al., 2007). Mg^{2+} is removed from solution in the form of $Mg(OH)_2$ when the pH value reaches 10.7 (Ali and

Schneider, 2008; Wang et al., 2005). Considering these factors, this study investigated the effect of pH on the MAP crystallization by varying pH value from 9 to 10 while maintaining other process parameters unchanged. In view of P recovery, both the P recovery efficiency and the MAP purity are vital. Thus, they were used as focal criteria for evaluation of MAP crystallization in this study. The effect of solution pH on MAP recovery was illustrated in Fig.7.1 while Fig.7.2 displayed the SEM images of the harvested precipitate at different pH values. It was found that the P recovery percentage increased from 88.7 to 93.73% when pH rose in the range between 9 and 10. On the contrary, the MAP proportion was reduced from 91.88 to 87.38% with the above pH augmentation. These findings are consistent with results reported by Hao et al. (2008) and Li et al. (2012). As the difference in the P recovery efficiency was not significant, and MAP was a favored recovered product, the pH 9 was selected as the optimal pH and used for other crystallization experiments. This is supported by Garcia-Belinchón et al. (2013), who recommended recovering MAP at a lower pH value among different tested pH values to mitigate the chemical costs. A similar optimal pH (9.0) was applied by Perera et al. (2007) for MAP recovery from swine biogas digester effluent.

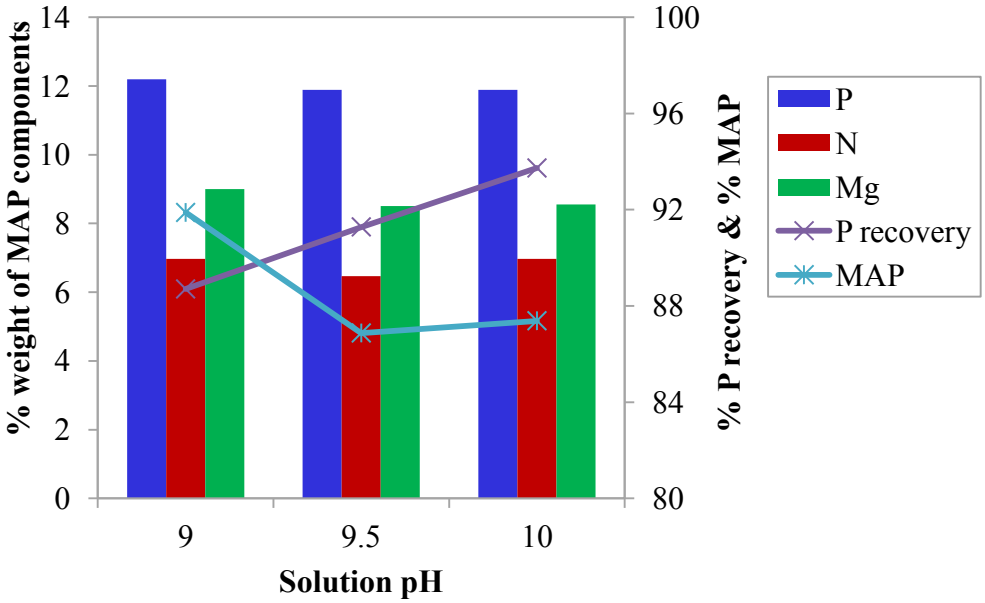

Figure 7.1 Effect of pH on the MAP crystallization from desorption solution (C_i = 139 mg P/L, Mg: N: P molar ratio = 2:2:1, 120 rpm, room temperature)

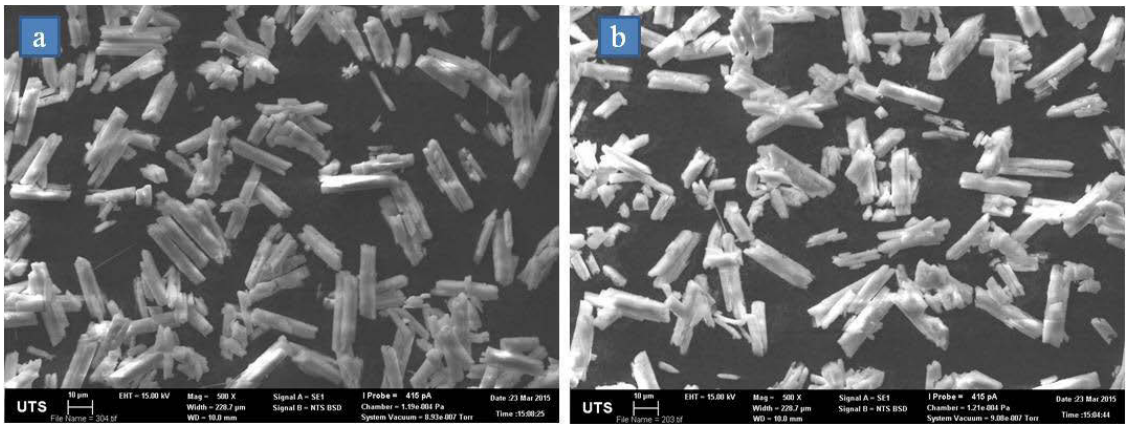

Figure 7.2 SEM images of MAP recovered from P desorption solution at various pH conditions: a) pH = 9, and b) pH = 10

7.3.2 Molar ratio of Mg: N: P

It is well recognized that Mg: N: P molar ratio plays an important role in MAP crystallization. On the one hand, there is a trend to use high Mg: N: P molar ratio to ensure that phosphorus is not a rate controlling factor for MAP formation (Li et al., 2012). On the other hand, there is a warning that the use of an extremely high Mg: N: P molar ratio may have adverse impacts on the environment or add more cost to the crystallization process (Huchzermeier, 2011; Jia, 2014). The low N: P molar ratio in the effluent is responsible for the nutrient imbalance in the agricultural land when the effluent was used for irrigation (Perera et al., 2007). The proper treatment of residual Mg in the effluent is costly (Lanning, 2008). For these reasons, 1:1:1 has been considered as the optimal Mg: N: P molar ratio in many previous studies (Foletto et al., 2013; Nur, 2014; Pastor et al., 2010).

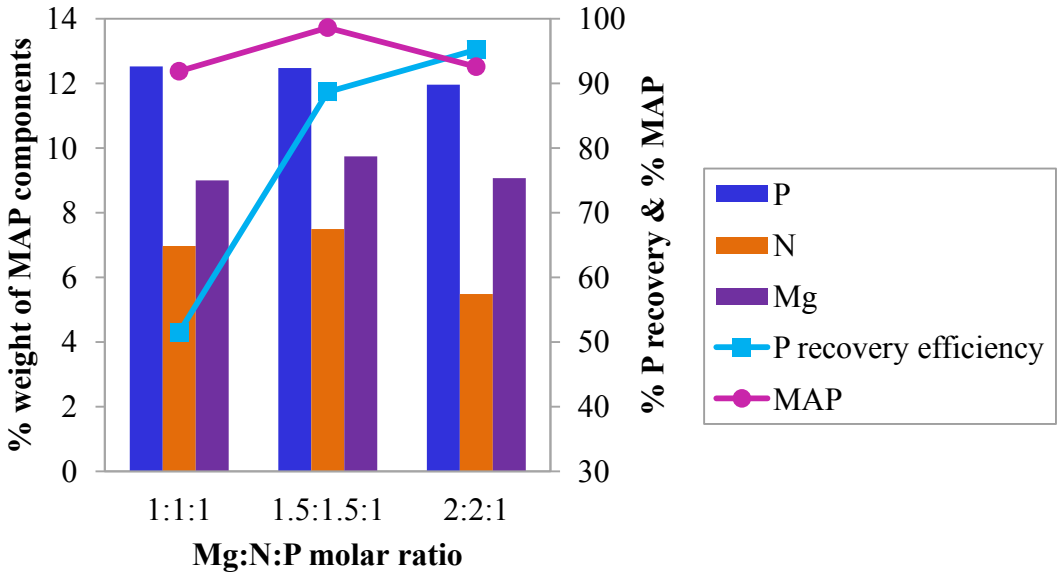

Figure 7.3 Effect of Mg: N: P molar ratio on the MAP crystallization from desorption solution (pH = 9, C_i = 156 mg P/L, stirring speed = 120 rpm, reaction temperature = 22 °C, NH_4Cl + $MgCl_2.6H_2O$)

Three Mg: N: P molar ratios have been tested, namely 1:1:1, 1.5:1.5:1, and 2:2:1. The best molar ratio was selected based on the high P recovery efficiency and MAP purity. The effect of Mg: N: P molar ratio on MAP synthesis is presented in Fig.7.3. The P recovered percentage was escalated from 51.5 to 95.19% with a growth in the Mg: N: P molar ratio from 1:1:1 to 2:2:1. Undoubtedly, the phosphorus recovery efficiency was greatly enhanced at the higher Mg: N: P molar ratio. The Mg: P molar ratio greater than 1:1 has been also used by many researchers, e.g. 1.4:1 (Song et al., 2007), 1.6:1 (Xu et al., 2012), 2.0:1 (Çelen et al., 2007), 3.0:1 (Warmadewanthi, 2009), and 4.2:1 (Wilsenach, 2007). Conversely, the elevation of Mg: N: P molar ratio seemed not to have a substantial effect on the MAP purity. However, the SEM analysis results showed that the MAP crystals precipitated at the lower molar ratio were a bit longer than those obtained at the higher molar ratios.

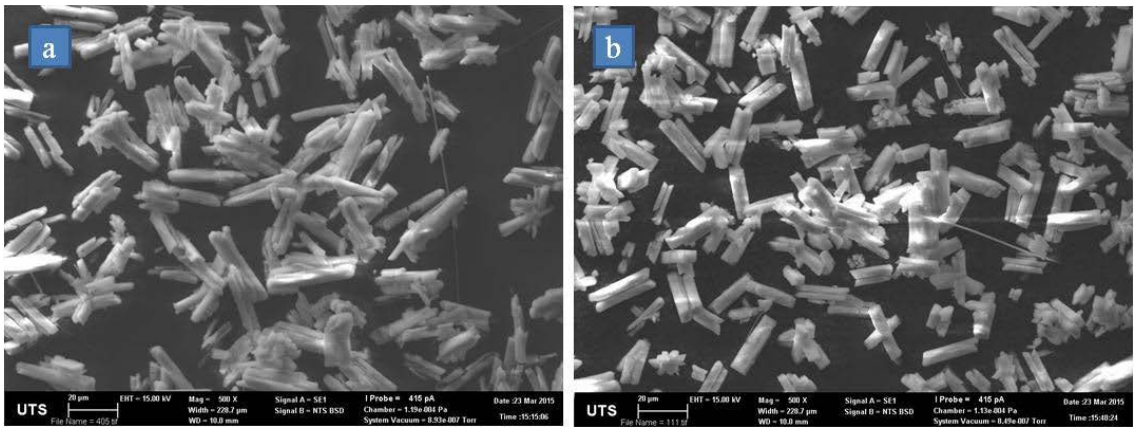

Figure 7.4 SEM images of MAP recovered from P desorption solution at different Mg: N: P molar ratios: a) 1:1:1, and b) 2:2:1

The highest percentage of MAP (98.63%) in the precipitate was attained at the Mg: N: P molar ratio of 1:1.5:1.5. Nevertheless, the phosphorus recovery efficiency at the molar ratio of 1:1.5:1.5 (88.69%) was much lower than that at the molar ratio of 1:2:2 (95.19%). The MAP percentage of the precipitate at the molar ratio of 1:2:2 was relatively high (92.59%). For these reasons, the Mg: N: P molar ratio of 2:2:1 was selected as the optimal molar ratio for MAP crystallization.

7.3.3 Magnesium and ammonium sources

The concentrations of NH_4^+ and Mg^{2+} in desorption solution are typically lower than that of PO_4^{3-}. Hence, the addition of external sources of Mg^{2+} and NH_4^+ is necessary to make the P recovery feasible. In an attempt to improve the MAP recovery performance and reduce the cost of reclaimed MAP, several sources of Mg^{2+} and NH_4^+ have been tested. This study evaluates two combinations, which were NH_4Cl + $MgCl_2.6H_2O$ and $(NH_4)_2SO_4$ + $MgSO_4.7H_2O$, in term of phosphorus recovery efficiency, MAP purity and morphology of the harvested precipitates. Fig.7.5 shows that the recovery efficiency of phosphorus was increased from 91.64 to 94.87% while the MAP purity was decreased from 81.97 to 77.79% when the combination of NH_4Cl + $MgCl_2.6H_2O$ was replaced by $(NH_4)_2SO_4$ + $MgSO_4.7H_2O$. This can be explained by the fact that Ca^{2+} in desorption solution may react with SO_4^{2-} to form $CaSO_4$ as impurities. Apparently, $(NH_4)_2SO_4$ + $MgSO_4.7H_2O$ was not as good as NH_4Cl + $MgCl_2.6H_2O$ for MAP recovery, with respect to MAP purity. These results are consistent with those reported by Jia (2014) and Kumar and Pal (2013). This is further confirmed by the SEM images depicted in Fig.7.6. When a combination of NH_4Cl and $MgCl_2.6H_2O$ was used, the majority of MAP crystals had the same size, which averaged between 20 and 25 µm. However, the size of MAP crystals varied in a wider range from 5 to 35 µm when

$(NH_4)_2SO_4$ + $MgSO_4.7H_2O$ applied. The results proved that MAP crystals obtained with NH_4Cl + $MgCl_2.6H_2O$ had better quality than those synthesized with $(NH_4)_2SO_4$ + $MgSO_4.7H_2O$. For these reasons, $(NH_4)_2SO_4$ + $MgSO_4.7H_2O$ should not be used as additional ammonium and magnesium sources in this study. Due to the cost concern, alternative sources of magnesium (e.g. sea water, MgO by-products from Mg mining) and ammonium (e.g. urine, NH_4^+ rich wastewater) should be tested in the future research (Karabegovic et al., 2013).

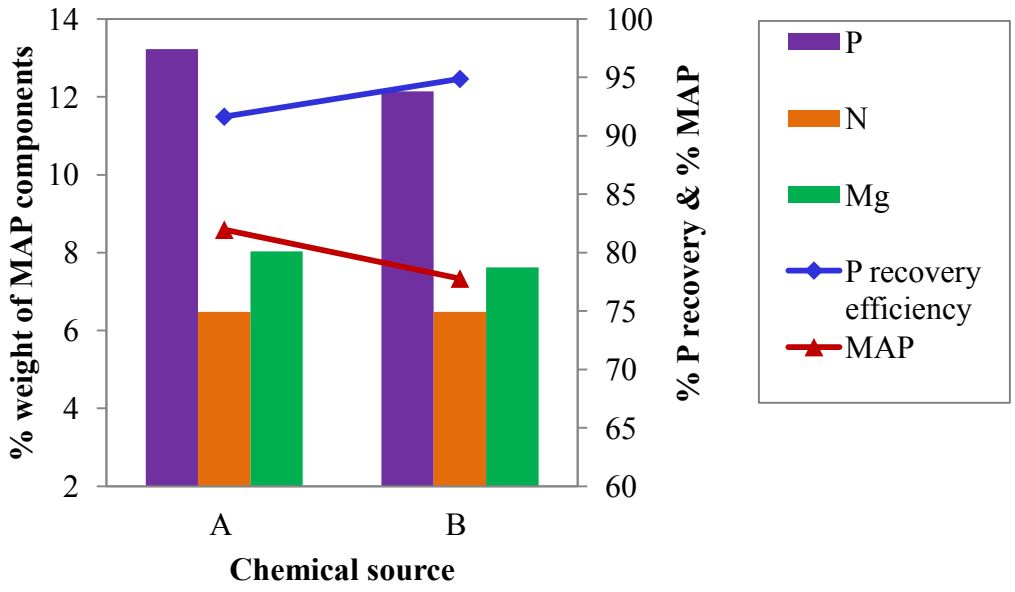

Figure 7.5 Effect of magnesium and ammonium sources on MAP recovery from desorption solution: A. NH_4Cl+$MgCl_2.6H_2O$, B. $(NH_4)_2SO_4$ + $MgSO_4$ (pH = 9, Mg: N: P molar ratio = 2:2:1, C_i = 189 mg P/L, stirring speed = 120 rpm, reaction temperature = 22 °C)

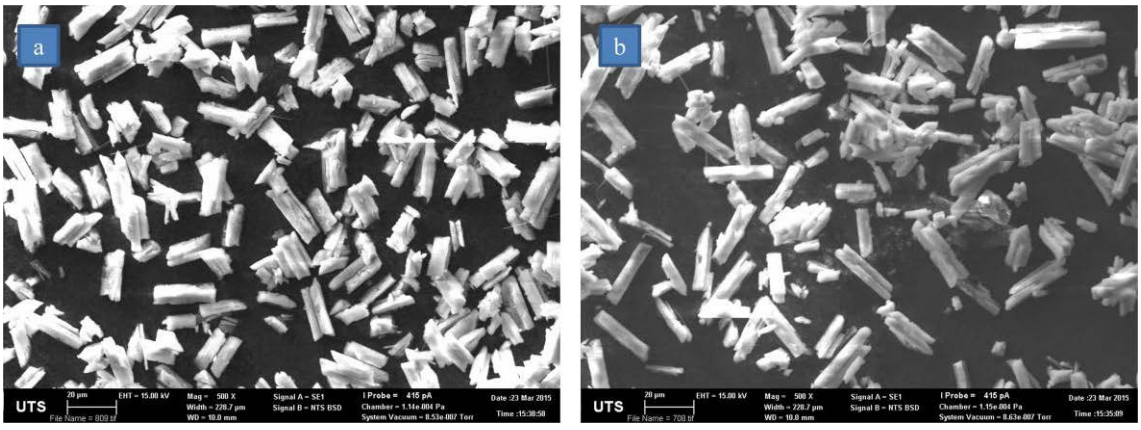

Figure 7.6 SEM images of MAP recovered from P desorption solution using different magnesium and ammonium sources: a) NH_4Cl + $MgCl_2.6H_2O$, and b) $(NH_4)_2SO_4$ + $MgSO_4.7H_2O$

7.3.4 Reaction temperature

The solution temperature is known to influence the MAP crystallization as it affects the MAP components activity and MAP crystals solubility. However, the temperature is supposed to play a less important role than pH and molar ratio in MAP synthesis (Le Corre et al., 2009). This study explores the effects of reaction temperatures (8^{o}C and 22^{o}C) on MAP recovery, concerning P recovery efficiency, MAP purity and morphology of the reclaimed crystals.

Fig.7.7 shows that the P recovery efficiency reduced from 85.84 to 75% with the augmentation of the solution temperature from 8 to 22^{o}C. Similar trend was reported by Adnan et al. (2003), who observed that the P recovery efficiency was decreased from 37.8 to 27.1% when the reaction temperature escalated from 8 to 22^{o}C. Likewise, Le Corre et al. (2009) stated that the formation of MAP was favored by low reaction temperature. In the same trend, the ratio of MAP to the precipitate was diminished from 79.22 to 78.60% with the increasing reaction temperature from 8 to 22^{o}C. As can be seen from Fig.7.8, the reaction temperature did not seem to have obvious impact on the shape of MAP crystals. Nevertheless, the increase in reaction temperature from 8 to 22^{o}C led to a slight reduction in the size of MAP crystals. This is in good agreement with the finding by Jia (2014), who reported that the size of MAP crystals was reduced from 30 to 14 μm with the enhancement of reaction temperature from 298 to 308 K. Equally, Rouff (2013) reported that the size of MAP crystals dropped from 1 mm to less than 25 μm with a rise of reaction temperature from 298 to 573 K. The decrease in the size of MAP crystals at higher temperature could be ascribed to the higher MAP solubility product at a greater temperature (Le Corre et al., 2009). In view of phosphorus recovery, the large size of MAP crystals is beneficial for MAP separation since it enables the crystal settling. That is why the reaction temperature range from 298 to 308 K is often used to perform MAP production (Le Corre et al., 2009). From the industrial application point of view, this study has chosen the room temperature (22^{o}C) as the ideal temperature for crystallization tests.

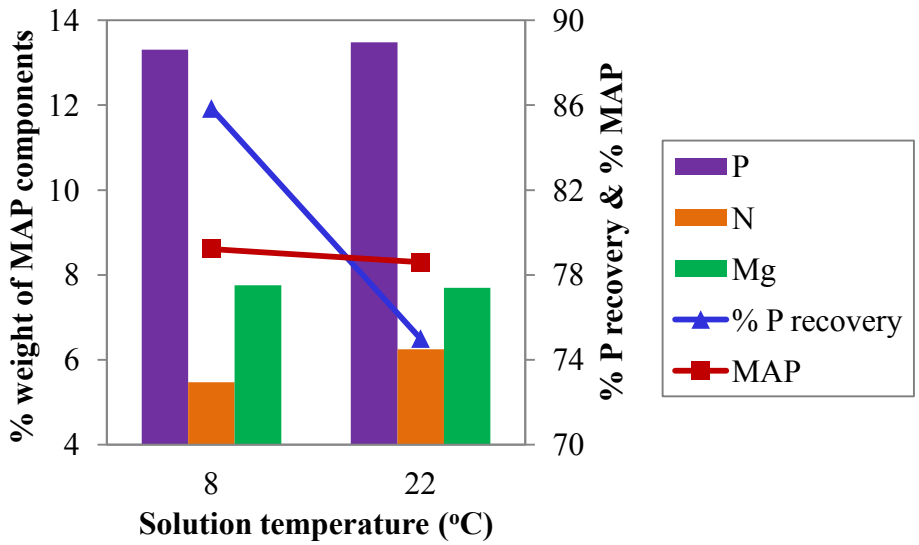

Figure 7.7 Effect of solution temperature on MAP crystallization from desorption solution (pH = 9, Mg: N: P molar ratio = 2:2:1, C_i = 171.6 mg P/L, stirring speed = 120 rpm, $NH_4Cl + MgCl_2.6H_2O$)

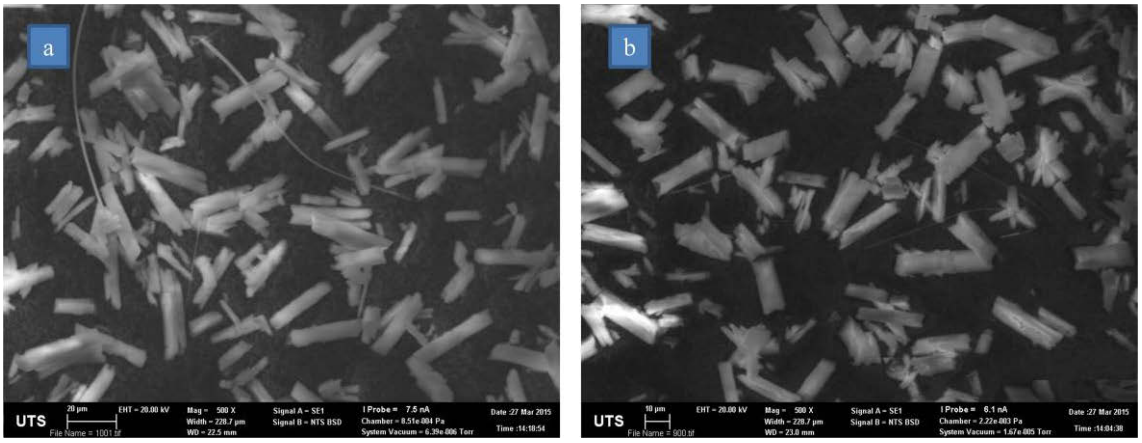

Figure 7.8 SEM images of MAP recovered from desorption solution at varying solution temperatures: a) 8°C, and b) 22°C

Table 7.2 MAP recovery from desorption solution at various conditions

Crystallization condition	% P recovery	% P	% Mg	%N	% MAP	P:Mg:N molar ratio
pH 9	88.70	12.19	9.0	6.97	91.88	0.80:0.76:1.01
pH 9.5	91.28	11.89	8.51	6.47	86.87	0.82:0.76:0.99
pH10	93.73	11.89	8.56	6.97	87.38	0.84:0.78:1.09
1:1:1	51.50	12.53	9.00	6.97	91.88	0.52:0.48:0.64
1:1.5:1.5	88.69	12.48	9.74	7.49	98.63	0.89:0.9:1.19
1:2:2	95.19	11.96	9.07	5.48	92.59	0.96:0.94:0.97
$NH_4Cl+MgCl_2.6H_2O$	91.64	13.23	8.03	6.48	81.97	1.12:0.88:1.21
$(NH_4)_2SO_4+MgSO_4.7H_2O$	94.87	12.14	7.62	6.48	77.79	1.16:0.94:1.37
22 °C	75	13.48	7.7	6.25	78.60	0.83:0.61:0.85
8 °C	85.84	13.31	7.76	5.47	79.22	0.95:0.72:0.86

7.4 EVALUATION OF THE HAVERSTED PRECIPITATES

The crystallization condition that resulted in high MAP purity and phosphorus recovery efficiency was considered as the optimal condition. Based on the selection criterion described above, the optimal crystallization condition was characterized as follows: pH = 9, P: Mg: N molar ratio = 1:2:2, influent phosphorus concentration = 156 mg/L, stirring speed = 120 rpm, reaction temperature = 295 K. The precipitate harvested at the optimal condition was selected for characterization, which was conducted by multi techniques, including element, XRD, SEM, FTIR, and P-bioavailability analyses.

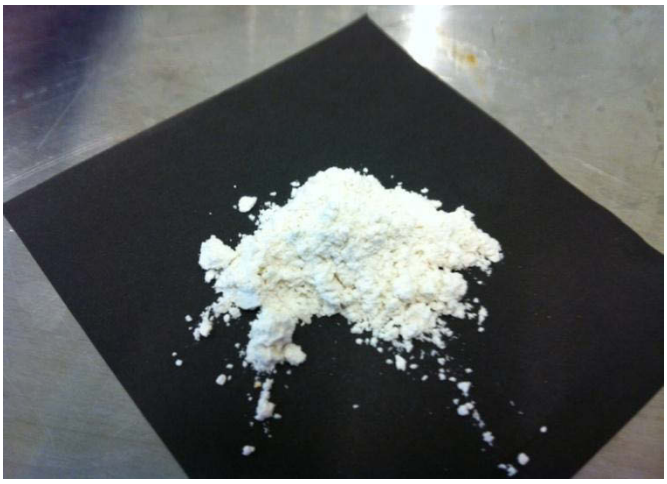

Figure 7.9 MAP recovered from municipal wastewater by adsorption onto ZLO

7.4.1 Crystal characterization

A. Elemental analysis

The main components of MAP reclaimed at the optimal crystallization condition were determined by dissolution method combined with elemental analysis. Table 7.3 shows the comparison between the recovered MAP and the standard MAP with respect to the elemental composition. It was found that the weight percentages of P (11.96%), Mg (9.07%), and N (5.48%) in the recovered MAP were very similar to those in the standard MAP. This confirmed the formation of high-purity MAP from phosphorus desorption solution after $MgCl_2.6H_2O$ and NH_4Cl addition. According to Kalmykova et al. (2013), phosphate ores can be classified as low grade (up to 3 wt. % P), intermediate - grade (4-5 wt. % P), and high-grade (6-8 wt. % P). The phosphorus content in the recovered product was 11.96%. Based on the evaluation criterion described above, the recovered MAP can be placed among high-grade phosphate ores. The elemental analysis also demonstrated that the contents of common heavy metals in the reclaimed MAP were much lower than the permissible limits regulated in Germany, Turkey and Australia (Table 7.4). Due to the high ratio of P and low content of heavy metals, it is safe to apply the recovered precipitate in agricultural land.

Table 7.3 Elemental composition of MAP recovered from desorption solution at the optimal condition

Element	Weight (%)	
	MAP recovered from desorption solution	Standard MAP (Sigma)
Phosphorus	11.96	12.65
Magnesium	9.07	9.80
Nitrogen	5.48	5.71

Table 7.4 Comparison of heavy metal contents in MAP recovered from desorption solution with legal limits

Heavy metal (ppm)	Legal limits*			MAP recovered from
	Germany	Turkey	Queensland	Raw municipal wastewater
Copper (Cu)	70	ND	ND	5
Zinc (Zn)	1000	1100	ND	11
Lead (Pb)	150	ND	100	3.0
Cadmium (Cd)	1.5	ND	350	0.1
Chrome (Cr)	2	270	ND	1.0
Nickel (Ni)	80	120	ND	1.0

Notation: * - Adapted from Liu et al. (2013), ND: not detected.

B. XRD analysis

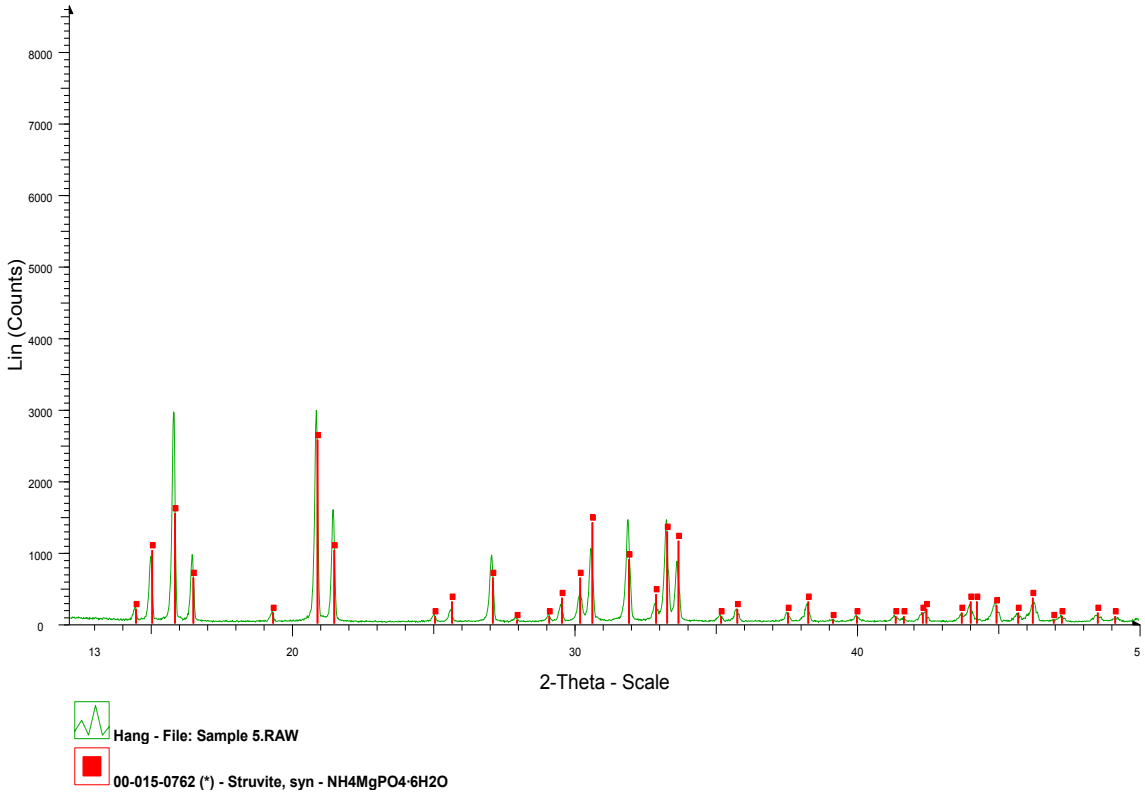

Figure 7.10 XRD pattern of MAP recovered from desorption solution at the optimal crystallization condition

The crystal structure of the recovered precipitate was analyzed using Siemens D5000 X-ray Diffractometer. The XRD patterns of the precipitate and the standard

struvite (MAP) are illustrated in Fig.7.10 for comparison purpose. As the figure shows, the XRD pattern of the harvested precipitate almost coincides with that of the reference struvite ($MgNH_4PO_4.6H_2O$), with respect to the position and the intensity of peaks. The result indicated that the reclaimed precipitate was mainly MAP crystals. A minor difference in the peak intensity between these two XRD patterns could be attributed to the presence of impurities in trivial quantities. Similar locations of the peaks were observed by Foletto et al. (2013), Hao et al. (2008), Jia (2014), Muster et al. (2013), Nur (2014), and Xu et al. (2012).

C. SEM analysis

The morphology of the precipitate obtained at the optimal condition was studied by Zeiss Evo LS15 SEM (Germany). The SEM analysis results are shown in Fig.7.11. Fig.7.11 indicates that no amorphous phase was found. It is noted that MAP crystals can be formed in different types, such as orthorhombic structure (Karabegovic et al., 2013), needle-like structure (Hao et al., 2008, Li et al., 2012; Muster et al., 2013; Song et al., 2007), and quasi-spherical structure (Foletto et al., 2013).

In this study, a majority of the settled solids were orthorhombic crystals. The precipitates were white and had a crystal size range of 2-50 μm, with an average length of 40 μm. It is well-documented that the small size of MAP crystals is responsible for their weak settling, leading to the separation problem. Due to the low weight, it will take much time for small-size MAP crystals to settle. Therefore, several measures have been proposed to enlarge the size of MAP crystals including continuous feeding, low-speed stirring, lengthy retention time, and seeding (Karabegovic et al., 2013; Lanning, 2008). Nevertheless, this is still a challenge to researchers. In the previous studies, the MAP crystals were found to be as long as 0.25 μm (Foletto et al., 2013), 2 μm (Karabegovic et al., 2013), 5 μm Lanning, 2008), 10 μm (Huchzermeier, 2011), 20 μm (Ackerman, 2012; Jia, 2014), 50 μm (Song et al., 2007), and 80 μm (Li et al., 2012; Muster et al., 2013). The comparison with earlier studies has placed the recovered MAP in this study among the medium-sized crystals. It was also found that a majority of MAP crystals were settled in 30 min. Clearly, the precipitates reclaimed at the optimal condition have the typical shape of MAP crystals with the advantageous crystal size.

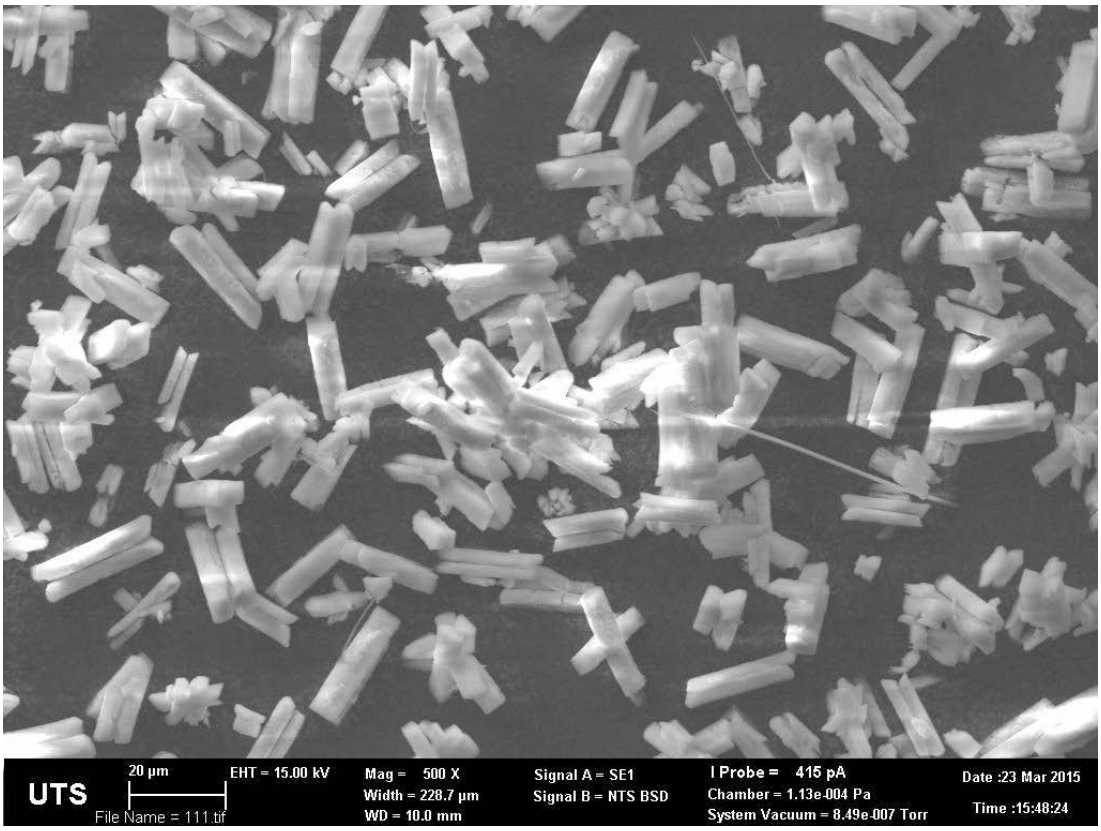

Figure 7.11 SEM image of MAP recovered from desorption solution at the optimal crystallization condition

D. FTIR analysis

The functional groups on the surface of the recovered precipitate were determined by FTIR technique. The IR spectroscopy was recorded in Fig.7.12. The peak at 2889.49 cm^{-1} represents O-H (very broad) in carboxylic acids and derivatives. The peak at 2343.61 cm^{-1} arises from phosphorus functions (P-H phosphine, med & shp). A broad band in the range between 1595.2 and 1581.7 cm^{-1} can be assigned to NH_2 scissoring (1^o amines) in amines. The band at 1437.03 cm^{-1} suggests the presence of C-O-H bending in carboxylic acids and derivatives. The peak at 987.6 cm^{-1} is attributed to the P-H phosphine (P-H pending) in phosphorus functions. The bands seen over the range of 885.36-750.34 cm^{-1} correspond to NH_2 and N-H wagging (shifts on H-bonding) in amines. Similar adsorption bands have been detected by Nur (2014) for MAP synthesized from synthetic wastewater. The adsorption peaks occurring at 1640 and 882 cm^{-1} was assigned to N-H bending vibration and NH_4-water H-bonding, respectively, whereas the band corresponding to 1063 cm^{-1} was associated with ionic phosphate. Equally, Foletto et al. (2013) suggested that the band at 2500 cm^{-1} was assigned to water - phosphate H-bonding, the peaks observed over the range from 1600 to 1400 cm^{-1}

represented HNH deformation modes of NH_4, and the peaks seen at 890 cm^{-1} was responsible for NH_4-water H-bonding. In the same way, Li et al. (2012) ascribed the adsorption peak at 1004.9 cm^{-1} to phosphate. Based on the IR data obtained in this study, it can be reasonably concluded that PO_4 and NH_4 are main components of the recovered phosphorus product.

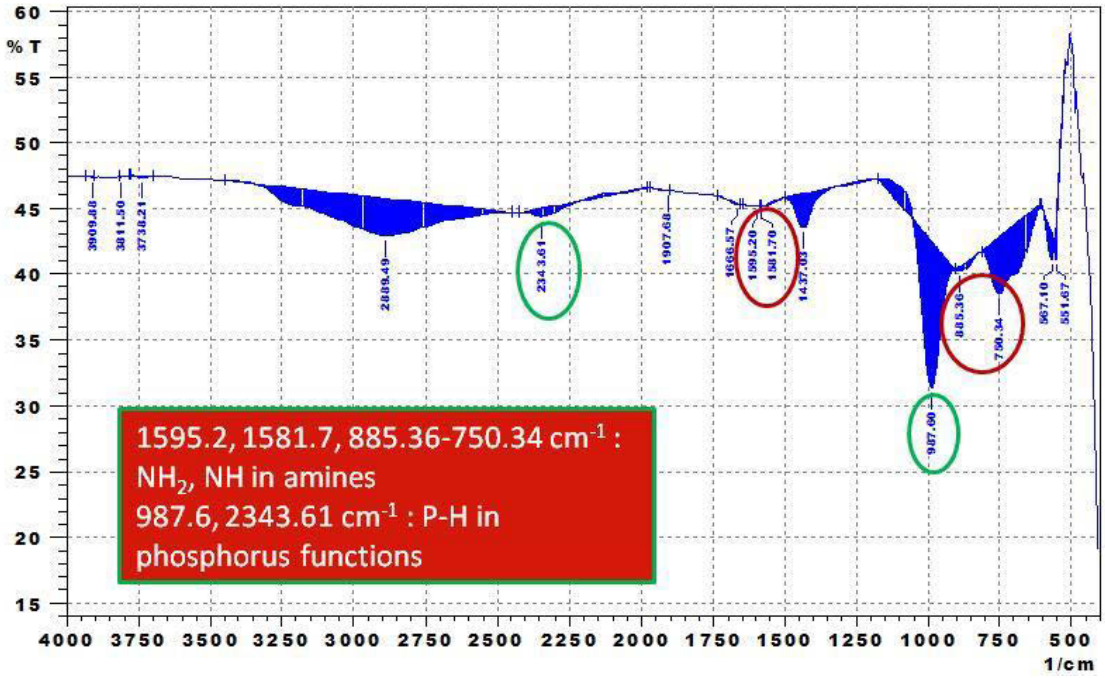

Figure 7.12 FTIR spectrum of MAP recovered from desorption solution at the optimal crystallization condition

7.4.2 MAP purity evaluation

It is common that the MAP content in the precipitate is calculated from NH_4^+-N content (Hao et al., 2008). This method is appropriate as long as no external ammonium compounds are remained in the precipitate. However, this is not true in the reality. It was observed that the residual ammonium compounds were present in the precipitate even though the precipitate was washed 7 times. Thus, in this study, MAP purity was determined according to the minimum molar number of MAP components. Accordingly, 2.48 g of the precipitate recovered at the optimal crystallization condition was dissolved with 1 L of Milli-Q water. The millimolar numbers of P, Mg, and N were calculated to be 9.58, 9.38, and 9.72, respectively. Thus, the millimolar number of MAP was 9.38, and the percentage of MAP in the precipitate was 92.59%.

7.4.3 Phosphorus bioavailability

The bioavailability of the recovered phosphorus product is indicated by its solubility in 2% citric acid (Nieminen, 2010). It was found that the citric acid solubility of the harvested precipitate was approximately 89% by mass, which was superior to that of conventional single superphosphate (87%). A similar result (94%) was reported by Xu et al. (2012) in case of reclaiming phosphorus as MAP from sewage sludge ash. Due to high P-availability together with low levels of heavy metals, the harvested MAP can be used as a high-quality fertilizer.

7.5 ECONOMIC ASSESSEMENT

7.5.1 Based on analytical grade chemical prices

A. The cost of ZLO development

This study employed analytical grade chemicals for ZLO preparation. Therefore, the cost of developed ZLO was first estimated based on the prices of analytical grade chemicals. The cost of ZLO included the following items: (i) modifying chemicals (NaOH and $ZrOCl_2.8H_2O$), (ii) electricity consumption for drying and stirring, and (iii) okara transportation from Nhu Quynh tofu and soy milk workshop to the Environmental Laboratory of University of Technology, Sydney. The calculation was made with the assumption that Zr^{4+} solution was recycled 10 times using add-on technique. The cost of ZLO prepared from analytical grade chemicals was estimated to be 198 USD/kg. The cost of ZLO was found to be still lower than the cost of Whatman QA 52 - a commercial anion exchange resin (436 USD/kg) (Wartelle and Marshall, 2006). However, it was much higher when compared to the cost of quaternized corn stover - another AWBs based phosphorus adsorbent (7.40 USD/kg). In an attempt to reduce the cost of ZLO, the calculation of the cost of ZLO was made based on the prices of industrial grade chemicals as follows.

Table 7.5 Comparing ZLO with other AWBs based adsorbents and commercial adsorbents in term of the cost

Adsorbent	Cost ($/kg)	Reference
Zirconium loaded okara (Zr^{4+} recycled)	8.69	This study
Quaternized corn stover (CHMAC recycled)	7.40	Wartelle and Marshall, 2006
Whatman QA 52	436	Wartelle and Marshall, 2006
DOWEX™ ion exchange resins	350	(1)
Amberlite® IRA400 chloride form	463.6	(2)

Notation: Available at

(1) http://msdssearch.dow.com/PublishedLiteratureDOWCOM/dh_0123/0901b80380123b04.pdf?filepath=liquidseps/pdfs/noreg/177-01806.pdf&fromPage=GetDoc

(2) http://www.sigmaaldrich.com/catalog/product/aldrich/247669?lang=en&region=AU

B. The cost of MAP recovery

To evaluate the economic feasibility of the P recovery from municipal wastewater as MAP by adsorption coupled with crystallization, the chemical consumption was taken into account in combination with other factors, such as energy requirement, the frequency of column cleaning and adsorbent replacement. The economic evaluation of MAP recovery was carried out with the following assumptions:

- ZLO was repeatedly used up to 10 times.
- The MAP yield in this study was 0.014 kg MAP/m^3.
- The price of the synthetic MAP was 1240 USD/kg (www.scbio.de/datasheet-268526-ammonium-magnesium-phosphate-hexahydrate.html)
- The price of the industrial MAP was 1885 USD/ton (Seymour, 2009).
- The price of analytical grade NH_4Cl was 3850 AUD/kg, which was equivalent to 2926 USD/kg (www.sigmaaldrich.com/catalog/product/aldrich/254134?lang=en&region=AU)
- The electricity rate was 0.1 €/kWh, which was equivalent to 0.109 USD/kWh (Garcia-Belinchón et al., 2013).

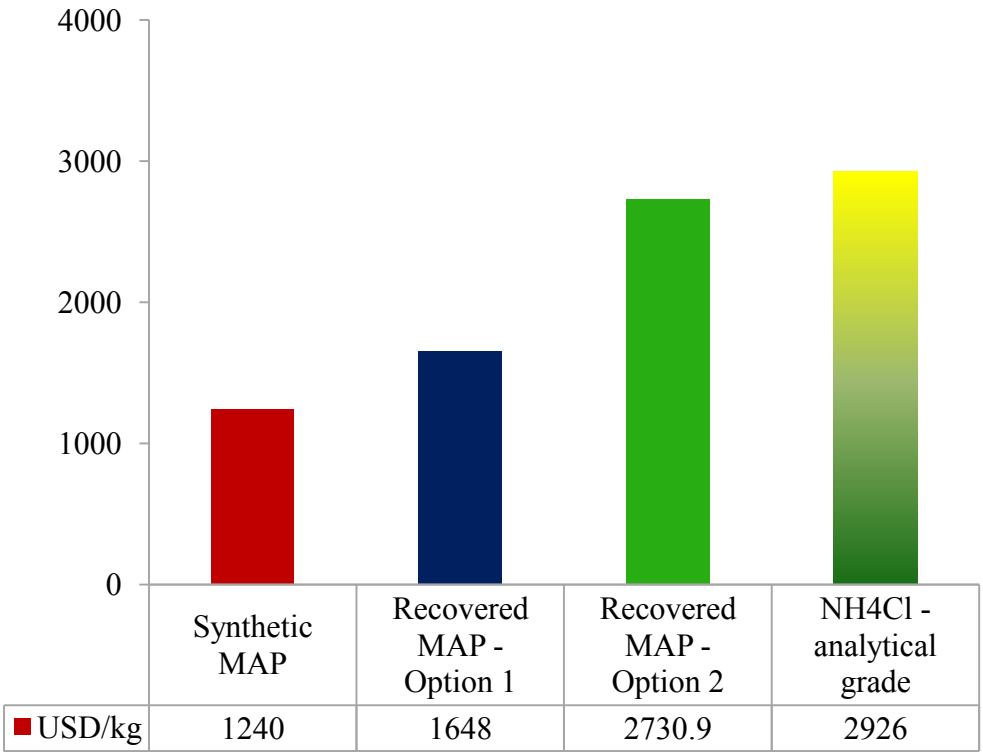

Figure 7.13 Comparing the recovered MAP with the synthetic MAP in term of price (based on analytical grade chemical prices)

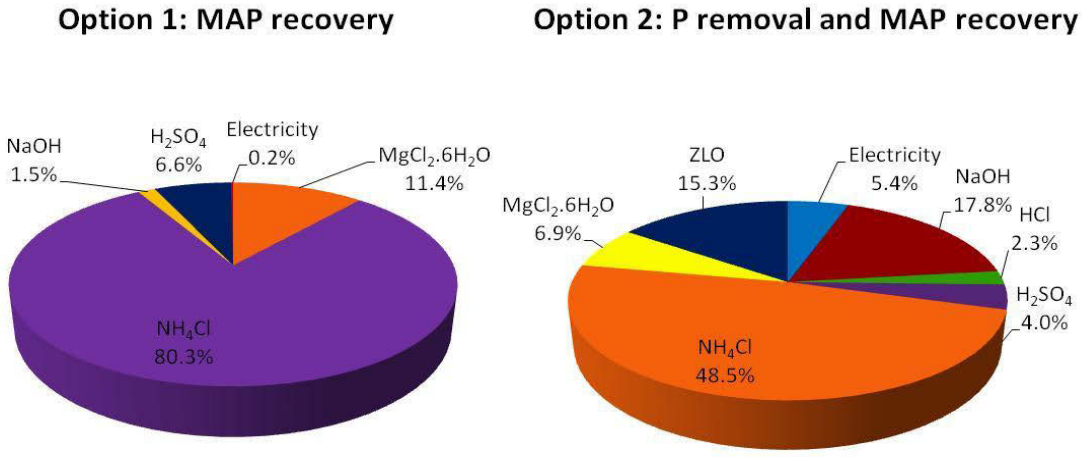

Figure 7.14 Components of the recovered MAP price (based on analytical grade chemical prices)

The cost of the recovered MAP was calculated for two options. In the Option 1, the cost of the recovered MAP was estimated for only MAP recovery. In the Option 2, the cost of the recovered MAP included those for both P removal and MAP recovery. The results are displayed in Figure 7.13. It was found that for Option 1, the cost of the recovered MAP was 1648 USD/kg, which was a little bit higher than the cost of synthetic MAP (1240 USD/kg). However, for Option 2, the cost of the harvested MAP

(2730.9 USD/kg) was more than double of the cost of synthetic MAP (1240 USD/kg). The higher cost of the recovered MAP in Option 2 was attributed to the P removal from municipal wastewater by adsorption onto ZLO. The high costs of the recovered MAP for both options can be ascribed to the high cost of analytical grade NH_4Cl (2926 USD/kg). This finding was further supported by two pie charts (Figure 7.14), which showed that NH_4Cl contributed up to 80.3% and 48.5%, respectively. The results implied that using analytical grade chemicals for MAP recovery resulted in extremely high cost of the recovered MAP. For that reason, the cost of the recovered MAP has been estimated using the industrial grade chemicals as follows.

7.5.2 Based on industrial grade chemical prices

A. The cost of ZLO development

In an attempt to reduce the cost of ZLO development, the prices of industrial chemicals (NaOH and $ZrOCl_2.8H_2O$) have been examined. The calculations were made based on the lower purity of industrial grade chemicals, and thus higher amounts of used chemicals. The cost of ZLO estimated using industrial grade chemical prices was 8.69 USD/kg ZLO. This was comparable to the cost of quaternized corn stover (7.40 USD/kg) but substantially lower than cost of Whatman QA 52 - a commercial anion exchange resin (436 USD/kg) (Wartelle and Marshall, 2006). The results indicated that the use of industrial grade chemicals significantly reduced the cost of the developed adsorbent. A low-cost can be considered as a significant advantage of ZLO over commercial anion exchange resins in the P decontamination from wastewater.

B. The cost of MAP recovery

The costs of the recovered MAP were calculated for Option 3 (MAP recovery only) and Option 4 (P removal and MAP recovery), using industrial grade chemical prices. The results are displayed in Figure 7.15. As shown by the figure, in Option 3 the cost of the recovered MAP (4.09 USD/kg) was comparable to that of industrial MAP (1.885 USD/kg). Nevertheless, in Option 4, the cost of recovered MAP (173.6 USD/kg) was considerably higher than the cost of the industrial MAP (1.885 USD/kg). However, the cost of the recovered MAP in Option 4 (173.6 USD/kg) was still much lower as compared to that of the synthetic MAP (1240 USD/kg). The results demonstrated that the use of industrial grade chemicals led to a dramatic reduction in the cost of the recovered MAP. The pie charts in Figure 7.16 indicated that when industrial grade chemicals were applied, not the chemicals but the electricity accounted for a major part

in the total cost of the recovered MAP. The percentages of electricity in the total cost of the recovered MAP in Option 3 and Option 4 were 74.44% and 86.29%, respectively. The electricity cost was particularly high in Option 4. This can be explained as follows. The direct MAP recovery from municipal wastewater is not efficient, due to low P concentration (~5 mg/L) and high volume of wastewater needs to be treated (Schick et al., 2009). Thus, in this study P in municipal wastewater was pre-concentrated in advance by adsorption onto ZLO. Since peristaltic pumps had to work for a long time, the electricity consumption was extensive. This can be cited as a main drawback of adsorption - crystallization hybrid process. However, the high purity of the recovered MAP can be considered as a compensation for the high cost. As electricity played an important part in the total cost of the recovered MAP when industrial grade chemicals are utilized, to reduce further the cost of the recovered MAP, efforts should be made to minimize the cost of electricity. It is expected that the electricity cost will be diminished if renewable energy, such as solar or wind energy can be applied. Moreover, it should be kept in mind that P is non-lasting resource, and thus its reserve will be depleted sooner or later. In the light of this, the hybrid adsorption-crystallization process for MAP recovery from municipal wastewater should be examined with additional measures to diminish the cost of the recovered MAP.

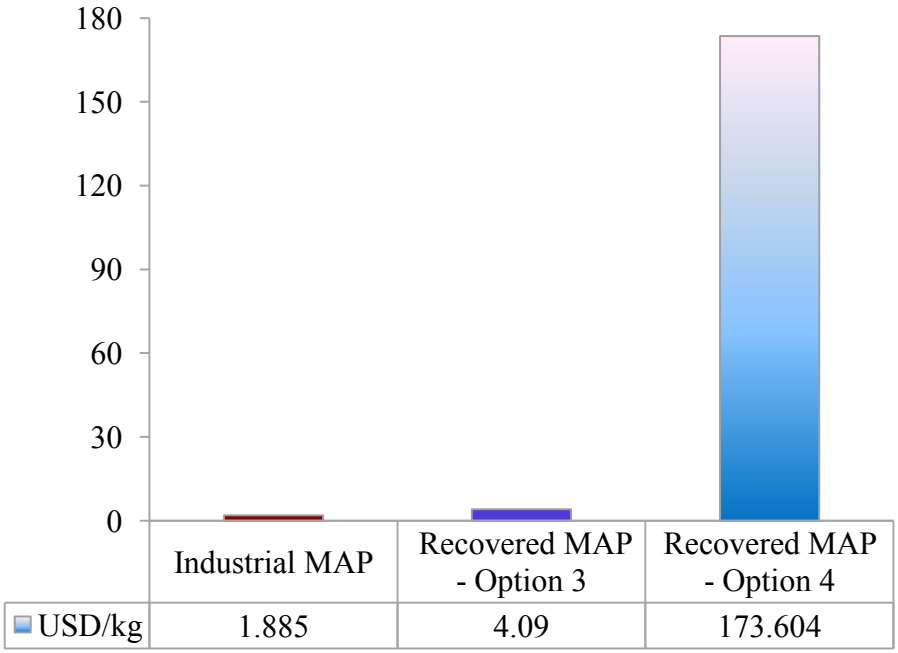

Figure 7.15 Comparing the recovered MAP with the synthetic MAP in term of price (based on industrial grade chemical prices)

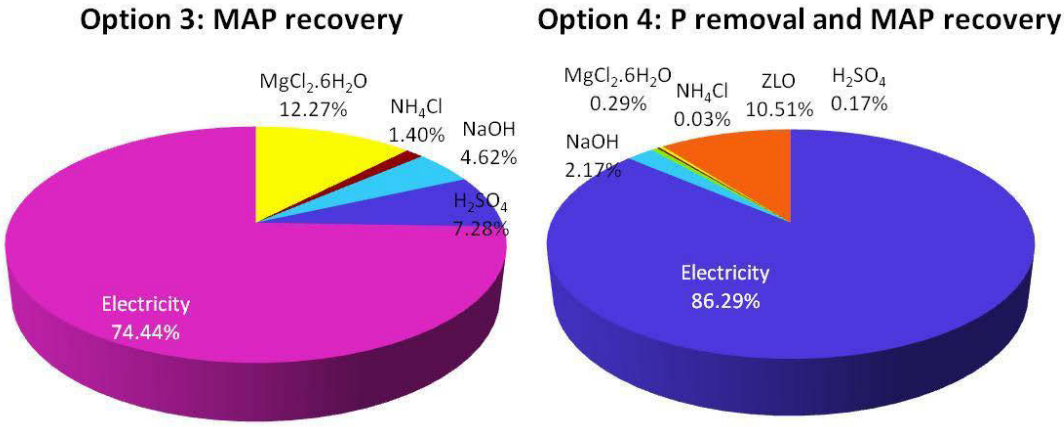

Figure 7.16 Components of the recovered MAP price (based on industrial grade chemical prices)

7.6 DISPOSAL OF THE EFFLUENT AFTER MAP CRYSTALLIZATION

It is important to evaluate the features of the effluent after MAP crystallization to ensure the safe discharge into the environment. Depending on the Mg: N: P molar ratio used for MAP synthesis, the effluent may suffer from high levels of nitrogen and/or magnesium, as well as high pH value. It has been reported that the wastewater with N: P ratio of 4:1 to 9:1 was suitable for irrigation without adverse impact on the nutrient balance of the agricultural land (Perera et al., 2007). In this study, the effluent after MAP crystallization had the pH value of 8.7, the N: P molar ratio of 10.72, and Mg^{2+} concentration of 168 mg/L. Due to the high pH and the presence of Mg^{2+} in the effluent, it is recommended not to employ the effluent after crystallization for irrigation. Alternatively, it can be mixed with new desorption solution in the next crystallization process. By this way, the residual Mg^{2+}, NH_4^+, and PO_4^{3-} can be used for the MAP recovery. As the phosphorus concentration in desorption solution was ≥150 mg/L, at the mixing ratio of 1:1, the phosphorus concentration of the mixture is supposed to be higher than the recommended P level (50 mg/L) to ensure the economical MAP recovery (Nieminen, 2010). Moreover, high pH value in the effluent after crystallization can help reduce the amount of NaOH for the pH increment to the optimal value.

7.7 CONCLUSION

The recovery of phosphorus from municipal wastewater is still a challenge to researchers, due to the low concentration of phosphorus and high volume of wastewater to be treated. This study examines a novel technique for phosphorus recovery from

municipal wastewater using adsorption followed by crystallization. The below are significant concluding remarks:

- A new insight was achieved that using a semi-pilot scale ZLO column adsorption-desorption system could pre-concentrate phosphorus from municipal wastewater up to 28.36 times, fitting well the minimum requirement (50 mg P/L) for the economical MAP recovery.
- Up to 95.19% of dissolved phosphorus in desorption solution was recovered at pH = 9, Mg: N: P molar ratio = 2:2:1, using a combination of $MgCl_2.6H_2O$ and NH_4Cl. The harvested MAP exhibited high purity (92.59%), high P-availability (89% by mass), and extremely low levels of heavy metals.
- It was noteworthy that the cost of ZLO was still lower than those of commercial anion exchange resins if analytical grade chemical prices were applied. However, use of industrial grade chemical prices made the cost of ZLO comparable to those of other AWBs based phosphorus adsorbents.
- The proposed MAP recovery process was currently not economically feasible, due to high prices of analytical grade chemicals and electricity. However, it can be economically acceptable when cheaper sources of chemicals and energy are applied alternatively.
- In view of the non-renewable P resource, the proposed MAP recovery process should receive more attention, because of the formation of high-quality and safe-to-use phosphorus.

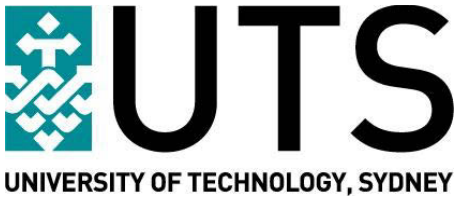

CHAPTER 8

CONCLUSIONS AND FUTURE RESEARCH

The previous Chapters provide insights into different aspects of removing and recovering phosphorus from water and wastewater by adsorption onto ZLO and crystallization as MAP. The overall concluding remarks of this thesis, the unsolved problems, and the direction for future work are major contents of Chapter 8.

8.1 OVERALL CONCLUSIONS

8.1.1 Key findings

This study demonstrated that metal loading method was an efficient means to activate the phosphate adsorption capability of AWBs. The Zr^{4+} cationic ions deposited on ZLO was responsible for the retention of PO_4^{3-} anionic ions onto ZLO. The recycling of Zr^{4+} as metal loading solution up to 10 times was viable with a minor reduction in the P removal percentage of ZLO. Among three developed adsorbents, ZLO was found to be the best.

Batch experiments indicated that ZLO could work competently in a wide range of pH (2-11) and the presence of several foreign anions (SO_4^{2-}, NO_3^-, and Cl^-). This can be considered as advantages of ZLO when used in treating real wastewater. The Langmuir adsorption capacity of ZLO was 58.93 mg PO_4/g adsorbent, which was favorably comparable to other adsorbents in the literature. This was probably owing to the existence of positively charged Zr^{4+} cationic ions on the adsorbent. Isotherm data was best fitted by the Freundlich model, indicating the heterogeneous surface of ZLO. The kinetic study demonstrated that phosphorus removal by ZLO was rapid, and the removal efficiency reached 95% in 30 min. The Pseudo-second order model most satisfactorily described the kinetic data, suggesting the dominance of chemisorptions mechanism. Thermodynamic analysis revealed that adsorption of phosphate onto ZLO was a feasible, spontaneous, and endothermic process. Finally, the desorption results showed that 94.25% of the adsorbed phosphate was eluted by 0.2 M NaOH. The spent ZLO could be successfully regenerated by 0.1 M HCl, with the reductions in phosphate sorption and desorption capacities of ZLO after five consecutive cycles were 12.46% and 7.40%, respectively.

The column experiments showed that it was feasible to eliminate phosphorus from water and wastewater using a ZLO packed bed column. The lower flow rate, higher bed depth, smaller feed phosphorus concentration, smaller particle size, and the lower solution pH value resulted in higher treated volume and longer service time. The highest

dynamic adsorption capacity of ZLO was 16.43 mg P/g adsorbent (~50.35 mg PO_4/g adsorbent), which accounted for 85.44% its equilibrium adsorption capacity (58.93 mg PO_4/g adsorbent). The Thomas and BDST models satisfactorily described the column adsorption behavior. The adsorbed P was quantitatively eluted by 0.2 M NaOH, and the desorbed ZLO was successfully regenerated with 0.1 M HCl. After three cycles of adsorption - desorption, the phosphorus uptake of ZLO was reduced by 18.64%, while the weight loss was 8.7%. In a semi-pilot scale test, the recommended discharge standard for phosphorus (1 mg/L) could be met for 41.67 h, equivalent to 132.5 L of treated volume by percolating municipal wastewater through a column packed with 100 g of ZLO. Zr^{4+} leaching from ZLO could not be detected during its performance.

This study proved that phosphorus can be successfully recovered from municipal wastewater by adsorption onto ZLO coupled with crystallization as MAP. Using a semi-pilot scale ZLO column adsorption-desorption system could pre-concentrate phosphorus from municipal wastewater up to 28.36 times, fitting well the minimum phosphorus concentration requirement (50 mg/L) for economical MAP recovery. Considering the P removal efficiency, MAP purity and real applicability, the optimal condition for MAP reclamation was determined as pH = 9, Mg: N: P molar ratio = 2:2:1, the chemical combination of $MgCl_2.6H_2O$ and NH_4Cl, and room temperature. The MAP harvested at the optimum condition was characterized by the P recovery efficiency of 95.19%, the MAP purity of 92.59%, and the P-availability of 89% by mass. It is recommended to use the reclaimed MAP as a fertilizer in agricultural production or a raw material in the phosphate industry.

The economic evaluation showed that ZLO could be developed at a price comparable to that of other AWBs based adsorbents, and significantly lower than that of commercial adsorbents. In contrast, the phosphorus recovery from municipal wastewater by adsorption onto ZLO combined with crystallization as MAP was currently not economically feasible. This can be explained by large energy consumption for phosphorus pre-concentration in the adsorption stage. To further reduce the cost of the recovered MAP, use of renewable energy, cheap and abundant sources of chemicals should be examined.

8.1.2 Contributions to the field

The original contributions of this research to the field of phosphorus removal and recovery using AWBs based adsorbents include:

- A determination that okara contains some phosphorus inside. This provides a foundation for mining phosphorus from okara.
- Development of a technique for recycling of metal loading solution. This helps reduce the cost of adsorbent preparation and the need to dispose of the metal loading solution after use. This technique can be applied whenever AWBs based phosphorus adsorbents are prepared according to metal loading method.
- A determination that in a column adsorption system, an adsorbent should be used in a combination of different particle sizes. By this way, the phosphorus removal efficiency of the column is improved, while the column clogging is mitigated. As a result, the adsorbent can be saved, and the frequency of the column maintenance will be diminished.
- Discovery that for a successful phosphorus recovery from desorption solution, both the volume and the phosphorus concentration of desorption solution are significant. Thus, the optimal flow rate should be applied. In view of phosphorus recovery, both the recovery efficiency and MAP purity are vital. Hence, these factors should be taken into account when the optimal crystallization conditions are determined.
- Development of a technique to obtain a desorption solution with a sufficiently high concentration of phosphorus. Accordingly, the exhausted desorption should not be implemented. Alternatively, desorption should be stopped when the desirable concentration of phosphorus is reached. This technique is suitable for adsorbents, whose desorption profiles show that the majority of desorption is completed in a very short time.
- Finding that activation with an acid solution is an efficient means to regenerate the phosphorus adsorbent after desorption. As adsorbent can repeatedly be used for several times, the cost of water treatment can be decreased.

8.2 RECOMMENDATIONS FOR FURTURE RESEARCH

8.2.1 Evaluation of ZLO safety

This study showed that ZLO did not suffer from Zr^{4+} bleeding during its performance. During the absence of Zr in the effluent and thus in the receiving water bodies, ZLO will not pose any risk to the aquatic creatures. However, to minimize the possible harmful effects on the public health, the toxicology tests with ZLO should be conducted before its application for drinking water treatment.

8.2.2 Agronomic study of the recovered MAP

The good quality of the recovered MAP was evidenced by high purity and P-bioavailability in this study. However, in the reality, the efficacy of the harvested MAP can vary, depending on the pH and the type of soils on which the MAP is applied. Thus, it is suggested that the field tests with the reclaimed MAP should be conducted to verify its agronomic values in the real conditions.

8.2.3 Alternative sources of chemicals and energy

The reclamation of P as MAP requires the addition of chemicals for pH alternation and crystallization. The use of analytical grade chemicals for these purposes often results in a very high cost of the recovered MAP. To make MAP recovery process economically viable, the substitutes for analytical grade chemicals should be explored. Considering the abundant availability and low cost, the natural resources (e.g. sea water), wastes/by-products (e.g. MgO by-products from Mg mining, urine, NH_4^+ rich wastewater), industrial grade chemicals (e.g. $ZrOCl_2.8H_2O$, NaOH, H_2SO_4) should be closely examined. Moreover, a study on the use of renewable energy (solar, wind energy) for P recovery is also necessary.

8.2.4 Recycling of chemicals

The recycling of Zr^{4+} loading solution should be applied in the preparation of phosphorus adsorbents from other AWBs. Additionally, the reuse of the effluent after MAP recovery as a substitute for desorption solution should be investigated to reduce the cost of water treatment and mitigate adverse impacts on the environment.

8.2.5 Use of ZLO for arsenate removal

The similarities in chemistry between arsenate (AsO_4^{3-}) and phosphate (PO_4^{3-}) have been well-documented in the literature (Gibbons, 2009; Nur, 2014). As ZLO was found to have a strong affinity for PO_4^{3-} anions, it is expected to be effective in eliminating AsO_4^{3-} anions as well. Therefore, it is recommended to use ZLO for

purification of arsenate contaminated underground waters. If it is successful, the practical application of ZLO will be extended.

8.2.6 Recovery of phosphorus from agricultural by-products

Phosphorus is found to be a component of many important compounds in plants, such as deoxyribonucleic acid (DNA), ribonucleic acid (RNA), adenosine triphosphate (ATP), and phospholipids. Thus, some AWBs may contain high contents of phosphorus. This provides a foundation for mining phosphorus from AWBs. In connection to that, the selection of potential AWBs and the development of efficient extraction methods are most important.

8.2.7 Simultaneous removal nitrogen and phosphorus

In the reality, there are many kinds of wastewater containing high levels of both ammonium (NH_4^+) and phosphate (PO_4^{3-}). In these cases, it would be appropriate to produce MAP by exploiting both ammonium (NH_4^+) and phosphate (PO_4^{3-}) sources in wastewater. As mentioned in the Section 7.5.1, using analytical grade chemicals for MAP recovery results in an extremely high cost of the recovered MAP. Therefore, by simultaneous removal of both ammonium (NH_4^+) and phosphate (PO_4^{3-}) from wastewater, the cost of the recovered MAP is expected to reduce significantly.

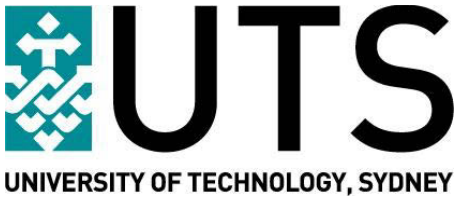

REFERENCES

[1] Abdul, A., Aberuagba, F., 2005. Comparative study of the adsorption of phosphate by activated charcoal from corncobs, groundnut shells and rice husks. AU J. T. 9, 59-63.

[2] Ackerman, J.N., 2012. Reclaiming phosphorus as struvite from hog manure (Doctoral thesis). University of Manitoba, Winnipeg, Canada.

[3] Adachi, A., Hamamoto, H., Okano, T., 2005. Use of lees materials as an adsorbent for removal of organochlorine compounds or benzene from wastewater. Chemosphere 58, 817-822.

[4] Adam, C., 2011. Case study: Phosphorus recovery from sewage sludge - Results of the European FP6- and FP7-projects SUSAN and SUSYPHOS. *International Conference on Environmental (Bio) Technologies and EU-FP7 Environment Brokerage Event*, 5-8 September, Gdańsk, Pomeranian, Poland.

[5] Adnan, A., Mavinic, D. S., Koch, F. A., 2003. Pilot-scale study of phosphorus recovery through struvite crystallization - examining the process feasibility. J. Environ. Eng. Sci. 2, 315-324.

[6] Ali, M.I., Schneider, P.A., 2008. An approach of estimating struvite growth kinetic incorporating thermodynamic and solution chemistry, kinetic and process description. Chem. Eng. Sci. 63, 3514-3525.

[7] Anirudhan, T.S, Senan, P., 2011. Adsorption of phosphate ions from water using novel cellulose based adsorbent. J. Chem. Ecol. 27, 147-164.

[8] Anirudhan, T.S., Noelin, B.F., Manohar, D.M., 2006. Phosphate removal from wastewaters using a weak anion exchanger prepared from a lignocellulosic residue. Environ. Sci. Technol. 40, 2740-2745.

[9] Australian water and wastewater association, 1997. Australian guidelines for sewerage systems - Effluent management. Available at http://www.environment.gov.au/system/files/resources/e52e452b-a821-4abe-9987-23988790e353/files/sewerage-systems-effluent-man-paper11.pdf. (Accessed on March 15, 2015).

[10] Awual, Md. R., Jyo, A., 2011. Assessing of phosphorus removal by polymeric anion exchangers. Desalin. 281, 111-117.

[11] Behnamfard, A., Salarirad, M.M., 2009. Equilibrium and kinetic studies on free cyanide adsorption from aqueous solution by activated carbon. J. Hazard. Mater. 170, 127-133.

[12] Benyoucef, S., Amrani, M., 2011a. Adsorption of phosphate ions onto low cost Aleppo pine adsorbent. Desalin. 275, 231-236.

[13] Benyoucef, S., Amrani, M., 2011b. Removal of phosphorus from aqueous solutions using chemically modified sawdust of Aleppo pine (*Pinus halepensis Miller*): Kinetics and isotherm studies. Environmentalist 31, 200-207.

[14] Bhojappa, S., 2009. Removal of phosphorus and selenium from aqueous solution by adsorption processes (Master of Science thesis). West Virginia University, Morgantown, West Virginia, USA.

[15] Biswas, B.K., 2008. Removal and recovery of arsenic and phosphorus by means of adsorption onto orange waste, an available agricultural by-product (Doctoral thesis). Saga University, Saga, Japan.

[16] Biswas, B.K., Inoue, K., Ghimire, K.N., Harada, H., Ohto, K., Kawakita, H., 2008. Removal and recovery of phosphorus from water by means of adsorption onto orange waste gel loaded with zirconium. Bioresour. Technol. 99, 8685-8690.

[17] Biswas, B.K., Inoue, K., Ghimire, K.N., Ohta, S., Harada, H., Ohto, K., Kawakita, H., 2007. The adsorption of phosphate from an aquatic environment using metal-loaded orange waste. J. Colloid Interf. Sci. 312, 241-223.

[18] Bottini, A., Rizzo, L., 2012. Phosphorus recovery from urban wastewater treatment plant sludge liquor by ion exchange. Separ. Sci. Technol. 47, 613-620.

[19] Boujelben, N., Bouzid, J., Elouear, Z., Feki, M., Jamoussi, F., Montiel, A., 2008. Phosphorus removal from aqueous solution using iron coated natural and engineered sorbents. J. Hazard. Mater. 151, 103-110.

[20] Boyer, T.H., Persaud, A., Banerjee, P., Palomino, P., 2011. Comparison of low-cost and engineered materials for phosphorus removal from organic-rich surface water. Water Res. 45, 4803-4814.

[21] Bradford-Hartke, Z., Lant, P., Leslie, G., 2012. Phosphorus recovery from centralized municipal water recycling plants. Chem. Eng. Res. Des. 90, 78-85.

[22] Bulgariu, D., Bulgariu, L., 2013. Sorption of Pb(II) onto a mixture of algae waste biomass and anion exchanger resin in a packed bed column. Bioresour. Technol. 129, 374-380.

[23] Carvalho, W.S., Martins, D.F., Gomes, F.R., Leite, I.R., Gustavo da Silva, L., Ruggiero, R., Richter, E.M., 2011. Phosphate adsorption on chemically modified sugarcane bagasse fibers. Biomass Bioenergy 35, 3913-3919.

[24] Çelen, I., Buchanan, J.R., Burns, R.T., Robinson, R.B., Raman, D.R., 2007. Using a chemical equilibrium model to predict amendments required to precipitate phosphorus as struvite in liquid swine manure. Water Res. 41, 1689-1696.

[25] Chen, S., Yue, Q., Gao, B., Li, Q., Xu, X., Fu, K., 2012a. Adsorption of hexavalent chromium from aqueous solution by modified corn stalk: A fixed bed column study. Bioresour. Technol. 113, 114-120.

[26] Chen, W.T., Lin, C.W., Shih, P.K., Chang, W.L., 2012b. Adsorption of phosphate into waste oyster shell: thermodynamic parameters and reaction kinetics. Desalin. Water Treat. 47, 86-95.

[27] Cheng, X., Wang, Y., Sun, Z., Sun, D., Wang, A., 2013. Pathways of phosphate uptake from aqueous solution by Zn/Al layered double hydroxides. Water Sci. Technol. 67, 1757-1763.

[28] Choi, J., Lee, S., Kim, J., Park, K., Kim, D., Hong, S., 2012. Comparison of surface modified adsorbents for phosphate removal in water. Water Air Soil Poll. 223, 2881-2890.

[29] Chu, A.D., Pham, M.C., Nguyen, M.K., 2010. Characteristic of urban wastewater in Hanoi City - nutritive value and potential risk in using for agriculture. VNU J. Sci., Earth Sci. 26, 42-47.

[30] Clark, D.L., Vanrolleghem, P., 2010. A survey of global and national nutrient regulatory approaches. *Chesapeake Bay program - Real world wastewater technologies workshop*. Available at http://www.chesapeake.org/stac/presentations/211_Clark_Survey%20of%20global%20and%20national%20nutrient%20regulatory%20approaches.pdf (Accessed on March 16, 2015).

[31] Cooper, J., Lombardi, R., Boardman, D., Marquet, C.C., 2011. The future distribution and production of global phosphate rock reserves. Resour. Conserv. Recycl. 57, 78-86.

[32] Cornel, P., Schaum, C., 2009. Phosphorus recovery from wastewater: needs, technologies and costs. Water Sci. Technol. 59, 1069-1076.

[33] Damte, E.M., 2006. Removal of fluoride from water using granular aluminum hydroxide: adsorption in a fixed-bed column (Master of Science thesis). Addis Abada University, Addis Ababa, Ethiopia.

[34] De-Bashan, L. E.., Bashan, Y., 2004. Recent advances in removing phosphorus from wastewater and its future use as fertilizer (1997-2003). Water Res. 38, 4222-4246.

[35] De Lima, A.C.A., Nascimento, R.F., de Sousa, F.F., Filho, J.M., 2012. Modified coconut shell fibbers: A green and economical sorbent for the removal of anions from aqueous solutions. Chem. Eng. J. 185-186, 274-284.

[36] Diwania, G.E., Rafiea, S.E., Ibiaria, N.N.E., El-Ailab, H.I., 2007. Recovery of ammonia nitrogen from industrial wastewater treatment as struvite slow releasing fertilizer. Desalin. 214, 200-214.

[37] Eberhardt, T.L., Min, S.H., 2008. Biosorbents prepared from wood particles treated with anionic polymer and iron salt: effect of particle size on phosphate adsorption. Bioresour. Technol. 99, 626-630.

[38] Eberhardt, T.L., Min, S.H., Han, J.S., 2006. Phosphate removal by refined aspen wood fibber treated with carboxymethyl cellulose and ferrous chloride. Bioresour. Technol. 97, 2371-2376.

[39] Ebie, Y., Kondo, T., Kadoya, N., Mouri, M., Maruyama, O., Noritake, S., Inamori, Y., Xu, K., 2008. Recovery oriented phosphorus adsorption process in decentralized advanced Johkasou. Water Sci. Technol. 57, 1977-1981.

[40] Eldho, T.I., 2014. Indian standards in wastewater treatment - An overview. *IFAT*, October 9-11, 2014, Mumbai, India.

[41] Eljamal, O., Okawauchi, J., Hiramatsu, K., Harada, M., 2013. Phosphorus sorption from aqueous solution using natural materials. Environ. Earth Sci. 68, 859-863.

[42] Foletto, E.L., dos Santos, W.R.B., Mazutti, M.A., Jahn, S.L., Gündel, A., 2013. Production of struvite from beverage waste as phosphorus source. Mater. Res. 16, 242-245.

[43] Foo, K.Y., Lee, L.K., Hameed, B.H., 2013. Preparation of tamarind fruit seed activated carbon by microwave heating for the adsorptive treatment of landfill leachate: A laboratory column evaluation. Bioresour. Technol. 133, 599-605.

[44] Frost, R.C., 2009. EU practice in setting wastewater emission limit values. Available at http://www.wgw.org.ua/publications/ELV%20-%20EU%20practice.pdf. (Accessed on March 15, 2015).

[45] Gao, J., Sia, C., Hea, Y., 2015. Application of soybean residue (okara) as a low-cost adsorbent for reactive dye removal from aqueous solution. Desalin. Water Treat. 53, 2266-2277.

[46] Garcia-Belinchón, C., Rieck, T., Bouchy, L., Gali, A., Rouge, P., Fabregas, C., 2013. Struvite recovery: pilot scale results and economic assessment of different scenarios. Water Practice Technol. 8, 119-130.

[47] Gibbons, M.K., 2009. The use of water treatment residual solids for arsenate and phosphate adsorption (Doctoral thesis). Dalhousie University, Nova Scotia, Canada.

[48] Gorazda, K., Kowalski, Z., Wzorek, Z., 2012. From sewage sludge ash to calcium phosphate fertilizers. Pol. J. Chem. Tech. 14, 54-58.

[49] Green, C.J., Johnson, P., Allen, V.G., Crossland, S.L., 2004. Treatment technologies for phosphorus removal from water derived from cattle feed yards. Available at http://www.tcfa.org/Research/92_treatment_technologies_green.pdf. (Accessed on September 25, 2013).

[50] Greenlee, L.F., Lawler, D.F., Freeman, B.D., Marrot, B., Moulin, P., 2009. Reverse osmosis desalination: Water sources, technology, and today's challenge. Water Res. 43, 2317-2348.

[51] Gupta, M.D., 2011. Removal and recovery of nutrients by ion exchange from water and wastewater (Master of Engineering thesis). University of Technology, Sydney, NSW, Australia.

[52] Han, J.S., Min, S.H., Kim, Y.K., 2005. Removal of phosphorus using AMD-treated lignocellulosic material. Forest Prod. J. 55, 48-53.

[53] Hao, X.D., Wang, C.C., Lan, L., van Loosdrecht, M.C.M., 2008. Struvite formation, analytical methods and effects of pH and Ca^{2+}. Water Sci. Technol. 58, 1687-1692.

[54] Henze, M., Comeau, Y., 2008. Wastewater characterization, in: Henze, M., van Loosdrecht, M.C.M, Ekama, G.A., Brdjanovic, D. (Eds.), Biological wastewater treatment: principles, modeling and design. IWA Publishing, London, 33-52.

[55] Huang, M., Yu, Y., Wu, R., 2010. Researches on the treatment of phosphorous wastewater with oyster shells. Chin. J. Struct. Chem. 29, 1886-1892.

[56] Huang, X., Liao, X., Shi, B., 2009. Adsorption removal of phosphate in industrial wastewater by using metal loaded skin split waste. J. Hazard. Mater. 166, 1261-1265.

[57] Huchzermeier, M.P., 2011. Overcoming challenges to struvite recovery from anaerobically digested dairy manure (Master of Science thesis). State University of New York, New York, USA.

[58] Ismail, Z.Z., 2012. Kinetic study for phosphate removal from water by recycled date-palm wastes as agricultural by-products. Int. J. Environ. Stud. 69, 135-149.

[59] Jain, M., Garg, V.K., Kadirvelu, K., 2013. Cadmium(II) sorption and desorption in a fixed bed column using sunflower waste carbon calcium-alginate beads. Bioresour. Technol. 129, 242-248.

[60] Jeanmaire, N., Evans, T., 2001. Technico-economic feasibility of P-recovery from municipal wastewaters. Environ. Technol. 22, 1355-1361.

[61] Jeon, D.J., Yeom, S.H., 2009. Recycling wasted biomaterial, crab shells, as an adsorbent for the removal of high concentration of phosphate. Bioresour. Technol. 100, 2646-2649.

[62] Jia, G., 2014. Nutrient removal and recovery by the precipitation of magnesium ammonium phosphate (Master of Science thesis). The University of Adelaide, South Australia, Australia.

[63] Jordaan, E.M., Ackerman, J., Cicek, N., 2010. Phosphorus removal from anaerobically digested swine wastewater through struvite precipitation. Water Sci. Technol. 61, 3228-3234.

[64] Jutidamrongphan, W., Park, K.Y., Dockko, S., Choi, J.W., Lee, S.H., 2012. High removal of phosphate from wastewater using silica sulfate. Environ. Chem. Lett. 10, 21-28.

[65] Jyothi, M.D., Kiran, K.R., Ravindhranath, K., 2012. Phosphate pollution control in waste waters using new biosorbents. Int. J. Water Res. Environ. Eng. 4, 73-85.

[66] Kalmykova, Y., Fedje, K., 2013. Phosphorus recovery from municipal solid waste incineration fly ash. Waste Manage. 33, 1403-1410.

[67] Karabegovic, L., Uldal, M., Werker, A., Morgan-Sagastume, F., 2013. Phosphorus recovery potential from a waste stream with high organic and nutrient contents via struvite precipitation. Environ. Technol. 34, 871-883.

[68] Karachalios, A.P., 2012. Nutrient removal from water by various quaternized wood agricultural residues using a choline based ionic liquid analogue (Doctoral thesis). Stevens Institute of Technology, New Jersey, United States.

[69] Karthikeyan, K.G., Tshabalala, M.A., Wang, D., Kalbasi, M., 2004. Solution chemistry effects on orthophosphate adsorption by cationized solid wood residues. Environ. Sci. Technol. 38, 904-911.

[70] Karthikeyan, K.G., Tshabalala, M.A., Wang, D., 2002. Use of lignocelluloses materials for sorption media for phosphorus removal. *ASAE Annual International Meeting/ CIGR XVth World Congress*, Chicago, Illinois, USA, July 28-31.

[71] Kihampa, C., 2013. Heavy metal contamination in water and sediment downstream of municipal wastewater treatment plants, Dar es Salaam, Tanzania. Int. J. Environ. Sci. 3, 1407-1415.

[72] Kim, D., Ryu, H.D., Kim, M.S., Kim, J., Lee, S., 2007. Enhancing struvite precipitation potential for ammonia nitrogen removal in municipal landfill leachate. J. Hazard. Mater. 146, 81-85.

[73] Köse, T. E., Kıvanç, B., 2011. Adsorption of phosphate from aqueous solutions using calcined waste eggshell. Chem. Eng. J. 178, 34-39.

[74] Krishnan, K.A., Haridas, A., 2008. Removal of phosphate from aqueous solutions and sewage using natural and surface modified coir pith. J. Hazard. Mater. 152, 527-535.

[75] Kumar, R., Pal, P., 2013. Turning hazardous waste into value-added products: production and characterization of struvite from ammoniacal waste with new approaches. J. Clean Prod. 43, 59-71.

[76] Kumar, R., Bhatia, D., Sigh, R., Rani, S., Bishnoi, N.R., 2011. Sorption of heavy metals from electroplating effluent using immobilized biomass *Trichodermaviride* in a continuous packed-bed column. Int. Biodeter. Biodegr. 65, 1133-1139.

[77] Kumar, P., Sudha, S., Chand, S., Srivastava,V.C., 2010. Phosphate removal from aqueous solution using coir pith activated carbon. Separ. Sci. Technol. 45, 1463-1470.

[78] Kumar, U., Bandyopadhyay, M., 2006. Fixed bed column study for Cd(II) removal from wastewater using treated rice husk. J. Hazard. Mater. B129, 253-259.

[79] Kuzma, M., 2011. Phosphorus removal and recovery in wastewater: How far can we go? *Online seminar*, September 30, 2011. Available at http://www.azwater.org/common/files/committees/e8fbf236-e225-4d3b-8e17-d94ae7beb19d/Matt%20Kuzma%20-

%20Phosphorus%20Removal%20and%20Reocvery%20from%20Wastewater%20Oct%202nd%202011.pdf. (Accessed on September 19, 2013).

[80] Lanning, M.C.E., 2008. Phosphate recovery from wastewaters comparing two different sources of magnesium oxide in the precipitation of struvite (Master of Science thesis). The University of Guelph, Ontario, Canada.

[81] Le Corre, K.S., Valsami-Jones, E., Hobbs, P. Parsons, S.A.., 2009. Phosphorus recovery from wastewater by struvite crystallization: A review. Crit. Rev. Environ. Sci. Technol. 39, 433-477.

[82] Le Corre, K.S., Valsami-Jones, E., Hobbs, P., Parsons, S.A., 2005. Impact of calcium on struvite crystal size, shape and purity. J. Cryst. Growth 283, 514-522.

[83] Li, N., Ren, J., Zhao, L., Wang, Z., 2013. Fixed bed adsorption study on phosphate removal using nanosized FeOOH-modified anion resin. J. Nanomater. 2013, January 2013, Article No. 7, http://dx.doi.org/10.1155/2013/736275.

[84] Li, B., Qiao, M., Lu, F., 2012. Composition, nutrition, and utilization of okara (soybean residue). Food Rev. Int. 28, 231-252.

[85] Li, H., Ye, Z., Wang, F., 2012. Phosphorus recovery as struvite from eutrophic waters by XDA-7 resin. Water Sci. Technol. 65, 2091-2097.

[86] Li, L., 2009. Adsorption of Cd(II) and Zn(II) from aqueous solutions by raw bean dregs (Master of Science thesis). Human University, Hunan, China.

[87] Li, Y.J., Wang, L.H., Lan, Y.Z., 2009. Experimental study on phosphorus removal by activated alumina adsorbents. Journal Kunming Metallurgy College 25, 59-65.

[88] Litke, D.W., 1999. Review of phosphorus control measures in the United States and their effects on water quality. Available at http://pubs.usgs.gov/wri/wri994007/pdf/wri99-4007.pdf. (Accessed on March 15, 2015).

[89] Liu, Y.H., Kumar, S., Kwag, J.H., Ra, C.S., 2013. Magnesium ammonium phosphate formation, recovery and its application as valuable resources: a review. J. Chem. Technol. Biotechnol. 88, 181-189.

[90] Loganathan, P., Vigneswaran, S., Kandasamy, J., Bolan, N.S., 2014. Removal and recovery of phosphate from water using sorption. Crit. Rev. Environ. Sci. Technol. 44, 847-907.

[91] Long, Y., Lei, D., Ni, J., Ren, Z., Chen, C., Xu, H., 2014. Packed bed column studies on lead (II) removal from industrial wastewater by modified *Agaricusbisporus*. Bioresour. Technol. 152, 457-463.

[92] Mallampati, R., Valiyaveettil, S., 2013. Apple peel - a versatile biomass for water purification. ACS Appl. Mater. Interfaces 5, 4443-4449.

[93] Marshall, W.E., Wartelle, L.H., 2004. An anion exchange resin from soybean hulls. J. Chem. Technol. Biotechnol. 79, 1286-1292.

[94] Martin, B.D., Parsons, S.A., Jefferson, B., 2009. Removal and recovery of phosphate from municipal wastewaters using a polymeric anion exchanger bound with hydrated ferric oxide nanoparticles. Water Sci. Technol. 60, 2637-2645.

[95] Martín, M., Gargallo, S., Hernández-Crespo, C., Oliver, N., 2013. Phosphorus and nitrogen removal from tertiary treated urban wastewaters by a vertical flow constructed wetland. Ecol. Eng. 61, 34-42.

[96] Mateo-Sagasta, J., Raschid-Sally, L., Thebo, A., 2015. Global wastewater and sludge production, treatment and use, in: Drechsel, P., Qadir, M., Wichelns, D. (Eds.), Wastewater economic asset in an urbanizing world. Springer, 15-24.

[97] Matouq, M., 2008. The potential for reusing treated municipal wastewater for irrigation in the Hashemite Kingdom of Jordan. Int. J. Water 4, 105-120.

[98] Mezenner, N.Y., Bensmaili, A., 2009. Kinetics and thermodynamic study of phosphate adsorption on iron hydroxide eggshell waste. Chem. Eng. J. 147, 87-96.

[99] Midorikawa, I., Aoki, H., Ormori, A., Shimizu, T., Kawaguchi, Y., Kassai, K., Murakami, T., 2008. Recovery of high purity phosphorus from municipal wastewater secondary effluent by a high-speed adsorbent. Water Sci. Technol. 58, 1601-1607.

[100] Min, S.H., Han, J.S., Shin, E.W., Park, J.K., 2004. Improvement of cadmium ion removal by base treatment of juniper fiber. Water Res. 38, 1289-1295.

[101] Ministry of the Environment - Government of Japan. National effluent standards. Available at http://www.env.go.jp/en/water/wq/nes.html. (Accessed on March 16, 2015).

[102] Moerman, W., Carballa, M., Vandekerckhove, A., Derycke, D., Verstraete, W., 2009. Phosphate removal in agro-industry: Pilot and full scale operational considerations of struvite crystallization. Water Res. 43, 1887-1892.

[103] Mohammed, W.T., Rashid, S.A., 2012. Phosphorus removal from wastewater using oven dried alum sludge. Int. J. Chem. Eng. Volume 2012, Article ID 125296, 11 pages, http://dx.doi.org/10.1155/2012/125296.

[104] Molinos-Senante, M., Hernández-Sancho, F., Sala-Garrido, R., Garrido-Baserba, M., 2011. Economic feasibility study for phosphorus recovery processes. Ambio 40, 408-416.

[105] Muster, T.H., Douglas, G.B., Sherman, N., Seeber, A., Wright, N., Güzükara, Y., 2013. Towards effective phosphorus recycling from wastewater: quantity and quality. Chemosphere 91, 676-684.

[106] Nada, A.M.A., Hassan, M.L., 2006. Ion exchange properties of carboxylated bagasse. J. Appl. Polym. Sci. 102, 1399-1404.

[107] Namasivayam, C., Sakoda, A., Suzuki, M., 2005. Removal of phosphate by adsorption onto oyster shell powder - kinetic studies. J. Chem. Technol. Biotechnol. 80, 356-358.

[108] Namasivayam, C., Sangeetha, D., 2004. Equilibrium and kinetic studies of adsorption of phosphate onto $ZnCl_2$ activated coir pith carbon. J. Colloid Interf. Sci. 280, 359-365.

[109] Neethling, J.B., 2011. Impact of phosphorous removal to low limits. Available at http://www.azwater.org/common/files/committees/e8fbf236-e225-4d3b-8e17-d94ae7beb19d/Phosphorus%202.pdf. (Accessed on January 20, 2013).

[110] Nguyen, T.A.H., Ngo, H.H., Guo, W.S., Pham, T.Q., Li, F.M., Nguyen, T.V., Bui, X.T., 2015. Adsorption of phosphate from aqueous solutions and sewage using zirconium loaded okara (ZLO): Fixed-bed column study. Sci. Total Environ. 523, 40-49.

[111] Nguyen, T.A.H., Ngo, H.H., Guo, W.S., Nguyen, T.V., Zhang, J., Liang, S., Chen, S.S., Nguyen, N.C., 2014a. A comparative study on different metal loaded soybean milk by-product 'okara' for biosorption of phosphorus from aqueous solution. Bioresour. Technol. 169, 291-298.

[112] Nguyen, T.A.H., Ngo, H.H., Guo, W.S., Zhang, J., Liang, S., Lee, D.J., Nguyen, P.D., Bui, X.T., 2014b. Modification of agricultural waste/by-products for enhanced phosphate removal and recovery: Potential and obstacles. Bioresour. Technol. 169, 750-762.

[113] Nguyen, T.A.H., Ngo, H.H., Guo, W.S., Zhou, J.L., Wang, J., Liang, H., Li, G., 2014c. Phosphorus elimination from aqueous solution using 'zirconium loaded okara' as a biosorbent. Bioresour. Technolo. 170, 30-37.

[114] Nguyen, T.A.H., Ngo, H.H., Guo, W.S., Zhang, J., Liang, S., Tung, K.L., 2013. Feasibility of iron loaded 'okara' for biosorption of phosphorus in aqueous solutions. Bioresour. Technol. 150, 42-49.

[115] Nguyen, T.A.H., Ngo, H.H., Guo, W.S., Nguyen, T.V., 2012. Phosphorous removal from aqueous solutions by agricultural by-products: A critical review. J. Water Sustain. 2, 193-207.

[116] Nieminen, J., 2010. Phosphorus recovery and recycling from municipal wastewater sludge (Master of Science thesis). Aalto University, Espoo, Finland.

[117] Ning, P., Bart, H., Li, B., Lu, X., Zhang, Y., 2008. Phosphate removal from wastewater by model La(III) zeolite adsorbents. J. Environ. Sci. 20, 670-674.

[118] Nur, T., 2014. Nitrate, phosphate and fluoride removal from water using adsorption process (Doctoral thesis). University of Technology, Sydney, NSW, Australia.

[119] Nur, T., Johir, M.A.H., Loganathan, P., Nguyen, T, Vigneswaran, S., Kandasamy, J., 2014a. Phosphate removal from water using an iron oxide impregnated strong base anion exchange resin. J. Ind. Eng. Chem. 20, 1301-1307.

[120] Nur, T., Shim, W.G., Johir, M.A.H., Vigneswaran, S., Kandasamy, J., 2014b. Modeling of phosphorus removal by ion-exchange resin (Purolite FerrIX A33E) in fixed-bed column experiments. Desalin. Water Treat. 52, 784-790.

[121] Ogata, F., Tominaga, H., Kangawa, M., Inoue, K., Kawasaki, N., 2012. Characteristics of granular boehmite and its ability to adsorb phosphate from aqueous solution. Chem. Pharm. Bull. 60, 985-988.

[122] Ohura, S., Harada, H., Biswas, B.K., Kondo, M., Ishikawa, S., Kawakita, H., Ohto, K., Inoue, K., 2011. Phosphorus recovery from secondary effluent and side-stream liquid in a sewage treatment plant using zirconium-loaded saponified orange waste. J. Mater. Cycles Waste Manag.13, 293-297.

[123] Okano, K., Uemoto, M., Kagami, J., Miura, K., Aketo, T., Toda, M., Honda, K., Ohtake, H., 2013. Novel technique for phosphorus recovery from aqueous solutions using amorphous calcium silicate hydrates (A-CSHs). Water Res. 47, 2251-2259.

[124] Okochi, N.C., 2013. Phosphorus removal from storm water using electric ARC furnace steel slag (Doctoral thesis). University of Regina, Saskatchewan, Canada.

[125] Onyango, M.S., Kuchar, D., Kubota, M., Matsuda, H., 2007. Adsorptive removal of phosphate ions from aqueous solutions using synthetic zeolite. Ind. Eng. Chem. Res. 46, 894-900.

[126] Özkütük, E.B., Ersöz, A., Denizli, A., Say, R., 2008. Preconcentration of phosphate ion onto ion-imprinted polymer. J. Hazard. Mater. 157, 130-136.

[127] Parsons, S., Smith, J.A., 2008. Phosphorus removal and recovery from municipal wastewaters. Elem. 4, 109-112.

[128] Pastor, L., Mangin, D., Ferrer, J., Seco, A., 2010. Struvite formation from the supernatants of an anaerobic digestion pilot plant. Bioresour. Technol. 101, 118-125.

[129] Paudyal, H., Pangeni, B., Inoue, K., Kawakita, H., Ohto, K., Alam, S., 2013. Adsorptive removal of fluoride from aqueous medium using a fixed bed column packed with Zr(IV) loaded dried orange juice residue. Bioresour. Technol., 146, 713-720.

[130] Peleka, E.N., Deliyanni, E.A., 2009. Adsorptive removal of phosphates from aqueous solutions. Desalin. 245, 357-371.

[131] Peng, F., He, P., Luo, Y., Lu, X., Liang, Y., Fu, J., 2012. Adsorption of phosphate by biomass chars deriving from fast pyrolysis of biomass waste. Clean - Soil Air Water 40, 493-498.

[132] Penn, C.J., Bryant, R.B., Kleinman, P.J.A., Allen, A.L., 2007. Removing dissolved phosphorus from drainage ditch water with phosphorus sorbing materials. J. Soil Water Conserv. 62, 269-276.

[133] Perera, P.W.A., Han, Z.Y-., Chen, Y.X., Wu, W.X., 2007. Recovery of nitrogen and phosphorous as struvite from swine waste biogas digester effluent. Biomed. Environ. Sci. 20, 343-350.

[134] Petzet, S., Peplinski, B., Cornel, P., 2012. On wet chemical phosphorus recovery from sewage sludge ash by acidic or alkaline leaching and an optimized combination of both. Water Res. 46, 3769-3780.

[135] Quintelas, C., Pereira, R., Kaplan, E., Tavares, T., 2013. Removal of Ni(II) from aqueous solutions by an Arthrobacterviscosus biofilm supported on zeolite: from laboratory to pilot scale. Bioresour. Technol., 142, 368-374.

[136] Reyahi-khoram, M., Sobhanardakani, S. 2014. Investigation of heavy metals concentration in community wastewater of Hamedan city and its effects on the environment. Adv. Environ. Biol. 8, 273-277.

[137] Riahi, K., Thayer, B.B., Mammou, A.B., Ammar, A.B., 2009. Biosorption characteristics of phosphates from aqueous solution onto Phoenix dactylifera L. date palm fibers. J. Hazard. Mater. 170, 511-519.

[138] Rouff, A.A., 2013. Temperature dependent phosphorus precipitation and chromium removal from struvite saturated solutions. J. Colloid Interf. Sci. 392, 343-348.

[139] Ruixia, L., Jinlong, G., Hongxiao, T., 2002. Adsorption of fluoride, phosphate and arsenate ions on a new type of ion exchange fibber. J. Colloid Interf. Sci. 248, 268-274.

[140] Saka, C., Sahin, Ö., Küçük, M.M., 2012. Applications on agricultural and forest waste adsorbents for the removal of lead (II) from contaminated waters. Int. J. Environ. Sci. Technol. 9, 379-394.

[141] Samuel, J., Pulimi, M., Paul, M.L., Maurya, A., Chandrasekaran, N., 2013. Batch and continuous flow studies of adsorptive removal of Cr(VI) by adapted bacterial consortia immobilized in alginate beads. Bioresour. Technol.128, 423-430.

[142] Sartorius, C., Horn, J.V., Tettenborn, F., 2012. Phosphorus recovery from wastewater - expert survey on present use and future potential. Water Environ. Res. 84, 313-322.

[143] Schick, J., Kratz, S., Adam, C., Schnug, E., 2009. Techniques for P recovery from waste water and sewage sludge and fertilizer quality of P recycling products. http://www.mmm.fi/attachments/mmm/ministerio/5n8h6xg9T/presentation_judith_schick.pdf. (Accessed on April 30, 2015).

[144] Sengupta, S., Pandit, A., 2011. Selective removal of phosphorus from wastewater combined with its recovery as a solid phase fertilizer. Water Res. 45, 3318-3330.

[145] Seymour, D., 2009. Can nutrient recovery be a financially sustainable development objective? Available at http://www.pncwa.org/assets/documents/2009%20PNCWA-

%20Session%2014-1%20-%20Centrate%20to%20Fertilizer%20-%20David%20Seymour.pdf. (Accessed on June 16, 2015).

[146] Sharma, R., Singh, B., 2013. Removal of Ni(II) ions from aqueous solutions using modified rice straw in a fixed bed column. Bioresour. Technol., 146, 519-524.

[147] Shen, Y., Ogejo, J.A., Bowers, K.E., 2011. Abating the effects of calcium on struvite precipitation in liquid dairy manure. T. Asabe 54, 325-336.

[148] Shin, E.W., Karthikeyan, K.G., Tshabalala, M.A., 2005. Orthophosphate sorption onto lanthanum treated lignocellulosic sorbents. Environ. Sci. Technol. 39, 6273-6279.

[149] Shu, L., Schneider, P., Jegatheesan, V., Johnson, J., 2006. An economic evaluation of phosphorus recovery as struvite from digester supernatant. Bioresour. Technol. 97, 2211-2216.

[150] Song, Y., Yuan, P., Zheng, B., Peng, J., Yuan, F., Gao, Y., 2007. Nutrients removal and recovery by crystallization of magnesium ammonium phosphate from synthetic swine wastewater. Chemosphere 69, 319-324.

[151] Soy 20/20, 2005. Overview of current utilization. Available at http://www.soy2020.ca/pdfs/OverviewOfOkaraUtilization.pdf. (Accessed on March 29, 2014).

[152] Srivastava, S., Goyal, P., 2010. Novel biomaterials - Decontamination of toxic metals from wastewater. Springer Heidelberg Dordrecht, London, New York.

[153] Strom, P.F., 2006. Technologies to remove phosphorous from wastewater. Available at http://www.water.rutgers.edu/Projects/trading/p-trt-lit-rev-2a.pdf. (Accessed on January 4, 2013).

[154] Suzuki, K., Tanaka, Y., Osada, T., Waki, M., 2002. Removal of phosphate, magnesium and calcium from swine wastewater through crystallization enhanced by aeration.Water res. 36, 2991-2998.

[155] Tan, Z., Lagerkvist, A., 2011. Phosphorus recovery from the biomass ash: A review. Renew. Sust. Energ. Rev. 15, 3588-3602.

[156] Tasmania Environmental Protection Authority (EPA). Emission limit guidelines for sewage treatment plants that discharge pollutants into fresh and marine waters June 2001. Available at http://epa.tas.gov.au/epa/document?docid=40. (Accessed on March 16, 2015).

[157] TCVN 5945: 2005. Industrial waste water -Discharge standards. Available at http://www.gree-vn.com/pdf/TCVN5945-2005.pdf. (Accessed on March 16, 2015).

[158] The National environment regulations, 1999 (Standards for Discharge of Effluent into Water or on Land). Available at http://faolex.fao.org/docs/pdf/uga40868.pdf. (Accessed on March 16, 2015).

[159] Tshabalala, M.A., Karthikeyan, K.G., Wang, D., 2004. Cationized milled pine bark as an adsorbent for orthophosphate anions. J. Appl. Polym. Sci. 93, 1577-1583.

[160] Tyagi, V.K., Lo, S., 2013. Sludge: a waste or renewable source for energy and resources recovery. Renew. Sust. Energ. Rev. 25, 708-728.

[161] Unnithan, M.R., Vinod, V.P., Anirudhan, T.S., 2002. Ability of iron(III) loaded carboxylated polyacrylamide grafted sawdust to remove phosphate ions from aqueous solution and fertilizer industry wastewater: adsorption kinetics and isotherm studies. J. Appl. Polym. Sci. 84, 2541-2553.

[162] Vázquez, G., Mosquera, O., Freire, M.S., Antorrena, G., González-Álvarez, J., 2012. Alkaline pre-treatment of waste chestnut shell from a food industry to enhance cadmium, copper, lead and zinc ions removal. Chem. Eng. J. 184, 147-155.

[163] Volesky, B., 2007. Biosorption and me. Water Res. 41, 4017-4029.

[164] Wahab, M.A., Hassineb, R.B., Jellalia, S., 2011. *Posidonia oceanica* (L.) fibers as a potential low-cost adsorbent for the removal. J. Hazard. Mater. 191, 333-341.

[165] Wang, Z., Nie, E., Li, J., Yang, M., Zhao, Y., Luo, X., Zheng, Z., 2012. Equilibrium and kinetics of adsorption of phosphate onto iron doped activated carbon. Environ. Sci. Pollut. Res. 19, 2908-2917.

[166] Wang, W.Y., Yue, Q.Y., Xu, X., Gao, B.Y., Zhang, J., Li, Q., Xu, J.T., 2010. Optimized conditions in preparation of giant reed quaternary amino anion exchanger for phosphate removal. Chem. Eng. J. 157, 161-167.

[167] Wang, J., Burken, J.G., Zhang, X.Q., Surampalli, R., 2005. Engineered struvite precipitation: Impacts of component ion molar ratios and pH. J. Environ. Eng.-Asce 131, 1433-1440.

[168] Warmadewanthi, J.C.L, 2009. Recovery of phosphate and ammonium as struvite from semiconductor wastewater. Separ. Purif. Technol. 64, 368-373.

[169] Wartelle, L.H., Marshall, W.E., 2006. Quaternized agricultural by-products as anion exchange resins. J. Environ. Manage. 78, 157-162.

[170] Wilsenach, J. A., Schuurbiers, C.A.H., van Loosdrecht, M.C.M., 2007. Phosphate and potassium recovery from source separated urine through struvite precipitation. Water Res. 41, 458-466.

[171] Wu, Q., Bishop, P.L., 2004. Enhancing struvite crystallization from anaerobic supernatant. J. Environ. Eng. Sci. 3, 21-29.

[172] Xu, H., He, P., Gu, W., Wang, G., Shao, L., 2012. Recovery of phosphorus as struvite from sewage sludge ash. J. Environ. Sci. 24, 1533-1538.

[173] Xu, X., Gao, B., Yue, Q., Zhong, Q., 2011a. Sorption of phosphate onto giant reed based adsorbent: FTIR, Raman spectrum analysis and dynamic sorption/desorption properties in filter bed. Bioresour.Technol. 102, 5278-5282.

[174] Xu, X., Gao, Y., Gao, B., Tan, X., Zhao, Y.Q., Yue, Q., Wang, Y., 2011b. Characteristics of diethylenetriamine-crosslinked cotton stalk/wheat stalk and their biosorption capacities for phosphate. J. Hazard. Mater. 192, 1690–1696.

[175] Xu, X., Gao, B. Y., Yue, Q. Y., Zhong, Q. Q., Li, Q., 2011c. Preparation of new types of anion exchange resins from agricultural by-products and their utilization in the removal of various toxic anions from solutions. Chem. Eng. J. 167, 104-111.

[176] Xu, X., Gao, B., Yue, Q., Zhong, Q., Zhan, X., 2010a. Preparation, characterization of wheat residue based anion exchangers and its utilization for the phosphate removal from aqueous solution. Carbohyd. Polym. 82, 1212-1218.

[177] Xu, X., Gao, B.Y., Yue, Q.Y., Zhong, Q.Q., 2010b. Preparation of agricultural by-product based anion exchanger and its utilization for nitrate and phosphate removal. Bioresour. Technol. 101, 8558-8564.

[178] Xu, X., Gao, B., Wang, W., Yue, Q., Wang, Y., Ni, S., 2009. Adsorption of phosphate from aqueous solution onto modified wheat residue: Characteristics, kinetic and column studies. Colloids Surf., B 70, 46-52.

[179] Yeom, S.H., Jung, K., 2009. Recycling wasted scallop shell as an adsorbent for the removal of phosphate. J. Ind. Eng. Chem. 15, 40-44.

[180] Yetilmezsoy, K., Turkdogan-Aydinol, I., Gunay, A., Ozis, I., 2011. Post treatment of poultry slaughterhouse wastewater and appraisal of the economic outcome. Environ. Eng. Manage. J. 10, 1635-1645.

[181] Yue, Q.Y., Wang, W., Gao, B., Xu, X., Zhang, J., Li, Q., 2010. Phosphate removal from aqueous solution by adsorption on modified giant reed. Water Environ. Res. 82, 374-381.

[182] Zach-Maor, A., Semiat, R., Shemer, H., 2011. Fixed bed phosphate adsorption by immobilized nano-magnetite matrix: experimental and a new modeling approach. Adsorpt. 17, 929-936.

[183] Zhang, L., Wu, Wentao, W., Liu, J., Zhou, Q., Luo, J., Zhang, J., Wang, X., 2014. Removal of phosphate from water using raw and activated laterite: batch and column studies. Desalin. Water Treat. 52, 775-783.

[184] Zhang, J., Shan, W., Ge, J., Shen, Z., Lei, Y., Wang, W., 2012. Kinetic and equilibrium studies of liquid phase adsorption of phosphate on modified sugarcane bagasse. J. Environ. Eng. 138, 252-258.

[185] Zhang, L., Wan, L., Chang, N., Liu, J., Duan, C., Zhou, Q., Li, X., 2011. Removal of phosphate from water by activated carbon fiber loaded with lanthanum oxide. J. Hazard. Mater. 190, 848-855.

UNIVERSITY OF TECHNOLOGY, SYDNEY

APPENDIX

RESEARCH OUTCOMES

LIST OF PUBLICATIONS

Book Chapter

1. Ngo, H.H., Guo, W.S., **Nguyen, T.A.H.**, Surampali, R., Zhang, T., 2015. Chapter 25: Agricultural by-products for phosphorus removal and recovery from water and wastewater: A green technology, in: Ngo, H.H., Guo, W.S., Surampali, R., Zhang, T. (Eds.), Green technologies for sustainable water management. American Civil Engineering Society, USA (In press).

Peer Reviewed Journal Articles

1. **Nguyen, T.A.H.,** Ngo, H.H., Guo, W.S., Pham, T.Q., Li, F.M., Nguyen, T.V., Bui, X.T., 2015. Adsorption of phosphate from aqueous solutions and sewage using zirconium loaded okara (ZLO): Fixed-bed column study. *Sci. Total Environ.* 523, 40-49.
2. **Nguyen, T.A.H**., Ngo, H.H., Guo, W.S., Zhou, J.L., Wang, J., Liang, H., Li, G., 2014. Phosphorus elimination from aqueous solution using 'zirconium loaded okara' as a biosorbent. *Bioresour. Technol.* 170, 30-37.
3. **Nguyen, T.A.H**., Ngo, H.H., Guo, W.S., Zhang, J., Liang, S., Lee, D.J., Nguyen, P.D., Bui, X.T., 2014. Modification of agricultural waste/by-products for enhanced phosphate removal and recovery: Potential and obstacles. *Bioresour. Technol.* 169C, 750-762.
4. **Nguyen, T.A.H**., Ngo, H.H., Guo, W.S., Nguyen, T.V., Zhang, J., Liang, S., Chen, S.S., Nguyen, N.C., 2014. A comparative study on different metal loaded soybean milk by-product 'okara' for biosorption of phosphorus from aquaeous solution. *Bioresour. Technol.* 169, 291-298.
5. **Nguyen, T.A.H**., Ngo, H.H., Guo, W.S., Zhang, J., Liang, S., Tung, K.L., 2013. Feasibility of iron loaded 'okara' for biosorption of phosphorousin aqueous solutions. *Bioresour. Technol.* 150, 42-49.
6. **Nguyen, T.A.H**., Ngo, H.H., Guo, W.S., Zhang, J., Liang, S., Yue, Q.Y., Li, Q., Nguyen, T.V., 2013. Applicability of agricultural waste and by-products for adsorptive removal of heavy metals from wastewater. *Bioresour. Technol.* 148, 574-585.

7. **Nguyen, T.A.H**., Ngo, H.H., Guo, W.S., Nguyen, T.V., 2012. Phosphorous removal from aqueous solutions by agricultural by-products: A critical review. *J. Water Sustain.* 2, 193-207.

CONTRIBUTIONS TO SCIENTIFIC FORUMS

1. **Nguyen, T.A.H**., Ngo, H.H., Guo, W.S., 2014. Isotherm and kinetic studies on biosorption of phosphorus by zirconium-loaded okara (Oral presentation). *10th European Symposium on Biochemical Engineering Sciences (ESBES) and 6th International Forum on Industrial Bioprocesses (IFIBiop) in collaboration with ACS.* Lille, France, 7-10 September, 2014.
2. **Nguyen, T.A.H**., Ngo, H.H., Guo, W.S., Nguyen, T.V., 2012. A critical review on the application of agricultural wastes for heavy metals removal from wastewater (Oral presentation). *5th International Conference on Challenges in Environmental Science and Engineering (CESE).* Melbourne, Australia, 9-13 September, 2012.

AWARDS

1. 2015 Faculty of Engineering and Information Technology (FEIT) PhD Post Thesis Publication Scholarship.
2. 2014 HDR Students Publication Award from Faculty of Engineering and Information Technology (FEIT), University of Technology, Sydney (UTS) for publishing in high quality journals.
3. 2012 one-off scholarship from Centre for Technology in Water and Wastewater (CTWW), University of Technology, Sydney (UTS).

CURRICULUM VITAE

THI AN HANG NGUYEN

PERSONAL INFORMATION

Date of birth: 26 November 1975

Place of birth: Hanoi, Vietnam

Gender: Female

Marital status: Married

CONTACT INFORMATION

Address: School of Civil and Environmental Engineering,
University of Technology, Sydney (UTS)
P.O. Box 123
15 Broadway, Ultimo, NSW 2007, Australia

E-mail address: Anhang75@gmail.com

Telephone: +61-2-9514-9094 (office)
+61-2-8033-7005 (home)

EDUCATION

2015

Ph.D. in Environmental Engineering (PhD thesis under examination)

School of Civil and Environmental Engineering,

University of Technology, Sydney (UTS), AUSTRALIA

1998

M.Sc. in Soil Science and Environment

Vietnam National University, Hanoi - University of Science, (VNU-HUS), VIETNAM

1996

B.Sc. in Biology

Vietnam National University, Hanoi - University of Science, (VNU-HUS), VIETNAM

RECORD EMPLOYMENT

2011

Program Manager

Education for Nature – Vietnam (ENV),

Vietnam Union of Sciences and Technology Associations (VUSTA)

Hanoi, Vietnam

2009-2010

Project Manager

Centre for Education and Communication of theEnvironment (CEACE),

Vietnam Union of Sciences and Technology Associations (VUSTA)

Hanoi, Vietnam

1999-2008

Head of Division of Research and Development (2006-2008)

Vice Head of Division of Research and Development (2000-2005)

Researcher (1999-2004)

Centre for Regional Research and Development (CRD),

Ministry of Science, Technology and Environment (MOSTE)

Hanoi, Vietnam

PROFESSIONAL MEMBERSHIP

International Forum on Industrial Bioprocesses (IFIBiop)

Centre for Technology in Water and Wastewater (CTWW), University of Technology, Sydney (UTS)

INFORMATION TECHNOLOGY

Proficient in MS Office package

Basic knowledge of PASCAL and MATLAB

LANGUAGES

English (fluent speaker)

Vietnamese (native speaker)

Japanese and Russian (beginner)

REFEREES

1. Prof. Dr. Huu Hao Ngo
   School of Civil and Environmental Engineering,
   University of Technology, Sydney (UTS), Australia
   Email: ngohuuhao121@gmail.com

2. Prof. Dr. Van Khoa Le
   Faculty of Environmental Science
   University of Science, Vietnam National University, Hanoi (VNU-HUS)
   Email: khoavnu@gmail.com

3. Ass. Prof. Dr. Manh Khai Nguyen
   Faculty of Environmental Science
   University of Science, Vietnam National University, Hanoi (VNU-HUS)
   Email: khainm@gmail.com